Rational Design of Responsive Prodrug-based Nanomedicines for Antitumor Therapy

Inaugural-Dissertation

to obtain the academic degree

Doctor rerum naturalium (Dr. rer. nat.)

submitted to the Department of Biology, Chemistry and Pharmacy

of Freie Universität Berlin

by

Gregor Nagel

Berlin

2018

I hereby declare that the submitted thesis is my own work and was prepared autonomously without the aid of other sources than the ones cited and acknowledged. The work was not submitted to any other prior doctoral procedure.

Gregor Nagel Berlin, den 08.11.2018

The following PhD thesis was carried out from February 2015 until November 2018 in the research group of Prof. Dr. Marcelo Calderón at the department of Biology, Chemistry and Pharmacy of the Freie Universität Berlin.

1st Reviewer: Prof. Dr. Marcelo Calderón

2nd Reviewer: PD Dr. Fiorenza Rancan

Date of thesis defense: 11.12.2018

ACKNOWLEDGEMENTS

I would like to express my gratitude to **Prof. Dr. Marcelo Calderón** for giving me the opportunity to conduct my doctoral studies in his research group and for providing an outstanding research environment. Apart of the excellent scientific guidance, I am most thankful for the mentorship, scientific freedom, and fun times over the past years.
Herewith, I would also like to thank **PD Dr. Fiorenza Rancan** for being the co-referee of this thesis.

I am thankful to all former and present members of AG Calderón creating a special atmosphere over the years. In particular, I want to thank my long-time colleagues (and friends) Julián Bergueiro Álvarez, Laura Isabel Vossen, Michael Giulbudagian, Harald Rune Tschiche, Stefanie Wedepohl, Loryn Theune, Emanuel Glitscher, Ernesto Osorio Blanco, Enrico Miceli, Catalina Biglione, Lydia Bouchet, Mazdak Asadian-Birjand, Dogus Isik, Maria Molina Soler, and Ana Sousa-Herves.
I would like to thank all the people that were sharing the office with me including Julián Bergueiro Álvarez, Laura Isabel Vossen, Michael Giulbudagian, Emanuel Glitscher, Loryn Theune, Harald Rune Tschiche, and Mazdak Asadian-Birjand. I am thankful for the fruitful discussions not only related to science and for having an open ear for questions and problems.
I want to thank all my lab mates including Laura Isabel Vossen, Harald Rune Tschiche, Mrityunjoy Kar, Ana Sousa-Herves, Eva Clemente and all the visiting students. It was not always easy in the small lab, but it brought us closer together.
Special thanks go to Katrin Michel and Sebastian Heintze for their technical support and for keeping order in the laboratories.
I am grateful for the countless international visitors and colleagues for teaching me cultural aspects from all over the world and bringing an international atmosphere to the labs. Among others, I thank Smriti Arora, Marek Brzeziński, Eva Clemente, Sandra Arias Lopez, Katherine Cobos, Irene Dolz Perez, Nicolas Guillaume, Alexis Kassentini, Marcelo Kravicz, Amit Kumar, Anna Puiggalí Jou, Balram Rathi, Alberto Sanz de León, Ana Lygia dos Santos Camara, Fitsum Sahle, and Oscar Rojas. In this regard, I want to thank the whole Argentinian crew including Lydia Bouchet, Catalina Biglione, Lucila Navarro, Matias Picchio, Alexis Wolfel, Ana Sofia Sonzogni, Cecilia Samaniego Lopez, and Guido Rimondino. You guys are all loco.

I would like to thank João Paulo Figueiró Longo, Ana Lygia dos Santos Câmara, Matias Picchio, Irene Dolz Perez, Balram Rathi, Cecilia Samaniego Lopez, Johannes Stellmacher, and Pin Dong for successful collaborations. Special thanks go to Fiorenza Rancan and Patrick Graff to help me figure out the spheroid sectioning.

I enjoyed the coffee breaks in the morning with all members of the coffee group including pseudo Calderonis Felix Reisbeck, Mathias Dimde, and Olaf Wagner. Thanks for the good times.

Special thanks go to my supervisors and subgroup leaders Harald Rune Tschiche and Stefanie Wedepohl. Your excellent guidance helped me to improve professionally and personally. I want to thank Stefanie for her patience, guidance in the world of cell tests and proof reading.

I am grateful to my friends and fellow students for their and support during the last years. In particular, I want to thank Johannes Wunderlich, Emanuel Glitscher, Hendrik Schröder, Sebastian Sobottka, Max Bartetzko, Nandor Ziebart, Goswinus de Kruijff for the most motivational studying group and interesting travel experiences. I also would like to thank Sebastian Niether, Paul Sengstock, Julius Naperkowski, Frederico Göpelt und Henry Pörner for cheering me up and distracting me in my free time.

Most importantly, I am grateful to my parents, Helma and Thomas Nagel and my sister Franziska for their unconditional support and patience.

Above all, I want to express my gratitude to my friend and partner Martina Menger for endless support, patience, love and so much more. You always brighten my mood with your smile. I am grateful to have you in my life. Thank you.

Abstract

A major issue of conventional chemotherapy is the lack of selective delivery which results in high systemic exposure and severe side effects. The limitations of small molecular weight drugs for cancer therapy prompted the development of diverse nanocarrier systems for targeted drug delivery. The impressive progress in nanomaterial science and increased understanding of the nano-bio interface allowed the progression of these systems. However, the targeted delivery remains challenging due to obstacles that are encountered during the drug delivery process, particularly, in the tumor microenvironment (TME). (Multi)stimuli-responsive nanocarriers have the potential to overcome the faced barriers by taking advantage of altered pathological characteristics in the TME and/or intracellular signals.

The motivation of the presented work was to incorporate rational design features into novel responsive nanomedicines to address the limitations of conventional chemotherapeutic drugs and tackle issues of current drug delivery systems (DDS). For this purpose, prodrugs of the chemotherapeutic agent doxorubicin (Dox) were combined with three nanocarrier designs including polymer-drug conjugates, a nanoemulsion (NE), and nanogels (NGs). The Dox prodrugs comprised cleavable motifs which introduce a responsiveness towards endogenous stimuli into the nanocarriers. The nanocarrier architectures with different sizes and compositions were evaluated in terms of controlled drug release, drug-carrier compatibility, carrier degradability, and transport restrictions in the TME, all of which are important aspects for an efficient delivery process.

The choice of the cleavable linkage strongly affects the specificity of the desired responsive behavior. To address this aspect, Dox prodrugs with pH- or protease-cleavable bonds were evaluated regarding their impact on the intracellular drug release. Activatable fluorescence probes were utilized to follow the drug release from polymer-drug conjugates in real-time. This assessment of the linker formed the basis for the rational design of two prodrug-based nanomedicines with adjusted cleavage properties. First, a pH-sensitive Dox prodrug was entrapped in a NE to form a DDS with explicit intracellular drug release. The second design was based on dual-responsive nanogels as multistage delivery systems with specific extracellular response to protease and acid-mediated intracellular payload release.

Initially, we evaluated the impact of the cleavable linkage on the drug release using theranostic polymer conjugates (TPC) with activatable fluorescence probes. The TPC represent model DDS that consist of dendritic polyglycerol (dPG) as polymeric carrier labeled with an

indodicarbocyanine (IDCC) dye that quenches the fluorescence of Dox, conjugated through a cleavable linker. Cleavage of the conjugates was mediated either by acidic pH or protease activity. By tracking the fluorescence recovery in a cell-based microplate assay, we were able to obtain characteristic release profiles of Dox for different cell lines. Here, the pH-cleavable linker was found to be cleaved mainly intracellularly, whereas the protease-sensitive system suffered from extracellular drug release. The intracellular release was crucial to treat multidrug-resistant cells and overcome their resistance mechanisms. It can be highlighted that the modular synthetic approach, combined with the cell-based assay, has potential to extend the common *in vitro* methods to evaluate DDS performance.

The results of this study motivated us to develop a pH-sensitive Dox prodrug (C16-Dox) to efficiently dissolve the drug in the nanodroplets of an oil/water NE. By attaching a hydrophobic alkyl chain (C16), Dox was provided with an amphiphilic character for increased drug-carrier compatibility. pH-sensitive properties of the prodrug allowed the intracellular release of the drug from the NE by recovering the hydrophilic parent drug. The new formulation of Dox (NE-C16-Dox) was compared with free Dox in a murine breast cancer model. Enhanced delivery to tumor tissue and reduction of systemic toxicity allowed the administration of a higher Dox dose in the NE formulation as compared to the free drug. The high dosage significantly inhibited the primary tumor growth and prevented the formation of distant lung metastasis without signs of side effects. The improved chemotherapeutic index compared to free Dox indicates that NE-C16-Dox is a promising formulation for breast cancer treatment

At last, we combined protease- and pH-sensitive moieties into a multistage nanocarrier to enhance drug transport in tumor tissue. Matrix metalloproteinase (MMP)-sensitive NGs (pNGs) were developed which consists of a dPG scaffold crosslinked with a fluorogenic peptide. The crosslinker integrates biodegradability to the nanocarrier mediated by proteases in the TME. The intrinsic reporter moiety of the crosslinker allowed us to study the influence of different pNG compositions on the degradation profile in detail. One pNG candidate was chosen to conjugate the therapeutic drug Dox through a pH-sensitive linkage to dPG. The degradable multistage pNGs demonstrated deeper penetration into multicellular tumor spheroids (MCTS) as compared to their non-degradable counterparts. Hence, the triggered size reduction of the pNGs by enzymatic degradation facilitated the infiltration of the nanocarrier into dense tissue and thereby promoted the delivery of the therapeutic cargo.

Kurzzusammenfassung

Ein Hauptproblem der konventionellen Chemotherapie ist die hohe systemische Exposition, die zu schweren Nebenwirkungen führen kann. Die Schwierigkeiten in Verbindung mit niedermolekularen Wirkstoffen für die Krebstherapie führten zur Entwicklung verschiedener Nanotransportsysteme für den gezielten Wirkstofftransport (*targeted drug delivery*). Aufgrund des Fortschritts in der Nanomaterialforschung und des besseren Verständnisses der Nano-Bio-Grenzfläche können diese Systeme weiter verbessert werden. Der gezielte Wirkstofftransport bleibt jedoch aufgrund der physiologischen Hindernisse, die während des Transportprozesses, insbesondere im Tumormikromileu (TMM), auftreten eine Herausforderung. (Multi)-Stimuli-responsive Nanotransportern (*Nanocarrier*) haben das Potenzial, die Barrieren zu überwinden, indem sie die veränderten pathologischen Eigenschaften des TMM nutzen.

Die Motivation dieser Arbeit war es rationales Design in neuartige, Prodrug-basierte Nanotransporter zu integrieren, um die Komplikationen herkömmlicher Chemotherapeutika zu reduzieren und die Probleme derzeitiger Wirkstofftransportsystemen (*Drug delivery systems*) zu überwinden. Zu diesem Zweck wurden Prodrugs des Chemotherapeutikums Doxorubicin (Dox) mit drei Nanotransportsystemen kombiniert, darunter Polymer-Wirkstoff-Konjugate, eine Nanoemulsion (NE) und Nanogele (NGs). Die Dox-Prodrugs enthalten spaltbare Gruppen, die eine Reaktivität auf endogene Stimuli in die Nanotransporter einführen. Die Nanocarrier-Architekturen mit unterschiedlichen Größen und Zusammensetzungen wurden im Hinblick auf die kontrollierte Freisetzung von Medikamenten, die Kompatibilität mit dem Transporter und die Abbaubarkeit des Nanocarriers sowie Transportbeschränkungen im TMM untersucht.

Die Wahl der spaltbaren Verknüpfung beeinflusst stark die Spezifität der gewünschten Reaktivität. Um den Einfluss des gewählten Linkers auf die intrazelluläre Wirkstofffreisetzung zu bewerten, wurden Dox-Prodrugs mit pH- oder Protease-spaltbaren Bindungen in Kombination mit aktivierbaren Fluoreszenzsreportern verwendet. Die Reporter erlaubten es die Wirkstofffreisetzung von Polymer-Wirkstoff-Konjugaten in Echtzeit zu verfolgen. Die Evaluierung der spaltbaren Linker bildete die Grundlage für das rationale Design von zwei Prodrug-basierten Nanotransportern mit angepassten Spaltungseigenschaften. Zunächst wurde eine pH-empfindliche Dox-Prodrug in ein NE eingeschlossen, um ein DDS mit expliziter intrazellulärer Wirkstofffreisetzung zu erhalten. Das zweite Design basierte auf Nanogelen mit

zwei sensitiven Gruppen für ein mehrstufiges Transportersystem mit spezifischer Reaktion auf extrazelluläre Proteasen und säurekatalysierter intrazellulären Freisetzung des Wirkstoffs.
Zunächst wurde die Auswirkung von verschiedenen spaltbaren Bindungen auf die Wirkstofffreisetzung untersucht. Dazu wurden theranostischen Polymerkonjugaten (TPC) mit aktivierbarer Fluoreszenzreportern verwendet. Die TPC stellen Modell-Wirkstofftransporter dar, die aus dendritischen Polygycerol (dPG) als polymerem Träger bestehen, das mit einem Indodicarbocyanin (IDCC)-Farbstoff markiert ist Die Nähe des Farbstoffes zu Dox, das über eine spaltbare Bindung an das dPG konjugiert wurde, wurde die Fluoreszenz von Dox unterdrückt. Die Spaltung der Konjugate konnte entweder durch saure Hydrolyse oder durch die Aktivität von Protease geschehen. In einem zellbasierten, vergleichenden Assay konnte durch das Verfolgen des Fluoreszenzsignals charakteristische Freisetzungsprofile für verschiedene Zelllinien erhalten werden. Dabei wurde festgestellt, dass der pH-spaltbare Linker hauptsächlich intrazellulär gespalten wurde, während das proteaseempfindliche System extrazellulären Wirkstofffreisetzung zeigte. Die intrazelluläre Wirkstofffreisetzung war entscheidend, um multiresistente Zellen zu behandeln und ihre Resistenzmechanismen zu überwinden. Der modulare Syntheseansatz in Kombination mit dem zellbasierten Assay kann die üblichen In-vitro-Methoden zur Bewertung der Wirkstofftransporterperformance erweitern, da das Design leicht für verschiedene Träger/Linker-Systeme sowie verschiedene Zelllinien eingesetzt werden kann.
Die Ergebnisse dieser Studie haben uns motiviert, eine pH-empfindliche Dox-Prodrug (C16-Dox) zu entwickeln, um den Wirkstoff effizient in die Nanotröpfchen einer Öl/Wasser-NE einzubringen. Durch Bindung einer hydrophoben Alkylkette (C16) erhielt Dox einen amphiphilen Charakter, was die Wirkstoff-Carrier-Kompatibilität erhöhte. Die pH-empfindlichen Eigenschaften der Prodrug ermöglichten die intrazelluläre Freisetzung von Dox durch Rückbildung des freien Wirkstoffs. Die neue Dox-Formulierung (NE-C16-Dox) wurde in einem In-vivo-Brustkrebsmodell mit freiem Dox verglichen. Eine verbesserte Akkumulation im Tumorgewebe und eine Verringerung der systemischen Toxizität ermöglichten die Verabreichung einer höheren Dosis von Dox in der NE-Formulierung im Vergleich zum freien Wirkstoff. Die höhere Dosierung inhibierte das primäre Tumorwachstum signifikant und verhinderte die Bildung von Lungenmetastasen ohne Anzeichen von Nebenwirkungen. Der verbesserte chemotherapeutische Index im Vergleich zu freiem Dox weist darauf hin, dass NE-

C16-Dox eine vielversprechende Formulierung für die Behandlung von Brustkrebs sein und wird daher für klinische Studien in Betracht gezogen.

Schließlich kombinierten wir Protease- und pH-empfindliche Komponenten in einem multi-responsiven Nanocarrier, um den gehinderten Wirkstofftransport im Tumorgewebe zu verbessern. Dazu wurden Matrix-Metalloprotease (MMP)-sensitive NGs (pNGs) entwickelt, die aus einem dPG-Gerüst bestehen, das mit einem fluorogenen Peptid vernetzt ist. Der Vernetzer integriert biologische Abbaubarkeit in den Nanocarrier, die durch Proteasen im TME verursacht werden kann. Der intrinsische Reporter des Vernetzers erlaubte es uns, den Einfluss verschiedener pNG-Zusammensetzungen auf das Zerfallsprofil im Detail zu untersuchen. Ein pNG-Kandidat wurde ausgewählt, um den therapeutischen Wirkstoff Dox über eine pH-sensitive Bindung an dPG zu konjugieren. Die abbaubaren mehrstufigen pNGs zeigten eine tiefere Eindringtiefe in multizellulären Tumor-Sphäroiden (MCTS) im Vergleich zu ihren nicht abbaubaren Gegenstücken. Es konnte somit gezeigt werden, dass die endogen gesteuerte Verkleinerung der pNGs durch enzymatischen Abbau die Infiltration des Nanocarrier in dichtes Gewebe verbesserte und dadurch den Transport des therapeutischen Wirkstoffs förderte.

TABLE OF CONTENTS

1 INTRODUCTION 1

1.1 Nanomedicine 1

1.1.1 Rationale for nanomedicine in cancer therapy 1

1.1.2 Role of the nanoscale size 3

1.1.3 Impact of nanocarrier design on drug delivery 4

1.1.4 Prodrug concept 10

1.2 Stimuli-responsive nanomaterials 12

1.2.1 Exogenous stimuli 14

1.2.2 Endogenous stimuli 15

1.2.3 Multistimuli responsiveness 20

1.2.4 Nanotheranostics 22

1.3 Classes of nanocarriers 29

1.3.1 Polymeric nanostructures 29

1.3.2 Lipid-based nanocarriers 36

1.3.3 Clinical translation of nanomedicine 37

2 MOTIVATION & OBJECTIVE 39

3 PUBLICATIONS & MANUSCRIPTS 43

3.1 Modular approach for theranostic polymer conjugates with activatable fluorescence: impact of linker design on the stimuli-induced release of doxorubicin 43

3.2 Acid-sensitive lipidated doxorubicin prodrug entrapped in nanoemulsion impairs lung tumor metastasis in a breast cancer model 57

3.3 Matrix metalloproteinase-sensitive multistage nanogels enhance drug transport in 3D tumor model 74

4 CONCLUSION & OUTLOOK 109

5 REFERENCES 115

6 APPENDIX 126

6.1 Supporting information 126

6.2 Publications & conference contributions 180

6.3 Curriculum Vitae 182

1 INTRODUCTION

1.1 Nanomedicine

Even though nanoparticles have existed since long, the technological advances to investigate and control matter at the nanoscale prompted the development of new materials and applications. Nanotechnology is an advancing field with interdisciplinary research focusing on the control of material at the nanoscale by engineering structures on the molecular level. Within this field, nanomedicine encompasses the application of nanotechnology in the healthcare sector.[1] The aim of nanomedicine is the design of nano-sized multifunctional therapeutics and drug delivery systems (DDS) to yield more effective therapies.[2-5] In addition, analytical tools and devices for a better understanding of the molecular basis of disease, patient predisposition, and response to therapy are developed.[6] This opened up new perspectives, for instance, in regenerative medicine, for drug delivery strategies, medical diagnostics, and therapeutics and lead to rapidly emerging biomedical tools ranging from nanoparticle coated medicinal implants[7] to contrast agents for diagnostic imaging[8] and to potential drug and gene delivery vehicles.[9] In addition, versatile nanomaterials with novel optical properties[10] as well as nanomaterials with intrinsic therapeutic nature[11] were generated. The advances in nanotechnology knowledge now allow to include diverse properties into nanomaterials that can be modulated according to the desired applications.

1.1.1 Rationale for nanomedicine in cancer therapy

The efficient treatment of diseases is often limited by the intrinsic shortcomings of small molecular weight drugs. The lack of selective delivery of anticancer compounds to malignant tissue results in high systemic exposure leading to severe side effects. This causes dose-limits for the drug in question and therefore a poor therapeutic index. Besides low target specificity, a rapid drug clearance leads to poor bioavailability of the so-called ‘small molecule’ drugs. Another class of biotherapeutics including proteins, peptides, oligonucleotides, and antibodies is rapidly evolving and has demonstrated striking therapeutic activities as alternatives to conventional small molecule drugs. The clinical translation of therapeutic proteins is, however, severely hindered due to their possible fast degradation *in vivo*, poor cell penetration, and inefficient intracellular trafficking.[12] Furthermore, new drug candidates often fail the transition to clinical trials due to deficient physicochemical properties such as low water solubility. These limitations prompted the development of new formulation and

modification approaches to improve the therapeutic efficiency and patient survival compared to conventional therapies.[13-14] Nanocarriers have emerged that offer the multifunctionality to incorporate required features to revolutionize the delivery across all barriers.[15-16] For a targeted and on-demand delivery of therapeutics, carrier platforms must be carefully designed in coherence with the faced biological barriers. This can provide DDS with the capacity to reach the therapeutic target and carry out their functions with maximum efficacy.[17-18]

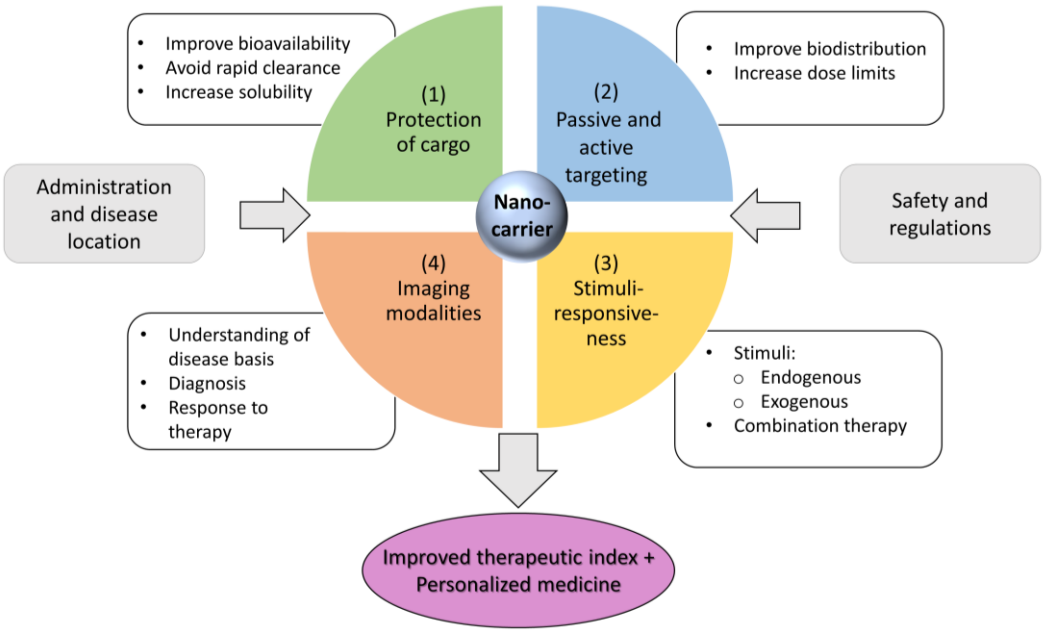

Figure 1. The rationale of nanomedicine for cancer therapy.

In Figure 1, the four main contributions of nanocarriers to improve cancer therapy are presented. (1) *Protection of the cargo*: The connection of the therapeutic agent with a carrier can enhance crucial parameters such as their solubility and *in vivo* stability resulting in improved bioavailability. Thereby, nanocarriers modulate both the pharmacokinetic and pharmacodynamic profiles of the loaded or conjugated drugs. (2) *Passive and active targeting*: The nanoscale size and surface properties of nanocarriers can be optimized to extend blood circulation time and to target diseased tissue which will be discussed in detail in the next chapter. (3) *Stimuli-responsiveness*: To enhance the targeted delivery, nanocarriers are provided with controlled drug release properties which can be triggered by external or internal stimuli (Chapter 1.2). (4) *Imaging modalities*: Beyond therapeutic moieties, imaging modalities can be added for diagnostic purposes and for monitoring of nanocarrier delivery paving the way for personalized therapy (chapter 1.2.4).

1.1.2 Role of the nanoscale size

Several reasons underline the potential of nanosized materials in nanomedicine. Particles in the nanoscale are characterized by an enormous surface area which allows the interaction with the surrounding environment with increased reactivity compared to macroscopic structures. Since processes in biological systems take place in the nanoscale, artificial nanosized particles enable to optimize the precise interaction with biological targets to develop new strategies for therapy and diagnostic. Moreover, quantum effects dominate the properties of materials at this scale. For instance, nanosized metal particles display altered optical properties. Upon interaction with visible or near infrared light, plasmon oscillation generates intense electromagnetic fields at the metal surface. These surface plasmons can decay by the emission of photons or non-radiative relaxation via heat irradiation. Both are used in nanomedicine to develop diagnostic and therapeutic approaches.[19]

With regards to tumor treatment, particles in the nanoscale can alter the biodistribution of loaded payloads. The particles with sizes between 10 and 200 nm avoid clearing mechanisms present in kidney and liver and therefore prolong half-life in the body. In addition, tumor physiology with rapidly dividing cancer cells results in the formation of the new vasculature that is architecturally abnormal and exhibits an increased permeability. The prolonged circulation in combination with leaky vasculature can yield enhanced accumulation of nanoscale particles in the tumor tissue. In addition, poor lymphatic drainage of the tumor increases retention of the nanoparticles. The phenomenon is referred to as the enhanced permeation an retention (EPR) effect (Figure 2a).[20]

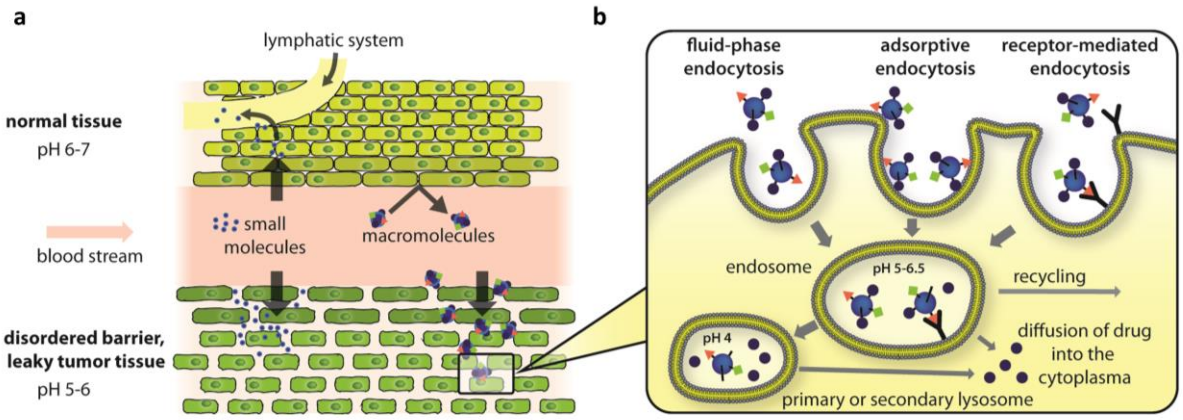

Figure 2. Schematic representation of (**a**) passive targeting by the EPR effect and (**b**) cell internalization mechanisms including active targeting. Adapted from Khandare et al.[5] with permission of reference 5. Copyright 2012 Royal Society of Chemistry.

In contrast, nanoparticles are less prone to pass through the epithelial wall of healthy tissue. The EPR effect has become the foundation of passive targeting of nanocarriers to solid tumors and is closely influenced by the size of the particles. Sizes in the range of 20–200 nm were found to be optimal to take advantage of the effect.[21]It is noteworthy that tumor heterogeneity and complexity observed for different kind of cancers strongly influences tumor extravasation and accumulation. Thus, the EPR effect was found to be highly variable with large differences between tumor types, metastasis, between animals and human, and even between single patients and appear to be only effective in certain subgroups of patients. A pioneering study has been done by Harrington et al., who quantified EPR-mediated passive tumor accumulation using ^{111}In-labeled PEGylated liposomes a radiolabeled nanocarrier (^{111}In-labeled PEGylated liposomes) in patients suffering from different types of tumors.[22] In total, the levels of accumulation varied from 2.7 to 53.0% of injected dose (ID)/kg of tumor. The highest accumulation was observed in head and neck cancer (33 ± 16% ID/kg), intermediate accumulation was noted in lung carcinoma (18 ± 6% ID/kg), and relatively low levels were detected in breast cancer (5 ± 3% ID/kg). The results indicated that a high degree of heterogeneity in tumor uptake of for this nanomedicine, both between patients with different types of tumors and between patients with the same tumor type is present.[23] Due to the variability of the EPR effect, nanoparticles are designed with active targeting ligands that can bind to specific receptor on the cell surface (Figure 2b). Here, the strategy is based on the overexpression of receptors on tumor cell compared to healthy cells. Therefore, the probability to bind to the intended target is increased. However, the non-specific interaction with plasma proteins impair active-targeting strategies since the adhered proteins may shield targeting ligands and these nanocarriers might lose their targeting capability.[24]

1.1.3 Impact of nanocarrier design on drug delivery

Despite efforts to develop non-invasive administration (for example, oral, pulmonary, nasal and transdermal) in cancer therapy, most nanocarriers are administered intravenously for systemic transport to the malignant tissue. Multiple biological steps in the systemic delivery can influence the fate of the nanotherapeutic including nanocarrier-protein interaction, blood circulation, extravasation into and interaction with the perivascular tumor microenvironment (TME), tumor tissue penetration and cell internalization. Conversely, the properties of nanocarriers such as size, surface features, geometry, elasticity, rigidity, composition and

targeting ligand can influence these biological processes; thus, influencing the delivery of the therapeutic agent (Figure 3a).[25]

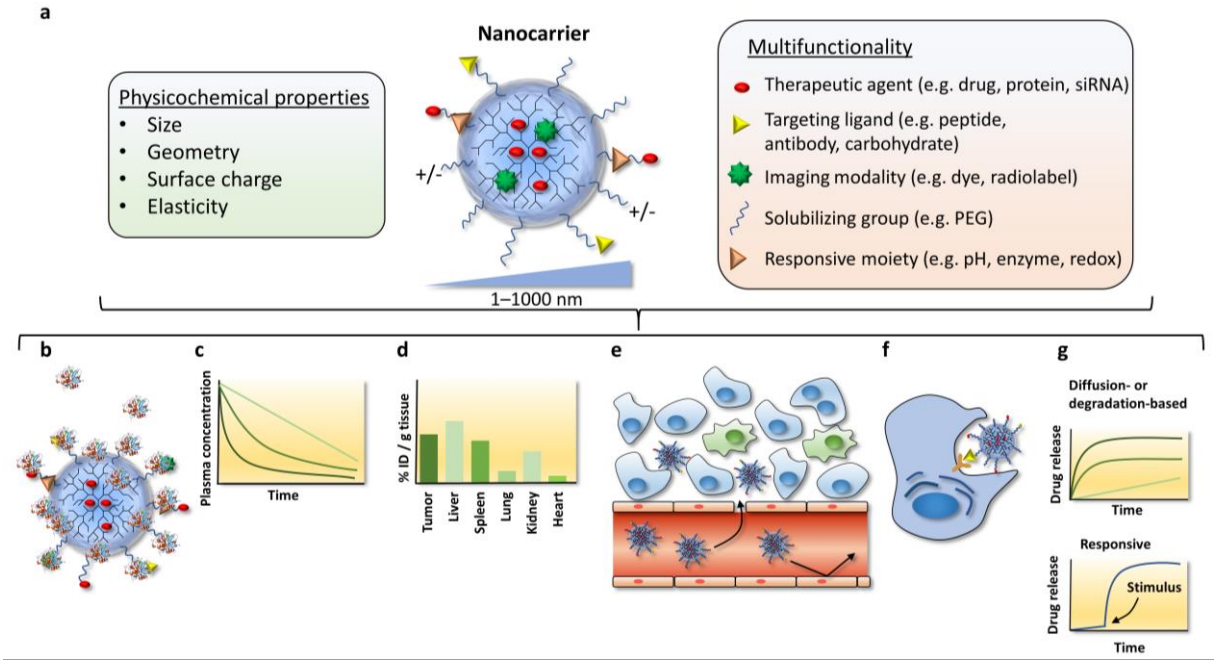

Figure 3. The impact of nanocarrier design on systemic delivery. (**a**) Nanocarriers from different materials have diverse physicochemical properties and can be modified with multiple functionalities. The properties affect the fate of the nanocarrier including (**b**) interactions with serum proteins, (**c**) blood circulation, (**d**) biodistribution, (**e**) extravasation to tumor microenvironment and penetration within the tumor tissue, and (**f**) tumor cell targeting and intracellular trafficking. (**g**) Nanocarriers can also display stimuli-sensitive behavior for controlled drug release (ID = injected dose).[15] Adapted from reference 15 with permission of Springer Nature. Copyright 2017.

Interaction with serum proteins

After injection, the nanocarrier's surface is immediately covered with serum proteins which yield the formation of a so-called protein corona (Figure 3b).[26-27] The adsorption of proteins alters the properties of injected nanoparticles in terms of particle size, stability and surface properties. Since the corona provides the exterior entity, it determines the physiological response which influences the biodistribution as well as cellular uptake and intracellular trafficking (Figure 3c–f). For instance, coverage with opsonins is recognized by the mononuclear phagocytic system (MPS) and leads to subsequent sequestration.[28] Vice versa, the nature of protein corona depends on nanoparticle properties including size, the surface chemistry, and hydrophobicity.[21] This can be used to prompt the binding of proteins which inhibit phagocytic uptake and improve delivery to specific organs.[29]

Blood circulation

There is a close connection between the blood circulation time and the effectiveness of passive extravasation and accumulation of the nanocarrier in tumor tissue (Figure 3c). Therefore, it is desirable to design nanoparticles that show prolonged circulation. The fast renal and biliary clearance usually is avoided by the application of nanocarriers with sizes above 10 nm and neutral charge. However, nanoparticles with sizes over 10 nm need to be biodegradable to avoid long-term accumulation in the body and to allow clearance from the body. The liver and spleen typically filter particles in the range of 200–500 nm, but do not necessarily excrete them.[30] Therefore, nanoparticles should be smaller for systemic applications or if larger than 200 nm, they need to display a soft and deformable nature to stay in circulation. Another major factor limiting circulation time is the nonspecific interaction between nanocarriers and serum proteins discussed above, which can promote opsonization, recognition, and sequestration by the MPS. The grafting of poly(ethylene glycol) (PEG) to the surface is a common strategy to reduce interaction with the plasma proteins since PEGylation provides a hydrated layer[31]. This provides the carrier with so-called 'stealth' properties as the hydrophilic and neutral nature of the polymer induces steric repulsion of plasma constituents. Another strategy is the coating of nanoparticles with cell membranes extracted, for instance, from red blood cells to provide a biomimetic surface.[32] The elasticity of particles has been recognized to influence MPS sequestration showing longer circulation times for soft and flexible particles.[33]

Extravasation to malignant tissue

At the site of disease, escaping the circulation is required to enter the diseased tissue (Figure 3d+e). For malignant tissue, disorganized vasculature due to uncontrolled angiogenesis leads to endothelial dysfunction and blood vessel fenestrations. This 'leakiness' is distinct from healthy tissue and promotes the accumulation of nanoparticle as mentioned before. Besides the abnormal tumor vasculature, the physicochemical properties of nanocarriers impact the tumor extravasation and accumulation. For instance, 30, 50, 70 and 100 nm polymeric micelles all demonstrated similar extravasation and therapeutic activity in hyperpermeable murine colon adenocarcinoma, whereas only the 30 nm micelles showed sufficient accumulation in hypopermeable pancreatic tumors.[34]. Interestingly, nanoparticle shapes with elongated structures tend to accumulate and adhere to endothelial cells better than spherical particles and can, therefore, enhance the extravasation into tumor tissue.[35]

Tumor penetration

While extravasation and accumulation are crucial in drug delivery, deep and uniform tumor penetration of nanotherapeutics need to be addressed for optimal therapeutic outcomes (Figure 3e). The TME present several physiological barriers to the delivery of nanomedicines such as heterogeneous tumor vasculature and constricted vessels due to growth-induced stress. Furthermore, a dense extracellular matrix composed of collagen fibers and other proteins, and the elevated interstitial fluid pressure (IFP) induced by hyperpermeability of the abnormal vasculature and lack of functional lymphatics in the tumor tissue impair the delivery (Figure 4).

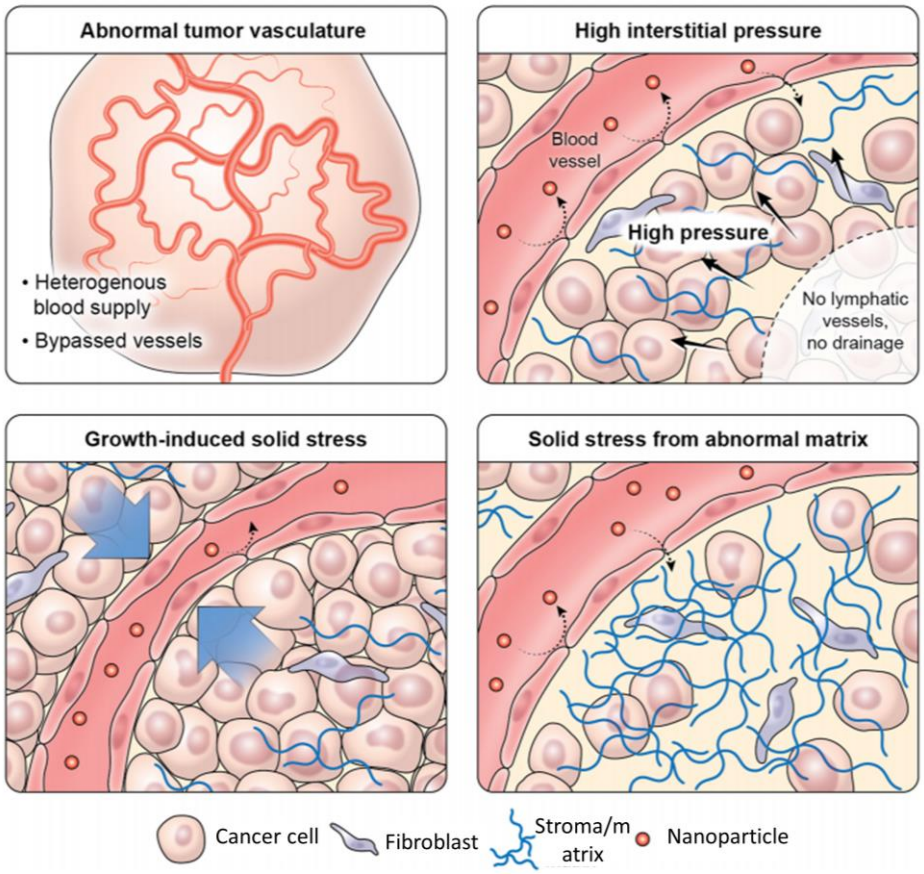

Figure 4. Intratumoral barriers to nanocarrier-based drug transport.[36] Reprinted with permission of reference 36. Copyright 2016 American Chemical Society.

The elevated interstitial fluid pressure reduces convective transport away from the site of extravasation, while dense extracellular matrix hinders diffusion of nanoparticles into the interstitial space.[37] This results in barely diffused tumor core which displays a harsh environment with low pH and low oxygen pressure.[38] Here, the most aggressive tumor cells are harbored that have the potential to regenerate the tumor if not eliminated completely.[39-40] Furthermore, low exposure of drug in some regions of the tumor could promote the

development of drug resistance.[41-42] Studies have demonstrated that size and binding affinity of the nanocarrier affect both diffusion kinetics and depth of tissue penetration. For optimal tumor penetration, the physicochemical properties of the nanocarrier need to be carefully tuned to penetrate the diffusional barriers.

Large sizes of nanoparticle impede the efficient penetration of the DDS since they become trapped in the dense extracellular matrix shortly after extravasation.[43] Cabral et al showed that nanocarriers aiming for high EPR-based accumulation (100 nm) do not easily penetrate into tumor tissue which leads to heterogeneous distribution of the DDS in the malignant tissue after extravasation of the nanoparticles from the vasculature.[36, 43-45]. Smaller nanocarriers (30 nm) could more readily diffuse within the tumor tissue. However, when the particles become very small particles (<5 nm) they are quickly cleared from the tissue. An optimal size that balances drug accumulation and penetration of tumors is critical for improving the therapeutic efficacy of nano-based drugs.

In addition, the high affinity of target ligands and antibodies has an impairing effect on the penetration because these structures are immobilized by the strong binding or the internalization into cells close to the extravasated area. Several strategies have been employed to improve the intratumoral delivery.[43, 46] The use of promoter drugs has been suggested. These physiologically active agents improve the exposure of tumor cells to anticancer drugs by increasing the blood flow or by reducing endothelial barrier function, interstitial pressure, or stromal barriers.[47] Another strategy is to employ hyperthermia to increase the vascular permeability of macromolecular delivery systems.[48] Directly modulating the tumor stroma by extracellular matrix (ECM) degrading enzymes like collagenase or hyaluronidase have also been employed to enhance nanocarrier distribution in tumors.[49] These strategies can be combined with nanomedicine in order to modulate the tumor tissue for a more effective nano-based treatment. With regards to the nanocarrier themselves, Surface modification with tumor penetrating peptides, such as the cyclic peptide CRGDK/RGPD/EC (also called iRGD), has been shown to increase the depth of delivery into tumor tissue.[50] Recently, multistage systems have been proposed to address the low penetration of nanoparticles.[51] When the particles reach the tumor, they release smaller entities upon exposure to the TME. These units can then more readily diffuse within the dense interstitial space.

Cell internalization

Cell internalization can also have an impact on enhancing retention in the tumor and usually, nanocarriers are expected to overcome the cell membrane to deliver its cargo for therapeutic effect in the cytoplasm or nucleus (Figure 3f). While small, hydrophobic molecules can simply diffuse through the membrane, nanoscale constructs usually require active uptake mechanisms. Several endocytic mechanisms can be prompted to facilitate the internalization of nanocarriers.[52] During endocytosis, plasma membrane invagination results in the internalization of externally disposed solutes, particles, or pathogens. The distinct mechanism of endocytosis is important as it determines the path of trafficking through various subcellular compartments. For example, clathrin-mediated endocytosis leads to localization in lysosomal compartments, whereas internalization through a caveolin-mediated process is not.[53] The upper size limit of a clathrin-coated vesicle is around 200 nm external diameter, which should be considered when designing a nanocarrier system. In clathrin-mediated endocytosis, the pathway eventually leads to lysosomes with harsh acidic and proteolytic conditions which contribute to the degradation of nanoparticles, drug, and genetic material. Here, endosomal escape is necessary to avoid degradation and to reach the desired cellular compartment. Multiple strategies have been tested to facilitate endosomal escape into the cytosol, such as pore-forming peptides and proteins or pH-buffering substances utilizing the “proton sponge effect”.[54] The mode of cellular internalization can be modulated by the attachment of ligands on the surface of nanoparticles (Figure 3f). For instance, folic acid, albumin, and cholesterol have been shown to promote uptake through caveolin-mediated endocytosis, whereas ligands for glycoreceptors trigger clathrin-mediated endocytosis.[55] As an alternative, the presentation of cell-penetrating peptides, such as a trans-activating transcriptional activator peptide on the surface of nanoparticles can facilitate macropinocytosis.[56] The nanoparticle surface properties also influence the internalization. In particular, cationic surface charge is associated with increased internalization for different cell lines. Since cationic particle can be recognized by the MPS, charge-conversion strategies aimed at site-specific switching of surface charge in response to environmental stimuli, such as pH.[57]

Finally, the therapeutic agent needs to be released at the site of disease which can be enabled by different modes including diffusion- and degradation-based mechanism (Figure 3g). To precisely control the drug release, stimuli-responsive bonds and moieties can be introduced into the nanocarrier which will be discussed in detail in chapter 1.2. In general, stimuli-

sensitive nanocarrier respond to environmental changes associated with the TME and tumor cells (e.g., pH, redox state, and enzymes) or can be activated by external stimuli (e.g., temperature, light, magnetic field, or ultrasound) to trigger the release of the payload.[58]

Takin all this into account, certain general requirements for the design of drug delivery vehicles for intravenous administration can be stated. These include the possibility to carry enough dose of the respective drug with high stability in circulation aiming for minimal elimination or degradation of the cargo. Moreover, the carrier should avoid non-specific interactions with plasma components and fast organ clearance to enable longer circulation. This provides the basis for active or passive targeting to the diseased tissue. The carrier should enable efficient distribution through the malignant tissue and the interaction with cells has to be tailored to ensure cellular internalization; e.g., by adsorption or endocytosis. Optimal would be a controlled drug release mechanism to increase the specificity of the DDS. In addition, nanocarriers should be biocompatible and non-immunogenic. As the parameters for maximum efficacy in drug delivery are better understood, a diverse range of nanostructures has been evolved to incorporate design features to address these requirements (Chapter 1.3).

1.1.4 Prodrug concept

An established concept in medicinal chemistry to reduce the side effects of parental drugs and improve targeted delivery is to suppress the activity and thereby mask the toxicity by attaching other chemical groups. These so-called prodrugs are chemically modified versions of the pharmacologically active agent that are converted by chemical or enzymatic reactions *in vivo* to release the active drug. Besides masking the toxicity, prodrugs can also improve physicochemical or pharmacokinetic properties of a drug, for instance, by enhancing membrane permeability or solubility, and by prolonging activity.[59] Esterification of charged groups such as carboxylic acids and phosphates is commonly used to enhance the lipophilicity of the parent drug improving the passive membrane permeability.[60] In a physiological environment, esters can be easily hydrolyzed by ubiquitous esterases found in the blood, liver and other organs and tissues.

Regarding cancer therapy, site-specific activity is crucial to reduce side effects. Elevated levels of enzymes in tumor tissue have been exploited to activate the prodrugs[61] As an example, capecitabine is an orally administered carbamate prodrug of 5-fluorouracil that undergoes three enzymatically catalyzed reactions to release the active drug (Scheme 1). Besides

enzymes, other stimuli can be employed to activate the drug at the site of tumor tissue; e.g., acidic pH, hypoxia, or reductive species.

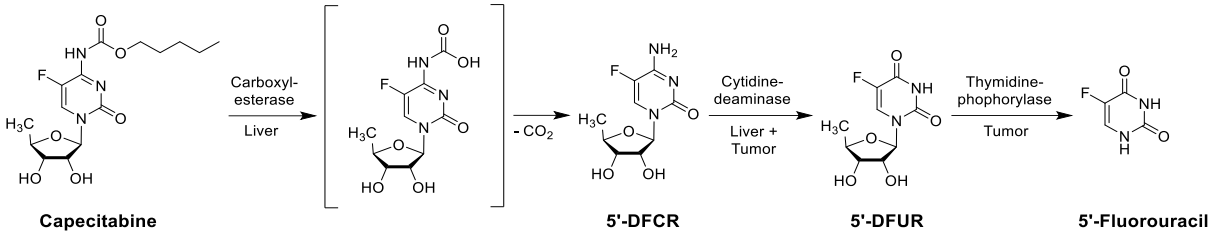

Scheme 1. Enzymatic bioconversion of capecitabine to 5'-fluorouracil.

In accordance with the prodrug concept, the conjugation of a drug through a cleavable linker to a polymeric carrier can result in a macromolecular prodrug (Chapter 1.3.1). This requires that the drug has distinctly decreased activity when bound to the carrier and upon cleavage of the linker under tumor-associated or intracellular conditions, the parental drug is released.

Overall, the use of prodrugs in drug delivery provides important benefits such as: (i) a controlled drug release mediated by chemical or enzymatic hydrolysis of the prodrug; (ii) an increase of the drug stability and solubility and, (iii) a reduced toxicity before activation.[59] The prodrug strategy provides a rationale for achieving tailor-made physico-chemical and pharmacological features.

1.2 Stimuli-responsive nanomaterials

Besides passive and active targeting, on-demand processes are a smart strategy to achieve nanomedicine-mediated tumor targeting. Nanomaterials offer a platform to incorporate stimuli-sensitive moieties into a drug delivery system, by exploiting different materials and interactions. Stimuli-responsive nanomaterials can be distinguished by the function that is performed upon stimulus such as drug release, morphological change (shrinkage/swelling/rearrangement), partial or complete disintegration, catalytic action or energy conversion (heat production) or by the stimulus that triggers the response. In general, these stimuli can be divided into the ones that originate from an external source or the ones that exploit internal alterations (Figure 5).

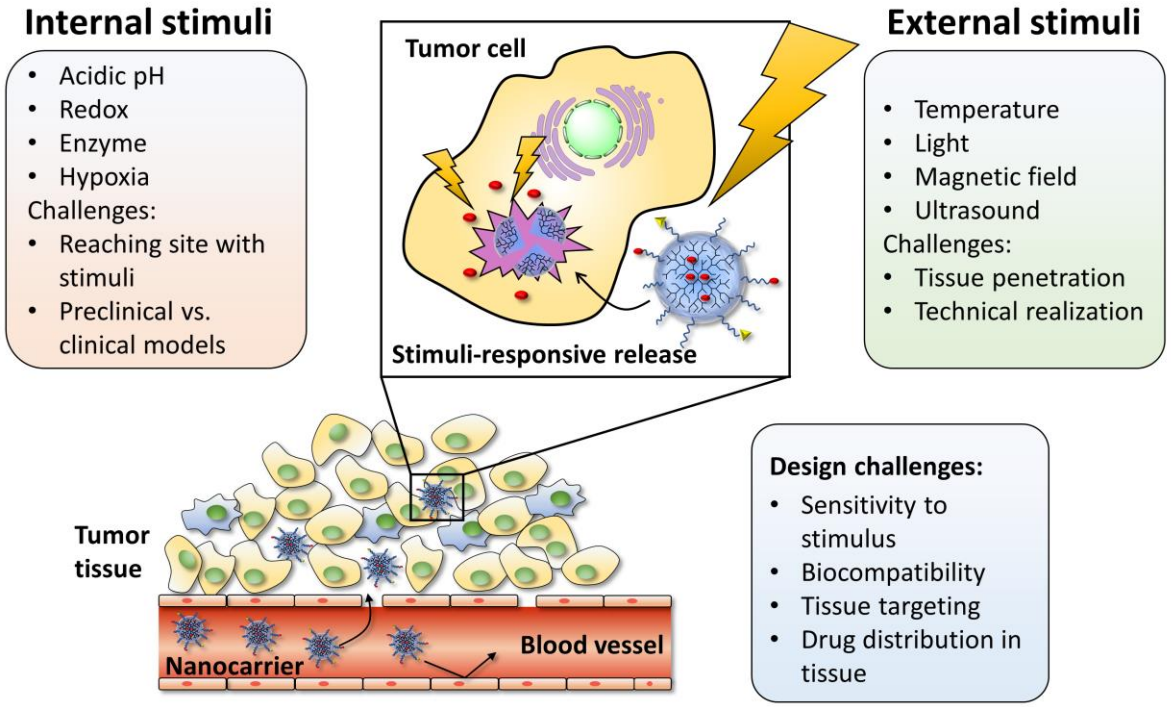

Figure 5. Overview of external and internal stimuli to trigger responsive drug release and associated design challenges.[13] Adapted with permission of reference 13 under Creative Commons license (http://creativecommons.org/licenses/by/4.0/).

Internal stimuli have the advantage that the nanocarrier can be triggered autonomously but it can be challenging to reach the site of action in the first place. In addition, the claimed alterations used as an internal trigger can differ between preclinical and clinical models. The challenges for external trigger lay in the selective application of the exogenous stimulus which may require elaborate techniques and equipment that may not be practical or cost-effective. Another problem with exogenous stimuli can arise from the depth of penetration required for

applications in the body. Furthermore, the need for site-specific application of the external stimulus implies that the diseased tissue can be spatially differentiated from healthy tissue, which could be questionable for certain diseases such as infiltrative neoplasms.

Since the stimulus is restricted to the site of the disease (endogenous) or is applied at the disease site (exogenous), a control over the spatiotemporal activation of the nanomedicine is obtained. This requires that the cargo is not active when associated with the carrier and that both form a stable linkage through either covalent or non-covalent interactions. This approach is complex as it requires the application of biocompatible materials that can undergo a specific response to an applied stimulus which may include protonation, hydrolytic cleavage, a molecular or supramolecular conformational change, or a response to specific physical stimulation (Figure 6).[58]

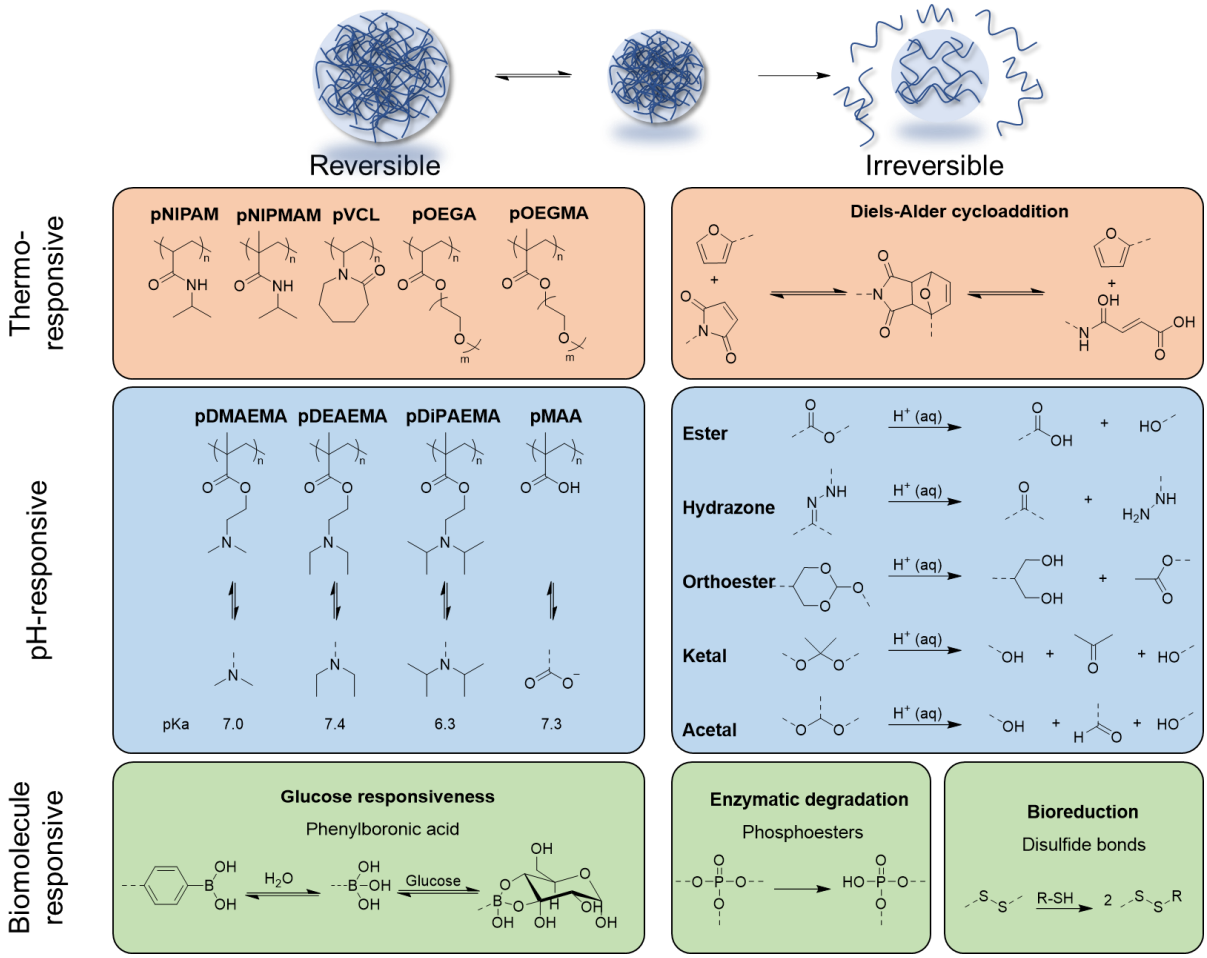

Figure 6. Chemical functionalities and polymers utilized for responsive behavior.[62] Adapted with permission from reference 62. Copyright 2018 Royal Society of Chemistry.

To introduce stimuli-sensitive behavior, dynamic covalent chemistry or non-covalent/supramolecular interactions are applied. Dynamic covalent chemistry relies on the reversible formation and cleavage of strong covalent bonds. Therefore, it combines the

rearrangement capability of supramolecular chemistry and the robustness of covalent bonds. Compared to supramolecular interactions, dynamic covalent reactions usually have slower kinetics and require the assistance of catalysts to achieve rapid equilibrium.[63] In the scope of drug delivery, these catalysts are the stimuli to trigger a specific response and include protons, enzymes, redox-active substances, among others.

1.2.1 Exogenous stimuli

Drug delivery systems that take advantage of externally applied stimuli such as ultrasound, magnetic field, light, and temperature, offer spatiotemporal control over the activation of materials. Here, the idea is that the activation or cargo release can be induced directly at the desired site by application of an external source.

Thermo-responsive polymers have been used as building blocks to create smart drug delivery system that present precise control of the response towards a thermal trigger.[64] Two types of thermoresponsive polymers can be distinguished which present either a lower critical solution temperature (LCST) or an upper critical solution temperature (UCST). LCST and UCST represent respectively the critical lower and upper temperature below and above the polymer and solvent are completely miscible.[65] Polymers that exhibit an LCST are perfectly soluble in water below the transition temperature. When the environment is heated above the LCST, the polymer chains dehydrate and become water insoluble caused by a change of the hydration state. Poly(N-isopropylacrylamide) (PNIPAm) is the most extensively studied thermoresponsive polymer with an LCST around 32 °C.[66] It is a versatile building block since the transition temperature can be conveniently adjusted by copolymerization with other acrylic monomers. If hydrophilic monomers like acrylic acid (AA) are incorporated randomly into the polymer, the phase transition temperature is increased.[67] Micelles based on block-co-polymers incorporated thermoresponsive polymers to use the hydrophilic-hydrophobic transition to assemble or disassemble and thereby trigger cellular uptake[68-69] or release an encapsulated guest.[70] Thermoresponsive NGs are a versatile tool for drug delivery. Thermoresponsive NGs incorporating acrylated dPG as macrocrosslinker into PNIPAm NGs have been introduced with tunable transition temperature depending on the dPG content. The hydrophilic dPG avoided macroscopic precipitation of the NGs but still showed a significant decrease in size above the LCST.[71] Other monomers, like N,N-diethylacrylamide, methylvinylether, N-vinyl caprolactam, Nethyl oxazoline, Poly(oligoethylene glycol) methacrylates, and N-isopropylmethacrylamide, as well as natural occurring peptide motifs

that show thermoresponsive behavior such as elastin, collagen, gelatin have been investigated as well. The most commonly employed UCST polymer in drug delivery is poly(2-vinylpyridine).

Ultrasound has been used as diagnostic tool but also as a trigger for drug release; e.g., from sensitive polymeric matrices by site-specific sonication. Ultrasonic contrast agents are encapsulated in the nanocarriers that release microbubbles which can be imaged for diagnostic purposes. This strategy has also been applied for ultrasound-mediated drug release from NE. Paclitaxel-loaded NE was locally converted into microbubbles in malignant tissue under the action of tumor-directed ultrasound.[72] In addition, ultrasound can promote the uniform distribution of nanocarriers and drug throughout the tumor tissue.[73]

The use of magnetic actuation can be employed to remotely guide the drug delivery system to the target site.[74] Furthermore, one intrinsic property of magnetic materials is their ability to produce heat when exposed to an alternating magnetic field which can be applied for hyperthermia treatment. In combination with thermoresponsive polymer, this can be used as an actuator for drug release.[75] Iron oxide nanoparticles are the most commonly used component to this end. To allow biomedical applications, magnetic particles are usually merged with polymeric materials. The magnetic particles are generally either embedded into the polymer matrix or core-shell type nanocarriers are employed.[74]

Light-sensitive nanodevices display a photochemical reaction upon irradiation.[76] Different mechanism for light-sensitive moieties have been employed that can undergo isomerization, oxidation, or bond cleavage which leads to disassembly of the nanocarrier or release of a therapeutic agent. In addition, surface plasmon absorption and photothermal effects are other forms of photochemical properties that can be used for therapy and diagnostic. Light usually suffers from low penetration depths (∼10 mm) as a result of strong scattering and absorption in soft tissue. Depending on the depth of penetration required for applications, penetration of the radiation may become an issue. Incorporation of bonds that are sensitive to longer wavelength allows the application of NIR laser (700−1000 nm) as the trigger which enables deeper tissue penetration.[77]

1.2.2 Endogenous stimuli

Endogenous stimuli refer to altered conditions within certain cellular compartments or in the diseased tissue. These stimuli include local environmental factors such as pH, redox potential, and temperature, as well as enzymes, ionic strength, small molecules, partial oxygen pressure,

osmotic pressure, nucleic acids, proteins, and peptides. Enzymatically catalyzed processes present ideal triggers for the selective responses due to the high specificity for their substrate and their catalytic properties. Highly specific cleavage-activated systems like enzyme activation and phosphorylation are widely found in biochemistry, and therefore inspiration should be taken from nature as a model I incorporate similar designs in drug delivery systems.

pH-sensitivity

Extra- and intracellular pH gradients are utilized as an endogenous trigger for DDS which selectively release their therapeutic cargo at the site of action. Nanocarriers with pH-sensitive modalities can facilitate the release of the payload at the targeted disease by either swelling, shrinkage or degradation of sensitive crosslinks.[78] The most obvious gradient with extreme pH values can be found in the gastro-intestinal systems from very acidic to basic (~2.0–8.0). This presents a challenge as well as an opportunity to design controlled release delivery systems for oral administration. In addition, pathological states such as in inflamed, infected, or malignant tissue are associated with lower pH values that differ from the physiological pH of 7.4. In cancer tissues, the cells predominantly produce their energy through a high rate of aerobic glycolysis followed by high lactate formation resulting in lower extracellular pH of 6–7.[79-80] During endocytic internalization, the pH decreases from typical extracellular pH values of 7.2-7.4 to reduced pH of 6-6.8 in endosomes. Further endosomal processing leads to pH 5-6 in the late endosome stage.[81] Finally, endocytosed materials may be delivered to the lysosomes with pH reduced to 4-5. Interestingly, viruses take advantage of those pH gradients to access the cytosol by a pH-triggered conformational change of viral proteins that allow them to penetrate, fuse with, or even completely disrupt the endosomal membrane. Polymeric micelles, polymersomes, and nanogels have been provided with tertiary amino, carboxyl or other ionizable groups that can act as pH-sensitive moieties as a change in pH can alter the protonation state of these basic/acidic functionalities. The change in protonation state can alter hydrophobicity, conformation, or electrostatics leading to morphological changes of the scaffold. Upon the variation of pH, these structures swell or collapse due to electrostatic repulsion or attraction, respectively. The most common polymers to incorporate pH-sensitivity by ionizable groups are poly(acrylamide), poly(acrylic acid), poly(methacrylic acid), poly(diethylaminoethyl methacrylate), and poly(dimethylaminoethyl methacrylate) (Figure 6).[82]

In polymer-drug conjugates, cleavage of the pH-sensitive linkage that connects the drug to the carrier presents a useful strategy to trigger intracellular drug release. For the conjugation of drugs to a polymeric backbone, pH-sensitive linkages such as hydrazone, acetal/ketal, orthoesters, cis-aconityl, and imines are broadly applied (Figure 7). The hydrolytic stability of these bonds depends on the chemical environment which allows the fine-tuning of the cleavability towards specific pH values. Therefore, DDS with stable carrier-drug linkage can be designed that avoid non-specific and premature release at neutral pH but allow release at lower pH for predominately intracellular release.

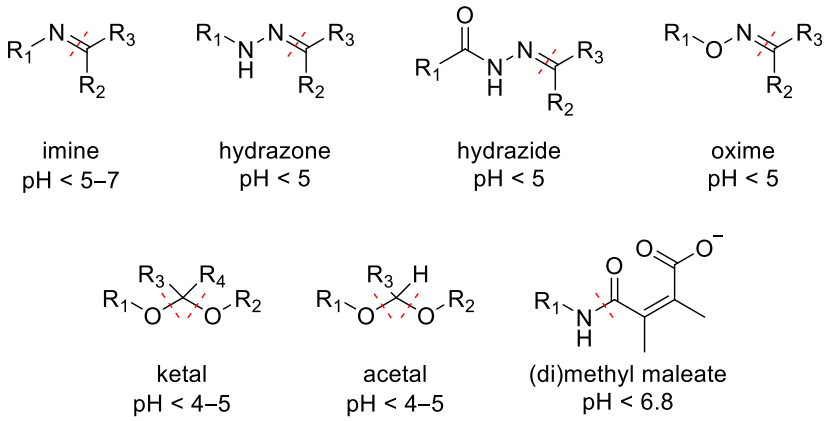

Figure 7. Overview of pH-sensitive bonds including pH values and cleavage site.[83] Adapted with permission from reference 83. Copyright 2014 Elsevier.

The Dox derivative aldoxorubicin contains a hydrazone bond which is one of the most successful pH-sensitive functionalities since it is stable at neutral pH but is readily cleaved in acidic intracellular compartments. Bearing further a maleimide group aldoxorubicin was developed as a thiol-binding prodrug for the auto conjugation to cysteine residues of albumin enhancing the circulation time of the drug to increase tumor accumulation. The linker remains stable during circulation and can release Dox at acidic conditions present in intracellular compartments. Aldoxorubicin is currently in phase III clinical studies for the treatment of soft tissue sarcoma and showed progression-free survival in leiomyosarcoma and liposarcoma and minimal cardiac toxicity, which represents a significant advantage to Dox.[84] Aldoxorubicin was also employed to prepare pH-sensitive macromolecular prodrugs based on dendritic polyglycerol that use the EPR effect and showed controlled release of the active drug in acidic environment .[85]

Enzyme-sensitivity

Many materials in living organisms respond to or are degraded by enzymes. Inspired by this, enzymes have been increasingly used as a trigger for responsive materials. In contrast to other stimuli-responsive systems, enzymes offer a high selectivity and specificity for their substrates and high catalytic activity. In pH- and temperature-responsive systems an equilibrium state is reached when the stimulus is applied. This also implies that it can be reverted to their original state when the stimulus is not present anymore. On the contrary, enzyme-sensitive systems often involve the formation or cleavage of bonds, which are mostly not reversible, except for some phosphatase/kinase systems. In general, enzyme-responsive moieties show not only structural conversion upon enzymatic reactions but all kinds of changes in functionality including variation in chemical as well as physical properties. The incorporation of enzyme-sensitive functionalities is often based on natural materials like peptide sequences or natural polymers. Beside peptide sequences, non-peptide substrates have been used including functional side groups (phenols), polysaccharides, and (phosphate-)esters. Besides bond formation and bond cleavage, oxidation and reduction, as well as isomerization reactions, can be performed by enzymes. In addition, other responses of material are possible upon enzyme action: change in hydrophilicity and steric effects, charges or functional groups may be introduced or removed, the chain length of block copolymers or crosslinks may be altered.

Concerning biomedical applications and in particular cancer therapy, the altered expression or activity of enzymes in association with the disease can be utilized as a suitable trigger for material response. As the enzyme expression is regulated by cells and therefore localized, a controlled response at the diseased site is possible. In the past, a range of different enzymes has been employed in enzyme-sensitive drug delivery systems. The most common classes are proteases, endonucleases, kinases (phosphorylation), and phosphatases (dephosphorylation). An overview of enzymes with altered expression in tumor tissue is given in Table 1. The altered expression patterns of enzymes represent biochemical signatures that can be used for diagnosis or in therapy as a site-specific trigger for drug release. This can be achieved by introducing specific substrate sequences either into the nanocarrier scaffold, e.g. as a crosslinker or in the linker segment through which the drug is conjugated to the nanoparticle. Overexpression of matrix metalloproteinases (MMPs) has been shown to be a relatively specific biomarker of malignant tissues. Intracellular proteases, such as cathepsin B, which

degrade proteins in lysosomes, have been intensively investigated for the site-specific release of drugs by the incorporation of specific peptide sequences.[86]

Table 1. Overview of enzymes for enzyme-responsive nanocarriers.[87-88]

Substrate	Enzyme	Function	Occurrence
Proteins	Cathepsin B Cathepsin H Cathepsin L	Lysosomal degradation of proteins	In mammalian cell lysosomes; over-expressed in various cancer types
	Cathepsin D	Degradation of extracellular matrix	Over-expressed in various cancer types
	Plasmin	Fibrinolysis, degradation of blood plasma proteins	In animals; increased concentrations present in cancer cells
	Urokinase-type plasminogen activator (uPA)	Degradation of extracellular matrix	In urine and the blood stream; implicated in cancer invasion and metastasis
	Matrix metalloproteinases	Degradation of extracellular matrix and collagens	In most multicellular organisms including animals and plants, implicated in several diseases including arthritis and cancer
Sugars	β-Glucuronidase	Hydrolysis of carbohydrate moieties from proteins	High concentrations in necrotic tissue and several cancer types
Phosphorylation	Kinases	Activation of signal transducers and activators of transcription factors	In the cell membrane; aberrantly activated in several cancer cells

Redox potential

The reductive environments found inside cells can be accounted to the high concentration of the tripeptide glutathione (GSH). Composed of L-glutamate, L-cysteine, and glycine, GSH presents a cellular reducing agent. Reduced GSH exists at millimolar (0.5–10 mM) concentrations in cellular fluids but is only found at micromolar (20–40 µM) levels in blood plasma.[89] In addition, GSH levels, determined *in vitro*, were found to be 7–10 fold higher in tumor cells than in normal cells.[90] The opposing redox environments of intra- and extracellular locations provide an opportunity for drug delivery. Disulfide bonds are formed through the oxidation of two thiols but can easily be cleaved by a reducing agent to two sulfhydryl moieties. These bonds play an important role in the structure and function of proteins, but exposed disulfide bonds are generally absent in intracellular proteins as a result of the redox

environment inside of cells.[91] In accordance, disulfide-containing structures are introduced to nanocarriers for targeted drug release exploiting the elevated GSH concentration associated with intracellular space in tumor tissue as stimulus. The nanocarriers equipped with disulfide moiety are stable during the transport in blood plasma but sensitive to intracellular GSH levels. By attaching a drug molecule through a disulfide bond to the nanocarrier, a drug can be guided to a particular location and be predominantly released in the cytosol. Alternatively, a drug can be entrapped in a nanocarrier that is connected by disulfide bonds. Once the disulfide bonds are reduced, the carrier disintegrates and releases the drug.

Taken together, nanocarriers with responsiveness to endogenous stimuli contain preprogrammed abilities to distinguish between diseased and healthy tissue and therefore proceed in an autonomous fashion to deliver the therapeutic cargo to the site of disease. Nowadays, multimodal system include materials or moieties that combine responsive to exogenous and endogenous stimuli into a single, elaborated system and will be discussed in the next chapter.[92]

1.2.3 Multistimuli responsiveness

As discussed in chapter 1.1.3, many obstacles; particularly, in the TME impair the successful delivery of the nanocarriers. To allow an adaption to diverse barriers, the response to one stimulus is often not enough to achieve effective delivery. For example, controlled release of the therapeutic payload by acidic pH or redox environment may not be effective to treat solid tumors with dense stroma due to poor penetration of nanoparticle when larger than 50 nm. Therefore, DDS are required that contain multi-responsive properties to tackle these obstacles (Figure 8).[93-94] The triggered responses can happen either in a simultaneous way at the target site or in a consecutive manner. When the stimuli-induced actions take place in a step-wise process in which the nanoparticles facilitate the transport by adapting to each physiological barrier encountered, they are also termed multistage delivery systems.[51] Here, specific stimuli in the TME such as pH or proteases are useful to achieve deeper tumor penetration, increased cellular uptake, and/or controlled drug release.

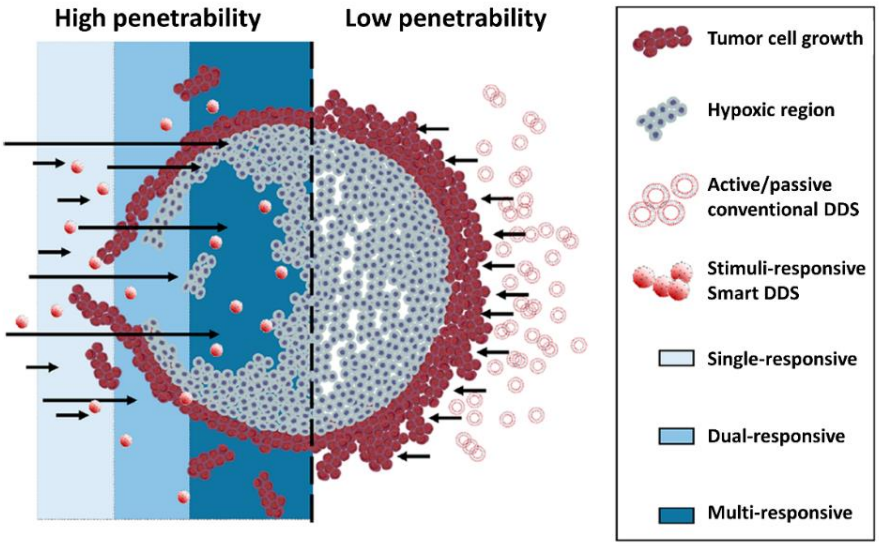

Figure 8. Schematic representation of the potential of multi-responsive DDS.[95] Adapted with permission from reference 95. Copyright 2018 American Chemical Society.

Nanocarriers have been reported that respond to the slightly acidic TME with size reduction by disintegration, sequential swelling/shrinking, or reorganization to facilitate the tumor penetration or cell internalization.[93, 96-98] It can be noted that the slightly acidic pH exploited for these delivery systems may be also found in other sites such as inflamed tissue and that the pH difference may be not distinct enough to trigger a response since acidic pH is associated with non-vascularized regions of the tumor. Several examples of gelatin nanoparticles that encapsulate smaller entities like quantum dots or gold nanoparticle have been presented.[99-101] Here, the idea is that the gelatin shell can be degraded in the TME by extracellular MMPs and thereby, the smaller entities are released which can then more readily diffuse within the dense interstitial space. Besides size reduction, the change of surface properties or the emergence of targeting units can be employed to improve tumor penetration by enhanced cell interaction. For example, the dissociation of a neutral PEG shell triggered by stimuli in the TME can be applied to expose positive charges or cell penetrating peptides that enhance surface-cell interaction.[102] Here, hypoxic., redox-, protease-, and acid-cleavable linker have been used to obtain PEG detachable nanocarriers. Figure 9 displays further strategies of nanocarriers that react to conditions in the TME to enhance the drug transport in tumor and overall the drug delivery

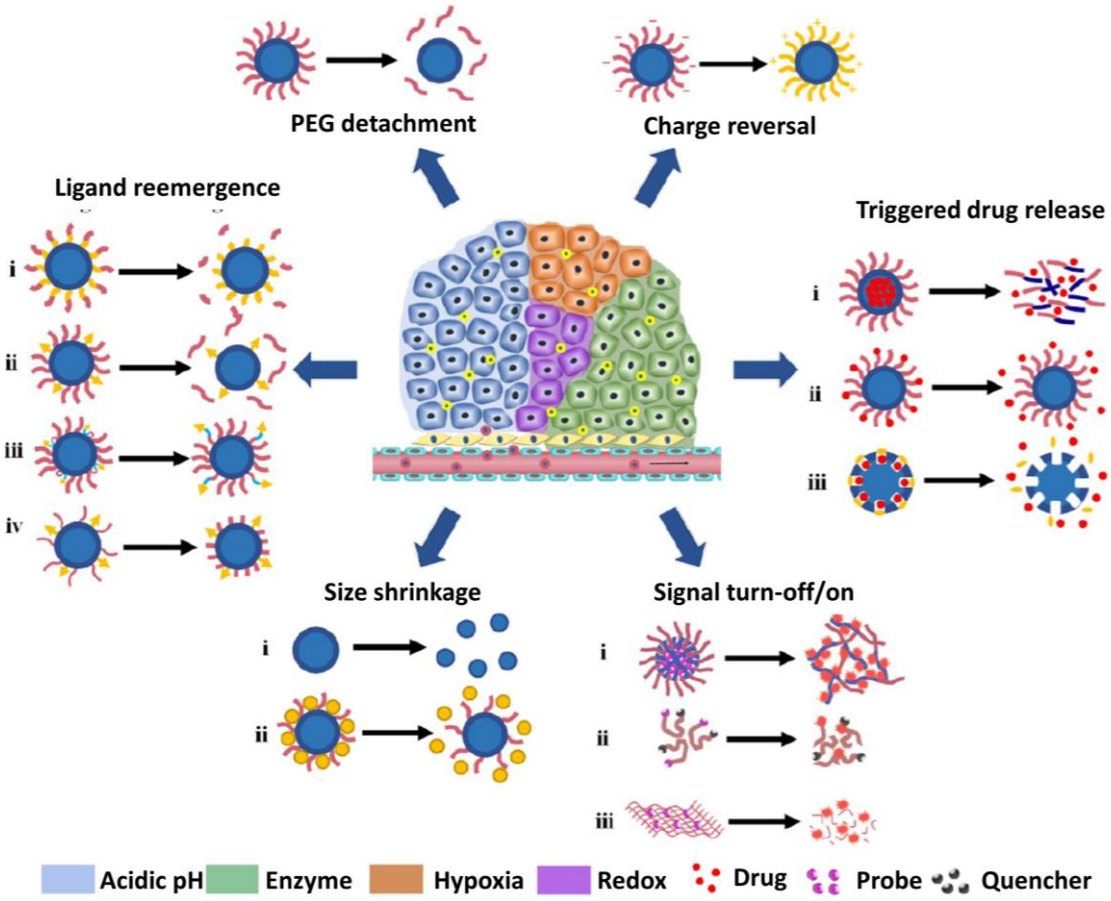

Figure 9. Responsive modes of nanocarriers activated by TME.[51] Adapted from reference 51 with permission of Ivyspring under the terms of the Creative Commons Attribution (CC BY-NC) License.

In addition, multi-responsive nanocarrier can also refer to a combination of different therapy approaches in one system with the goal to improve therapeutic outcome. For instance, when chemotherapy and hyperthermia are combined, the heating of the tumor leads to cell ablation, can facilitate the drug release, and at the same time widens the constricted blood vessels which allows a more effective distribution of the anticancer drug into deeper layers of the tumor.[103-104]

1.2.4 Nanotheranostics

The term theranostic was first mentioned by John Funkhouser 2002 describing his company's business model in developing diagnostic tests directly linked to the application of specific therapies.[105] Theranostics aim to combine therapeutic and diagnostic applications within a single formulation to individualize and improve treatments and has emerged as a highly interdisciplinary field since the early 2000s. The possibility of nanocarriers to incorporate multiple moieties with different functions in one device makes them an ideal tool for

theranostics. This coined the field of nanotheranostics for the application of nanoparticle for targeted therapy and diagnosis.

Imaging modalities

Different imaging modalities are available for non-invasive diagnostics including optical imaging, magnetic resonance imaging (MRI), ultrasound (US), and nuclear imaging (Positron emission tomography (PET)/ Single-photon emission computed tomography (SPECT)/ computed tomography (CT)).[8] Depending on the information that is required an appropriate imaging modality can be chosen. Among the mentioned techniques, CT, MRI, and US can be used for high resolution anatomical and morphological imaging, whereas nuclear imaging such as PET, SPECT and optical imaging are applied to image and quantify functional or molecular processes with high sensitivity (Figure 10).

In general, radiolabeling for PET and SPECT provides deep tissue penetration and high sensitivity due to distinctive detection of positron (PET) or gamma (SPECT) emission. These techniques are comparatively costly and special cautions must be applied in synthesis and handling due to ionizing radiation. MRI provides good soft tissue contrast and gives precise anatomical images with good spatial resolution (10-100 μm) and sensitivity. However, MRI, as well as CT and US, are semi-suitable for molecular imaging since these modalities require pre-scans, to determine the background level of MRI, CT, and US signal prior to contrast agent administration. Optical imaging offers great sensitivity with the ability to detect molecules in picomolar concentrations. Here, fluorescence, Raman, and luminescence imaging are included, where fluorescence imaging is to date the most utilized technique to detect information on the molecular level (molecular imaging). Optical imaging is frequently used for *in vivo* imaging of small animals because of its safety and time- and cost-effectiveness. However, it is impractical to image deep tissues or large living objectives due to low tissue penetration.

Multimodal imaging

Due to the limitations and possibilities of the individual modalities, hybrid imaging techniques have been developed in which the anatomical information obtained by CT or MRI is used to assist in the assignment of functional and molecular information to the organ or tissue. As an example, PET and SPECT have relatively poor spatial resolution and lack of anatomical information. To allocate the obtained information, they are often combined with MRI and CT,

which enable sensitive high resolution soft and hard tissue visualization. Optical imaging used in preclinical situations, it is difficult to accurately assign the signal to animal organs and consequently, moderately informative feedback on the biodistribution. Therefore, optical imaging also profits from hybrid imaging techniques; e.g., in combination with CT.

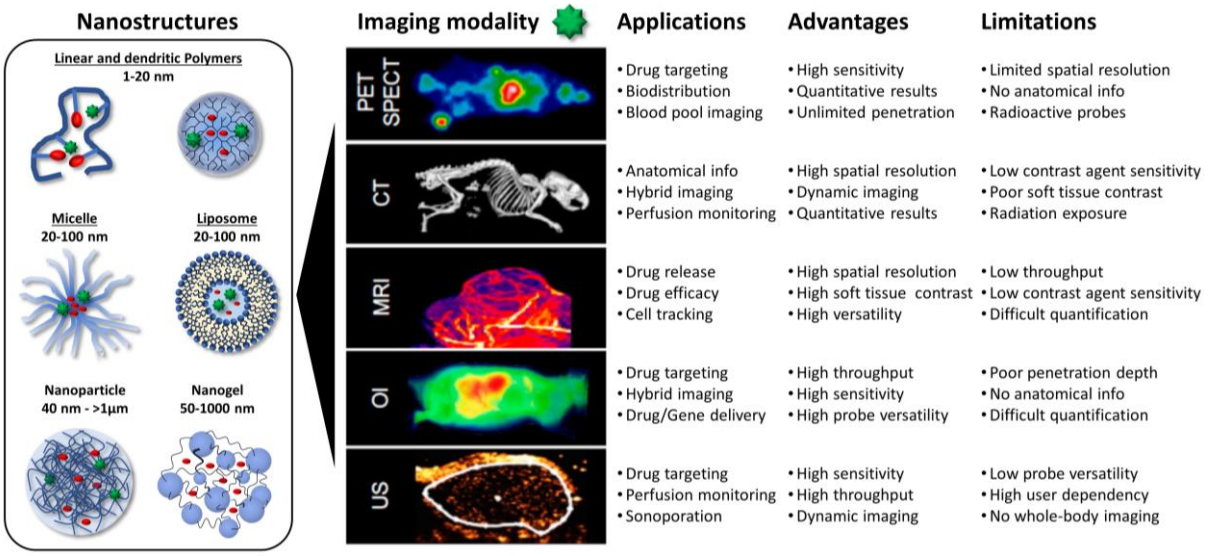

Figure 10. Non-invasive imaging modalities and overview of their applications, advantages, and limitation.[8] Adapted with permission from reference 8. Copyright 2015 American Chemical Society.

Theranostics in nanomedicine

To apply the mentioned imaging modalities, contrast agents are required. Most contrast agents used for various imaging modalities are low in molecular weight and therefore suffer from similar limitations as small drugs which result in short imaging duration and low signal to noise ratio. Consequently, the integration of nanotechnology can improve these limitations. Diagnostic agents may benefit from increased stability and a higher accumulation at the target site. For example, sizes of iron oxide nanoparticles are tuned in the nanoscale to target different organs such as liver, spleen, or lymph nodes for contrast-enhanced MRI (Resovist). Besides the improvement of the specificity of contrast agents, the association of diagnostic probes with therapeutic nanocarriers can be applied to understand and optimize drug delivery to pathological sites and evaluate nanomedicine performance in terms of therapeutic efficacy. In this sense, theranostics can help to get a grip on the variability of passive targeting using non-invasive and quantitative assessment of tumor targeting efficiency. As an example, Mulder et al developed a nanoreporter technique that predicts the efficacy of cancer nanotherapy by combining a liposomal nanocarrier with a PET probe.[106] Doxil (liposomal Dox

formulation) and a Doxil-mimic nanoreporter without Dox but with similar composition, size, and physicochemical properties were labeled with ^{89}Zr. When the radiolabeled nanoreporter and Doxil were co-administered, they could find a correlation in tumor accumulation. Therefore, the nanoreporter can be used to estimate the accumulation of Doxil in tumor with a single non-invasive PET session. Apart from liposomes, they were able to predict the efficacy of nanotherapy for nanoemulsion and PLGA particles. In addition, a close correlation was found between the potency of the EPR effect and treatment efficacy. This approach can be used to pre-select suitable patients with acceptable/high tumor accumulation of nanomedicine for further treatment and it might thereby provide a rational framework for personalizing nanomedicine treatments (Figure 11a).[107-108] Preselection of patients can be based on different functions of the nanodevice. Besides passive targeting, a selection of nanomedicine for a specific patient can be based on the expression receptors or enzyme activity which can be determined by non-invasive diagnosis.

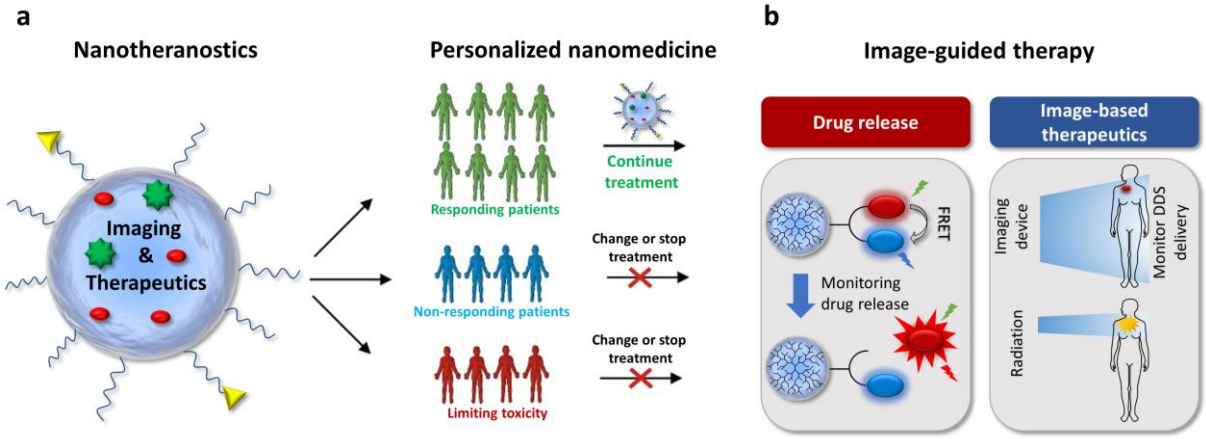

Figure 11. (**a**) Nanotheranostics can help evaluate nanomedicine performance in potential patients. Depending on the distribution optimized treatment is applied.[109] Copyright 2012 Elsevier. (**b**) Monitoring of therapeutic activity and response to therapy with the help of nanotheranostics.[110] Copyright 2016 Elsevier.

In addition, to decide whether to apply nanomedicine, it is also crucial to integrate imaging during the treatment by closely monitoring therapeutic responses. Here, clinical decisions can be facilitated whether a treatment should be continued or whether the drug doses should be adjusted. This image-guided therapy includes markers for malignant tissue in surgery and the monitoring of the nanomedicine in a non-invasive manner to precisely apply an external stimulus. In this regard, nanotheranostics has been discussed as a milestone towards precision medicine since it allows guided treatment as opposed to the strategy of “one fits all”-therapy (Figure 11b).[110]

Activatable theranostic prodrugs

Within optical image technologies, the most sophisticated imaging methods are functional or activatable probes to gain information on biological processes (molecular imaging). The physical phenomenon called fluorescence resonance energy transfer (FRET) is in particular useful as it allows to monitor molecular distances within a range of 1–10 nm in real time.[111] In general, FRET is a non-radiative process where an excited donor fluorophore transfers energy to a ground state acceptor through long-range dipole-dipole interactions. The energy transfer depends on many factors, such as the extent of spectral overlap, the relative orientation of the transition dipoles and, most importantly, the distance between the donor and acceptor dye.[112] The distance dependence makes FRET a useful tool to observe conformational changes and protein-protein interactions.[113] Furthermore, FRET is ideal to investigate bond cleavage or triggered release from a carrier in the context of a living system.[114]

In fundamental studies, Mulder et al. used activatable FRET-probes to follow not only the fate of the nanoparticle after intravenous administration but also the release of a model drug *in vivo*. They connected the fluorescent dye Cy5 (donor dye) to PLGA-PEG polymers that self-assemble to nanoparticles and used Cy7 (acceptor dye) with different hydrophobic tails as model drugs.[115] By disruption of FRET, they could follow the release of the model drug in real time and the biodistribution of the nanocarrier in a tumor mouse model. They evaluated how the model drug–carrier compatibility affected the drug release and found that the hydrophobicity of the drug and its miscibility with the nanoparticles determine its accumulation in the tumor. These findings were applied to improve delivery of the chemotherapeutic drug Dox by increasing its compatibility with the nanocarrier. For this purpose, Dox was modified with hydrophobic tails linked through a hydrazone bond, thereby generating a prodrug approach. The modified drug achieved better antitumor efficacy due to higher compatibility with the hydrophobic nanocarrier. These result help to elucidate the fate of nanomedicine *in vivo* fate and provide guidelines for efficient drug delivery of self-assembled nanocarriers.

Besides clinical and preclinical studies, theranostic probes can be used as a research tool to further elucidate the mechanisms of action that are present during the delivery process and thereby increase the understanding of fundamental processes crucial for a successful delivery.[116] For that purpose, activatable probes are designed that provide temporal and spatial information about the fate of the nanocarrier/drug and the occurrence of cleavage,

dissociation or conformational events during the delivery process on the cellular and even molecular level. Theranostic prodrugs have been shown to deliver and release the therapeutic drug Dox intracellularly mediated by biothiols in real time.[117] Zhang et al. reported a dual FRET prodrug with the capability of real-time drug-release monitoring and in situ cell-apoptosis imaging (Figure 12).[118] For this purpose, they connected the quencher dye 4-(dimethylaminoazo)benzene-4-carboxylic acid (Dabcyl) in proximity to DOX and 5(6)-carboxyfluorescein (FAM) which efficiently quenched the fluorescence of both. DOX was linked through a hydrazone bond that is cleaved under acidic conditions enabling the real-time monitoring of DOX release whereas FAM was connected through a caspase3 enzyme-responsive Asp-Glu-Val-Asp (DEVD) peptide sequence enabling caspase-3 imaging capabilities. This provides a cascaded imaging of real-time drug release and subsequent cell apoptosis, which enables the direct, precise and quantitative in situ detection of the cell response and the therapeutic efficacy for the evaluation of the prodrug.

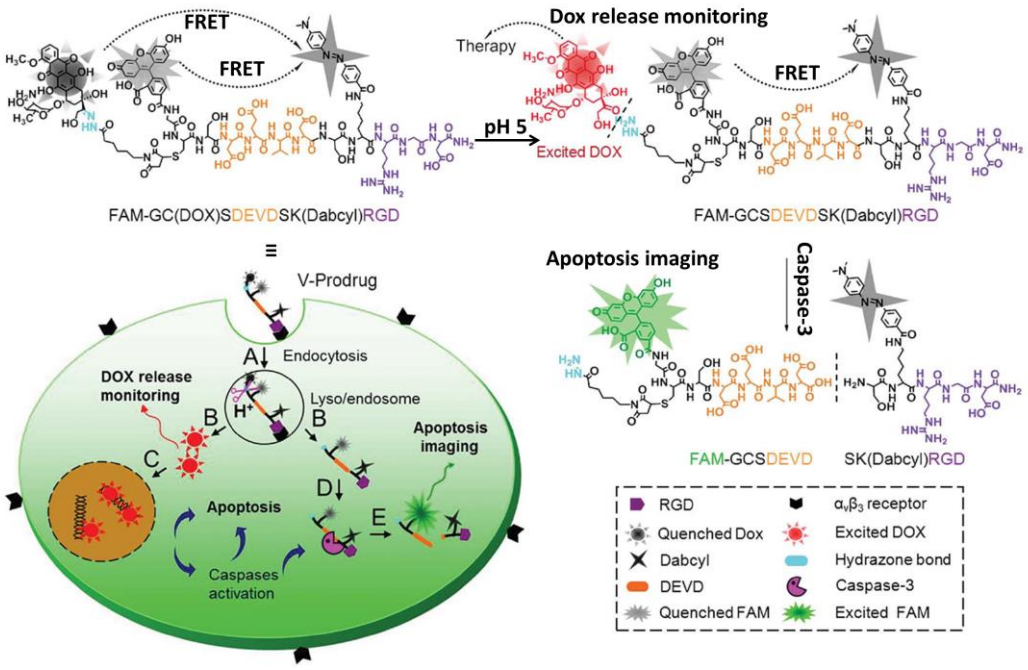

Figure 12. Double FRET theranostic probe allows imaging of drug release and therapeutic effect within one probe. Reprinted with permission from reference 118. [118] Copyright 2015 John Wiley and Sons.

The theranostic prodrug approach was also extended to evaluate also non-fluorescent drugs by the incorporation of an activatable reporter unit between the cleavable trigger moiety and the therapeutic drug. The self-immolative nature of the prodrugs leads to cascade reaction that leads to the activation of the reporter and release of drug at the same time. For the optical probe, examples exist using a pair of identical dyes that exhibit homo-FRET due to self-

quenching when in proximity and are activated by enzymatic activation,[119] a latent fluorophore that is activated upon substrate cleavage and rearrangement,[120] or recently a chemiluminescence diagnostic moiety that has superior signal-to-noise ratio during *in vivo* imaging.[121]

As the prodrug concept, the theranostic prodrugs can be adapted for polymeric systems by smart synthetic design that includes a nanocarrier, a therapeutic cargo, a trigger moiety and a reporter entity in one nanotheranostics system. Zhao et al. reported a prodrug-based supramolecular amphiphile that was formed via host-guest interaction for the delivery of camptothecin.[122] The prodrug host-guest complex self-assembled in aqueous solution to give nanosized vesicles that disassembled in the presence of glutathione. The assembled system was utilized as a drug/gene vector to achieve combinational gene therapy and chemotherapy with intracellular imaging of drug release in real time. For micellar architectures, the release of drug was followed by a light-induced change in polarity of the drug that can be followed by fluorescence due to the phototransformation to a fluorescent counterpart.[123]

Theranostic polymer-drug conjugates were designed based on N-(2-hydroxypropyl) methacrylamide (HPMA) copolymer for non-invasive intravital monitoring of drug release in real-time.[124] The fluorescence-based monitoring of site-specific drug release was feasible by a self-quenched near-infrared fluorescence probe. Two HPMA copolymer-based systems were presented where the diagnostic system consists of self-quenched Cy5 dyes and the therapeutic system contains the anticancer agent paclitaxel were linked by an enzymatically cleavable linkage. Both HPMA copolymer released the drug/dye upon enzymatic cleavage which was accompanied by the activation of the fluorophore. Therefore, the probes could be applied to image breast cancer progression and drug release in vivo.

1.3 Classes of nanocarriers

During the last decades, architectures for the delivery of pharmaceuticals with diverse forms, sizes, and surface properties have been designed that can be classified in polymer-, lipid-, and inorganic-based nanocarrier. [125] These include versatile architectures such as liposomes, polymer nanoparticles, micelles, dendrimers, as well as inorganic nanoparticles including quantum dots, iron oxide, gold, or metal oxide frameworks, among others (Figure 13). Eventually, also hybrid nanoparticles combining the materials and their characteristics of the mentioned ones evolved.

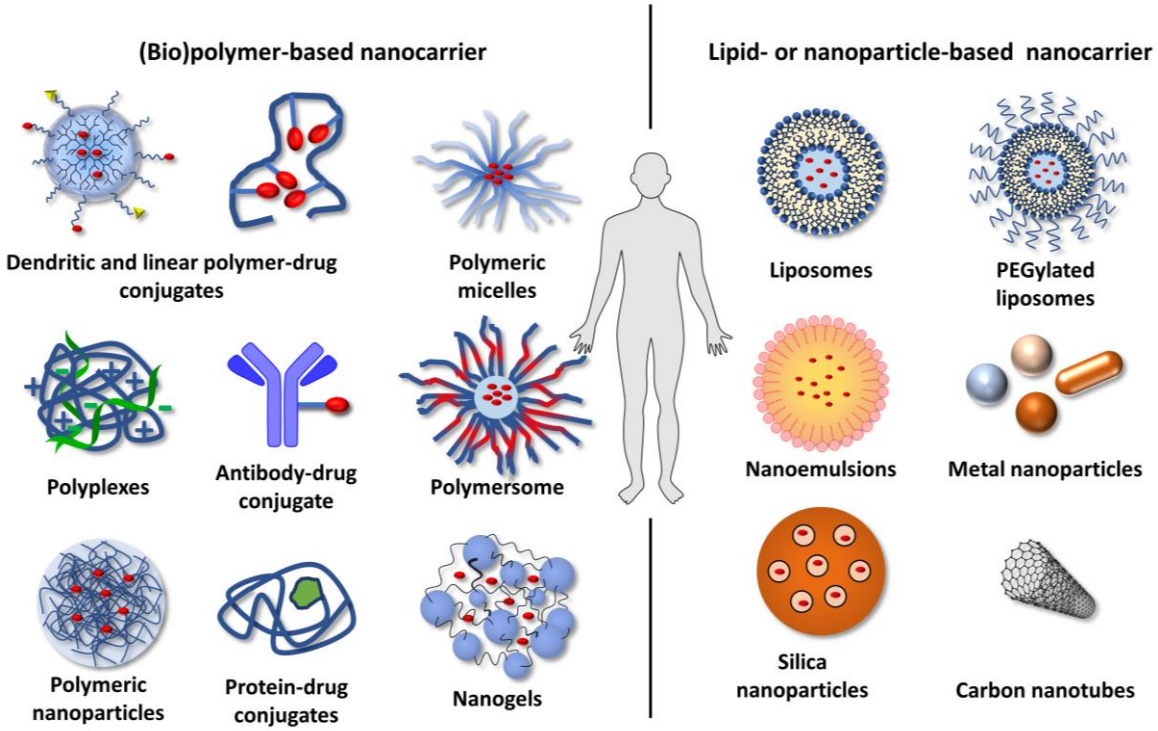

Figure 13. Schematic illustration of classes of nanoarchitectures used in drug delivery.

1.3.1 Polymeric nanostructures

The application of polymers or macromolecules as building blocks for nanocarrier platforms is widespread due to the variability and versatility in structure and physicochemical properties.[126-127] In the last decades, polymeric architectures evolved into more complex structures to encounter the requirements for effective drug delivery.[128] Nano-sized macromolecular architecture ordered from smaller to bigger structures (with overlap) include dendrimers/dendritic polymers (1–15 nm), polymer-drug/protein conjugates (5–20 nm), polyplexes (40–60 nm), polymeric micelles (20–100 nm), polymersomes (40–800 nm), nano- and microgels (50 nm-1 µm) and polymeric nano- and microparticles (40 nm–>1 µm)

(Figure 14). One key feature of these nanostructures is the opportunity to design multifunctional DDS that combine the (i) polymeric nanocarrier, (ii) a targeting moiety, (iii) a therapeutic agent, (iv) controlled therapeutic activation, and/or (v) an imaging probe.

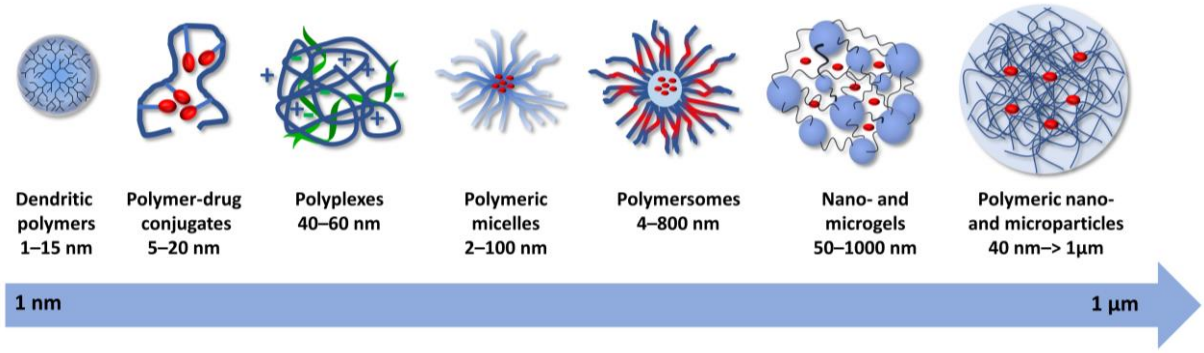

Figure 14. The dimensions of macromolecular nanostructures for drug delivery.

Polymer-drug conjugates

The concept of applying polymeric structures for drug conjugation has been introduced by Helmut Ringsdorf with his universal model that consists of a synthetic hydrophilic polymeric backbone with one or several drug molecules preferentially attached through cleavable linkers. He further proposed that the conjugates can be optimized by the attachment of functional moieties to increase the solubility, include active targeting or imaging probes for diagnostic.[129-130]

Together with other polymeric systems including polymeric drugs, protein–polymer conjugates, polymeric micelles covalently linked to drugs, multicomponent polyplexes and prodrug–protein complexes, polymer-drug conjugates are described with the term polymer therapeutic.[131] These systems are designed to address several of the key issues faced during drug delivery, including prolonged blood circulation times, targeting, accumulation and retention.[132]

Several polymeric materials from natural and synthetic origin have been explored for their potential as macromolecular nanocarriers. Natural polymers based on amino acids (peptides and proteins) or sugars (polysaccharides) have been evaluated as matrix material for nanocarriers for drug delivery owing to their intrinsic biocompatibility and biodegradability.[133] Polysaccharides include agarose, alginate, carrageenan, hyaluronic acid, dextran, and chitosan; whereas protein-based nanoparticles made of collagen, albumin, and gelatin are the most widely studied systems. Albumin was used in nanoparticulated systems as it offers specific binding sites for functionalization.[134] The albumin-based conjugates of paclitaxel,

Abraxane, is an approved therapeutic to treat breast cancer, lung cancer and pancreatic cancer.[135]

Synthetic polymers for biomedical application encompassed for a long time mainly linear, random-coil polymer. Among them are PEG; vinyl-based polymers such as poly(N-(2-hydroxypropyl) methacrylamide) (PHPMA), poly(vinylpyrrolidone) (PVP), and poly(vinyl alcohol) (PVA); polyesters like poly(lactide-co-glycolide) (PLGA) or poly(caprolactone) (PCL); and poly(amino acids) such as poly(L-lysine), poly(glutamic acid) (PGA), poly(malic acid) and poly(aspartamides).[136] The most widely applied macromolecule linked to the therapeutic to increase its solubility and circulation time is PEG. PEGylated nanoparticles have generally been considered to be benign and inert carriers. However, it has been found that PEG itself can evoke an immunogenic response and the search of alternatives is ongoing.[137-138] Nowadays, a diversity of linear branched and hyperbranched architectures and their hybrids are accessible that allow tailored composition of the nanocarrier scaffold (Figure 15). To achieve this structural diversity a tremendous effort has been undertaken to develop new polymerization methodologies including living anionic polymerization, controlled free-radical polymerization (atom transfer radical polymerization (ATRP) and reversible addition-fragmentation chain transfer (RAFT)), ring-opening polymerization (ROP), and ring opening metathesis polymerization (ROMP).

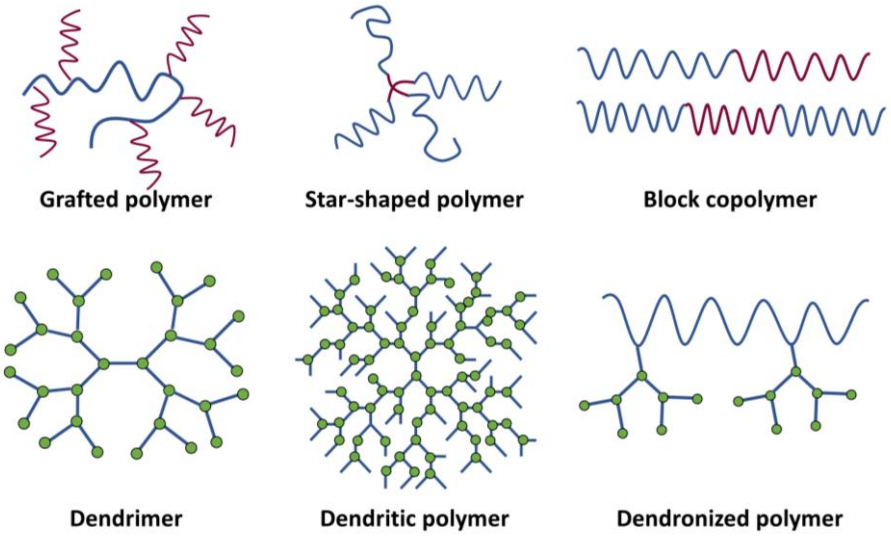

Figure 15. Examples of different polymer architectures for biomedical applications.[131] Adapted with permission from reference 131. Copyright 2003 Springer Nature.

A key feature to achieve an effective polymer-drug conjugate includes cleavable polymer–drug linkers that are stable during conjugate transport in blood and able to release drug at an

optimum rate upon arrival at the target site. Progress in this area will continue, especially, due to new linker methodologies. Synthetic effort has provided new cleavable linker that introduces controlled release properties to the conjugates. A promising strategy is the utilization of specific short peptide sequences that connect the drug molecules to the carrier. Peptide linkers for polymer–drug conjugation were popularized by the emergence of HPMA–Gly-Phe-Leu-Gly-doxorubicin conjugate (PK1).[139] This tetrapeptide linker is stable in the circulation but is cleaved by the lysosomal thiol-dependent protease cathepsin B following endocytic uptake. [140] pH-sensitive linkages have also been introduced as an alternative for drug conjugation. An HPMA copolymer conjugate containing doxorubicin bound via hydrazone linkages has shown significantly improved antitumor activity against lymphoma *in vivo* compared with the tetrapeptide conjugate.[141]

Two HPMA copolymer–doxorubicin conjugates with peptide linkers and one containing galactosamine (PK2) to promote liver targeting have subsequently progressed into Phase I/II evaluation. Even though they did not make into clinics, polymer-drug conjugates proved to be successful drug delivery strategy which leads to the translation of other polymer therapeutics into clinics and several are currently under clinical evaluation in clinics or clinical trial.[128]

Dendritic nanostructures

Dendritic polymers have tree-like structures and encompass hyperbranched polymers, dendronized polymers, dendrons, and dendrimers. While dendrimers represent perfectly branched systems with a well-defined molecular mass that are prepared in a tedious step by step manner, hyperbranched polymers are conveniently prepared in one step but are non-symmetrical and polydisperse. As nanocarrier, dendritic polymers offer defined and multiple functional groups to conjugate several drug molecules while adding targeting, imaging probes, and/or solubilizing modalities on the same construct in a controlled fashion.[142] A beneficial feature of dendritic polymers is the multivalent presentation of surface groups, which considerably enhances the binding to cell receptors. Dendritic molecules such as polyamidoamine, poly(propylene imine), polyaryl ethers, polylysine, polyester, polyamide, polyglycerol, and triazine dendrimers, have been introduced as DDS.[143]

Dendritic polyglycerol (dPG) presents a versatile platform for biomedical applications since it displays inertness in contact with biological systems.[144-146] The synthesis allows for a structural range of dPG architectures from perfect dendrons to well-defined hyperbranched polymers,

amphiphilic structures, core-shell system, nano-, micro-, and hydrogels that can be optimized towards the specific application. The hyperbranched version can be synthesized in a one-step anionic, ring-opening multi-branching polymerization of glycidol on a large scale with a predetermined molecular weight and degree of branching.[147] Materials based on dPG have been investigated several applications.[148] Besides utilization, for instance, as support for organic synthesis and catalysis[149] and for the preparation of surfaces with antifouling properties,[150] dPG has been extensively exploited to design nanocarriers[151-152] for drug-[83, 153-154] and gene-delivery,[155-157] In addition, polyglycerol-based nano-, micro-, and hydrogel formulations[158-161] were developed to investigate relevant architectures with various sizes for biological targets.

Nanogels

Among the macromolecular architectures, nanogels (NGs) are a promising platform for the creation of functional materials. Defined as nanometric aqueous dispersions of hydrogel particles that are formed by the physical or chemical crosslinking of polymer chains, NGs exhibit intrinsic features that are beneficial for the application in biomedicine. [62, 162] These polymeric nanoparticles usually possess a soft and hydrophilic nature, which helps to prevent unspecific interactions and prolongs circulation times compared to their hard counterparts.[163] The flexible and mechanical deformability enables the squeezing to otherwise inaccessible topologies.[164] In addition, the size range of NGs between 50 nm and several hundred nanometers allows the modulation towards the requirements of the specific application and towards similar dimension as biologically relevant structures, such as viruses.

Furthermore, NGs can incorporate stimuli-responsive polymers into their network to enable a triggered reaction ranging from morphological changes such as swelling or shrinkage to the disintegration of the polymer network.[62] These responsive properties can be exploited for the triggered release of cargo, morphological changes or degradation of the gels (Figure 16).[165] Herein, thermoresponsive nanogels allow the controlled release of drug upon shrinking when a thermal trigger is applied.[71] Apart from temperature-responsive NGs[64], stimuli-sensitive polymers and bonds have been introduced into the backbone or crosslinking points of nanogels that react to endogenous stimuli, for instance, to changes in pH,[166] redox potential,[167] or enzyme[168-169] action.

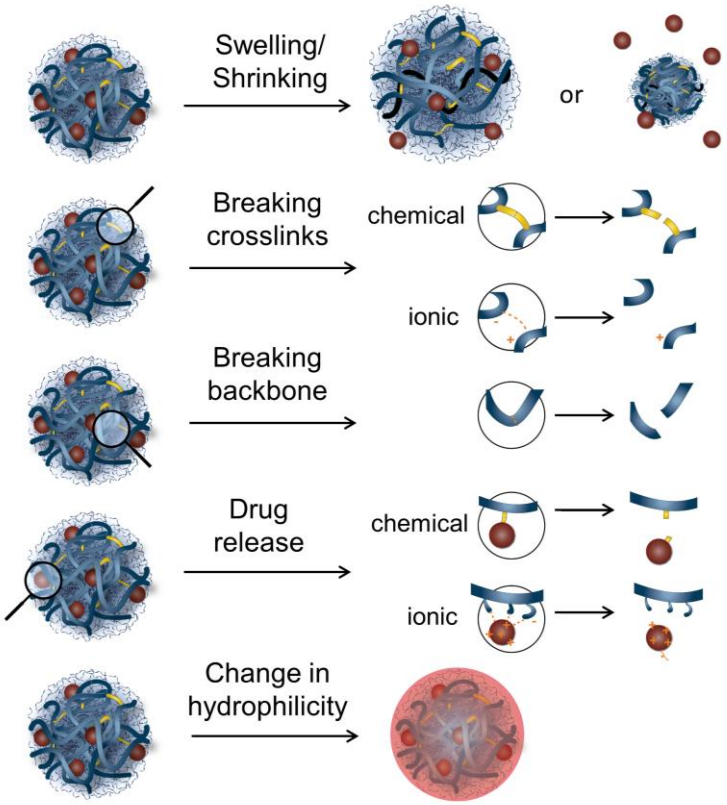

Figure 16. Possible stimuli-sensitive properties of nanogels.

For the fabrication of nanogels, multiple methodologies can be employed to obtain a crosslinked polymeric system. The most commonly employed methods are miniemulsion, precipitation and dispersion polymerization, inverse nanoprecipitation/solvent displacement, self-assembly, and template-assisted nanogel formation (lithographic methods, micromolding), as well as micelle crosslinking.[62] The crosslinking reactions include radical polymerization with the vinyl-functionalized monomer, click chemistry (alkyne-azide cycloaddition, thiol-ene, Michael addition), Schiff-base reaction to form imine or hydrazone bonds, thiol-disulfide exchange reaction, photo-induced crosslinking, ester/amide-based crosslinking, and enzyme-catalyzed crosslinking.[170] In addition, nanogels crosslinked by non-covalent bonds can be prepared using ionic or hydrophobic interactions as well as hydrogen bonding.[171] To form three-dimensional networks, at least one component, the so-called crosslinker, needs to present at least two or more reactive groups to form a network with the polymer chains. For radical polymerization, monomers can be polymerized in the presence of the crosslinker to build the network structure. Alternatively, preformed polymers with the corresponding functional groups are reacted in a template-assisted preparation method.

Polymeric micelles

Polymeric micelles are among the most studied macromolecular structures. These structures are constructed by the self-assembly of block copolymers to nano-scaled drug carriers forming a core-shell structure.[172] Kataoka et al. focused on the development of polymeric micelles, where the drug-loaded core consists of poly(amino acids) and is surrounded by a biocompatible PEG shell, with a narrowly distributed size controllable in the range of 10–100 nm.[173] The desired chemotherapeutic drugs can be incorporated by non-covalent interaction within the core or by covalent conjugation to the core-forming polymer block through a cleavable linker. Engineering the micelle-forming block copolymers endowed polymeric micelles with on-demand and smart functionalities such as stimuli-responsive behavior and active targeting abilities. The group was able to transfer several systems to clinical trials and has currently five micellar formulations incorporating PTX (NK105), cisplatin (NC-6004), SN-38 (NK102), DACH-platin (active complex of oxaliplatin) (NC-4016), or epirubicin (NC-6300/K-912) under clinical evaluation.[174] Polymeric micelles were found optimal to solubilize lipophilic drugs using amphiphilic block copolymers. However, important issues related to instability over long periods of time, the short duration of sustained release and poor bioavailability remain. Reversible crosslinking of the micelle core is one strategy to target these issues.[175]

Polymeric nanoparticles

Polymeric nanoparticles comprise of synthetic polymers forming a dense polymer matrix that is typically stabilized by hydrophobic interactions.[176]. Commonly used polymers for the formation of nanoparticles are polylactide and PLGA which degrade through hydrolysis of ester linkages.[177] PLGA-based formulations for drug delivery were limited due to issues with reproducibility and scalability of polymer synthesis, toxicity due to the premature release of therapeutic cargo from nanoparticles, and polymer interactions with the encapsulated drug. New biodegradable polymers have been synthesized addressing these concerns;[178] e.g., poly(caprolactone), poly(anhydrides),[179] poly(phosphazenes),[180] poly(phosphoesters);[181] poly(alkyl cyanoacrylates)[182-183]; and poly(orthoesters)[184] of which some are at different stages of clinical development. For drug encapsulation, methods such as nanoprecipitation, electrospray, and emulsification are used. A key advantage of these systems is that they enable the controlled release of various cargo, ranging from hydrophobic small molecules to large proteins and the release of the cargo can be controlled by the degradation rate.[185] As an example, solid poly(DL-lactide) (PLA) nanoparticles synthesized using an emulsion solvent

evaporation process were loaded with docetaxel and coated with both PEG and prostate-specific membrane antigen-targeting ligand. The PLA particles are currently in clinical trials for the treatment of prostate and lung cancer.[186]

1.3.2 Lipid-based nanocarriers

Liposomes

The most extensively studied among the classes of DDS are liposomes which are formed by self-assembly of amphiphilic phospholipids.[187] The liposomal formulation of doxorubicin (Doxil) was the first nano-drug that received clinical approval for cancer treatment and marks a milestone in the history of nanomedicine. Despite success in the clinical translation of liposome-based nanotechnology, some challenges remain.[188] The behavior of liposomes in a biological fluid is barely understood and their structural design is restricted. In addition, the loading capacities of liposomal formulations are comparably low. In combination with premature leakage, this results in insufficient drug amount reaching the target.

Nanoemulsions

Nanoemulsions (NEs) are biphasic dispersions of two immiscible liquids stabilized by an amphiphilic surfactant. The kinetically stable mixtures consist of either water in oil (W/O) or oil in water (O/W) nanodroplets with diameters of 20–500 nm.[25] In contrast to microscale emulsions, NE exhibit optical transparency at high droplet volume fractions, strong elasticity at low droplet volume fractions, enhanced diffusive transport and shelf stability. Despite their metastability, NE can be stable for years without showing coalescence. NEs are applied in drug delivery since the dispersed phase represents a large volume with high drug loading capability and the mechanical properties protect them against disruption.[189-190]

To form NE, usually, high shear stress using ultrasonication or homogenizer is applied to obtain small droplets of the dispersed phase. However, also low energy emulsification methods exist that utilize the energy stored in the system to produce ultra-fine droplets. Interactions of oil, surfactants, co-surfactants, drug, aqueous component, hydrophilic-lipophilic balance of utilized oil surfactant blend, and operative temperature must be optimized to enable low-energy emulsification.[191] Low-energy methods include spontaneous emulsification[192], phase inversion,[193] and the less utilized catastrophic phase inversion method.[194] Utilization of such method enables the production of NE in large scale without the need for complex equipment

or processes. Furthermore, these methods are of interest as they prevent the potential degradation of fragile encapsulated cargo compared to the high energy procedure. Drug release from NE involves partitioning of the drug from oil into surfactant layer and then into the aqueous phase. It has been shown that the drug release can be triggered by application of ultrasound by the formation of microbubbles from the NE.[72] When such external stimuli cannot be applied the drug retention within the formulation can be a concern. To facilitate this process, stimuli-sensitive prodrugs could be employed that change their partition coefficient after activation, and thereby allow the release of the cargo. Lipid or amphiphilic prodrugs can facilitate prodrug loading/insertion in lipid-based nanocarriers by membrane insertion. This strategy has been applied for liposomes, solid-lipid nanoparticles, and nanoemulsion and has appeared to be a valuable strategy to achieve improvements over conventional formulations.[115, 195]

1.3.3 Clinical translation of nanomedicine

Liposomes were the first class of therapeutic nanocarrier for cancer treatment to be successfully translated to clinics and Doxil received clinical approval in 1995. Along with other lipid-based DDS, liposomes still represent a large percentage of clinical-stage nanotherapeutics. Several other therapeutic nanocarrier platforms such as albumin nanoparticle, polymeric micelles, iron oxide nanoparticle, and polymeric nanoparticle have been approved for cancer treatment. Besides chemotherapy, new nanotechnology-based therapeutic modalities are under clinical investigation, including hyperthermia, radiation therapy, gene or RNA interference therapy, and immunotherapy (Table 2).

Even though the number of nanocarrier-based therapeutics for cancer therapy entering clinical trials is increasing, many of them fail translation to the market due to disappointing efficacy and barely improved survival rates. Major issues are the specificity of drug release which leads to severe side effect, the prevention of metastasis which still is a determinant factor that impairs patient's survival, and intratumoral barriers that impede homogenous drug transport in the malignant tissue. In this context, the EPR effect was shown to be highly variable depending on the tumor type and patient and is not sufficient for optimal targeted delivery.[196-197] However, novel nanocarriers approaches with multistage or multi-responsive characteristics show that nanomedicines can still offer promising solutions in cancer therapy even when long-lasting principles such as the EPR effect are compromised.

Table 2. Examples of approved and clinical-stage nanomedicines for cancer therapy.[15] Adapted from reference 15 with permission of Springer Nature.

Therapy modality	Generic or proprietary name	Nano-technology platform	Active pharmaceutical ingredients	Indication	Status
Non-targeted delivery	Liposomal doxorubicin (Doxil)	Pegylated liposome	Doxorubicin	HIV-related Kaposi sarcoma, ovarian cancer, and multiple myeloma	Approved by FDA
	Nab-paclitaxel (Abraxane)	Albumin NP	Paclitaxel	Breast, lung and pancreatic cancer	Approved by FDA
	SMANCS	Polymer conjugate	Neocarzinostatin	Liver and renal cancer	Approved in Japan
	Genexol-PM	Polymeric micelle	Paclitaxel	Breast cancer and non-small-cell lung cancer	Approved in Korea
	NK-105	Polymeric micelle	Paclitaxel	Metastatic or recurrent breast cancer	Phase III
	Nab-rapamycin (ABI-009)	Albumin NP	Rapamycin	Advanced malignant perivascular epithelioid cell tumors	Phase II
Targeted delivery	MM-302	HER2-targeting liposome	Doxorubicin	HER2-positive breast cancer	Phase II/III
	BIND-014	PSMA-targeting polymeric NP	Docetaxel	Non-small-cell lung cancer and metastatic castration-resistant prostate cancer	Phase II
	Anti-EGFR immunoliposomes	EGFR-targeting liposome	Doxorubicin	Solid tumors	Phase I
Stimuli-responsive delivery	ThermoDox	Liposome	Doxorubicin	Hepatocellular carcinoma	Phase III
Combinatorial delivery	CPX-351 or Vyxeos	Liposome	Cytarabine and daunorubicin (5:1)	High-risk acute myeloid leukemia	Phase III
	CPX-1	Liposome	Irinotecan and floxuridine (1:1)	Advanced colorectal cancer	Phase II
Hyperthermia	NanoTherm	Iron oxide NP	NA	Glioblastoma	Approved in Europe
	AuroLase	Silica core with a gold nanoshell	NA	Head and neck cancer, and primary and metastatic lung tumors	Pilot study
Radiotherapy	NBTXR3	Hafnium oxide NP	NA	Adult soft tissue sarcoma	Phase II/III
Gene or RNAi therapy	SGT53	TfR-targeting liposome	Plasmid	Recurrent glioblastoma and metastatic pancreatic cancer	Phase II
	CALAA-01	TfR-targeting polymeric NP	siRNA	Solid tumors	Phase I
Immunotherapy	Tecemotide	Liposome	MUC1 antigen	Non-small-cell lung cancer	Phase III
	JVRS-100	Lipid NP	Plasmid DNA	Relapsed or refractory leukemia	Phase I
	CYT-6091	Colloidal gold NP	tumor necrosis factor	Advanced solid tumors	Phase I

2 MOTIVATION & OBJECTIVE

Despite the high activity of conventional small molecular weight chemotherapeutic drugs, the lack of selective treatment results in severe side effects. The highly active anticancer drug doxorubicin (Dox) has been approved for several cancer types but shows major drawbacks as it is toxic to main organs, especially, the cardiotoxicity is life-threatening and therefore has dose-limiting effects. Using nanocarrier-based drug delivery platforms, side effects of therapeutic molecules and dose limits can be reduced by shielding the toxicity during transport and targeting the site of disease. Multiple barriers that are encountered during drug delivery, in particular in the tumor microenvironment (TME), impede nano-based drug delivery approaches indicating that conventional tumor targeting strategies alone are not sufficient to guide the therapy. However, the TME presents several features that can be utilized as endogenous triggers to activate nanotherapeutics. Hence, novel (multi)stimuli-responsive nanoarchitectures can be designed that adapt to the barriers by taking advantage of the altered conditions in the TME and improve targeted delivery by on-demand activation of therapeutics.

The main objective of this thesis is the incorporation of the prodrug concept into responsive nanocarrier designs to improve the pharmacological profile of chemotherapeutic drugs and tackle the issues of current nanomedicines. To approach this objective, nanocarrier architectures with different composition and sizes including polymer-drug conjugates, a nanoemulsion (NE), and nanogels (NGs) are combined with prodrugs of the chemotherapeutic drug Dox. The prodrugs contain cleavable motifs which provide the drug delivery system (DDS) with responsiveness for controlled drug release, change in hydrophilicity of the drug, or degradability of the carrier system, respectively (Figure 17).

The choice of the cleavable motif is a crucial factor for the specificity of response at the site of action. This aspect will be addressed using Dox prodrugs with different cleavable linkages for a specific response to an endogenous trigger. The different linkages will be evaluated in terms of intracellular cargo release and therapeutic activity using activatable fluorescence probes for real-time feedback. The assessment of cleavable linker forms the basis for the rational design of two prodrug-based nanomedicines with adjusted cleavage properties for intracellular drug release or dual-responsive behavior, respectively. In a first facile approach, a pH-sensitive prodrug will be combined with a NE as carrier to ensure intracellular Dox release. The second more complex nanomedicine aims for the combination of stimuli-

sensitive bonds with extracellular response to proteases and pH-mediated intracellular payload release.

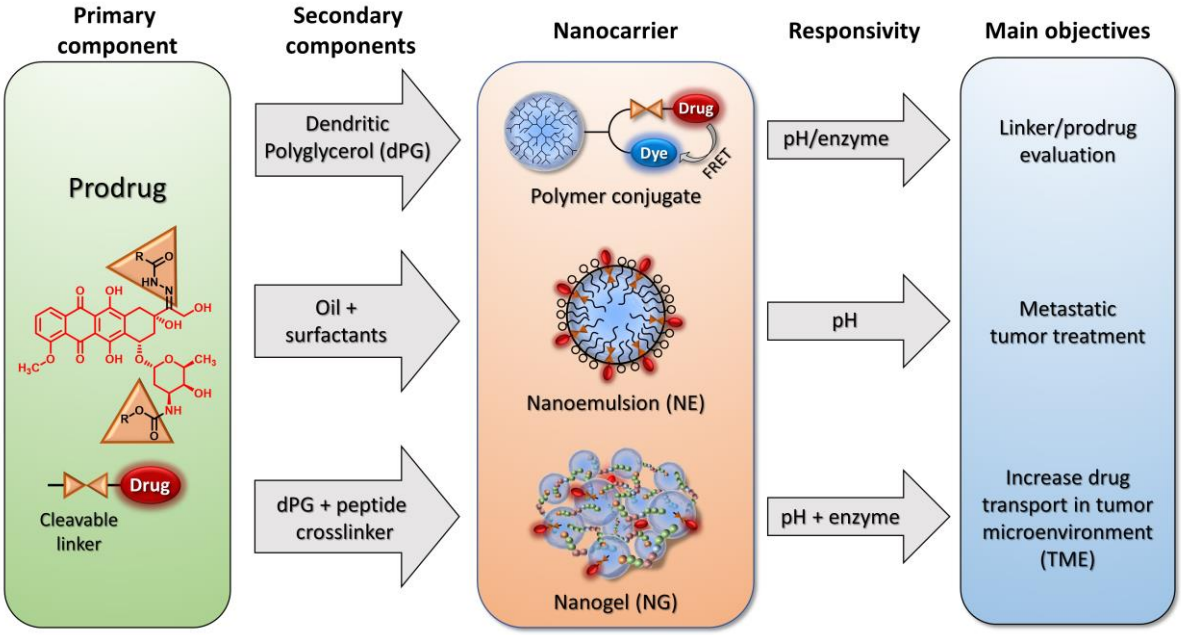

Figure 17. Main objectives of the thesis: incorporation of the prodrug concept into responsive nanocarrier designs to build smart nanomedicines for improved antitumor drug delivery.

To introduce on-demand activation of the delivery system, dynamic covalent chemistry is employed using the reversible formation and cleavage of strong covalent bonds. These linkages can provide stability for the drug-carrier connection but allow drug release or disintegration under specific conditions. To gain information on the performance of the devised DDS, activatable fluorescence probes are employed that give real-time information about the action of the nanocarrier. In combination, biological methods shall be established including cell-based microplate assays and multicellular tumor spheroids for detailed *in vitro* evaluation. This should help to characterize the systems in detail and understand the underlying processes in terms of drug-carrier compatibility, drug release, the fate of the carrier, and degradability.

Section 3 of this thesis comprises three chapters that describe the development and evaluation of responsive delivery approaches. Therefore, polymeric and lipid-based nanocarrier platforms are combined with prodrugs of the chemotherapeutic drug Dox.

In **section 3.1**, the synthesis of theranostic polymer-drug conjugates (TPC) with Dox conjugated through different cleavable linkers shall be developed. Cleavage of the conjugate is mediated either by acidic environment or by protease activity. These model DDS are based on dendritic polyglycerol (dPG) and comprise an activatable fluorescence imaging probe that should allow real-time observation of drug release. The TPC are employed to assess the

implications of the cleavable linker design on the cell-mediated Dox release using a simple cell-based microplate assay. The release profiles should give insight into the fate of the TMP as well as temporal information about the drug release depending on the linker and the cell line. This theranostic platform could contribute to the characterization of the TPC regarding their performance as DDS which, eventually, can be extended to other carrier systems with different linkers, drugs, and dyes. Thereby, we try to confirm that the microplate assay can be employed to extend the current *in vitro* methods to evaluate the potential of macromolecular DDS.

The assessed Dox prodrugs shall be employed in the design of novel nanocarrier systems with adjusted responsive behavior. In **section 3.2**, we aim for the development of a pH-sensitive Dox prodrug for the efficient entrapment of Dox into nanodroplets of an oil in water NE, as a new formulation approach. To achieve the entrapment, Dox shall be modified to provide it with an amphiphilic character for increased drug-carrier compatibility. In addition, the pH-cleavable bond should allow the regeneration of the parent drug and subsequent transition from the oil droplets to the aqueous phase endowing the system with controlled release capability. The Dox-loaded nanoemulsion will be evaluated *in vitro* to determine the character of drug release and cytotoxicity. *In vivo*, the new formulation of Dox may reduce off-target effects which would allow the administration of higher dosage. Thereby, the treatment of tumors should be more effective compared to the free drug and may prevent the formation of metastasis. The low-cost and easily scalable nanoemulsion approach could be a promising candidate for clinical application in the near future.

In **section 3.3**, dPG-based NGs are employed as alternative polymeric architecture to increase the size of the carrier endowing the system with improved pharmacokinetic and the possibility to incorporate multiple stimuli-responsive moieties. We aim for the combination of protease- and pH-sensitive moieties into one multistage delivery system that utilizes the proteolytic activity in TME and the intracellular drop in pH to enhance tumor penetration and drug distribution within diseased tissue. To implement the crucial design feature, matrix metalloproteinase (MMP)-sensitive NGs shall be developed that present suitable sizes to potentially accumulate in tumor tissue by the enhanced permeation and retention (EPR) effect. The incorporation of a fluorogenic peptide as crosslinker should integrate biodegradability into the nanocarrier and endow the nanocarrier with protease-mediated size reduction property in response to the TME. To complete the multistage design, a pH-

responsive Dox prodrug shall be covalently attached to the NGs allowing a stable transport of the drug and controlled drug release in the second stage of the delivery. To evaluate the potential of the pNGs to promote the penetration of Dox into dense tumor tissue, multicellular tumor spheroid shall be established as a 3D model that resembles the tumor tissue physiology and TME.

3 PUBLICATIONS & MANUSCRIPTS

In the following section, the published articles and submitted manuscripts are listed and the contributions of the author are specified.

3.1 Modular approach for theranostic polymer conjugates with activatable fluorescence: impact of linker design on the stimuli-induced release of doxorubicin

Gregor Nagel, Harald R. Tschiche, Stefanie Wedepohl, Marcelo Calderón, *Journal of Controlled Release* 285 (**2018**) 200–211. *Journal of Controlled Release* **2018**, *285*, 200–211.

Reprinted with permission from reference 198.[198] Copyright 2018 Elsevier.

The article is electronically available: https://doi.org/10.1016/j.jconrel.2018.07.015.

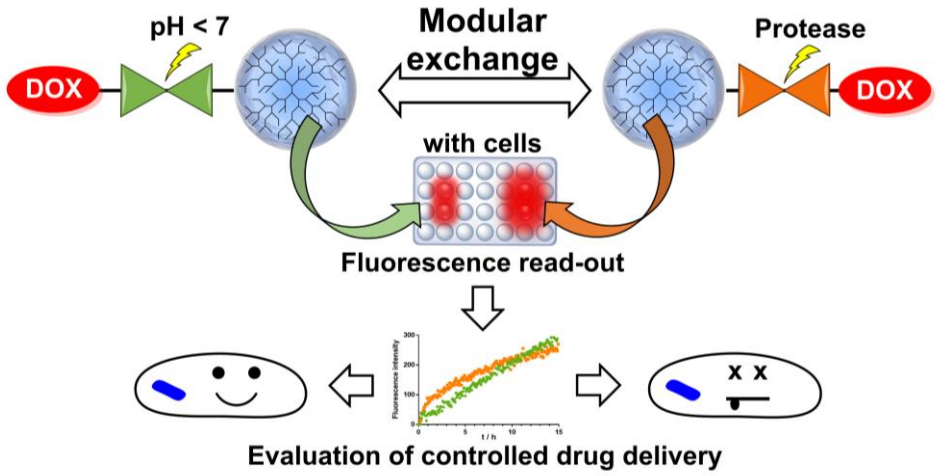

Figure 18. Schematic representation of modular theranostic polymer conjugates (TPC) for the evaluation of linker design. Reprinted with permission from reference 198. Copyright 2018 Elsevier.

Abstract:

The introduction of cleavable motifs by dynamic covalent chemistry is widely applied in the design of drug delivery systems (DDS) to introduce controlled release properties. Since the cleavable moieties can be triggered by various exogenous or endogenous stimuli, the choice of the linker has substantial implications on the performance of the DDS. In this project, a pair of theranostic polymer conjugates (TPC) is presented to study the influence of the cleavable bond on the cell-mediated drug release by a facile in vitro fluorescence assay. The TPC represent model DDS that consist of dendritic polyglycerol as polymeric carrier labeled with

an indodicarbocyanine (IDCC) dye and the chemotherapeutic drug doxorubicin (Dox) conjugated through different cleavable linkers. Cleavage of the conjugate can be mediated by either acidic environment or protease activity. The spatial proximity of the IDCC dye and the fluorescent drug led to effective quenching of Dox fluorescence when bound to the carrier. The stimuli-induced linker cleavage was correlated with the recovery of fluorescence giving real-time information about the stimuli-dependent drug release. By tracking the fluorescence recovery in a cell-based high throughput microplate assay, we were able to obtain characteristic release profiles of Dox for different cell lines. Here, we found that the pH-cleavable linker was more suitable for drug delivery applications since the enzyme-sensitive system suffered premature release due to the presence of extracellular proteases. This had a pronounced effect on the treatment of a multidrug-resistant cell line where an intracellular drug release is crucial to overcome the resistance mechanisms. We want to highlight that the modular synthetic approach combined with the cell-based assay has potential to extend the common in vitro methods to evaluate DDS performance and suitability as the design can be easily employed for diverse carrier/linker systems as well as various cell lines.

Author's contribution:

In this publication, the author contributed to the conceptual development of the theranostic polymer conjugates (TPC) and the microplate assay. The synthesis and characterization of the TPC were conducted by the author including organic synthesis of the linker and prodrugs as well as the conjugation to the polymeric carrier. Analytical methods for physicochemical characterization of the linkers, prodrugs and the conjugates using NMR, ESI-MS, DLS, GPC, fluorescence and UV/Vis measurements were performed and analyzed by the author. In addition, the biological testing and data evaluation including the microplate assay, cytotoxicity test, and cellular uptake using confocal laser scanning microscopy or cytometry was performed by the author. The author developed the outline and wrote the manuscript with assistance from the co- and corresponding authors.

3.2 Acid-sensitive lipidated doxorubicin prodrug entrapped in nanoemulsion impairs lung tumor metastasis in a breast cancer model

Ana Lygia dos Santos Câmara[‡], **Gregor Nagel[‡]**, Harald R Tschiche, Camila Magalhães Cardador, Luis Alexandre Muehlmann, Daniela Mara de Oliveira, Paula Queiroz Alvim, Ricardo Bentes Azevedo, Marcelo Calderón & João Paulo Figueiró Longo, *Nanomedicine (Lond.)* (**2017**) 12(15), 1751–1765. *Nanomedicine* **2017**, 12, 1751–1765.

[‡] Authors contributed equally.

The article is electronically available: https://doi.org/10.2217/nnm-2017-0091.

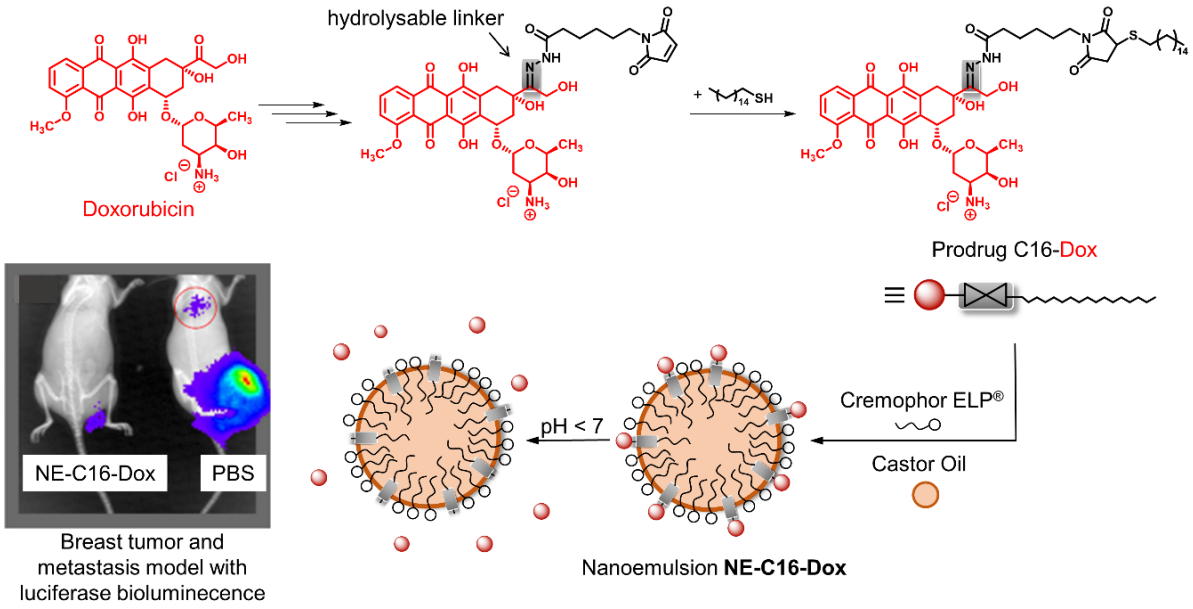

Figure 19. Schematic representation of the synthesis of acid-sensitive Dox prodrug C16-Dox, formulation into nanoemulsion (NE-C16-Dox), acid-mediated Dox release, and treatment of breast tumor model. Adapted with permission of reference 199. Copyright 2017 Future Medicine Ltd.

Abstract:

The highly active anticancer drug doxorubicin (Dox) has been approved for several cancer types but shows major drawbacks as it is toxic to main organs, especially, the cardiotoxicity is life-threatening and therefore has dose-limiting effects. To efficiently entrap Dox in the nanodroplets of an oil in water nanoemulsion (NE), we developed a novel Dox prodrug (C16-

Dox) that provides the drug with an amphiphilic character for increased drug-carrier compatibility. pH-sensitive properties of the prodrug allowed a controlled release of the drug from the NE. The new formulation of Dox (NE-C16-Dox) was evaluated by *in vitro* experiments in terms of cell internalization and cytotoxicity. In addition, the novel prodrug formulated in NE was tested in an *in vivo* breast cancer model in mice regarding its biocompatibility, Dox delivery to tumor tissues and the prevention of metastasis. Improved delivery to tumor tissue and reduction of systemic toxicity allowed the administration of higher doses of Dox as compared to the free drug. The tumor treatment in a murine 4T1 breast cancer model with NE-C16-Dox in high dosage significantly inhibited the primary tumor growth and prevented the formation of distant lung metastasis. This is an important finding since the presence of metastasis is as a determinant factor for patient survival. The improved chemotherapeutic index compared to free Dox indicates that NE-C16-Dox is a promising formulation for breast cancer treatment; thus, creating possibilities to translate this nanotechnology concept into clinical applications.

Author's contribution:

In this publication, the author contributed to the conceptual development of the Dox prodrug, the synthesis, and characterization of the same, and the preparation and characterization of the drug-loaded nanoemulsions such as drug release, stability, and data evaluation. Analytical data such as NMR and ESI-MS were evaluated by the author. In addition, the author contributed to the scientific discussion and experiment design of *in vitro* studies, the preparation of the manuscript, and assisted in writing the report in general.

3.3 Matrix metalloproteinase-sensitive multistage nanogels enhance drug transport in 3D tumor model

Gregor Nagel, Ana Sousa-Herves, Stefanie Wedepohl, Marcelo Calderón, *submitted manuscript.*

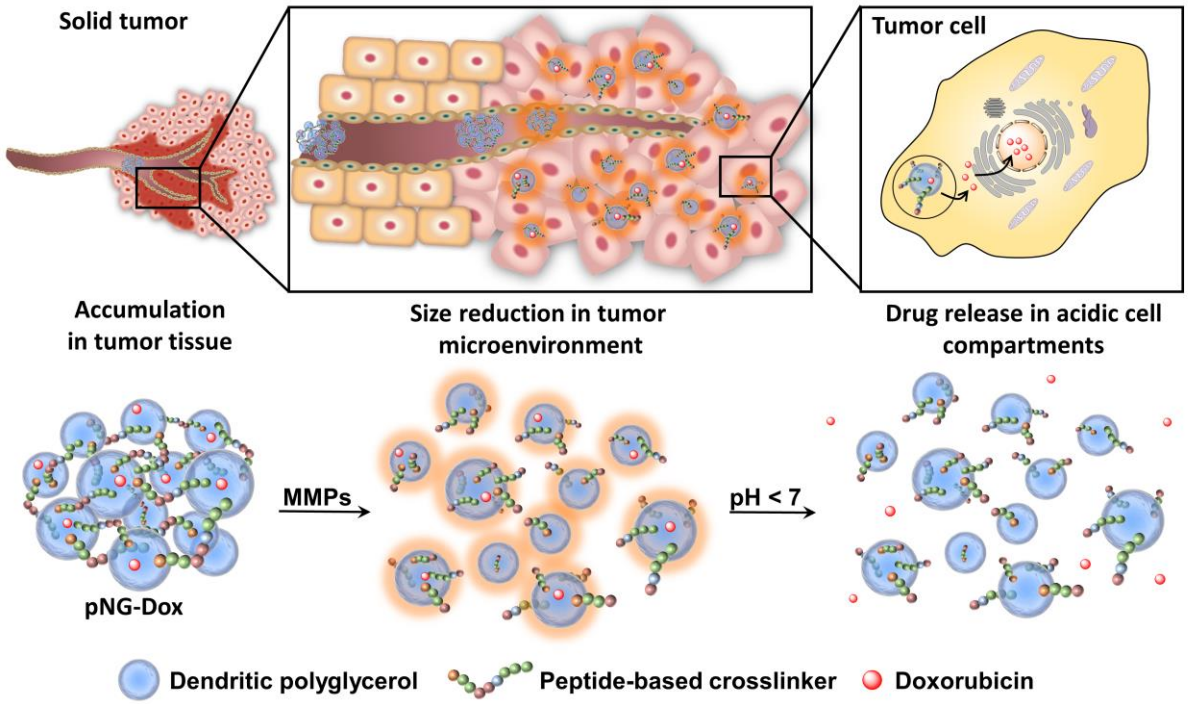

Figure 20. Schematic representation of the mechanism proposed for multistage drug delivery by peptide-crosslinked NG (pNG-Dox).

Abstract:

Physiological barriers inside of tumor tissue often result in poor interstitial penetration and heterogenous intratumoral distribution of nanoparticle-based drug delivery systems (DDS). Hence, novel matrix metalloproteinase (MMP)-sensitive peptide-crosslinked nanogels (pNGs) were developed as multistage DDS with a beneficial size reduction property to promote the process of deep tissue penetration. The pNG consists of dendritic polyglycerol (dPG) macrounits forming nanogel networks with an MMP-sensitive fluorogenic peptide crosslinker. The crosslinker integrates degradability to the nanocarrier comprised of otherwise non-degradable polymers. Surfactant-free inverse nanoprecipitation was employed to prepare the nanogels using strain-promoted click chemistry. The size and crosslinking density of the pNGs were controlled by the functionalization degree of dPG with cyclooctyne groups and by the peptide crosslinker fraction. The intrinsic reporter moiety of the crosslinker allowed us to study the influence of different pNG compositions on the degradation profile in detail. One

pNG candidate was chosen to conjugate the therapeutic drug Dox through a pH-sensitive linkage to the dPG macrounits. The degradable multistage pNGs demonstrated deeper penetration into multicellular tumor spheroids (MCTS) as compared to their non-degradable counterparts. Hence, the triggered size reduction of the pNGs by enzymatic degradation can facilitate the infiltration of the nanocarrier into dense tissue and thereby promote the delivery of the therapeutic cargo.

Author's contribution:

In this publication, the author contributed to the concept of dPG-based peptide-crosslinked nanogels (pNGs). The development of synthetic methodologies of the pNGs as well as their physicochemical characterization, dye labeling, drug release, and degradation studies were performed by the author. In addition, the author established a multicellular tumor spheroid model for the evaluation of drug and carrier penetration into dense tissue. The outline and manuscript were developed and written by the author with the assistance of the co- and corresponding authors.

Matrix metalloproteinase-sensitive multistage nanogels promote drug transport in 3D tumor model

Gregor Nagel, Ana Sousa-Herves, Stefanie Wedepohl, Marcelo Calderon*

Freie Universität Berlin, Institute of Chemistry and Biochemistry, Takustr. 3, 14195 Berlin, Germany.

*Corresponding author:

Prof. Dr. Marcelo Calderón

Freie Universität Berlin, Institute of Chemistry and Biochemistry

Takustr. 3, 14195 Berlin (Germany)

Tel.: +49 30 838 459368

E-mail: marcelo.calderon@fu-berlin.de

Homepage: http://www.bcp.fu-berlin.de/chemie/calderon

ABSTRACT

Physiological barriers inside of tumor tissue often result in poor interstitial penetration and heterogenous intratumoral distribution of nanoparticle-based drug delivery systems (DDS). We report novel matrix metalloproteinase (MMP)-sensitive peptide-crosslinked nanogels (pNGs) as multistage DDS with a beneficial size reduction property to promote the process of deep tissue penetration. The pNG consists of dendritic polyglycerol (dPG) forming nanogel networks crosslinked with a modified MMP-sensitive fluorogenic peptide. The crosslinker integrates degradability to the nanocarrier by endogenous stimulus present in the tumor microenvironment. Surfactant-free inverse nanoprecipitation was employed to prepare the nanogels using strain-promoted click chemistry. The size and crosslinking density of the pNGs were controlled by the functionalization degree of dPG with cyclooctyne groups and by the peptide crosslinker fraction. The intrinsic reporter moiety of the crosslinker allowed us to study the influence of different pNG compositions on the degradation profile in detail. One pNG candidate was chosen to conjugate the therapeutic drug Doxorubicin through a pH-sensitive linkage to dPG. The degradable multistage pNGs demonstrated deeper penetration into multicellular tumor spheroids (MCTS) as compared to their non-degradable counterparts. Hence, the triggered size reduction of the pNGs by enzymatic degradation can facilitate the infiltration of the nanocarrier into dense tissue, and thereby promote the delivery of its therapeutic cargo.

INTRODUCTION

Despite all the advances that have been achieved in the field of nanocarrier-driven drug delivery, many challenges remain.[1-4] One major obstacle is poor tumor penetration and heterogeneous distribution throughout the diseased tissue after extravasation of the nanoparticles from the vasculature.[5-6] While the accumulation of nanocarrier-based drug delivery in tumor tissue mediated by the enhanced penetration and retention (EPR) effect has been well established for many setups *in vivo*, the corresponding improvement of the therapeutic efficiency has often been deficient.[6-8] This can be accounted, for instance, to the hampered penetration and uneven distribution of the nanocarrier in deeper regions of the tumor which result from the heterogeneous vasculature, high interstitial fluid pressure, and dense interstitial matrix.[6, 9-10] Nanocarriers aiming for EPR-based delivery are typically in the size of 100-300 nm.[5] However, it was found that particles in this size range cannot easily

penetrate into the interstitial space,[11] leading to a heterogeneous distribution of particles within the malignant tissue. This impairs the treatment, and additionally, the barely perfused center of the tumor harbors the most aggressive cells that have the potential to regenerate the tumor if not eliminated completely.[12-14] Low exposure of drug in some regions of the tumor could even promote the development of drug resistance.[15-16] Conventional small molecule therapeutic agents show fast diffusion in tumor stroma, they are however also rapidly cleared from body and tissues.

One approach to improve intratumoral delivery is to carefully design multistage delivery systems that utilize specific stimuli in the tumor microenvironment such as pH or proteases to either achieve deeper tumor penetration, increased cellular uptake, and/or controlled drug release.[17-18] The nanocarriers possess design features that allow the response to specific stimuli encountered in a consecutive manner.[19] Examples have been reported that respond to the slightly acidic tumor microenvironment (pH 6–7) with a size reduction by disintegration, sequential swelling/shrinking, or reorganization to enhance the diffusive properties of the particles.[17, 20-22] However, the acidic pH is typically located far from the blood vessels (pH gradient) which would hinder the response in the perivascular regions. As enzymatic reactions are highly specific and enzyme activity is strongly dependent on location, cell type, or the state of the targeted tissue, introduction of enzyme-responsive moieties into NGs can aid to adapt the responsiveness of a drug delivery system (DDS) to the abundant proteases in the tumor microenvironment.[23-24] Therefore, nanoparticles based on the natural polymers gelatin have been presented that encapsulate smaller entities like quantum dots or gold nanoparticles.[25-27] The idea of these carriers is that the gelatin shell can be degraded by extracellular proteases and thereby release the smaller entities, which can then more readily diffuse within the dense interstitial space. Gelatin is a substrate for matrix metalloproteinases (MMPs), a family of extracellular endopeptidases with the ability to degrade components of the extracellular matrix (ECM). Upregulated MMP expression has been reported for several malignant conditions where they are involved in tumor proliferation and invasion as well as metastasis.[28-32] The enzymes are located in the extracellular space and can be used for early detection and as biomarkers of disease progression and metastasis.[33-35]. Alternative MMP-responsive moieties are peptides that can be applied as cleavable linkages to introduce site-specific biodegradation or drug release.[36-39]

Taking this into account, we designed multistage MMP-sensitive peptide-crosslinked nanogels (pNGs) that present suitable sizes to potentially accumulate in tumor tissue by the EPR effect and feature a protease-mediated size reduction property and acid-mediated drug release for enhanced tissue penetration. These degradable nanocarriers consist of a hydrophilic scaffold based on dendritic polyglycerol (dPG, Figure S1) that forms a three-dimensional network connected via MMP-specific peptide crosslinkers. The second building block was a rationally designed fluorogenic peptide crosslinker that comprises an MMP-specific amino acid sequence that is framed by a dye pair that exhibits fluorescence resonance energy transfer (FRET) and enables the monitoring of the peptide cleavage. The incorporation of the fluorogenic peptide as crosslinker integrates degradability to the nanocarrier comprised of otherwise non-degradable polymers, and additionally, the cleavage of the crosslinks can be conveniently monitored by the intrinsic fluorescence reporter. The design was inspired by hydrogels prepared by Janda and co-workers that include MMP-sensitive crosslinkers in acrylamide gels to introduce degradability into synthetic hydrogels.[40] To transfer this concept to the nanoscale, we choose NGs as the nanometric equivalents of hydrogels that have emerged as a platform for the development of novel nanocarrier-based strategies.[41] NGs are soft, hydrophilic hydrogel particles formed by physically or chemically crosslinked polymer chains that can incorporate stimuli-responsive moieties into their network to enable a triggered reaction ranging from morphological changes such as swelling or shrinkage to the disintegration of the polymer network.[42]

Classically, NGs are prone to efficiently encapsulate their cargo by physical interactions in the network structure. However, encapsulation can cause premature release of the payload by diffusion mediated leakage before reaching the site of action. Additionally, the release of the drug should be prevented after MMP-mediated degradation as this could cause fast clearance of the small molecular weight drugs. As an alternative, covalently bound therapeutics can prevent leakage, mediate enhanced solubility, and, when attached by dynamic covalent chemistry, can be released in a controlled manner.[43] To this end, we aimed to conjugate the chemotherapeutic drug doxorubicin (DOX) through a pH-sensitive linker to the dPG scaffold, thereby creating a multistage delivery system (pNG-DOX). In the first stage, pNGs can be degraded by MMPs which are present in the tumor microenvironment. After the resulting size reduction, the fragments constitute polymer-drug conjugates consisting of polyglycerol as polymeric carrier and DOX conjugated through an acid-cleavable linkage. These fragments

should facilitate the penetration into deeper areas of tumor tissue where the cargo could be released at acidic pH as present in intracellular compartments (pH 4-5) such as endosomes and lysosomes (Scheme 1).[44]

Scheme 1. Schematic representation of the mechanism proposed for the multistage drug delivery by pNG-DOX.

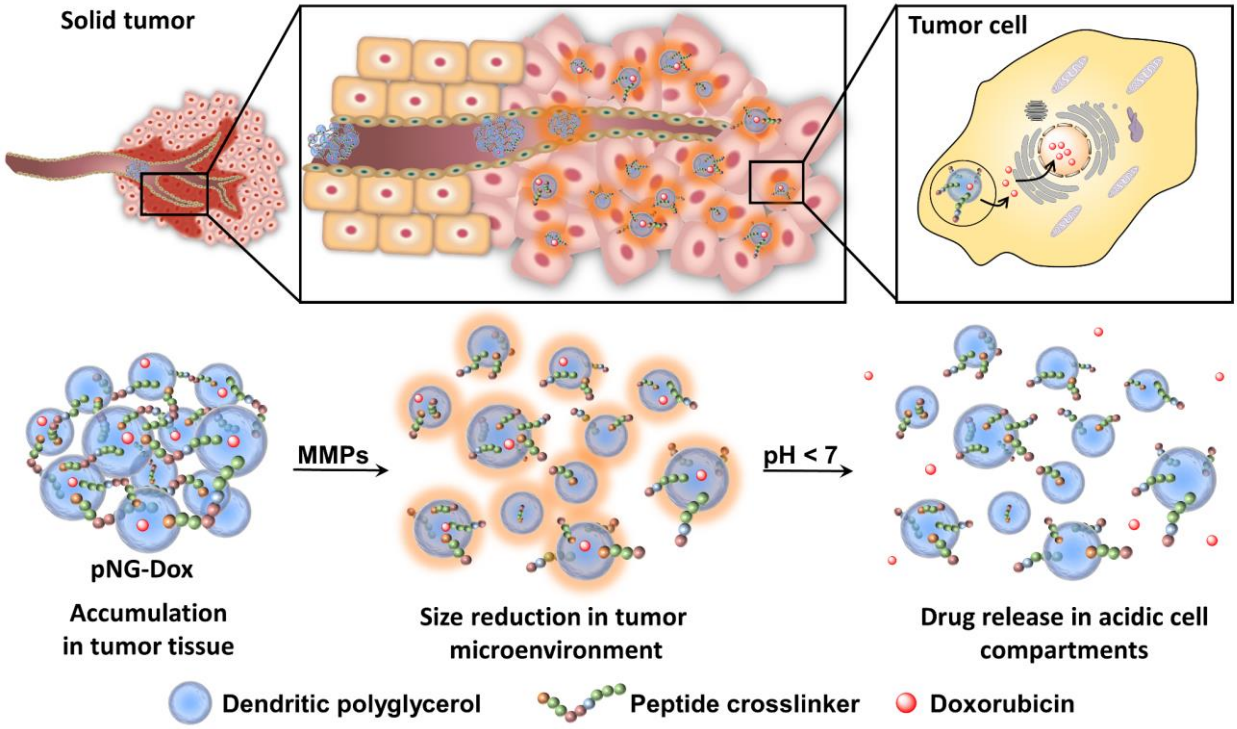

We expect that the synthetic approach based on multifunctional building blocks and directed incorporation of cleavable peptide allows precise control over the size and crosslinking density of the pNGs with varying the applied feed. Different crosslinking densities should result in different degradation profiles which can be tuned towards the specific application as multistage nanocarrier. In our system, the MMP-induced size reduction and degradation can be conveniently studied using the intrinsic fluorescence probe of the crosslinker. To prove the principle of the multistage drug delivery system, we investigate the diffusive transport of MMP-digested pNGs in a dense gel matrix mimicking the ECM. Furthermore, we want to confirm an enhanced penetration of the carrier fragments and the drug into multicellular tumor spheroids (MCTS) which should result in an improved therapeutic activity of the drug.

So far, the majority of the peptide-crosslinked nanocarriers only described the degradation to small fragments to release encapsulated cargo. To the best of our knowledge, the controlled introduction of peptide-based crosslinkers into nanogels and the application as a multistage delivery system has not been reported before.

EXPERIMENTAL SECTION

General Methods

All chemicals were purchased from Acros Organics, Alfa Aesar, Roth, Merck, Sigma-Aldrich (now Merck), Deutero GmbH, and used as received. The design of the peptide crosslinker was adapted and modified from the work of Janda et al.[40] and the strategy of the crosslinker synthesis was developed in cooperation with Protein Research Inc. (UK). Structure and peptide sequence: Mca-Lys((OEG)8-N3)-Pro-Leu-Gly-Leu-Lys(Dnp)-Ala-Arg-Lys((OEG)8-N3)-NH2 (Mca: 7-methoxycoumarinyl-4-acetic acid; Dnp: 2,4-dinitrophenyl; EG: ethylene glycol). Dendritic polyglycerol (dPG) was purchased from Nanopartica GmbH (Germany) with a weight average molecular weight (M_w) of 10 kDa (Dispersity Đ = 1.27). The cyclooctyne reagent (1R,8S,9s)-Bicyclo[6.1.0]non-4-yn-9-ylmethyl N-succinimidyl carbonate was purchased from Synaffix (AE Oss, Netherlands). Water used for the synthesis was obtained from a Millipore water purification system. The pH-sensitive (6-maleimidocaproyl) hydrazone derivative of DOX (aldoxorubicin), was synthesized starting from 6-aminocaproic acid following a procedure from literature.[45] ^{1}H NMR and ESI-MS spectra are shown in the SI.

HeLa cells (DSMZ-No. ACC-57, Leibnitz Institute DSMZ- German Collection of Microorganisms and Cell Cultures) were routinely maintained in RPMI 1640 medium (Lonza) containing 10% fetal bovine serum (FBS Superior, Merck), 1% Penicillin/Streptomycin (P/S, Thermo Fisher Scientific), and 1% MEM non-essential amino acids (Sigma-Aldrich) at 37 °C and 5% CO_2. Human dermal fibroblasts from juvenile foreskin were isolated in accordance to local ethics and biosafety regulations (ethical approval EA1/345/14 by the Charité ethical committee) and were routinely cultured in Dulbecco's Modified Eagle Medium (DMEM) with 15% FBS and 1% P/S at 37 °C and 5% CO_2.

Synthetic procedure

Functionalization of dPG

The hydroxyl groups of dPG were modified in three steps to obtain amine functionalities following published procedure (Scheme S1).[46] Briefly, dried dPG (250 mg dPG, 0.27 mmol OH's for 8%, 1.0 equiv.) was dissolved in DMF (25 mL) with triethyl amine (113 µL, 0.81 mmol, 3 equiv.) and cooled down to 0 °C. The hydroxy groups were activated by addition of methanesulfonyl chloride (23.0 µL, 0.30 mmol, 1.1 equiv.). The reaction was stirred overnight

(18 h) and allowed to reach rt. The reaction mixture was diluted with MeOH (4:1 v/v) and dialyzed against MeOH for 2 d (Molecular weight cut-off (MWCO) 1000 Da). The degree of functionalization was determined by ^{1}H NMR. Degrees of functionalization for dPG-BCN are given as a percentage of the total dPG hydroxyl groups (~ 135 hydroxyl groups for 10 kDa dPG). For the next step, the polymer was dissolved in DMF and sodium azide (87.8 mg, 1.35 mmol, 5 equiv.) was added to induce a nucleophilic substitution of the mesyl groups. The reaction mixture was heated to 60 °C and stirred for 3 d. After filtration, the filtrate was diluted with MeOH and dialyzed against MeOH for 2 d (1000 Da MWCO) to obtain dPG-azide. The appearance of a characteristic azide band was observed in the IR spectrum (2100 cm^{-1}) and the disappearance of the NMR signal for mesyl groups was monitored. To obtain dPG with amine functionalization, the azide groups were reduced by Staudinger reaction. Therefore, dPG-azide was dissolved in water/THF (1:1 v/v) and triphenylphosphine (213 mg, 0.81 mmol, 3 equiv.) was added before the solution was stirred for 3 d at 40 °C. Afterwards, TFA was evaporated and the remaining aqueous solution was filtered. The solution was dialyzed against MeOH for 3 d (MWCO 1000 Da). By this method, dPG-amine with 4% and 8% degrees of functionalization were obtained as determined by ^{1}H NMR.

Functionalization of dPG with bicyclononyne groups (BCN)

For the functionalization with cyclooctyne groups, dPG-amine (250 mg, 0.27 mmol amine groups for 8%, 1.0 equiv.) was dissolved in DMF (20 mL) before triethylamine (112.3 µL, 0.81 mmol, 3.0 equiv.) and (1R,8S,9s)-Bicyclo[6.1.0]non-4-yn-9-ylmethyl N-succinimidyl carbonate (86.5 mg, 0.30 mmol, 1.1 equiv.) were added. The reaction was stirred for 3 h at rt. Then, the solution was diluted with MeOH (4:1 v/v) and dialyzed against MeOH for 3 d (MWCO 1000 Da). The degree of functionalization was determined by ^{1}H NMR yielding dPG-BCN with 3.9% and 7.8% conversion (NMR in SI).

Preparation of pNGs

For the synthesis of the pNGs, nanoprecipitation was employed using different degrees of BCN-functionalization and different feed ratios (see Table 1). As an example, dPG-BCN (4% functionalization, 4.1 mg, $2.2 \cdot 10^{-3}$ mmol BCN groups) and peptide crosslinker (2.0 mg, $1.6 \cdot 10^{-3}$ mmol azide groups, 70 mol%) were dissolved separately in water (1 mL) and cooled down in an ice bath. The cooled solutions were mixed and directly injected into NaCl-saturated acetone (20 mL) under vigorous stirring (900 rpm). After injection, the stirring was stopped, and the

nanoprecipitation was left for 2 d at rt before the excess of BCN groups was quenched with either azidopropanol (pNG-OH), indocarbocyanine azide (pNG-ICC) or 11-Azido-3,6,9-trioxaundecan-1-amine (pNG-NH_2). The dispersion was left for 1 d more before of water (1 mL) was added and acetone was evaporated. The aqueous dispersion was dialyzed against water for 3 d (MWCO 50 kDa). For the preparation of non-degradable controls, the same methodology was applied using the peptide crosslinker comprised of D-amino acids.

Table 1: Composition of feed and resulting hydrodynamic diameters of prepared pNGs.

#	dPG-BCN (%OH groups converted)	Peptide crosslinker (w%)	Peptide crosslinker (mol%)	Reactant concentration (mg/mL)	size[a] in H_2O (nm)	Poly dispersity index
pNG 1	4	10	20	3.0	676	0.239
pNG 2	4	20	25	3.0	414	0.345
pNG 3	4	25	35	3.0	308	0.128
pNG 4	4	40	50	3.0	270	0.205
pNG 5	4	45	70	3.0	254	0.150
pNG 6	4	50	80	3.0	193	0.276
pNG 7	4	70	105	3.0	178	0.175
pNG 8	8	25	17.5	3.0	635	0.077
pNG 9	8	40	35	3.0	543	0.030
pNG 10	8	45	40	3.0	502	0.108
pNG 11	8	50	50	3.0	379	0.032
pNG 12	8	70	60	3.0	367	0.314
pNG 13	4	45	70	2.0	121	0.324
pNG 14	4	45	70	4.0	270	0.023
pNG 15	4	45	70	8.0	426	0.349

[a] Mean hydrodynamic diameter obtained by dynamic light scattering (DLS) measurements in H_2O at 25 °C. The intensity distribution is given.

Synthesis of multistage pNGs (pNG-DOX)

pNGs (5 mg) quenched with 11-Azido-3,6,9-trioxaundecan-1-amine were reacted with 2-iminothiolane hydrochloride (1.1 mg, $8.1 \cdot 10^{-3}$ mmol, 3 equiv. of maximum amine groups) to convert the amine groups to thiols. After 20 min, the dispersion was filtered through a desalting column (PD10 column; GE Healthcare) to separate remaining 2-iminothiolane. The

pNGs dispersion was concentrated by centrifugal filter devices (Vivaspin ®, MWCO 100 kDa) before DOX-EMCH (2.1 mg, $2.7 \cdot 10^{-3}$ mmol, 1 equiv.), dissolved in DMF (0.1 mL), was added and left to stir for 4 h at rt. The pNGs were purified by size exclusion chromatography (SEC) using Sephadex G-25 fine matrix and subsequently dialyzed for 2 d in water (MWCO 50 kDa). The NGs were stored as highly concentrated dispersions (5 mg/mL) at 4 °C. The same methodology was applied for the preparation of non-degradable controls using the peptide crosslinker comprised of D-amino acids.

Characterization of pNGs

Dynamic light scattering (DLS) and zeta potential

Size distribution and zeta potential of pNGs were measured at 25 °C by dynamic light scattering (DLS) using a Zetasizer Nano-ZS 90 (Malvern) equipped with a He-Ne laser (λ = 633 nm) at a scattering angle of 173°. Samples with the concentration of 1 mg/mL in phosphate buffered saline (10 mM phosphate salts, 150 mM NaCl, PBS) were equilibrated for 5 min at the respective temperature prior to the measurement. Particle size distributions are given as the average of three measurements from intensity distribution curves. As DLS measurements of the NGs were monomodal in distribution, with autocorrelation functions showing a single exponential decay. The hydrodynamic diameters are reported from the intensity distribution curves.

Transmission electron microscopy (TEM)

Transmission electron microscopy samples were prepared by blotting samples (1 mg/mL) onto carbon-coated copper grids (400 meshes, Quantifoil Micro Tools GmbH). Then a droplet (5 µL) of 1% (w/v) uranyl acetate solution was applied and kept for 60 s before the excess of contrasting material was removed by means of filter paper and the sample could dry in air. Samples were visualized by using the TEM detector on a Hitachi scanning electron microscope (SU8030, Hitachi, Tokyo, Japan) at 20–30 kV and 10 µA at different magnifications.

Degradation study of pNG

By DLS

To follow the degradation of the pNGs by DLS, recombinant human MMP-7 (R&D Systems) were activated at 100 µg/mL with 1 mM p-aminophenylmercuric acetate (APMA) in a solution

of 50 mM Tris base, 10 mM $CaCl_2$, 150 mM NaCl, 0.05% (w/v) Brij-35, and pH 7.5 (TCNB) for 1 h at 37 °C. The enzyme solution was diluted to 0.4 µg/mL. 50 µL of NGs solution at 1 mg/mL were filled into low volume cuvettes (Sarstedt) and placed in the Zetasizer Nano-ZS 90 (Malvern). The reaction was initiated by addition of enzyme solution (50 µL at 0.4 µg/mL). The particle size distributions were measured every 30 min at 37 °C over 16 h.

By fluorescence

The degradation was monitored by fluorescence intensity measurements over time following the fluorescence of 7-methoxycoumarin. pNG solutions of 0.01–1.0 mg/mL were prepared in TCNB buffer and 50 µL were loaded into a 96-well microplate. The reaction was started by adding 50 µL of the activated MMP-7 solution (0.02 µg per well). Plates included a substrate and background controls containing pNGs with buffer and buffer only. As a positive control, a fluorogenic peptide (Mca-Pro-Leu-Gly-Leu-Dpa-Ala-Arg-NH_2, Dpa: N-3-(2, 4-Dinitrophenyl)-L-2,3-diamino propionyl, R&D systems) was included at a concentration of 10 µM to confirm enzyme activity. The microplate was sealed with optically clear adhesive seal sheets (Absolute qPCR Seal, Thermo Scientific) and placed into a microplate reader (Infinite M200 Pro, Tecan) heated to 37 °C. The excitation and emission wavelengths were set to 320 nm and 405 nm (top read), respectively, and fluorescence intensity was recorded every 5 min for 15 h. The background signal of pNGs in assay buffer was subtracted and the fluorescence intensities expressed as changes relative to the starting point, were plotted versus time.

Release of DOX

pNG-DOX dispersions in H_2O were mixed with different buffers (1:1 v/v with acetate buffer (50 mM sodium acetate/acetic acid, 150 mM NaCl) at pH 5 or Tris buffer (50 mM Tris base, 10 mM $CaCl_2$, 150 mM NaCl, 0.05% w/v Brij-35, TCNB) at pH 7.5 with or without MMP-7) at 5 mg/mL and incubated at 37 °C. At specific time points (t = 0 min, 1 h, 2.5 h, 5 h, 8 h, 24 h) an aliquot of the solution was transferred to a SEC column containing Sephadex G-25 fine matrix to separate the free DOX from the NGs. The collected NG fraction was analyzed for remaining DOX by UV/Vis spectroscopy (absorption at 490 nm).

Diffusion in agarose gels

Agarose gels were prepared by heating a suspension of agarose in PBS (0.5 w%) in a microwave oven at 500 W for 30 seconds. The clear agarose solution was filled into

rectangular capillaries of borosilicate glass (Hilgenberg, LxBxW: 80x4.2x1.25 mm, wall thickness 120 µm). After gel formation at rt, NGs labeled with ICC (pNG-ICC, 0.1 mg) were incubated with either MMP-7 (final concentration 0.02 µg/mL) in TCNB buffer or in buffer alone. After 16 h, EDTA was added to inactivate the enzyme and 20 µL of the solution was filled into the capillaries on top of the agarose gel. In addition, free ICC in the same concentration was added to a capillary and then, the capillaries were kept at 37 °C in a humidified chamber for another 16 h. The gels were imaged using a gel imaging system (GelDoc XRS+, Bio-Rad) with green epi-illumination (0.2 s exposure time) and 605/50 nm filter. The images were analyzed by ImageJ software.

MCTS culture

HeLa cells or HeLa/fibroblast cell mixtures were cultured in hanging drops using the GravityPLUS^{TM} kit (InSphero AG). According to the manufacturer's instructions, drops of 40 µL at various cell densities ranging from 500 to 10000 cells per drop were seeded to observe the formation of spheroids of at least 500 µm in diameter. After 3 d at 37 °C and 5% CO_2, spheroids grew on the bottom of most of the drops. The spheroids were transferred to GravityTRAP™ plates, a non-adhesive coated 96-well microplate with conic wells for longtime cultivation, by adding 70 µL media to the drops and subsequent centrifugation of the plate at 300 rpm for 2 min to force the spheroids into the wells. The spheroids were stored at 37 °C and 5% CO_2. The medium was exchanged once per week. Between day 7 and 9 after seeding, spheroids reached a size of approximately 500–600 µm and showed dense circular structures and were ready to use for the penetration assay (Figure S2).

MCTS penetration

After 9 d in culture, spheroids were rinsed twice with PBS before fluorescently labeled pNGs-ICC, degradable and non-degradable control, or free ICC in RPMI medium without FBS and phenol red were added to the spheroids. The pNGs were added to a final concentration of 1.5 µM regarding the fluorescent dye. The spheroids were incubated for 2 or 16 h at 37 °C and 5% CO_2. Afterwards, the medium was discarded, spheroids were washed three times with PBS, and fixed for 40 min at rt in 10% neutral buffered formalin. Spheroids were washed again twice with PBS and cell nuclei were stained with DAPI solution (2.5 µg/mL in PBS, Sigma) for 1 h at rt. After washing with PBS, two complementary methods were applied to realize the visualization of the pNGs penetration into MCTS. For the first one, spheroids were transferred

using 1 mL pipetting tips onto microscope slides, squeezed under microscopy coverslips and mounted with ProTaqs MountFluor (Quartett GmbH) mounting medium. For the second method, the fixed spheroids were stained with methylene blue (0.1% in PBS) for 10 min at rt. After washing with PBS, spheroids were transferred to Peel-A-Way® S-22 embedding molds (Merck) embedding molds and embedded in Surgipath FSC 22 clear embedding compound (Leica) before the samples were frozen using liquid nitrogen. Then, the spheroids were cut into 16 µm-thick sections and mounted onto microscope slides. Images were acquired with a Leica SP8 CLSM using laser excitation at 488 nm (DOX) and 561 nm (ICC) with 20-fold and 64-fold magnification. Image analysis was performed with LASX software and ImageJ. The circumference was determined in the brightfield images and then transferred to the intensity images. Subsequently, the measuring function was used to determine the mean fluorescence intensity in the area of the MCTS. The same procedure was followed for analyzing the penetration of multistage pNGs (degradable and non-degradable and free DOX) into spheroids. Here, a concentration of 5µM regarding DOX was applied for all samples.

Cell viability assay

To assess cell viability and proliferation inhibition, 10000 cells per well were seeded into 96-well-plates (Sarstedt) with 100 µL of culture medium (RPMI for HeLa, DMEM for all other cell lines) with 10% FBS (FBS Superior, Merck), 1% Penicillin/Streptomycin (Thermo Fisher Scientific). The cells were incubated at 37 °C at 5% CO_2 overnight. Then, the media was replaced with fresh media containing various dilutions of the corresponding NG or free drug in duplicates and cells were incubated for 48 h at 37 °C and 5% CO_2. The cell culture supernatant was removed, and cells were washed twice with PBS (200 µL/well). Then, 100 µL/well fresh full medium including 10 µL/well MTT (Sigma-Aldrich, 5 mg/mL in PBS) were added and incubated for another 4 h at 37 °C. After development of formazan crystals, the cell culture supernatant was removed, and crystals were dissolved by addition of 100 µL/well of isopropanol containing 0.04 M HCl. Absorbance was read at 590 nm in a Tecan Infinite M200 Pro microplate reader. In case of the 3D-model, spheroids were incubated with the corresponding pNGs or the free drug with DOX concentrations of 10 µM in triplicates for 48 h at 37 °C and 5% CO_2. Afterwards, CellTiter-Glo® (Promega Corporation) viability assay solution was added and the contents were mixed for 5 min to induce lysis of the cells. The plate was incubated for 10 min at rt to stabilize the luminescence signal and luminescence was recorded

in the plate reader. Relative viabilities were calculated by dividing average absorbance or luminescence values of wells with treated cells by values of untreated cells (=100% viability). All tests were repeated 3 times independently and errors were expressed as standard error of the mean (SEM).

RESULTS AND DISCUSSION

We propose the use of peptide crosslinked nanogels (pNGs) as a multistage drug delivery systems (DDS) that feature MMP-mediated size reduction properties in response to the tumor microenvironment followed by controlled drug release at acidic pH conditions to aid enhancing tumor tissue penetration of attached DOX. To design a suitable pNG for this purpose, we needed to consider the initial size of the pNG that should potentially enable accumulation in tumor tissue by the EPR effect which requires rather large particle sizes (100–300 m).[8] In the tumor environment, extracellular MMPs would cleave the peptide linker and thereby cause a size reduction by degradation of the pNG that enables deeper tissue penetration of the fragments. The size of the degradation products must be carefully chosen as well, since particles smaller than 30 nm may be cleared from tumor tissue while larger particles are retained and continue to accumulate.[47] It has been reported that micelles in size range of 50 nm are able to penetrate tumor tissues and at the same time are more likely to be retained in the tumor tissue while smaller micelles of 30 nm are susceptible to more rapid clearance.[5, 7, 48] Therefore, we first systematically investigated the synthetic parameters and the influence of the different building blocks on the resulting properties of the pNGs with the goal to find a suitable candidate for proposed multistage DDS.

Formation and characterization of pNGs

In the first step, we developed the methodology for the preparation of the MMP-sensitive NGs. The pNGs consist of dendritic polyglycerol (dPG) crosslinked by a fluorogenic peptide that can be cleaved by MMPs, as well as a chemotherapeutic drug attached via an acid labile linker to the polymer. The hyperbranched polymer dPG was chosen to form the hydrophilic scaffold of the pNGs and to allow facile functionalization.[49] Furthermore, dPG served as a polymeric carrier of DOX after fragmentation. The hydroxy groups of dPG were converted to amine groups in a three-step approach following a known procedure.[46] Afterwards, the amines were reacted with (1R,8S,9s)-Bicyclo[6.1.0]non-4-yn-9-ylmethyl N-succinimidyl carbonate to introduce cyclooctyne groups (dPG-BCN, Scheme S2).

To employ the fluorogenic peptide as crosslinker, it was modified with two terminal azide groups. These groups were attached through the γ-amino groups of lysine side chains including an 8-unit oligoethylene glycol (OEG)-chain as spacer leading to the final structure: Mca-Lys((OEG)8-N3)-Pro-Leu-Gly-Leu-Lys(Dnp)-Ala-Arg-Lys((OEG)8-N3)-NH2 (Scheme 2). The additional OEG chains were introduced to increase the water solubility and the accessibility for the proteases. The functional groups allow the strain-promoted alkyne-azide cycloaddition (SPAAC), a biorthogonal, metal-free click reaction that can be performed under mild conditions. Therefore, the reaction type allows the crosslinking of the building blocks without damaging the sensitive peptide and potentially could enable the encapsulation of sensitive cargos.[50]

Scheme 2. Schematic representation of the building blocks, synthesis, and structure of multistage pNG-Dox.

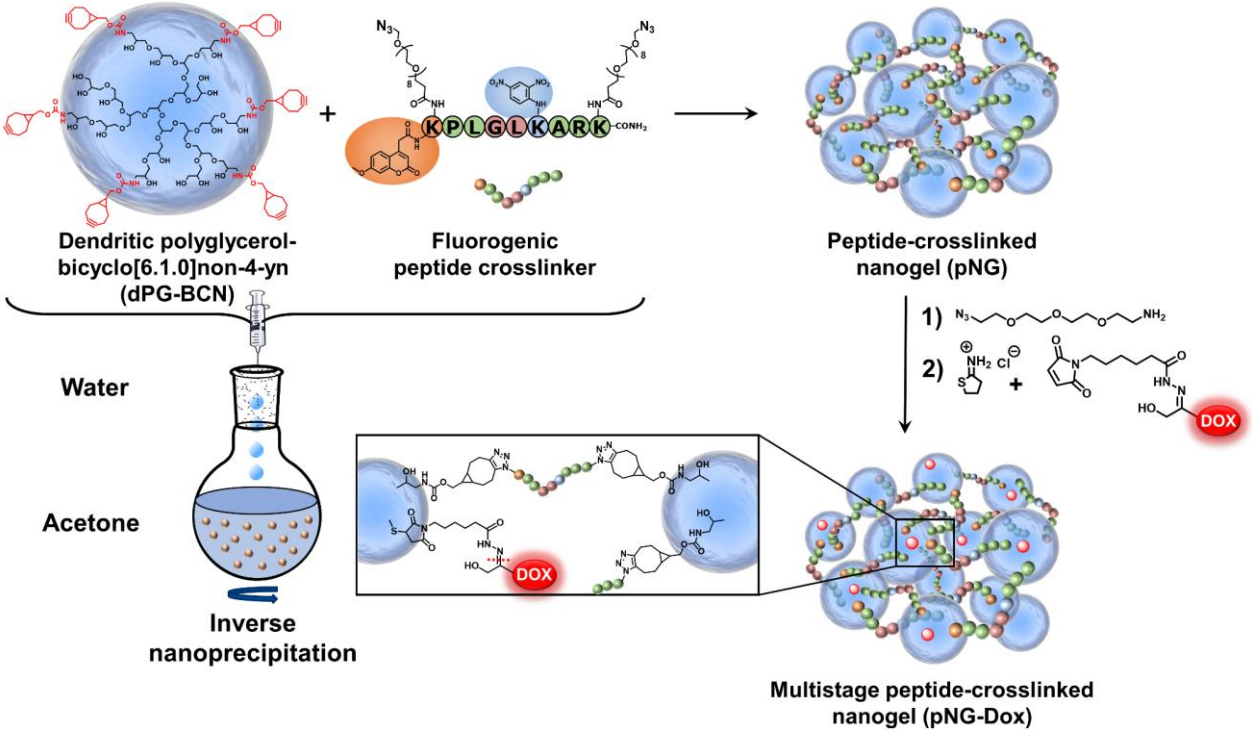

NGs are usually prepared by templating the polymer in confined spaces and subsequent crosslinking inside these templates.[51] The most common methods are the mini- or microemlusion.[52] However, the high shear stress impairs the encapsulation of sensitive cargos and the high amount of surfactants may alter surface properties when not carefully removed during purification. To bring the presented building blocks into nanosized assemblies, we employed the inverse nanoprecipitation technique.[53-55] This mild method avoids extended stirring/sonification (shear stress) and is surfactant-free. For the inverse nanoprecipitation,

water was used as solvent and acetone was chosen as non-solvent. A constant polymer concentration of 3 mg/mL and a solvent/non-solvent ratio of 1:20 were selected as working parameters. These conditions were found to be optimal to obtain stable dispersions and were maintained for synthetic screening. The cyclooctyne functionalities were used in excess and were quenched with azidopropanol, or alternatively, with an azide-functionalized indocarbocyanine dye (ICC) as florescent label. The crosslinking reaction was monitored by FT-IR spectroscopy which showed the disappearance of the azide signal at 2100 cm^{-1} indicating the formation of triazoles by SPAAC (Figure 1a).

We hypothesized that by varying the fraction of the peptide crosslinker in the feed and the crosslinking points on the dPG surface, different sizes and network densities would be obtained. The size is crucial for the fate of the pNGs in a biological environment and the network has an influence on the degradation rate of the pNG which can be optimized for the size reduction or alternatively to tune the release of an encapsulated cargo. Therefore, a rational screening included the variation of dPG-BCN functionalization degree and the fraction of peptide crosslinker in the feed to study their effect on the composition of the polymeric particles. Two degrees of BCN functionalization with 4% and 8% of converted hydroxy groups (~ 5 and 10 groups per dPG) were tested and the peptide crosslinker feed was varied from 10 to 70 w%. The hydrodynamic diameters and polydispersity indices (PDI) as determined by DLS showed narrow, monomodal distributions for the prepared pNGs (Table 1). To complement these results, we confirmed the formation of spherical particles by TEM measurements. The sizes determined by statistical analysis of the TEM images revealed smaller diameters compared to the DLS measurements, which is due to drying and associated deswelling of the particles. For example, particle sizes of ~270 nm were determined for pNG4 by DLS, while TEM images revealed sizes of ~180 nm. Interestingly, pNG7 with a higher peptide feed displayed a size of 180 nm measured by DLS and only slightly smaller sizes of 150 nm were determined by TEM indicating a denser network (Figure 1b).

Overall, the screening of BCN functionalization and peptide feed confirmed that the sizes could be modulated in a broad range between 150 and 650 nm (Figure. 1c). As expected, the nanogel size depended on the weight fraction of the peptide crosslinker. Here, smaller particle sizes were obtained with increasing peptide feed. The higher amount of crosslinker allows a stronger interconnection and additionally may provide stabilization during the nucleation and aggregation process yielding smaller particles. For higher BCN functionalization, we expected

denser and smaller structures. Interestingly, an increase in sizes was observed when the number of BCN groups were doubled while maintaining the same peptide fraction. Besides the solvent/non-solvent and polymer concentration, eventually, the character of the polymer is responsible for the stabilization of the aggregates to prevent coalescence or Ostwald ripening in the nanoprecipitation process.[56] Therefore, a higher functionalization of dPG seems to impair the potential of the polymer to stabilize smaller aggregates that has been observed for other dPG-based nanoparticles prepared by inverse nanoprecipitation.[53, 55] Our screening revealed that the stabilization by dPG in inverse nanoprecipitation is reduced by functionalization with hydrophobic groups. Nevertheless, the tested feed composition allows an application-optimized size adaptation in a broad size range.

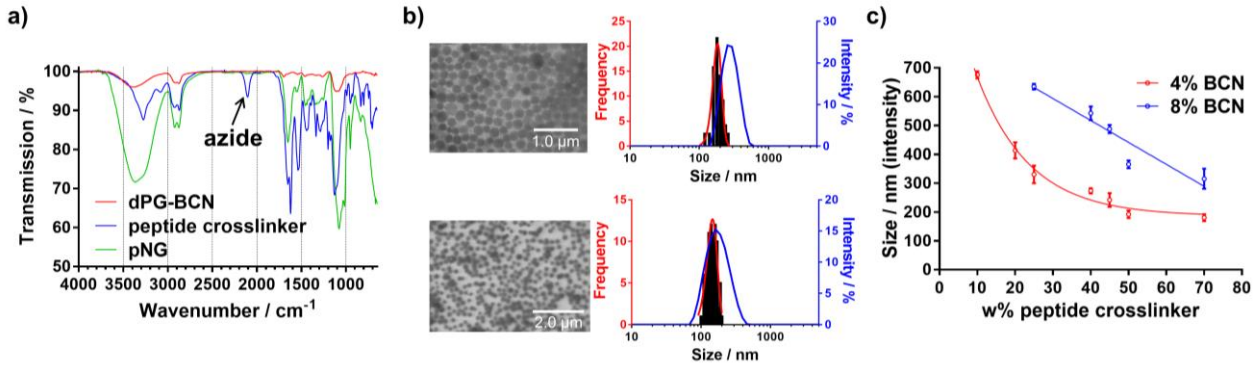

Figure 1. Characterization of pNGs: (a) FT-IR spectra of dPG-BCN (red), peptide crosslinker (blue), and pNGs (green). (b) Representative TEM images of pNGs with 4% BCN functionalization and 40 w% (pNG4) and 70 w% (pNG7) peptide crosslinker and the corresponding statistical analysis of the particle size distribution. (c) Influence of the peptide crosslinker feed and dPG functionalization on pNGs size.

Size reduction and degradation kinetics of pNGs

For the MMP-specific peptide sequence it was reported before that MMP-7 was able to efficiently hydrolyze the crosslinker sequence which resulted in an increased fluorescence signal when incubated with the fluorogenic crosslinker (Figure S3).[40, 57] To confirm the degradability of the prepared nanogels, pNG6 (BCN 4%, 50 w%) was incubated in the presence and absence of the protease MMP-7. Subsequently, particle sizes were monitored by DLS over time. In the first 4 hours, we observed a slight increase in size indicating a swelling of the particles, which we think is due to partial cleavage of crosslinking points and hence loosening of the network. After this time, apparent particle sizes were decreasing suggesting a disintegration of the pNG networks to smaller portions (Figure 2a). For pNG6, size reduction

of approximately 75% compared to the initial size was observed after 16 h (Figure 2b top). As controls for the specific degradation, pNGs were prepared by the same procedure but using a peptide crosslinker comprised of D-amino acids, which cannot be hydrolyzed by MMP-7 (Figure S3). As seen in Figure 2b bottom, these non-cleavable pNGs were stable upon incubation with the protease. These results confirm the MMP-mediated degradability and consequently a size reduction of the pNGs. The degradation was also confirmed by GPC measurements. Here, longer retention times for pNGs were observed after incubated with MMP-7 (Figure S4).

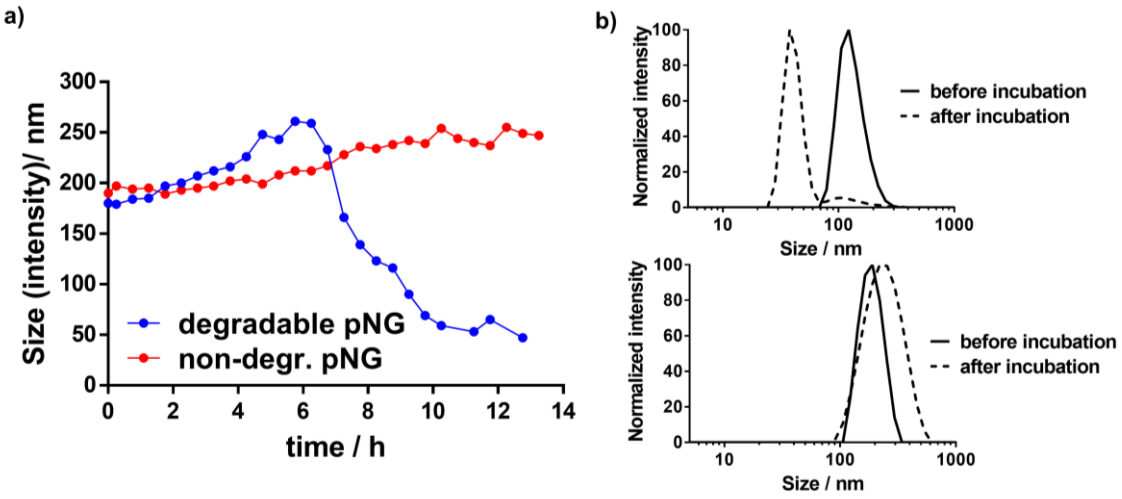

Figure 2. (a) Hydrodynamic diameters of degradable and non-degradable pNGs incubated with MMP-7 over time determined by DLS. (b) Normalized size distributions of degradable (top) and non-degradable (bottom) pNG before and after incubation with MMP-7 for 16 h.

The fluorogenic peptide crosslinker was introduced to conveniently follow the degradation of pNGs by fluorescence measurement since upon cleavage of the peptide crosslinks, the fluorescence of the quenched 7-methoxycoumarin (Mca) dye is regained. A library consisting of four pNGs with 4% and 8% BCN functionalization as well as with low and high peptide crosslinker feed were incubated with MMP-7 and the fluorescence intensities were followed over time. The peptide feed and the BCN functionalization in the pNG formation should affect the interior composition. More BCN groups of the nanogels and higher peptide crosslinker feed should result in a denser network structure which eventually should be reflected in slower degradation rates. The plot of the fluorescence intensities versus time showed indeed that higher BCN functionalization and constant peptide fraction resulted in slower degradation indicating a denser network structure (Figure 3). Faster degradation was observed when the fraction of the peptide was reduced during the synthesis suggesting

network structures, which are easier accessible for the proteases. Since the number of crosslinking points on the dPG was kept constant, higher peptide fractions can form denser networks which eventually lead to smaller particles as observed in the synthetic screening. The effect of peptide fraction on the degradation rate was more pronounced for pNGs prepared with 4% BCN functionalization. Here, the time constant, which describes how rapidly the degradation process occurs, was nearly increased threefold when the peptide fraction was doubled (1.3 h to 3.7 h), whereas, for 8% functionalization, only a minor increase was observed (6.6 Table S1). It can be noted that the non-degradable pNGs did not show an increase of fluorescence signal when incubated with MMP-7 indicating that these NGs are stable at proteolytic conditions (Figure S5).

Since the pNGs are used as DDS, we were interested to see if cells were able to induce the degradation. Therefore, pNGs were incubated with HeLa cells and the fluorescence intensities of Mca were measured over time. Even though with a slower rate, the fluorescence signal was increasing over time suggesting a digestion of the pNGs by cells is feasible (Figure S6).

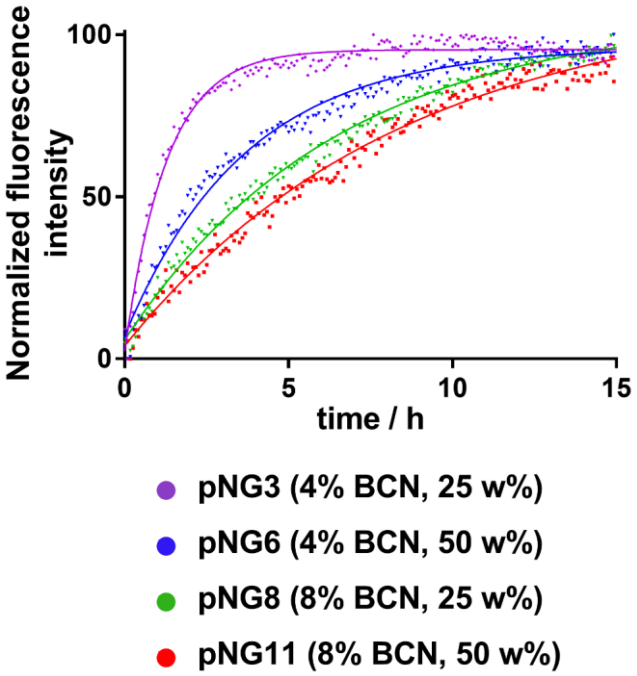

Figure 3. Degradation of pNGs with MMP-7 monitored by an increase of fluorescence signal at 405 nm with time constants of pNGs obtained by the exponential fit. Normalized fluorescence intensity

The incorporation of the fluorogenic peptide crosslinker allowed us to study the impact of different feed ratios and the dPG functionalization degree on the degradation rates which

translates to different interior compositions of the pNGs. By varying the functionalization of dPG and the fraction of the peptide, the degradation rates showed time constants in the range of about 1 h to 6 h. Hence, we demonstrated that the formation of pNGs with an increased feed of peptide crosslinker generated higher crosslinking densities which correspond to the slower cleavage rate. This should allow the tuning of the release kinetics of encapsulated cargo from rather fast to sustained release depending on the desired application.

Conjugation of Dox to obtain multistage pNGs

Considering the previous data, we chose pNG6 as a suitable candidate because the nanogels presented sizes around 200 nm appropriate for the accumulation process by the EPR effect and constant degradation rates with the desired MMP-mediated size shrinkage to 40–50 nm fragments. To realize the conjugation of DOX through a pH-sensitive linkage, we chose a known prodrug of the anticancer drug, namely aldoxorubicin. This prodrug comprises a maleimide group readily reacting with free thiols. This thiol-binding DOX derivative was designed to hitchhike albumin as a carrier in the blood stream by probing a specific cysteine of the serum protein.[58-60] After the crosslinking process, the pNGs were easily modified by quenching the excess of BCN groups with an azide-functionalized cyanine dye (ICC-azide) to label the pNGs or with 1-Azido-4,7,10-trioxa-13-tridecanamine (N_3-TOTA) to introduce amine groups. The ICC label is used to follow the pNGs and the degradation fragments in the following diffusion and penetration experiments. After purification, the free amine groups were thiolated using 2-iminothiolane. The formed thiols readily reacted in a Michael addition reaction with the maleimide groups of aldoxorubicin yielding multistage pNGs (Scheme 2). The approach of in situ thiolation was chosen to avoid crosslinking of the reactive precursors. As before, non-degradable control pNGs were prepared using a peptide crosslinker synthesized with D-amino acids. The hydrodynamic diameters were barely affected by the modification of the pNGs, but the slightly positive surface charge was marginally increased by the attachment of aldoxorubicin HCl salt. The DOX content of the degradable and non-degradable pNGs was determined by UV/Vis spectroscopy with 1.8 w% and 2.0 w%, respectively (Figure S7). All synthesized pNGs had similar sizes and dye/drug loadings allowing to compare their potential to increase the penetration efficiency (Table 2). The acid-mediated release of DOX from the pNGs was confirmed by incubation of the multistage pNGs at pH 7.4 and pH 5 as well as in the presence of MMP-7. Here, we found that the release of DOX is accelerated in acidic pH and in the first 24 h ~50% of DOX was released. In earlier studies, we reported a release of 60% at

pH 5 for aldoxorubicin-derived polymer-drug conjugates,[61] which is slightly higher than observed here, probably caused by interaction with the nanogel network. Therefore, an increase in the release is expected when the pNGs are first digested with MMP and subsequently, exposed to acidic pH values. Indeed, under these conditions, the release was increased to ~60% (Figure S8). At pH 7.4, a minor release of ~25% was observed indicating that DOX is partially encapsulated and can leak out of the nanogel network by diffusion. A small fraction of encapsulated DOX always remained in the network even after intensive purification by dialysis and SEC column. In the mentioned polymer-drug conjugates, release at pH 7.4 was marginal with less than 10% over several days. Therefore, we think that the peptide crosslinker may affect the hydrolysis of the hydrazone which leads to increased release at pH 7.4.

Table 2. Physicochemical characterization of multistage pNGs.

Sample	Peptide linker	Size[a] in nm (DLS)	PDI (DLS)	ζ-potential[b] in mV	Functionalization[c] w%
pNG-NH_2	cleavable	214	0.117	+4	-
pNG-DOX	cleavable	218	0.220	+9	1.8
pNG-ICC	cleavable	244	0.105	+2	0.8
pNG- NH_2	non-cleavable	193	0.043	+5	-
pNG-DOX	non-cleavable	220	0.100	+9	2.0
pNG-ICC	non-cleavable	212	0.026	+3	0.8

[a] Mean hydrodynamic diameter obtained by DLS measurements in H_2O at 25 °C. The intensity distribution is given; b For ζ-potential measurements, electrophoretic mobility of the NGs was analyzed following application of a 20 Vcm^{-1} electric field. *c* Determined by UV/Vis spectroscopy using the extinction coefficient of the ICC dye and DOX, respectively

Diffusive transport in an agarose matrix

The potential of pNGs fragmentation by MMPs to enhance diffusive transport was studied by the penetration of digested and undigested pNGs in dense agarose matrix mimicking the dense ECM in tissue. For this, we first brought solutions of ICC-labeled pNGs and the non-degradable control pNGs before and after incubation with MMP-7 in contact with the agarose gel and incubated for 16 h at 37 °C. Before digestion, degradable and non-degradable pNGs

presented negligible penetration into the agarose gel. However, after incubation with MMP-7, the smaller fragments were able to penetrate deep into the agarose matrix (Figure 4a). The intensity profiles of the fluorescence signal in the gel were plotted in Figure 4b. The signals for non-digested particles and for non-degradable control pNGs incubated with MMP-7 descends to 50% of the initial value after ~2.5 mm, whereas the intensity of digested pNGs was reduced to 50% of the initial value only after 8.9 mm indicating that the penetration is enhanced.

Having confirmed an increased diffusion after pNG degradation using a dye-labeled model NG, we investigated the performance of the multistage DDS pNG-DOX in agarose gel diffusion. In this case, the intrinsic fluorescence of DOX allowed us to follow the infiltration. Before the incubation with MMP, only marginal penetration of DOX was observed (50% after 4.0 mm), whereas after incubation with MMP, the particles diffused into the gel matrix (50% after 6.8 mm; Figure 4c+d).

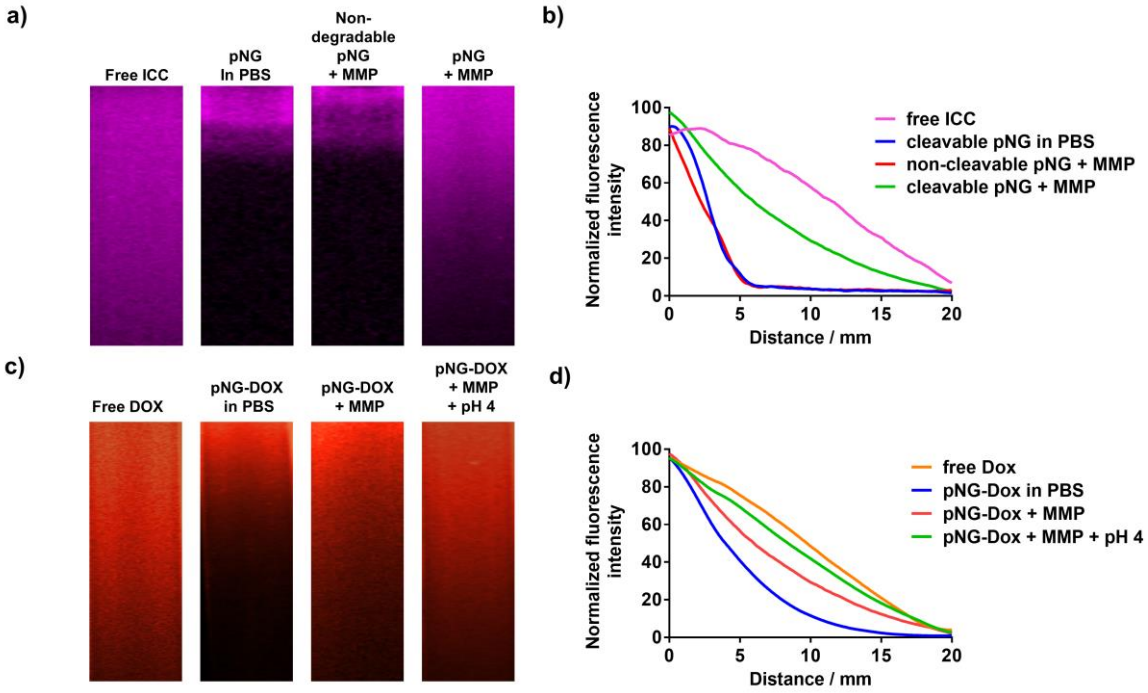

Figure 4. (a) Diffusion of free ICC and ICC-labeled pNGs in agarose gel before and after incubation with MMP-7. (b) Normalized intensity profiles of free ICC and ICC-labeled pNG in agarose gel. (c) Diffusion of free DOX and pNG-DOX in agarose gel before and after incubation with MMP-7 and at acidic pH. (d) Normalized intensity profiles of free DOX and pNG-DOX in agarose gel.

To emulate the second step in the multistage delivery—the pH-dependent release of DOX from dPG by cleavage of the linking hydrazone bond—we further incubated the digested pNGs at acidic pH. Penetration of DOX into the agarose matrix was notably increased to 50% after 8.3 mm. This experiment confirmed an improved diffusion efficiency for degradable pNGs indicating that the fragmentation of the pNG could improve the penetration into the interstitial matrix of tumor tissue.

Penetration into multicellular tumor spheroids

To confirm that the MMP-induced size reduction of pNGs can enable penetration into tumor tissue, we employed multicellular tumor spheroids to test the hypothesis in a tumor-resembling 3D model. MCTS capture complex 3D tissue physiology such as the presence of ECM as well as pH, oxygen, metabolic, and proliferative gradients and provides a useful technique to study anticancer strategies *in vitro*. [62-66] In particular; diffusion-based transport of nanoparticles in an environment that resembles the structural and microenvironmental conditions associated with solid tumors is of great interest.[65, 67] For modeling the cellular diversity in tumor tissues, a variety of spheroid-based co-culture systems have been developed, e.g., with fibroblasts and endothelial cells.[68] Among the major cell types that seem to be important for conditioning the microenvironment are fibroblasts.[69] This cell type is known to be involved in tumor proliferation by promoting invasion to other tissue and by contributing to the formation of metastasis.[70-71] In particular, fibroblasts contribute to tumor invasiveness by producing MMPs which regulate the remodeling of the surrounding ECM.[70, 72] Therefore, co-cultures of cancer cell lines and fibroblasts enable the formation of 3D spheroids models that resemble the tumor physiology and microenvironment and also provide the proteases necessary to degrade the pNGs.

To grow MCTS, HeLa cells and primary fibroblasts at different ratios and cell numbers were screened to reproducibly obtain spheroids with sizes of ~500 µm. For a mixture of HeLa and fibroblasts in ratio 2:1, spheroids were obtained after 4 days and further grew to dense circular structures with sizes of approximately 500 µm after 7–9 days (Figure S2).

To investigate the diffusion properties of the DDS in MCTS, we first used the dye-labeled model pNGs. MCTS with sizes of around 500 µm were treated with ICC-labeled degradable (pNG-ICC) and non-degradable pNGs (non-degradable pNG-ICC). In the first set of experiments, spheroids were washed after incubation with the compounds for 16 h, fixed, and

directly imaged using a CLSM. The z-stack function was used to optically section the spheroids in 20 µm steps. Here, we could indeed observe that the free dye and degradable pNGs penetrate deeper compared to the non-degradable control. However, when the images were compared with the brightfield image (Figure S9), it appeared that only the surface of the spheroids was imaged as the laser light is absorbed by the tumoroid tissue resulting in a limited penetration depth. To compensate for the absorption of the laser light in large objects, the spheroids were mounted between a microscope slide and cover glass and were thereby slightly squeezed (Figure 5b). With these MCTS, optical sectioning in the confocal microscope allowed to image the central region of the spheroids since the laser light does not need to penetrate into deeper layers. We found that the free dye used to label the pNGs had penetrated to the interior of the MCTS to a point where the signal abruptly decreased (Figure 5a) because the light absorption of the tissue is too large to obtain proper signals. Nevertheless, optical sections of spheroids treated with the degradable control displayed an efficient penetration into the spheroid. Compared to the free dye, the distribution of the fluorescence signal is not as homogeneous as for the degradable pNGs indicating that larger fragments may accumulate in more spacious regions of the spheroid. A distinct difference is apparent in comparison to the non-degradable control. Here, all sections displayed a low intensity and only a marginal signal was observed in deeper layers confirming that the non-degradable pNGs are not able to diffuse into the MCTS.

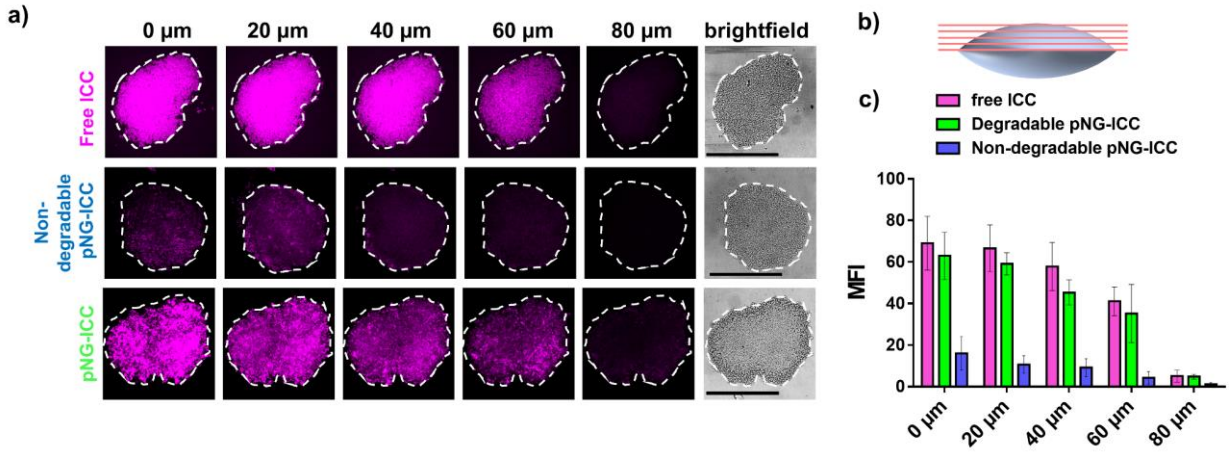

Figure 5. a) Penetration of free ICC, degradable, and non-degradable pNGs into MCTS in different layers. The black bars in the brightfield images represent 500 µm. (b) Schematic representation of the flattened spheroids and the optical sections. (c) Mean fluorescence intensities of ICC in the area of the MCTS for increasing depth.

The graph in Figure 5c shows the mean fluorescence intensity (MFI) over the area of the spheroid section illustrating that free dye and the degradable nanogel display similar intensity with a slow decrease for deeper sections.

To confirm the results obtained from optical sections, cryosections of the spheroids incubated with labeled pNG-ICC for 2 h and 16 h were prepared. Representative cryosections from the mid-region of spheroids were imaged by fluorescence microscopy. Free ICC and DAPI were found to be homogeneously distributed throughout the sections at both time points indicating an unhindered diffusion of the free dye through the spheroid (Figure 6a). Only minor intensity was observed at the margins of the spheroids for the degradable pNGs and the non-degradable control after 2 h. For longer incubation time, we found minimally increased fluorescence intensity when treated with the non-degradable pNGs. At the periphery, intense signals were observed, however, the intensity was rapidly declining over the first 20 to 30 µm towards the center of the section. When the degradable pNGs was incubated for 16 h with the MCTS, intense fluorescence was observed throughout the section area (Figure 6b). The sections showed a gradient with higher fluorescence intensity at the periphery that decreased towards the core which is apparent from the images with higher magnification (Figure 6c). It is notable that the core still possessed distinct fluorescence intensity suggesting that the degradation products penetrated to the core of the spheroids. These observations support the results of the optical sections and confirm that the degradable property of the pNGs enables an efficient penetration of the tumor-resembling 3D model. Since we have shown before that the fragmentation of the pNGs is caused by proteases (Figure 2), we can assume that fragmentation in the tumor model is also caused by expressed proteases. It has been reported that MMPs are indeed expressed by cancer cell lines and in particular in co-cultures using primary cells.[73-74]

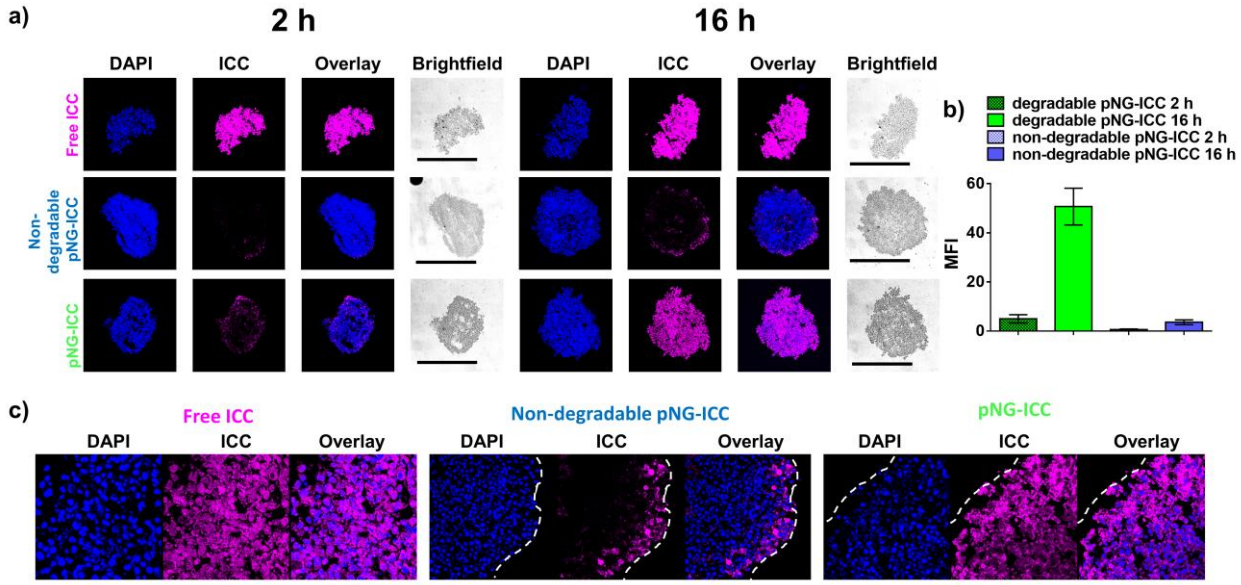

Figure 6. (a) CLSM images of MCTS cryosections with 20-fold magnification. MCTS were incubated with free ICC, degradable, and non-degradable pNG-ICC for 2 h and 16 h, respectively. Images were obtained with flattened spheroids and optical sectioning. (b) Mean fluorescence intensity over the area of spheroid sections. (c) CLSM images of cryosections with 64-fold magnification.

To demonstrate that the results obtained from the dye-labeled pNG can be transferred to the performance of the multistage pNG-Dox, spheroids were incubated with the multistage pNGs, free DOX, and the non-degradable control. After incubation, we could see that the free drug was distributed homogeneously throughout the spheroids with slightly decreasing fluorescence intensity for deeper regions. In comparison, the penetration for the degradable pNG-DOX was considerably higher than for the non-degradable control especially for deep sections of the tumor spheroids (Figure 7a). This indicates that pNGs are degraded and that the small fragments possessed an advantage in penetrating into deep regions of the 3D tumor model. Comparing to the penetration study using dPG-ICC, it can be noted that the DOX penetration for the non-degradable system was higher than for the non-degradable dPG-ICC (Figure 7b). This can be explained by either premature DOX release or diffusion of small fractions of encapsulated DOX. The confocal images at higher magnification illustrate the enhanced penetration of DOX for the degradable pNGs (Figure 7c).

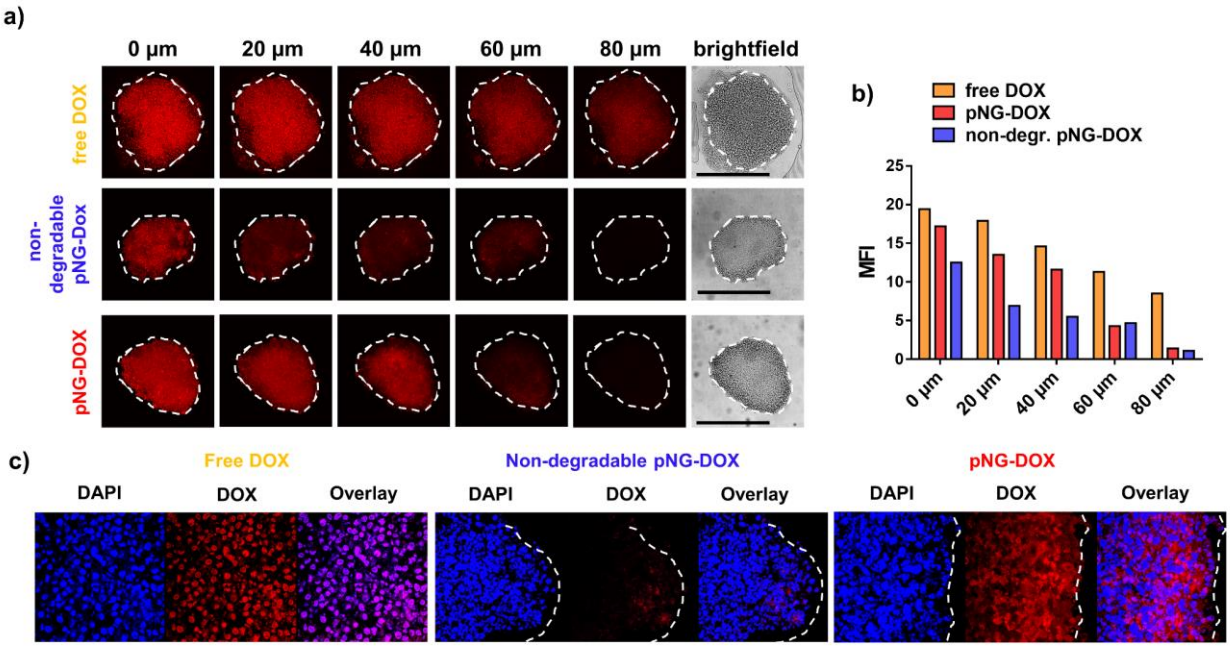

Figure 7. (a) Penetration of dPG-DOX into MCTS: Comparison of free DOX, degradable multistage pNGs, and the non-degradable control. The black bars in the brightfield images represent 500 µm. (b) Mean fluorescence intensity of DOX in the area of the MCTS for different penetration depth. (c) CLSM images of cryosections with 64-fold magnification.

To complement this data, cryosections of MCTS incubated with pNG-DOX and controls were prepared for 2 h and 16 h (Figure S11). For the degradable dPG-Dox a time-dependent increase in penetration depth of DOX fluorescence was observed, whereas for the non-degradable control no change was visible over time. These observations support the results of the optical sections and confirm that the size reduction property of the pNGs enhances the transport of the therapeutic agent into the tumor-resembling 3D model

Therapeutic activity of multistage pNG

To confirm that DOX is still therapeutically active after multistage degradation of the pNG and deep tissue penetration, we analyzed the activity of DOX on cell viability after the incubation with pNGs in monolayer culture as well as in MCTS. For the monolayered culture, the viability was determined by the ability of the cells to metabolize MTT. Since we obtained low signals with MTT for the evaluation of the spheroid model, we assessed the viability of cells in spheroids by measuring intracellular ATP content using the CellTiter-Glo® assay. The bare pNGs did not display any toxicity towards HeLa cells up to the highest concentration tested (0.25 mg/mL), whereas free DOX and the multistage pNG-DOX reduced the viability of HeLa

cells for higher DOX concentrations (Figure 8a). Interestingly, minor toxicity towards HeLa cells was also observed for the non-degradable control indicating that the degradability of the pNGs plays a crucial role in the therapeutic activity. Since the release of DOX for the pNGS was marginal at pH 7.4 but increased under acidic conditions as found in intracellular compartments this result suggest that the non-degradable pNG are internalized less by the cells and that the small fragments of the degradable pNGs can be taken up more easily. This observation is supported by the magnified images of the cryosections where we see the fluorescence associated with the digested pNGs and the drug is localized inside the cells (Figure 6c+7c).

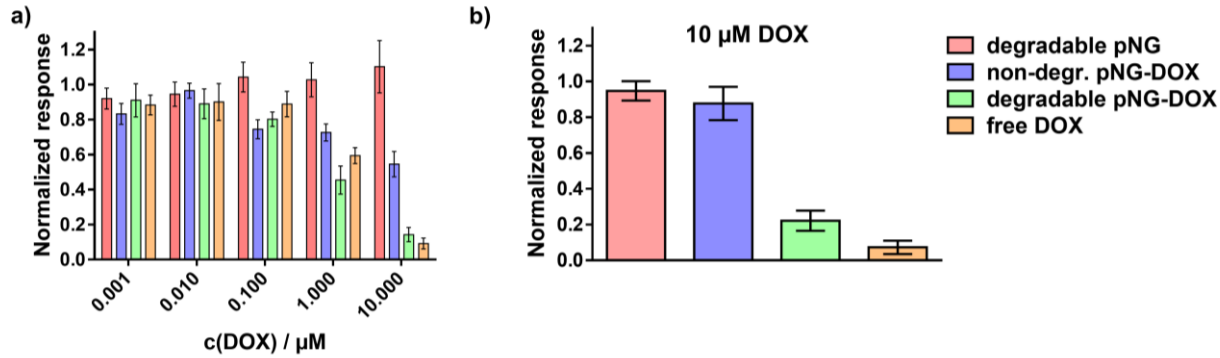

Figure 8. Therapeutic activity of DOX in the multistage DDS. Cell viability: (a) After treatment with different concentration of pNG-DOX and controls in monolayer culture of HeLa cells. (b) After treatment with pNG-DOX and controls at 10 µM DOX concentration in MCTS model after 48 h of treatment, respectively.

For the 3D model, the non-degradable control marginally inhibited the proliferation of the spheroids when treated with a DOX concentration of 10 µM. In contrast, when treated with the degradable pNG-DOX, ATP concentrations were reduced to 22% relative to the untreated control (Figure 8b). The difference emphasizes that degradation-induced penetration is crucial for the treatment of the tumor model to deliver the drug to the inner regions. Therefore, we suggest the two-stage strategy of the presented multistage pNGs as potential nanocarrier-based DDS for systemically applied drug delivery. After extravasation to the tumor tissue, the protease-mediated fragmentation could enhance the tumor penetration to promote uniform drug distribution.

CONCLUSIONS

In summary, we prepared a novel MMP- and pH-sensitive multistage delivery system in the form of pNGs. The incorporation of a smart fluorogenic peptide crosslinkers into a hydrophilic, dPG-based scaffold provided degradability into synthetic NGs comprised of otherwise non-degradable polymers. The size reduction of these particles can be triggered by an endogenous stimulus in the tumor microenvironment, and thereby promotes the penetration of polymer-drug conjugates. The pNGs were prepared by surfactant-free inverse nanoprecipitation using strain-promoted click chemistry. The procedure yielded NGs with spherical morphology and good to excellent size distribution. The variation of BCN functionalization on dPG and the fraction of the peptide crosslinker allowed control over the size and the degree of crosslinking. The size reduction property of the pNGs in the presence of MMP was demonstrated by time-dependent size measurements showing the desired reduction from several 100 nm to sub-50 nm fragments. The MMP-mediated degradation was studied in detail by fluorescence measurements following fluorescence recovery of the intrinsic reporter moiety of the crosslinker. Here, we found that the degradation rate depends on the feed ratio and BCN functionalization with slower rates for higher crosslinker feed. This feature could be used to tune the release rate of an encapsulated cargo. The pNGs were post-synthetically modified to covalently attach the chemotherapeutic drug DOX through an acid-sensitive hydrazone linkage. The size and surface charge were barely affected by the modification, and the release of DOX from the pNGs was enhanced at acidic conditions. The digested multistage pNGs showed enhanced diffusive transport through a dense gel matrix and we could successfully demonstrate in tumor resembling MCTS models that the size-changing property of the pNGs can promote the infiltration of the functional chemotherapeutic drug into deeper tissue regions. Therefore, the multistage dPG constitutes a potential nanocarrier for systemic application to promote drug delivery in solid tumors.

ACKNOWLEDGEMENT

The authors gratefully acknowledge financial support from the Bundesministerium für Bildung und Forschung (BMBF) through the NanoMatFutur award (ThermoNanogele, 13N12561), the Freie Universität Focus Area Nanoscale, and the Deutsche Forschungsgemeinschaft (DFG) through the Collaborative Research Center 1112 (SFB 1112), project A04. The authors acknowledge Emanuel Glitscher and Dr. Julián Bergueiro Álvarez for performing the TEM measurements as well as Sebastian Heintze for maintenance of the cell culture and his help

with performing cytotoxicity assays and spheroid culture. Dr. Julián Bergueiro Álvarez and Ernesto Rafael Osorio Blanco are acknowledged for his help to prepare the graphical art work. We thank Dr. Anke Hoppensack and Johanna Scholz for the preparation of the fibroblasts.

REFERENCES

1. Tong, R.; Kohane, D. S., New Strategies in Cancer Nanomedicine. *Annual Review of Pharmacology and Toxicology* **2016,** *56* (1), 41-57.
2. Tran, S.; DeGiovanni, P.-J.; Piel, B.; Rai, P., Cancer nanomedicine: a review of recent success in drug delivery. *Clinical and Translational Medicine* **2017,** *6* (1), 44.
3. Shi, J.; Kantoff, P. W.; Wooster, R.; Farokhzad, O. C., Cancer nanomedicine: progress, challenges and opportunities. *Nature Reviews Cancer* **2016,** *17*, 20-37.
4. Blanco, E.; Shen, H.; Ferrari, M., Principles of nanoparticle design for overcoming biological barriers to drug delivery. *Nature Biotechnology* **2015,** *33*, 941.
5. Wang, J.; Mao, W.; Lock, L. L.; Tang, J.; Sui, M.; Sun, W.; Cui, H.; Xu, D.; Shen, Y., The Role of Micelle Size in Tumor Accumulation, Penetration, and Treatment. *ACS Nano* **2015,** *9* (7), 7195–7206.
6. Jain, R. K.; Stylianopoulos, T., Delivering nanomedicine to solid tumors. *Nature Reviews Clinical Oncology* **2010,** *7*, 653.
7. Maeda, H.; Wu, J.; Sawa, T.; Matsumura, Y.; Hori, K., Tumor vascular permeability and the EPR effect in macromolecular therapeutics: a review. *Journal of Controlled Release* **2000,** *65* (1), 271-284.
8. Maeda, H.; Tsukigawa, K.; Fang, J., A Retrospective 30 Years After Discovery of the Enhanced Permeability and Retention Effect of Solid Tumors: Next-Generation Chemotherapeutics and Photodynamic Therapy—Problems, Solutions, and Prospects. *Microcirculation* **2016,** *23* (3), 173-182.
9. Nakamura, Y.; Mochida, A.; Choyke, P. L.; Kobayashi, H., Nanodrug Delivery: Is the Enhanced Permeability and Retention Effect Sufficient for Curing Cancer? *Bioconjugate Chemistry* **2016**.
10. Dreher, M. R.; Liu, W.; Michelich, C. R.; Dewhirst, M. W.; Yuan, F.; Chilkoti, A., Tumor Vascular Permeability, Accumulation, and Penetration of Macromolecular Drug Carriers. *JNCI: Journal of the National Cancer Institute* **2006,** *98* (5), 335-344.
11. Cabral, H.; Matsumoto, Y.; Mizuno, K.; Chen, Q.; Murakami, M.; Kimura, M.; Terada, Y.; Kano, M. R.; Miyazono, K.; Uesaka, M.; Nishiyama, N.; Kataoka, K., Accumulation of sub-100 nm polymeric micelles in poorly permeable tumours depends on size. *Nature Nanotechnology* **2011,** *6*, 815.
12. Helmlinger, G.; Yuan, F.; Dellian, M.; Jain, R. K., Interstitial pH and pO2 gradients in solid tumors in vivo: high-resolution measurements reveal a lack of correlation. *Nat Med* **1997,** *3* (2), 177-82.
13. Brown, J. M.; Giaccia, A. J., The Unique Physiology of Solid Tumors: Opportunities (and Problems) for Cancer Therapy. *Cancer Research* **1998,** *58* (7), 1408-1416.
14. Helmlinger, G.; Yuan, F.; Dellian, M.; Jain, R. K., Interstitial pH and pO2 gradients in solid tumors in vivo: High-resolution measurements reveal a lack of correlation. *Nature Medicine* **1997,** *3*, 177.
15. Giaccone, G.; Pinedo, H. M., Drug Resistance. *The Oncologist* **1996,** *1* (1), 82-87.
16. Trédan, O.; Galmarini, C. M.; Patel, K.; Tannock, I. F., Drug Resistance and the Solid Tumor Microenvironment. *JNCI: Journal of the National Cancer Institute* **2007,** *99* (19), 1441-1454.
17. Ju, C.; Mo, R.; Xue, J.; Zhang, L.; Zhao, Z.; Xue, L.; Ping, Q.; Zhang, C., Sequential Intra-Intercellular Nanoparticle Delivery System for Deep Tumor Penetration. *Angewandte Chemie International Edition* **2014,** *53* (24), 6253-6258.
18. Yim, H.; Park, S.-j.; Bae, Y. H.; Na, K., Biodegradable cationic nanoparticles loaded with an anticancer drug for deep penetration of heterogeneous tumours. *Biomaterials* **2013,** *34* (31), 7674–7682.
19. Chen, B.; Dai, W.; He, B.; Zhang, H.; Wang, X.; Wang, Y.; Zhang, Q., Current Multistage Drug Delivery Systems Based on the Tumor Microenvironment. *Theranostics* **2017,** *7* (3), 538-558.

20. Li, H.-J.; Du, J.-Z.; Du, X.-J.; Xu, C.-F.; Sun, C.-Y.; Wang, H.-X.; Cao, Z.-T.; Yang, X.-Z.; Zhu, Y.-H.; Nie, S.; Wang, J., Stimuli-responsive clustered nanoparticles for improved tumor penetration and therapeutic efficacy. *Proceedings of the National Academy of Sciences* **2016,** *113* (15), 4164-4169.
21. Zan, M.; Li, J.; Luo, S.; Ge, Z., Dual pH-triggered multistage drug delivery systems based on host–guest interaction-associated polymeric nanogels. *Chemical Communications* **2014,** *50* (58), 7824-7827.
22. Li, J.; Han, Y.; Chen, Q.; Shi, H.; ur Rehman, S.; Siddiq, M.; Ge, Z.; Liu, S., Dual endogenous stimuli-responsive polyplex micelles as smart two-step delivery nanocarriers for deep tumor tissue penetration and combating drug resistance of cisplatin. *Journal of Materials Chemistry B* **2014,** *2* (13), 1813-1824.
23. de la Rica, R.; Aili, D.; Stevens, M. M., Enzyme-responsive nanoparticles for drug release and diagnostics. *Advanced Drug Delivery Reviews* **2012,** *64* (11), 967-978.
24. Zhu, Q.; Chen, X.; Xu, X.; Zhang, Y.; Zhang, C.; Mo, R., Tumor-Specific Self-Degradable Nanogels as Potential Carriers for Systemic Delivery of Anticancer Proteins. *Advanced Functional Materials* **2018,** *28* (17), 1707371.
25. Wong, C.; Stylianopoulos, T.; Cui, J.; Martin, J.; Chauhan, V. P.; Jiang, W.; Popović, Z.; Jain, R. K.; Bawendi, M. G.; Fukumura, D., Multistage nanoparticle delivery system for deep penetration into tumor tissue. *Proceedings of the National Academy of Sciences* **2011,** *108* (6), 2426–2431.
26. Ruan, S.; Zhang, L.; Chen, J.; Cao, T.; Yang, Y.; Liu, Y.; He, Q.; Gao, F.; Gao, H., Targeting delivery and deep penetration using multistage nanoparticles for triple-negative breast cancer. *RSC Advances* **2015,** *5* (79), 64303-64317.
27. Hu, G.; Wang, Y.; He, Q.; Gao, H., Multistage drug delivery system based on microenvironment-responsive dendrimer-gelatin nanoparticles for deep tumor penetration. *RSC Advances* **2015,** *5* (104), 85933-85937.
28. Kessenbrock, K.; Plaks, V.; Werb, Z., Matrix Metalloproteinases: Regulators of the Tumor Microenvironment. *Cell* **2010,** *141* (1), 52-67.
29. Nielsen, B. S.; Timshel, S.; Kjeldsen, L.; Sehested, M.; Pyke, C.; Borregaard, N.; Danø, K., 92 kDa type IV collagenase (MMP-9) is expressed in neutrophils and macrophages but not in malignant epithelial cells in human colon cancer. *International Journal of Cancer* **1996,** *65* (1), 57-62.
30. Brown, P. D.; Bloxidge, R. E.; Anderson, E.; Howell, A., Expression of activated gelatinase in human invasive breast carcinoma. *Clinical & Experimental Metastasis* **1993,** *11* (2), 183-189.
31. Iwata, H.; Kobayashi, S.; Iwase, H.; Masaoka, A.; Fujimoto, N.; Okada, Y., Production of Matrix Metalloproteinases and Tissue Inhibitors of Metalloproteinases in Human Breast Carcinomas. *Japanese Journal of Cancer Research* **1996,** *87* (6), 602-611.
32. Takao Nakagawa; Toshihiko Kubota; Masanori Kabuto; Kazufumi Sato; Hirokazu Kawano; Taro Hayakawa; Yasunori Okada, Production of matrix metalloproteinases and tissue inhibitor of metalloproteinases-1 by human brain tumors. *Journal of Neurosurgery* **1994,** *81* (1), 69-77.
33. Page-McCaw, A.; Ewald, A. J.; Werb, Z., Matrix metalloproteinases and the regulation of tissue remodelling. *Nature reviews. Molecular cell biology* **2007,** *8* (3), 221-233.
34. Roy, R.; Yang, J.; Moses, M. A., Matrix Metalloproteinases As Novel Biomarker s and Potential Therapeutic Targets in Human Cancer. *Journal of Clinical Oncology* **2009,** *27* (31), 5287–5297.
35. Han, J.-C.; Li, X.-D.; Du, J.; Xu, F.; Wei, Y.-J.; Li, H.-B.; Zhang, Y.-J., Elevated matrix metalloproteinase-7 expression promotes metastasis in human lung carcinoma. *World Journal of Surgical Oncology* **2015,** *13* (1), 1–10.
36. Andrieu, J.; Kotman, N.; Maier, M.; Mailänder, V.; Strauss, W. S. L.; Weiss, C. K.; Landfester, K., Live Monitoring of Cargo Release From Peptide-Based Hybrid Nanocapsules Induced by Enzyme Cleavage. *Macromolecular Rapid Communications* **2012,** *33* (3), 248–253.
37. Maier, M.; Kotman, N.; Friedrichs, C.; Andrieu, J.; Wagner, M.; Graf, R.; Strauss, W. S. L.; Mailänder, V.; Weiss, C. K.; Landfester, K., Highly Site Specific, Protease Cleavable, Hydrophobic Peptide–Polymer Nanoparticles. *Macromolecules* **2011,** *44* (16), 6258–6267.
38. Wei, X.; Luo, Q.; Sun, L.; Li, X.; Zhu, H.; Guan, P.; Wu, M.; Luo, K.; Gong, Q., Enzyme- and pH-Sensitive Branched Polymer–Doxorubicin Conjugate-Based Nanoscale Drug Delivery System for Cancer Therapy. *ACS Applied Materials & Interfaces* **2016,** *8* (18), 11765–11778.

39. Calderón, M.; Graeser, R.; Kratz, F.; Haag, R., Development of enzymatically cleavable prodrugs derived from dendritic polyglycerol. *Bioorganic & Medicinal Chemistry Letters* **2009,** *19* (14), 3725-3728.
40. Moss, J. A.; Stokols, S.; Hixon, M. S.; Ashley, F. T.; Chang, J. Y.; Janda, K. D., Solid-phase synthesis and kinetic characterization of fluorogenic enzyme-degradable hydrogel cross-linkers. *Biomacromolecules* **2006,** *7* (4), 1011–1016.
41. Asadian-Birjand, M.; Sousa-Herves, A.; Steinhilber, D.; Cuggino, J. C.; Calderon, M., Functional nanogels for biomedical applications. *Current medicinal chemistry* **2012,** *19* (29), 5029-43.
42. Ekkelenkamp, A. E.; Elzes, M. R.; Engbersen, J. F. J.; Paulusse, J. M. J., Responsive crosslinked polymer nanogels for imaging and therapeutics delivery. *Journal of Materials Chemistry B* **2018,** *6* (2), 210-235.
43. Calderón, M.; Welker, P.; Licha, K.; Fichtner, I.; Graeser, R.; Haag, R.; Kratz, F., Development of efficient acid cleavable multifunctional prodrugs derived from dendritic polyglycerol with a poly(ethylene glycol) shell. *Journal of Controlled Release* **2011,** *151* (3), 295-301.
44. Murphy, R. F.; Powers, S.; Cantor, C. R., Endosome pH measured in single cells by dual fluorescence flow cytometry: rapid acidification of insulin to pH 6. *The Journal of cell biology* **1984,** *98* (5), 1757-62.
45. Willner, D.; Trail, P. A.; Hofstead, S. J.; King, H. D.; Lasch, S. J.; Braslawsky, G. R.; Greenfield, R. S.; Kaneko, T.; Firestone, R. A., (6-Maleimidocaproyl)hydrazone of doxorubicin. A new derivative for the preparation of immunoconjugates of doxorubicin. *Bioconjugate Chemistry* **1993,** *4* (6), 521-527.
46. Roller, S.; Zhou, H.; Haag, R., High-loading polyglycerol supported reagents for Mitsunobu- and acylation-reactions and other useful polyglycerol derivatives. *Molecular Diversity* **2005,** *9* (4), 305-316.
47. Mikhail, A. S.; Eetezadi, S.; Ekdawi, S. N.; Stewart, J.; Allen, C., Image-based analysis of the size- and time-dependent penetration of polymeric micelles in multicellular tumor spheroids and tumor xenografts. *International Journal of Pharmaceutics* **2014,** *464* (1), 168-177.
48. Cabral, H.; Matsumoto, Y.; Mizuno, K.; Chen, Q.; Murakami, M.; Kimura, M.; Terada, Y.; Kano, M. R.; Miyazono, K.; Uesaka, M.; Nishiyama, N.; Kataoka, K., „ Accumulation of sub-100 nm polymeric micelles in poorly permeable tumours depends on size. *Nat Nano* **2011,** *6* (12), 815–823.
49. Frey, H.; Haag, R., Dendritic polyglycerol: a new versatile biocompatible material. *Reviews in Molecular Biotechnology* **2002,** *90* (3–4), 257–267.
50. Jiang, Y.; Chen, J.; Deng, C.; Suuronen, E. J.; Zhong, Z., Click hydrogels, microgels and nanogels: Emerging platforms for drug delivery and tissue engineering. *Biomaterials* **2014,** *35* (18), 4969–4985.
51. Oh, J. K.; Drumright, R.; Siegwart, D. J.; Matyjaszewski, K., The development of microgels/nanogels for drug delivery applications. *Progress in Polymer Science* **2008,** *33* (4), 448–477.
52. Crespy, D.; Landfester, K., Miniemulsion polymerization as a versatile tool for the synthesis of functionalized polymers. *Beilstein Journal of Organic Chemistry* **2010,** *6*, 1132-1148.
53. Steinhilber, D.; Witting, M.; Zhang, X.; Staegemann, M.; Paulus, F.; Friess, W.; Küchler, S.; Haag, R., Surfactant free preparation of biodegradable dendritic polyglycerol nanogels by inverse nanoprecipitation for encapsulation and release of pharmaceutical biomacromolecules. *Journal of Controlled Release* **2013,** *169* (3), 289–295.
54. Giulbudagian, M.; Asadian-Birjand, M.; Steinhilber, D.; Achazi, K.; Molina, M.; Calderon, M., Fabrication of thermoresponsive nanogels by thermo-nanoprecipitation and in situ encapsulation of bioactives. *Polymer Chemistry* **2014,** *5* (24), 6909–6913.
55. Vossen, L.; Wedepohl, S.; Calderón, M., A Facile, One-Pot, Surfactant-Free Nanoprecipitation Method for the Preparation of Nanogels from Polyglycerol–Drug Conjugates that Can Be Freely Assembled for Combination Therapy Applications. *Polymers* **2018,** *10* (4), 398.
56. Schubert, S.; Delaney, J. J. T.; Schubert, U. S., Nanoprecipitation and nanoformulation of polymers: from history to powerful possibilities beyond poly(lactic acid). *Soft Matter* **2011,** *7* (5), 1581-1588.
57. Neumann, U.; Kubota, H.; Frei, K.; Ganu, V.; Leppert, D., Characterization of Mca-Lys-Pro-Leu-Gly-Leu-Dpa-Ala-Arg-NH2, a fluorogenic substrate with increased specificity constants for collagenases and tumor necrosis factor converting enzyme. *Analytical Biochemistry* **2004,** *328* (2), 166–173.

58. Kratz, F.; Müller-Driver, R.; Hofmann, I.; Drevs, J.; Unger, C., A Novel Macromolecular Prodrug Concept Exploiting Endogenous Serum Albumin as a Drug Carrier for Cancer Chemotherapy. *Journal of Medicinal Chemistry* **2000,** *43* (7), 1253-1256.
59. Kratz, F.; Warnecke, A.; Scheuermann, K.; Stockmar, C.; Schwab, J.; Lazar, P.; Drückes, P.; Esser, N.; Drevs, J.; Rognan, D.; Bissantz, C.; Hinderling, C.; Folkers, G.; Fichtner, I.; Unger, C., Probing the Cysteine-34 Position of Endogenous Serum Albumin with Thiol-Binding Doxorubicin Derivatives. Improved Efficacy of an Acid-Sensitive Doxorubicin Derivative with Specific Albumin-Binding Properties Compared to That of the Parent Compound. *Journal of Medicinal Chemistry* **2002,** *45* (25), 5523-5533.
60. Kratz, F., DOXO-EMCH (INNO-206): the first albumin-binding prodrug of doxorubicin to enter clinical trials. *Expert Opinion on Investigational Drugs* **2007,** *16* (6), 855-866.
61. Krüger, H. R.; Schütz, I.; Justies, A.; Licha, K.; Welker, P.; Haucke, V.; Calderón, M., Imaging of doxorubicin release from theranostic macromolecular prodrugs via fluorescence resonance energy transfer. *Journal of Controlled Release* **2014,** *194* (Supplement C), 189–196.
62. Acker, H.; Carlsson, J.; Mueller-Klieser, W.; Sutherland, R. M., Comparative pO2 measurements in cell spheroids cultured with different techniques. *British Journal Of Cancer* **1987,** *56*, 325.
63. Nederman, T.; Norling, B.; Glimelius, B.; Carlsson, J.; Brunk, U., Demonstration of an Extracellular Matrix in Multicellular Tumor Spheroids. *Cancer Research* **1984,** *44* (7), 3090-3097.
64. Rotin, D.; Robinson, B.; Tannock, I. F., Influence of Hypoxia and an Acidic Environment on the Metabolism and Viability of Cultured Cells: Potential Implications for Cell Death in Tumors. *Cancer Research* **1986,** *46* (6), 2821-2826.
65. Huang, B.-W.; Gao, J.-Q., Application of 3D cultured multicellular spheroid tumor models in tumor-targeted drug delivery system research. *Journal of Controlled Release* **2018,** *270*, 246-259.
66. Griffith, L. G.; Swartz, M. A., Capturing complex 3D tissue physiology in vitro. *Nature Reviews Molecular Cell Biology* **2006,** *7*, 211.
67. Hirschhaeuser, F.; Menne, H.; Dittfeld, C.; West, J.; Mueller-Klieser, W.; Kunz-Schughart, L. A., Multicellular tumor spheroids: An underestimated tool is catching up again. *Journal of Biotechnology* **2010,** *148* (1), 3-15.
68. Wenger, A.; Kowalewski, N.; Stahl, A.; Mehlhorn, A. T.; Schmal, H.; Stark, G. B.; Finkenzeller, G., Development and Characterization of a Spheroidal Coculture Model of Endothelial Cells and Fibroblasts for Improving Angiogenesis in Tissue Engineering. *Cells Tissues Organs* **2005,** *181* (2), 80-88.
69. Österholm, C.; Lu, N.; Lidén, Å.; Karlsen, T. V.; Gullberg, D.; Reed, R. K.; Kusche-Gullberg, M., Fibroblast EXT1-Levels Influence Tumor Cell Proliferation and Migration in Composite Spheroids. *PLOS ONE* **2012,** *7* (7), e41334.
70. Kalluri, R.; Zeisberg, M., Fibroblasts in cancer. *Nature Reviews Cancer* **2006,** *6*, 392.
71. Bhowmick, N. A.; Neilson, E. G.; Moses, H. L., Stromal fibroblasts in cancer initiation and progression. *Nature* **2004,** *432*, 332.
72. Nyga, A.; Cheema, U.; Loizidou, M., 3D tumour models: novel in vitro approaches to cancer studies. *Journal of Cell Communication and Signaling* **2011,** *5* (3), 239.
73. Paduch, R.; Kandefer-Szerszeń, M., Expression and activation of proteases in co-cultures. *Experimental and Toxicologic Pathology* **2011,** *63* (1), 79-87.
74. Morini, M.; Mottolese, M.; Ferrari, N.; Ghiorzo, F.; Buglioni, S.; Mortarini, R.; Noonan, D. M.; Natali, P. G.; Albini, A., The α3β1 integrin is associated with mammary carcinoma cell metastasis, invasion, and gelatinase B (mmp-9) activity. *International Journal of Cancer* **2000,** *87* (3), 336-342.

TABLE OF CONTENTS

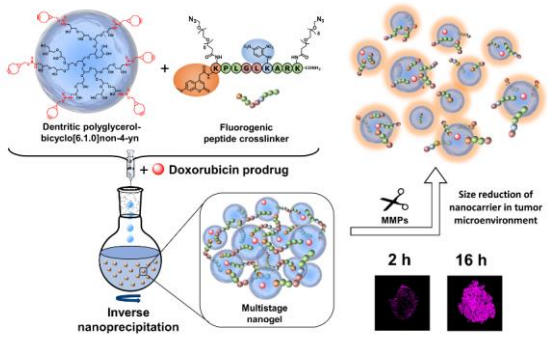

4 CONCLUSION & OUTLOOK

The development of nanocarriers was prompted by the goal to revolutionize drug delivery by improving pharmacokinetic profiles and the therapeutic index of conventional drugs by targeted delivery. Indeed, advances in the field lead to a multitude of delivery platforms that could improve common therapy strategies. However, the deficient clinical translation indicates that many challenges remain since the DDS often fail to overcome all the barriers that are encountered during the drug delivery process. The incorporation of stimuli-responsive moieties into drug delivery system allows the adaptation to certain biological barriers and thereby help to optimize targeted delivery and controlled therapeutic activation. The present thesis consists of three main projects that deal with the incorporation of the prodrug concept to build stimuli-responsive nanocarriers for drug delivery. Prodrugs of the chemotherapeutic drug Dox were combined with nanoarchitectures to exploit the advantageous properties of nanocarriers and to introduce stimuli-responsiveness with the goal to improve the performance of the parent drug. The presented systems include theranostic polymer-drug conjugates (TPC) for the evaluation of *in vitro* drug release by activatable fluorescence probes. The results of this assessment were incorporated in the rational design of a NE approach for the treatment of a metastatic breast cancer in mice model and peptide-crosslinked NGs as a multistage delivery system.

Stimuli-sensitive covalent chemistry is a versatile tool to introduce controlled cleavability into DDS that can enable controlled drug release, degradability, or other functional and morphological changes. Here, the choice of the cleavable moiety is crucial to fit the desired applications. In the first project, we aimed to assess the implication of the cleavable linkers in polymer-drug conjugates on the cell-mediated drug release, and subsequently, on the therapeutic efficacy of the DDS. A pair of TPC was synthesized that enabled the *in situ* monitoring of the cell-mediated drug release triggered by an acidic environment or enzymatic activity. The modular synthesis of the conjugates allowed the preparation of equal polymer-drug conjugates comprised of high molecular weight dPG as a polymeric carrier with Dox as a therapeutic agent and reporter unit connected via different cleavable linkers to the polymer. Importantly, the fluorescence of Dox was efficiently quenched by the proximity of an indodicarbocyanine (IDCC) dye. The FRET between Dox and IDCC suppressed the fluorescence of the drug when bound to the carrier. Consequently, regeneration of Dox fluorescence could be correlated with the release of Dox-induced by endogenous stimuli. The theranostic

conjugates proved to be sensitive to their environment regarding the pH and protease concentration, respectively and enabled the monitoring of the drug release in real-time by measurement of fluorescence recovery.

In a compatible microplate assay which allowed parallel screening of different cell lines and DDS, TPC were incubated with four cell lines (HeLa, A549, MDA-MB-231, KB-V1) to obtain characteristic release profiles for Dox by following the fluorescence signal. The correlation of the cell-mediated Dox release profiles with the cytotoxicity of the conjugates demonstrated the theranostic character of the conjugates and gave valuable information about the implication of the linker design on the drug release.

For the linkers investigated, the pH-cleavable linker was found to be more suitable for the drug delivery approach, since premature, extracellular Dox release was observed for the protease-sensitive system. This was particularly important for the treatment of multidrug-resistant KB-V1 cells where the intracellular drug release is crucial to circumvent the resistance mechanism. In contrast, the protease-sensitive conjugate proved to be more effective to inhibit the cell proliferation in MDA-MB-231 cells as the Dox release was hindered for the pH-sensitive system for this cell line. These results suggest that the linker design must be carefully chosen according to the target characteristics. The approach for targeted drug delivery cannot be fulfilled by a “one fits all” solution but there is rather a need to design the DDS in compliance with the disease characteristics and patient-specific requirements. Here, the modular nanocarrier-based delivery system could be conceived that can be adjusted to the specific needs.

It can be emphasized that the cell-based assay combined with activatable fluorescence probes, could be a valuable tool to expand the commonly used methods for the *in vitro* evaluation and screening of DDS in various cell lines. The modular approach for the synthetic methodology allows the systematic screening of different carrier architectures, a cleavable linker, and drug/dyes regarding their impact on the DDS performance. To improve the evaluated TPC towards an effective DDS, the application of more specific peptide sequences or disulfide units for the cleavable linker should ensure an intracellular drug release. The theranostic concept can be extended to non-fluorescent drugs when an additional fluorescent dye is introduced between the drug and the IDCC dye. The release of drug and dye could be realized by the application of self-immolative linkers. [119] By the application of NIR light

emitting dyes or chemiluminescence probes, the principle could be applied to track the release in an *in vivo* environment.

Even though highly active, the chemotherapeutic drug Dox displays major drawbacks such as a short half-life which impairs delivery to the tumor tissue. At the same time, Dox is widely distributed into healthy tissue which results in severe side effects leading to dose limits. The results of the first project served as the basis for the simple but effective design of pH-sensitive prodrug-based nanomedicines to improve the pharmacologic profile of Dox. In the second project, Dox was modified to be efficiently entrapped in an oil/water NE consisting of castor oil, PEG-35-castor oil as a surfactant, and water. By attaching a C16-alkyl chain, the lipophilicity of Dox was increased giving an amphiphilic character that allowed to dissolve the prodrug in the nanodroplets of the NE which serve as a nanocarrier for the drug. The Dox-loaded NE (NE-C16-Dox) showed droplet sizes of around 30 nm with an almost transparent appearance as well as high stability over long-time and in a large pH range. As responsive moiety, an acid-sensitive hydrazone linkage was applied between the alkyl chain and the drug. In intracellular acidic conditions, the hydrazone bond is hydrolyzed inducing a change in hydrophobicity of Dox which facilitates the partitioning from the NE. Indeed, it was observed that Dox remains encapsulated at neutral pH and is only released in acidic conditions. The cell internalization of the Dox-loaded NE showed fast uptake even compared to the free drug. While the free drug accumulated directly in the nucleus, Dox from the NE was first localized in the cytoplasm and was then transferred to nucleus over time. Interestingly, none of the tested endocytic blocker and neither incubation at 4 °C could inhibit the uptake of NE-C16-Dox indicting an energy-independent diffusion pathway. The internalization may occur by the fusion of nanodroplets with cell membranes as it has been observed before for surfactant-lipid droplets.[200]
When evaluated in a murine breast cancer tumor model, Dox-loaded NE presented prolonged circulation leading to higher accumulation in the tumor as compared to free Dox. In addition, reduced systemic toxicity for NE-C16-Dox was indicated by an increase of body weight during treatment and reduction of cardiac toxicity. Even when the doubled concentration of the Dox dose limit was applied as NE formulation, it did not show any signals of toxic effects indicating an overall reduction of systemic toxicity. Due to the increased dose-limit, the NE formulation was eventually able to significantly inhibit the primary tumor growth, whereas treatment with free Dox and NE with the same Dox concertation did not show a significant reduction. Interestingly, the treatment with NE-C16-Dox impaired the formation of distant lung

metastasis compared to the treatment with the free drug. This is an important finding since the presence of metastasis is as a determinant factor for patient survival.[201]

Related to this work, it has been shown by Mulder *et al.* that the miscibility and hydrophobicity of nanocarrier and drug is a major factor for the effectiveness of tumor delivery and subsequently the success of the treatment.[106] In their study, the release of model dyes modified with a hydrophobic tail was monitored *in vivo* using FRET technology. They evaluated how the model drug–carrier compatibility affected the targeted delivery and drug release and found that the hydrophobicity of the drug and its miscibility with the nanoparticles determine its accumulation in the tumor. This supports the validity of our approach to modify the parent drug with a hydrophobic entity to improve the miscibility with the chosen lipid nanocarrier. In addition, the hydrolyzable moiety allows the regeneration of the native Dox which is crucial to ensure partitioning from the NE, delivery to the nucleus, and therapeutic activity.

To gain a fundamental understanding of the processes that are involved in the cell internalization, investigation using fluorescence life time imaging microscopy are ongoing to elucidate the mechanism of action of the NE-C16-Dox-mediated intracellular delivery of Dox. We further hypothesize that the intracellular delivery can help to circumvent resistance mechanism in multi-drug resistant cell lines which should be studied in the future.

The increase of size from the first polymer therapeutics around 10 nm to larger polymeric architecture of 100–200 nm proved to be beneficial for the loading capacity of anti-cancer drugs and has been shown to improve the biodistribution with regards to higher tumor accumulation in tumor tissue. However, intratumoral barriers impede the distribution of these bigger structures leading to limited penetration into avascular regions of the tumor. In the third project, enzyme- and pH-responsive features were combined to design a two-stage drug delivery system in the form of peptide-crosslinked nanogels (pNGs) that has size reduction properties mediated by MMP followed by controlled drug release at acidic pH conditions. The MMP-sensitive pNGs were prepared by incorporation of fluorogenic peptides as crosslinkers into a hydrophilic, polymeric scaffold. The peptides introduced degradability into synthetic NGs comprised of otherwise non-degradable dPG. Inverse nanoprecipitation in combination with strain-promoted click chemistry was utilized to prepare pNGs in a surfactant-free and mild manner. The synthetic methodology allowed control over the pNG size and degree of crosslinking to optimize for the desired application. In the presence of MMP, pNGs displayed fragmentation from several 100 nm to sub-50 nm particles. The rate of MMP-mediated

degradation was adjusted by the crosslinker feed and was characterized by fluorescence measurements enabled by the intrinsic fluorogenic reporter moiety of the crosslinker.

For the multistage system, pNGs were post-synthetically modified by covalent attachment of the chemotherapeutic drug Dox through an acid-sensitive hydrazone thereby creating a multistage delivery system. In the first stage, pNGs can be degraded by MMPs which are present in the TME. After the resulting size reduction, the fragments constitute polymer-drug conjugates consisting of polyglycerol as polymeric carrier and Dox conjugated through an acid-cleavable linkage (pNG-Dox). It was confirmed that the release of Dox was enhanced at acidic conditions indicating that the cargo could be released at acidic pH as present in intracellular compartments such as endosomes and lysosomes (pH 4-5). The digested multistage pNGs showed enhanced diffusive transport through a gel matrix mimicking the dense extracellular space. These fragments after digestion should facilitate the penetration into deeper areas of tumor tissue. As proof of concept, a multicellular tumor spheroid model (MCTS) was established resembling the TME. The size-reduction property to smaller entities was able to promote the infiltration of the nanocarrier and the functional chemotherapeutic drug into deeper regions of the MCTS.

In the future, the control over the size and crosslinking density can be utilized to tune the encapsulation of therapeutic molecules with different molecular weight as well as the release rate of cargo. To confirm different densities in the pNG network, rigidity and flexibility could be determined by advanced atomic force microscopy (AFM) methods.

The employed MCTS model cannot take dynamic processes into account that affect the transport of the nanocarrier and its cargo. To extend the validity of the spheroid model, microfluidic-based systems could be realized that simulate the blood flow and interstitial fluid pressure.[202] Other studies related to the 3D model also enable to study tumor growth inhibition, drug sensitivity, targeting efficiency.

Taken together, rational design was employed to integrate stimuli-responsive moieties in drug delivery systems combining prodrugs and nanocarriers to improve different aspects of antitumor therapy. Theranostic polymer conjugates allowed to evaluate the impact of the cleavable linker design on the cell-mediated drug release by integration of an activatable fluorescence probe. Based on this assessment, two nanocarrier systems of different compositions were developed that integrated the pH-sensitive linker design for intracellular release and protease-sensitivity for extracellular degradation.

The first system allowed the elegant entrapment of Dox in an oil in water NE by the development of an amphiphilic and pH-sensitive prodrug of the chemotherapeutic agent. The Dox-loaded formulation impeded tumor growth and prevented metastasis in a murine model, and therefore represents a simple, easily scalable, and economical DDS that could be translated into clinical application in the near future.

In the second approach, NGs were designed that integrated dual-stimuli response to prepare a multistage DDS with the goal to overcome intratumoral barriers. Here, a protease-sensitive part was utilized to trigger the size reduction of the NGs by extracellular MMPs in the TME. Together with the pH-sensitive conjugation of Dox, which allowed acid-mediated intracellular drug release, the system successfully enhanced the drug transport in 3D tumor models. This NGs presents a rather complex approach that is designed for the complex nature of the tackled disease. At the moment, there are only a few examples of multistimuli-responsive DDS entering clinical trials but due to the complexity of tumor biology, it will be necessary to establish these nanocarriers for an efficient delivery.

5 REFERENCES

1. Duncan, R.; Gaspar, R., Nanomedicine(s) under the Microscope. *Molecular Pharmaceutics* **2011,** *8* (6), 2101–2141.
2. Shi, J.; Votruba, A. R.; Farokhzad, O. C.; Langer, R., Nanotechnology in drug delivery and tissue engineering: from discovery to applications. *Nano Lett* **2010,** *10* (9), 3223-30.
3. Kearney, C. J.; Mooney, D. J., Macroscale delivery systems for molecular and cellular payloads. *Nat Mater* **2013,** *12* (11), 1004-17.
4. Smith, D. M.; Simon, J. K.; Baker, J. R., Jr., Applications of nanotechnology for immunology. *Nature reviews. Immunology* **2013,** *13* (8), 592-605.
5. Khandare, J.; Calderón, M.; Dagia, N. M.; Haag, R., Multifunctional dendritic polymers in nanomedicine: opportunities and challenges. *Chemical Society Reviews* **2012,** *41* (7), 2824-2848.
6. Yao, J.; Yang, M.; Duan, Y., Chemistry, Biology, and Medicine of Fluorescent Nanomaterials and Related Systems: New Insights into Biosensing, Bioimaging, Genomics, Diagnostics, and Therapy. *Chemical Reviews* **2014,** *114* (12), 6130-6178.
7. Nakano, K.; Egashira, K.; Masuda, S.; Funakoshi, K.; Zhao, G.; Kimura, S.; Matoba, T.; Sueishi, K.; Endo, Y.; Kawashima, Y.; Hara, K.; Tsujimoto, H.; Tominaga, R.; Sunagawa, K., Formulation of nanoparticle-eluting stents by a cationic electrodeposition coating technology: efficient nano-drug delivery via bioabsorbable polymeric nanoparticle-eluting stents in porcine coronary arteries. *JACC. Cardiovascular interventions* **2009,** *2* (4), 277-83.
8. Kunjachan, S.; Ehling, J.; Storm, G.; Kiessling, F.; Lammers, T., Noninvasive Imaging of Nanomedicines and Nanotheranostics: Principles, Progress, and Prospects. *Chemical Reviews* **2015,** *115* (19), 10907-10937.
9. Petros, R. A.; DeSimone, J. M., Strategies in the design of nanoparticles for therapeutic applications. *Nat Rev Drug Discov* **2010,** *9* (8), 615-27.
10. Kelly, K. L.; Coronado, E.; Zhao, L. L.; Schatz, G. C., The Optical Properties of Metal Nanoparticles: The Influence of Size, Shape, and Dielectric Environment. *The Journal of Physical Chemistry B* **2003,** *107* (3), 668-677.
11. Wei, L.; Lu, J.; Xu, H.; Patel, A.; Chen, Z.-S.; Chen, G., Silver nanoparticles: synthesis, properties, and therapeutic applications. *Drug Discovery Today* **2015,** *20* (5), 595-601.
12. Zelikin, A. N.; Ehrhardt, C.; Healy, A. M., Materials and methods for delivery of biological drugs. *Nature Chemistry* **2016,** *8*, 997.
13. Rosenblum, D.; Joshi, N.; Tao, W.; Karp, J. M.; Peer, D., Progress and challenges towards targeted delivery of cancer therapeutics. *Nature Communications* **2018,** *9* (1), 1410.
14. Cheng, Z.; Al Zaki, A.; Hui, J. Z.; Muzykantov, V. R.; Tsourkas, A., Multifunctional nanoparticles: cost versus benefit of adding targeting and imaging capabilities. *Science* **2012,** *338* (6109), 903-10.
15. Shi, J.; Kantoff, P. W.; Wooster, R.; Farokhzad, O. C., Cancer nanomedicine: progress, challenges and opportunities. *Nature Reviews Cancer* **2016,** *17*, 20-37.
16. Riehemann, K.; Schneider, S. W.; Luger, T. A.; Godin, B.; Ferrari, M.; Fuchs, H., Nanomedicine—Challenge and Perspectives. *Angewandte Chemie International Edition* **2009,** *48* (5), 872-897.
17. Blanco, E.; Shen, H.; Ferrari, M., Principles of nanoparticle design for overcoming biological barriers to drug delivery. *Nature Biotechnology* **2015,** *33*, 941.
18. Petros, R. A.; DeSimone, J. M., Strategies in the design of nanoparticles for therapeutic applications. *Nature Reviews Drug Discovery* **2010,** *9*, 615.
19. Pastoriza-Santos, I.; Kinnear, C.; Pérez-Juste, J.; Mulvaney, P.; Liz-Marzán, L. M., Plasmonic polymer nanocomposites. *Nature Reviews Materials* **2018**.
20. Maeda, H.; Nakamura, H.; Fang, J., The EPR effect for macromolecular drug delivery to solid tumors: Improvement of tumor uptake, lowering of systemic toxicity, and distinct tumor imaging in vivo. *Adv Drug Deliv Rev* **2013,** *65* (1), 71-9.

21. Nel, A. E.; Mädler, L.; Velegol, D.; Xia, T.; Hoek, E. M. V.; Somasundaran, P.; Klaessig, F.; Castranova, V.; Thompson, M., Understanding biophysicochemical interactions at the nano–bio interface. *Nature Materials* **2009,** *8*, 543.
22. Harrington, K. J.; Mohammadtaghi, S.; Uster, P. S.; Glass, D.; Peters, A. M.; Vile, R. G.; Stewart, J. S. W., Effective Targeting of Solid Tumors in Patients With Locally Advanced Cancers by Radiolabeled Pegylated Liposomes. *Clinical Cancer Research* **2001,** *7* (2), 243-254.
23. Maeda, H., Toward a full understanding of the EPR effect in primary and metastatic tumors as well as issues related to its heterogeneity. *Advanced Drug Delivery Reviews* **2015,** *91*, 3-6.
24. Salvati, A.; Pitek, A. S.; Monopoli, M. P.; Prapainop, K.; Bombelli, F. B.; Hristov, D. R.; Kelly, P. M.; Åberg, C.; Mahon, E.; Dawson, K. A., Transferrin-functionalized nanoparticles lose their targeting capabilities when a biomolecule corona adsorbs on the surface. *Nature Nanotechnology* **2013,** *8*, 137.
25. Singh, Y.; Meher, J. G.; Raval, K.; Khan, F. A.; Chaurasia, M.; Jain, N. K.; Chourasia, M. K., Nanoemulsion: Concepts, development and applications in drug delivery. *Journal of Controlled Release* **2017,** *252*, 28-49.
26. Mahmoudi, M.; Lynch, I.; Ejtehadi, M. R.; Monopoli, M. P.; Bombelli, F. B.; Laurent, S., Protein−Nanoparticle Interactions: Opportunities and Challenges. *Chemical Reviews* **2011,** *111* (9), 5610-5637.
27. Monopoli, M. P.; Åberg, C.; Salvati, A.; Dawson, K. A., Biomolecular coronas provide the biological identity of nanosized materials. *Nature Nanotechnology* **2012,** *7*, 779.
28. Tenzer, S.; Docter, D.; Kuharev, J.; Musyanovych, A.; Fetz, V.; Hecht, R.; Schlenk, F.; Fischer, D.; Kiouptsi, K.; Reinhardt, C.; Landfester, K.; Schild, H.; Maskos, M.; Knauer, S. K.; Stauber, R. H., Rapid formation of plasma protein corona critically affects nanoparticle pathophysiology. *Nature Nanotechnology* **2013,** *8*, 772.
29. Dong, Y.; Love, K. T.; Dorkin, J. R.; Sirirungruang, S.; Zhang, Y.; Chen, D.; Bogorad, R. L.; Yin, H.; Chen, Y.; Vegas, A. J.; Alabi, C. A.; Sahay, G.; Olejnik, K. T.; Wang, W.; Schroeder, A.; Lytton-Jean, A. K.; Siegwart, D. J.; Akinc, A.; Barnes, C.; Barros, S. A.; Carioto, M.; Fitzgerald, K.; Hettinger, J.; Kumar, V.; Novobrantseva, T. I.; Qin, J.; Querbes, W.; Koteliansky, V.; Langer, R.; Anderson, D. G., Lipopeptide nanoparticles for potent and selective siRNA delivery in rodents and nonhuman primates. *Proc Natl Acad Sci U S A* **2014,** *111* (11), 3955-60.
30. Moghimi, S. M.; Hunter, A. C.; Murray, J. C., Long-circulating and target-specific nanoparticles: theory to practice. *Pharmacological reviews* **2001,** *53* (2), 283-318.
31. Gref, R.; Minamitake, Y.; Peracchia, M. T.; Trubetskoy, V.; Torchilin, V.; Langer, R., Biodegradable long-circulating polymeric nanospheres. *Science* **1994,** *263* (5153), 1600-3.
32. Hu, C.-M. J.; Zhang, L.; Aryal, S.; Cheung, C.; Fang, R. H.; Zhang, L., Erythrocyte membrane-camouflaged polymeric nanoparticles as a biomimetic delivery platform. *Proceedings of the National Academy of Sciences* **2011,** *108* (27), 10980-10985.
33. Anselmo, A. C.; Zhang, M.; Kumar, S.; Vogus, D. R.; Menegatti, S.; Helgeson, M. E.; Mitragotri, S., Elasticity of nanoparticles influences their blood circulation, phagocytosis, endocytosis, and targeting. *ACS Nano* **2015,** *9* (3), 3169-77.
34. Cabral, H.; Matsumoto, Y.; Mizuno, K.; Chen, Q.; Murakami, M.; Kimura, M.; Terada, Y.; Kano, M. R.; Miyazono, K.; Uesaka, M.; Nishiyama, N.; Kataoka, K., ,, Accumulation of sub-100 nm polymeric micelles in poorly permeable tumours depends on size. *Nat Nano* **2011,** *6* (12), 815–823.
35. Smith, B. R.; Kempen, P.; Bouley, D.; Xu, A.; Liu, Z.; Melosh, N.; Dai, H.; Sinclair, R.; Gambhir, S. S., Shape matters: intravital microscopy reveals surprising geometrical dependence for nanoparticles in tumor models of extravasation. *Nano Lett* **2012,** *12* (7), 3369-77.
36. Nakamura, Y.; Mochida, A.; Choyke, P. L.; Kobayashi, H., Nanodrug Delivery: Is the Enhanced Permeability and Retention Effect Sufficient for Curing Cancer? *Bioconjugate Chemistry* **2016**.
37. Jain, R. K.; Baxter, L. T., Mechanisms of heterogeneous distribution of monoclonal antibodies and other macromolecules in tumors: significance of elevated interstitial pressure. *Cancer Res* **1988,** *48* (24 Pt 1), 7022-32.
38. Helmlinger, G.; Yuan, F.; Dellian, M.; Jain, R. K., Interstitial pH and pO2 gradients in solid tumors in vivo: high-resolution measurements reveal a lack of correlation. *Nat Med* **1997,** *3* (2), 177-82.

39. Brown, J. M.; Giaccia, A. J., The Unique Physiology of Solid Tumors: Opportunities (and Problems) for Cancer Therapy. *Cancer Research* **1998,** *58* (7), 1408-1416.
40. Helmlinger, G.; Yuan, F.; Dellian, M.; Jain, R. K., Interstitial pH and pO2 gradients in solid tumors in vivo: High-resolution measurements reveal a lack of correlation. *Nature Medicine* **1997,** *3*, 177.
41. Giaccone, G.; Pinedo, H. M., Drug Resistance. *The Oncologist* **1996,** *1* (1), 82-87.
42. Trédan, O.; Galmarini, C. M.; Patel, K.; Tannock, I. F., Drug Resistance and the Solid Tumor Microenvironment. *JNCI: Journal of the National Cancer Institute* **2007,** *99* (19), 1441-1454.
43. Jain, R. K.; Stylianopoulos, T., Delivering nanomedicine to solid tumors. *Nature Reviews Clinical Oncology* **2010,** *7*, 653.
44. Dreher, M. R.; Liu, W.; Michelich, C. R.; Dewhirst, M. W.; Yuan, F.; Chilkoti, A., Tumor Vascular Permeability, Accumulation, and Penetration of Macromolecular Drug Carriers. *JNCI: Journal of the National Cancer Institute* **2006,** *98* (5), 335-344.
45. Curry, F.-R. E., Redefining tumour vascular barriers. *Nature Nanotechnology* **2016,** *11*, 494.
46. Durymanov, M. O.; Rosenkranz, A. A.; Sobolev, A. S., Current Approaches for Improving Intratumoral Accumulation and Distribution of Nanomedicines. *Theranostics* **2015,** *5* (9), 1007-20.
47. Marcucci, F.; Corti, A., How to improve exposure of tumor cells to drugs — Promoter drugs increase tumor uptake and penetration of effector drugs. *Advanced Drug Delivery Reviews* **2012,** *64* (1), 53-68.
48. Kong, G.; Braun, R. D.; Dewhirst, M. W., Hyperthermia Enables Tumor-specific Nanoparticle Delivery: Effect of Particle Size. *Cancer Research* **2000,** *60* (16), 4440-4445.
49. EIKENES, L.; TUFTO, I.; SCHNELL, E. A.; BJØRKØY, A.; DE LANGE DAVIES, C., Effect of Collagenase and Hyaluronidase on Free and Anomalous Diffusion in Multicellular Spheroids and Xenografts. *Anticancer Research* **2010,** *30* (2), 359-368.
50. Ruoslahti, E., Tumor penetrating peptides for improved drug delivery. *Advanced Drug Delivery Reviews* **2017,** *110-111*, 3-12.
51. Chen, B.; Dai, W.; He, B.; Zhang, H.; Wang, X.; Wang, Y.; Zhang, Q., Current Multistage Drug Delivery Systems Based on the Tumor Microenvironment. *Theranostics* **2017,** *7* (3), 538-558.
52. Zhang, S.; Gao, H.; Bao, G., Physical Principles of Nanoparticle Cellular Endocytosis. *ACS Nano* **2015,** *9* (9), 8655-8671.
53. Le Roy, C.; Wrana, J. L., Clathrin- and non-clathrin-mediated endocytic regulation of cell signalling. *Nature Reviews Molecular Cell Biology* **2005,** *6*, 112.
54. Sahay, G.; Querbes, W.; Alabi, C.; Eltoukhy, A.; Sarkar, S.; Zurenko, C.; Karagiannis, E.; Love, K.; Chen, D.; Zoncu, R.; Buganim, Y.; Schroeder, A.; Langer, R.; Anderson, D. G., Efficiency of siRNA delivery by lipid nanoparticles is limited by endocytic recycling. *Nature Biotechnology* **2013,** *31*, 653.
55. Bareford, L. M.; Swaan, P. W., Endocytic mechanisms for targeted drug delivery. *Adv Drug Deliv Rev* **2007,** *59* (8), 748-58.
56. Torchilin, V. P., Cell penetrating peptide-modified pharmaceutical nanocarriers for intracellular drug and gene delivery. *Biopolymers* **2008,** *90* (5), 604-10.
57. Yuan, Y.-Y.; Mao, C.-Q.; Du, X.-J.; Du, J.-Z.; Wang, F.; Wang, J., Surface Charge Switchable Nanoparticles Based on Zwitterionic Polymer for Enhanced Drug Delivery to Tumor. *Advanced Materials* **2012,** *24* (40), 5476-5480.
58. Mura, S.; Nicolas, J.; Couvreur, P., Stimuli-responsive nanocarriers for drug delivery. *Nat Mater* **2013,** *12* (11), 991–1003.
59. Rautio, J.; Kumpulainen, H.; Heimbach, T.; Oliyai, R.; Oh, D.; Järvinen, T.; Savolainen, J., Prodrugs: design and clinical applications. *Nature Reviews Drug Discovery* **2008,** *7*, 255.
60. Kevin, B.; Robert, W.; Iain, G.; Kevin, D., Design of Ester Prodrugs to Enhance Oral Absorption of Poorly Permeable Compounds: Challenges to the Discovery Scientist. *Current Drug Metabolism* **2003,** *4* (6), 461-485.
61. Miwa, M.; Ura, M.; Nishida, M.; Sawada, N.; Ishikawa, T.; Mori, K.; Shimma, N.; Umeda, I.; Ishitsuka, H., Design of a novel oral fluoropyrimidine carbamate, capecitabine, which generates 5-fluorouracil selectively in tumours by enzymes concentrated in human liver and cancer tissue. *Eur J Cancer* **1998,** *34* (8), 1274-81.

62. Ekkelenkamp, A. E.; Elzes, M. R.; Engbersen, J. F. J.; Paulusse, J. M. J., Responsive crosslinked polymer nanogels for imaging and therapeutics delivery. *Journal of Materials Chemistry B* **2018,** *6* (2), 210-235.
63. Jin, Y.; Yu, C.; Denman, R. J.; Zhang, W., Recent advances in dynamic covalent chemistry. *Chemical Society Reviews* **2013,** *42* (16), 6634-6654.
64. Bergueiro, J.; Calderón, M., Thermoresponsive Nanodevices in Biomedical Applications. *Macromolecular Bioscience* **2015,** *15* (2), 183-199.
65. Ward, M. A.; Georgiou, T. K., Thermoresponsive Polymers for Biomedical Applications. *Polymers* **2011,** *3* (3), 1215.
66. Heskins, M.; Guillet, J. E., Solution Properties of Poly(N-isopropylacrylamide). *Journal of Macromolecular Science: Part A - Chemistry* **1968,** *2* (8), 1441-1455.
67. Eeckman, F.; Moës, A. J.; Amighi, K., Synthesis and characterization of thermosensitive copolymers for oral controlled drug delivery. *European Polymer Journal* **2004,** *40* (4), 873-881.
68. Hiruta, Y.; Shimamura, M.; Matsuura, M.; Maekawa, Y.; Funatsu, T.; Suzuki, Y.; Ayano, E.; Okano, T.; Kanazawa, H., Temperature-Responsive Fluorescence Polymer Probes with Accurate Thermally Controlled Cellular Uptakes. *ACS Macro Letters* **2014,** *3* (3), 281-285.
69. Akimoto, J.; Nakayama, M.; Sakai, K.; Okano, T., Thermally Controlled Intracellular Uptake System of Polymeric Micelles Possessing Poly(N-isopropylacrylamide)-Based Outer Coronas. *Molecular Pharmaceutics* **2010,** *7* (4), 926-935.
70. Johnson, R. P.; Jeong, Y. I.; John, J. V.; Chung, C.-W.; Kang, D. H.; Selvaraj, M.; Suh, H.; Kim, I., Dual Stimuli-Responsive Poly(N-isopropylacrylamide)-b-poly(l-histidine) Chimeric Materials for the Controlled Delivery of Doxorubicin into Liver Carcinoma. *Biomacromolecules* **2013,** *14* (5), 1434-1443.
71. Cuggino, J. C.; Alvarez I, C. I.; Strumia, M. C.; Welker, P.; Licha, K.; Steinhilber, D.; Mutihac, R.-C.; Calderon, M., Thermosensitive nanogels based on dendritic polyglycerol and N-isopropylacrylamide for biomedical applications. *Soft Matter* **2011,** *7* (23), 11259–11266.
72. Rapoport, N. Y.; Kennedy, A. M.; Shea, J. E.; Scaife, C. L.; Nam, K.-H., Controlled and targeted tumor chemotherapy by ultrasound-activated nanoemulsions/microbubbles. *Journal of Controlled Release* **2009,** *138* (3), 268-276.
73. Gao, Z.-G.; Fain, H. D.; Rapoport, N., Controlled and targeted tumor chemotherapy by micellar-encapsulated drug and ultrasound. *Journal of Controlled Release* **2005,** *102* (1), 203-222.
74. Thévenot, J.; Oliveira, H.; Sandre, O.; Lecommandoux, S., Magnetic responsive polymer composite materials. *Chemical Society Reviews* **2013,** *42* (17), 7099-7116.
75. Sanson, C.; Diou, O.; Thévenot, J.; Ibarboure, E.; Soum, A.; Brûlet, A.; Miraux, S.; Thiaudière, E.; Tan, S.; Brisson, A.; Dupuis, V.; Sandre, O.; Lecommandoux, S., Doxorubicin Loaded Magnetic Polymersomes: Theranostic Nanocarriers for MR Imaging and Magneto-Chemotherapy. *ACS Nano* **2011,** *5* (2), 1122-1140.
76. Fomina, N.; Sankaranarayanan, J.; Almutairi, A., Photochemical mechanisms of light-triggered release from nanocarriers. *Advanced Drug Delivery Reviews* **2012,** *64* (11), 1005-1020.
77. Pansare, V. J.; Hejazi, S.; Faenza, W. J.; Prud'homme, R. K., Review of Long-Wavelength Optical and NIR Imaging Materials: Contrast Agents, Fluorophores, and Multifunctional Nano Carriers. *Chemistry of Materials* **2012,** *24* (5), 812-827.
78. Gao, W.; Chan, J. M.; Farokhzad, O. C., pH-Responsive Nanoparticles for Drug Delivery. *Molecular Pharmaceutics* **2010,** *7* (6), 1913-1920.
79. Vaupel, P.; Kallinowski, F.; Okunieff, P., Blood Flow, Oxygen and Nutrient Supply, and Metabolic Microenvironment of Human Tumors: A Review. *Cancer Research* **1989,** *49* (23), 6449-6465.
80. Vander Heiden, M. G.; Cantley, L. C.; Thompson, C. B., Understanding the Warburg Effect: The Metabolic Requirements of Cell Proliferation. *Science (New York, N.Y.)* **2009,** *324* (5930), 1029-1033.
81. Murphy, R. F.; Powers, S.; Cantor, C. R., Endosome pH measured in single cells by dual fluorescence flow cytometry: rapid acidification of insulin to pH 6. *The Journal of cell biology* **1984,** *98* (5), 1757-62.

82. Liu, J.; Huang, Y.; Kumar, A.; Tan, A.; Jin, S.; Mozhi, A.; Liang, X.-J., pH-Sensitive nano-systems for drug delivery in cancer therapy. *Biotechnology Advances* **2014,** *32* (4), 693-710.
83. Fleige, E.; Achazi, K.; Schaletzki, K.; Triemer, T.; Haag, R., pH-Responsive Dendritic Core–Multishell Nanocarriers. *Journal of Controlled Release* **2014,** *185*, 99-108.
84. Sachdev, E.; Sachdev, D.; Mita, M., Aldoxorubicin for the treatment of soft tissue sarcoma. *Expert Opinion on Investigational Drugs* **2017,** *26* (10), 1175-1179.
85. Calderón, M.; Welker, P.; Licha, K.; Fichtner, I.; Graeser, R.; Haag, R.; Kratz, F., Development of efficient acid cleavable multifunctional prodrugs derived from dendritic polyglycerol with a poly(ethylene glycol) shell. *Journal of Controlled Release* **2011,** *151* (3), 295-301.
86. Mohamed, M. M.; Sloane, B. F., Cysteine cathepsins: multifunctional enzymes in cancer. *Nat Rev Cancer* **2006,** *6* (10), 764–775.
87. Fleige, E.; Quadir, M. A.; Haag, R., Stimuli-responsive polymeric nanocarriers for the controlled transport of active compounds: Concepts and applications. *Advanced Drug Delivery Reviews* **2012,** *64* (9), 866–884.
88. Zelzer, M.; Todd, S. J.; Hirst, A. R.; McDonald, T. O.; Ulijn, R. V., Enzyme responsive materials: design strategies and future developments. *Biomaterials Science* **2013,** *1* (1), 11–39.
89. Jones, D. P.; Carlson, J. L.; Samiec, P. S.; Sternberg, P.; Mody, V. C.; Reed, R. L.; Brown, L. A. S., Glutathione measurement in human plasma: Evaluation of sample collection, storage and derivatization conditions for analysis of dansyl derivatives by HPLC. *Clinica Chimica Acta* **1998,** *275* (2), 175-184.
90. Hassan, S. S. M.; Rechnitz, G. A., Determination of glutathione and glutathione reductase with a silver sulfide membrane electrode. *Analytical Chemistry* **1982,** *54* (12), 1972-1976.
91. Lomaestro, B. M.; Malone, M., Glutathione in Health and Disease: Pharmacotherapeutic Issues. *Annals of Pharmacotherapy* **1995,** *29* (12), 1263-1273.
92. Pasparakis, G.; Manouras, T.; Vamvakaki, M.; Argitis, P., Harnessing photochemical internalization with dual degradable nanoparticles for combinatorial photo–chemotherapy. *Nature Communications* **2014,** *5*, 3623.
93. Ju, C.; Mo, R.; Xue, J.; Zhang, L.; Zhao, Z.; Xue, L.; Ping, Q.; Zhang, C., Sequential Intra-Intercellular Nanoparticle Delivery System for Deep Tumor Penetration. *Angewandte Chemie International Edition* **2014,** *53* (24), 6253-6258.
94. Yim, H.; Park, S.-j.; Bae, Y. H.; Na, K., Biodegradable cationic nanoparticles loaded with an anticancer drug for deep penetration of heterogeneous tumours. *Biomaterials* **2013,** *34* (31), 7674–7682.
95. El-Sawy, H. S.; Al-Abd, A. M.; Ahmed, T. A.; El-Say, K. M.; Torchilin, V. P., Stimuli-Responsive Nano-Architecture Drug-Delivery Systems to Solid Tumor Micromilieu: Past, Present, and Future Perspectives. *ACS Nano* **2018**.
96. Li, H.-J.; Du, J.-Z.; Du, X.-J.; Xu, C.-F.; Sun, C.-Y.; Wang, H.-X.; Cao, Z.-T.; Yang, X.-Z.; Zhu, Y.-H.; Nie, S.; Wang, J., Stimuli-responsive clustered nanoparticles for improved tumor penetration and therapeutic efficacy. *Proceedings of the National Academy of Sciences* **2016,** *113* (15), 4164-4169.
97. Zan, M.; Li, J.; Luo, S.; Ge, Z., Dual pH-triggered multistage drug delivery systems based on host–guest interaction-associated polymeric nanogels. *Chemical Communications* **2014,** *50* (58), 7824-7827.
98. Li, J.; Han, Y.; Chen, Q.; Shi, H.; ur Rehman, S.; Siddiq, M.; Ge, Z.; Liu, S., Dual endogenous stimuli-responsive polyplex micelles as smart two-step delivery nanocarriers for deep tumor tissue penetration and combating drug resistance of cisplatin. *Journal of Materials Chemistry B* **2014,** *2* (13), 1813-1824.
99. Wong, C.; Stylianopoulos, T.; Cui, J.; Martin, J.; Chauhan, V. P.; Jiang, W.; Popović, Z.; Jain, R. K.; Bawendi, M. G.; Fukumura, D., Multistage nanoparticle delivery system for deep penetration into tumor tissue. *Proceedings of the National Academy of Sciences* **2011,** *108* (6), 2426–2431.
100. Ruan, S.; Zhang, L.; Chen, J.; Cao, T.; Yang, Y.; Liu, Y.; He, Q.; Gao, F.; Gao, H., Targeting delivery and deep penetration using multistage nanoparticles for triple-negative breast cancer. *RSC Advances* **2015,** *5* (79), 64303-64317.

101. Hu, G.; Wang, Y.; He, Q.; Gao, H., Multistage drug delivery system based on microenvironment-responsive dendrimer-gelatin nanoparticles for deep tumor penetration. *RSC Advances* **2015,** *5* (104), 85933-85937.
102. Gordon, M. R.; Zhao, B.; Anson, F.; Fernandez, A.; Singh, K.; Homyak, C.; Canakci, M.; Vachet, R. W.; Thayumanavan, S., Matrix Metalloproteinase-9-Responsive Nanogels for Proximal Surface Conversion and Activated Cellular Uptake. *Biomacromolecules* **2018**.
103. Frazier, N.; Ghandehari, H., Hyperthermia approaches for enhanced delivery of nanomedicines to solid tumors. *Biotechnol Bioeng* **2015,** *112* (10), 1967-83.
104. Yatvin, M. B.; Weinstein, J. N.; Dennis, W. H.; Blumenthal, R., Design of liposomes for enhanced local release of drugs by hyperthermia. *Science* **1978,** *202* (4374), 1290-3.
105. J, F., Reinventing Pharma: The Theranostic Revolution. *Curr. Drug Discovery* **2002,** *2*, 17–19.
106. Pérez-Medina, C.; Abdel-Atti, D.; Tang, J.; Zhao, Y.; Fayad, Z. A.; Lewis, J. S.; Mulder, W. J. M.; Reiner, T., Nanoreporter PET predicts the efficacy of anti-cancer nanotherapy. *Nature Communications* **2016,** *7*, 11838.
107. Miller, M. A.; Gadde, S.; Pfirschke, C.; Engblom, C.; Sprachman, M. M.; Kohler, R. H.; Yang, K. S.; Laughney, A. M.; Wojtkiewicz, G.; Kamaly, N.; Bhonagiri, S.; Pittet, M. J.; Farokhzad, O. C.; Weissleder, R., Predicting therapeutic nanomedicine efficacy using a companion magnetic resonance imaging nanoparticle. *Sci Transl Med* **2015,** *7* (314), 314ra183.
108. Lammers, T.; Rizzo, L. Y.; Storm, G.; Kiessling, F., Personalized Nanomedicine. *Clinical Cancer Research* **2012,** *18* (18), 4889-4894.
109. Mura, S.; Couvreur, P., Nanotheranostics for personalized medicine. *Advanced Drug Delivery Reviews* **2012,** *64* (13), 1394-1416.
110. Blau, R.; Krivitsky, A.; Epshtein, Y.; Satchi-Fainaro, R., Are nanotheranostics and nanodiagnostics-guided drug delivery stepping stones towards precision medicine? *Drug Resistance Updates* **2016,** *27*, 39-58.
111. Sun, Y.; Wallrabe, H.; Seo, S.-A.; Periasamy, A., FRET Microscopy in 2010: The Legacy of Theodor Förster on the 100th Anniversary of his Birth. *ChemPhysChem* **2011,** *12* (3), 462-474.
112. Sapsford, K. E.; Berti, L.; Medintz, I. L., Materials for Fluorescence Resonance Energy Transfer Analysis: Beyond Traditional Donor–Acceptor Combinations. *Angewandte Chemie International Edition* **2006,** *45* (28), 4562-4589.
113. Giepmans, B. N. G.; Adams, S. R.; Ellisman, M. H.; Tsien, R. Y., The Fluorescent Toolbox for Assessing Protein Location and Function. *Science* **2006,** *312* (5771), 217-224.
114. Yang, J.; Chen, H.; Vlahov, I. R.; Cheng, J.-X.; Low, P. S., Evaluation of disulfide reduction during receptor-mediated endocytosis by using FRET imaging. *Proceedings of the National Academy of Sciences* **2006,** *103* (37), 13872-13877.
115. Zhao, Y.; Fay, F.; Hak, S.; Manuel Perez-Aguilar, J.; Sanchez-Gaytan, B. L.; Goode, B.; Duivenvoorden, R.; de Lange Davies, C.; Bjørkøy, A.; Weinstein, H.; Fayad, Z. A.; Pérez-Medina, C.; Mulder, W. J. M., Augmenting drug–carrier compatibility improves tumour nanotherapy efficacy. *Nature Communications* **2016,** *7*, 11221.
116. Lee, M. H.; Sharma, A.; Chang, M. J.; Lee, J.; Son, S.; Sessler, J. L.; Kang, C.; Kim, J. S., Fluorogenic reaction-based prodrug conjugates as targeted cancer theranostics. *Chemical Society Reviews* **2018,** *47* (1), 28-52.
117. Hu, Y.; Zeng, F., A theranostic prodrug based on FRET for real-time drug release monitoring in response to biothiols. *Materials Science and Engineering: C* **2017,** *72*, 77–85.
118. Li, S. Y.; Liu, L. H.; Rong, L.; Qiu, W. X.; Jia, H. Z.; Li, B.; Li, F.; Zhang, X. Z., A Dual-FRET-Based Versatile Prodrug for Real-Time Drug Release Monitoring and In Situ Therapeutic Efficacy Evaluation. *Advanced Functional Materials* **2015,** *25* (47), 7317-7326.
119. Redy, O.; Shabat, D., Modular theranostic prodrug based on a FRET-activated self-immolative linker. *Journal of Controlled Release* **2012,** *164* (3), 276-282.
120. Redy-Keisar, O.; Ferber, S.; Satchi-Fainaro, R.; Shabat, D., NIR Fluorogenic Dye as a Modular Platform for Prodrug Assembly: Real-Time in vivo Monitoring of Drug Release. *ChemMedChem* **2015,** *10* (6), 999–1007.

121. Gnaim, S.; Scomparin, A.; Das, S.; Blau, R.; Satchi-Fainaro, R.; Shabat, D., Direct Real-Time Monitoring of Prodrug Activation by Chemiluminescence. *Angewandte Chemie International Edition* **2018,** *57* (29), 9033-9037.
122. Chen, H.; Jia, H.; Tham, H. P.; Qu, Q.; Xing, P.; Zhao, J.; Phua, S. Z. F.; Chen, G.; Zhao, Y., Theranostic Prodrug Vesicles for Imaging Guided Codelivery of Camptothecin and siRNA in Synergetic Cancer Therapy. *ACS Applied Materials & Interfaces* **2017,** *9* (28), 23536-23543.
123. Aibani, N.; da Costa, P. F.; Masterson, J.; Marino, N.; Raymo, F. M.; Callan, J.; Callan, B., The integration of triggered drug delivery with real time quantification using FRET; creating a super 'smart' drug delivery system. *Journal of Controlled Release* **2017,** *264*, 136-144.
124. Ferber, S.; Baabur-Cohen, H.; Blau, R.; Epshtein, Y.; Kisin-Finfer, E.; Redy, O.; Shabat, D.; Satchi-Fainaro, R., Polymeric nanotheranostics for real-time non-invasive optical imaging of breast cancer progression and drug release. *Cancer Letters* **2014,** (0).
125. Nicolas, J.; Mura, S.; Brambilla, D.; Mackiewicz, N.; Couvreur, P., Design, functionalization strategies and biomedical applications of targeted biodegradable/biocompatible polymer-based nanocarriers for drug delivery. *Chemical Society Reviews* **2013,** *42* (3), 1147-1235.
126. Haag, R.; Kratz, F., Polymer therapeutics: concepts and applications. *Angewandte Chemie (International ed. in English)* **2006,** *45* (8), 1198-215.
127. Vicent, M. J.; Ringsdorf, H.; Duncan, R., Polymer therapeutics: Clinical applications and challenges for development. *Advanced Drug Delivery Reviews* **2009,** *61* (13), 1117-1120.
128. Kakkar, A.; Traverso, G.; Farokhzad, O. C.; Weissleder, R.; Langer, R., Evolution of macromolecular complexity in drug delivery systems. *Nature Reviews Chemistry* **2017,** *1*, 0063.
129. Ringsdorf, H., Structure and properties of pharmacologically active polymers. *Journal of Polymer Science: Polymer Symposia* **1975,** *51* (1), 135-153.
130. Khandare, J.; Minko, T., Polymer–drug conjugates: Progress in polymeric prodrugs. *Progress in Polymer Science* **2006,** *31* (4), 359-397.
131. Duncan, R., The dawning era of polymer therapeutics. *Nat Rev Drug Discov* **2003,** *2* (5), 347-60.
132. Duncan, R., Polymer therapeutics as nanomedicines: new perspectives. *Current Opinion in Biotechnology* **2011,** *22* (4), 492-501.
133. Pillai, O.; Panchagnula, R., Polymers in drug delivery. *Current Opinion in Chemical Biology* **2001,** *5* (4), 447-451.
134. Elzoghby, A. O.; Samy, W. M.; Elgindy, N. A., Albumin-based nanoparticles as potential controlled release drug delivery systems. *Journal of controlled release : official journal of the Controlled Release Society* **2012,** *157* (2), 168-82.
135. Gradishar, W. J., Albumin-bound paclitaxel: a next-generation taxane. *Expert opinion on pharmacotherapy* **2006,** *7* (8), 1041-53.
136. Brocchini, S.; Duncan, R., Pendent drugs, release from polymers. *Encyclopaedia of controlled drug delivery* **1999,** *2*, 786-816.
137. Garay, R. P.; El-Gewely, R.; Armstrong, J. K.; Garratty, G.; Richette, P., Antibodies against polyethylene glycol in healthy subjects and in patients treated with PEG-conjugated agents. *Expert Opinion on Drug Delivery* **2012,** *9* (11), 1319-1323.
138. Knop, K.; Hoogenboom, R.; Fischer, D.; Schubert, U. S., Poly(ethylene glycol) in drug delivery: pros and cons as well as potential alternatives. *Angewandte Chemie (International ed. in English)* **2010,** *49* (36), 6288-308.
139. Duncan, R.; Cable, H. C.; Lloyd, J. B.; Rejmanová, P.; Kopeček, J., Polymers containing enzymatically degradable bonds, 7. Design of oligopeptide side-chains in poly[N-(2-hydroxypropyl)methacrylamide] copolymers to promote efficient degradation by lysosomal enzymes. *Die Makromolekulare Chemie* **1983,** *184* (10), 1997-2008.
140. Rejmanova, P.; Kopecek, J.; Duncan, R.; Lloyd, J. B., Stability in rat plasma and serum of lysosomally degradable oligopeptide sequences in N-(2-hydroxypropyl) methacrylamide copolymers. *Biomaterials* **1985,** *6* (1), 45-8.

141. Etrych, T.; Jelinkova, M.; Rihova, B.; Ulbrich, K., New HPMA copolymers containing doxorubicin bound via pH-sensitive linkage: synthesis and preliminary in vitro and in vivo biological properties. *Journal of controlled release : official journal of the Controlled Release Society* **2001,** *73* (1), 89-102.
142. Paleos, C. M.; Tsiourvas, D.; Sideratou, Z.; Tziveleka, L.-A., Drug delivery using multifunctional dendrimers and hyperbranched polymers. *Expert Opinion on Drug Delivery* **2010,** *7* (12), 1387-1398.
143. Gillies, E. R.; Frechet, J. M., Dendrimers and dendritic polymers in drug delivery. *Drug Discov Today* **2005,** *10* (1), 35-43.
144. Frey, H.; Haag, R., Dendritic polyglycerol: a new versatile biocompatible material. *Reviews in Molecular Biotechnology* **2002,** *90* (3–4), 257–267.
145. Haag, R.; Sunder, A.; Stumbé, J.-F., An Approach to Glycerol Dendrimers and Pseudo-Dendritic Polyglycerols. *Journal of the American Chemical Society* **2000,** *122* (12), 2954-2955.
146. Khandare, J.; Mohr, A.; Calderon, M.; Welker, P.; Licha, K.; Haag, R., Structure-biocompatibility relationship of dendritic polyglycerol derivatives. *Biomaterials* **2010,** *31* (15), 4268-77.
147. Sunder, A.; Hanselmann, R.; Frey, H.; Mülhaupt, R., Controlled Synthesis of Hyperbranched Polyglycerols by Ring-Opening Multibranching Polymerization. *Macromolecules* **1999,** *32* (13), 4240-4246.
148. Calderón, M.; Quadir, M. A.; Sharma, S. K.; Haag, R., Dendritic Polyglycerols for Biomedical Applications. *Advanced Materials* **2010,** *22* (2), 190–218.
149. Rainer Haag, S. R., Dendritic Polymers as High-Loading Supports for Organic Synthesis and Catalysis. In *Polymeric Materials in Organic Synthesis and Catalysis*, 2005.
150. Wei, Q.; Becherer, T.; Noeske, P.-L. M.; Grunwald, I.; Haag, R., A Universal Approach to Crosslinked Hierarchical Polymer Multilayers as Stable and Highly Effective Antifouling Coatings. *Advanced Materials* **2014,** *26* (17), 2688-2693.
151. Krämer, M.; Stumbé, J.-F.; Türk, H.; Krause, S.; Komp, A.; Delineau, L.; Prokhorova, S.; Kautz, H.; Haag, R., pH-Responsive Molecular Nanocarriers Based on Dendritic Core-Shell Architectures. *Angewandte Chemie International Edition* **2002,** *41* (22), 4252-4256.
152. Radowski, M. R.; Shukla, A.; von Berlepsch, H.; Böttcher, C.; Pickaert, G.; Rehage, H.; Haag, R., Supramolecular Aggregates of Dendritic Multishell Architectures as Universal Nanocarriers. *Angewandte Chemie International Edition* **2007,** *46* (8), 1265-1269.
153. Calderón, M.; Graeser, R.; Kratz, F.; Haag, R., Development of enzymatically cleavable prodrugs derived from dendritic polyglycerol. *Bioorganic & Medicinal Chemistry Letters* **2009,** *19* (14), 3725-3728.
154. Calderon, M.; Welker, P.; Licha, K.; Fichtner, I.; Graeser, R.; Haag, R.; Kratz, F., Development of efficient acid cleavable multifunctional prodrugs derived from dendritic polyglycerol with a poly(ethylene glycol) shell. *Journal of controlled release : official journal of the Controlled Release Society* **2011,** *151* (3), 295-301.
155. Mehrabadi, F. S.; Hirsch, O.; Zeisig, R.; Posocco, P.; Laurini, E.; Pricl, S.; Haag, R.; Kemmner, W.; Calderón, M., Structure–activity relationship study of dendritic polyglycerolamines for efficient siRNA transfection. *RSC Advances* **2015,** *5* (96), 78760-78770.
156. Dimde, M.; Neumann, F.; Reisbeck, F.; Ehrmann, S.; Cuellar-Camacho, J. L.; Steinhilber, D.; Ma, N.; Haag, R., Defined pH-sensitive nanogels as gene delivery platform for siRNA mediated in vitro gene silencing. *Biomater Sci* **2017,** *5* (11), 2328-2336.
157. Malhotra, S.; Bauer, H.; Tschiche, A.; Staedtler, A. M.; Mohr, A.; Calderón, M.; Parmar, V. S.; Hoeke, L.; Sharbati, S.; Einspanier, R.; Haag, R., Glycine-Terminated Dendritic Amphiphiles for Nonviral Gene Delivery. *Biomacromolecules* **2012,** *13* (10), 3087-3098.
158. Sisson, A. L.; Steinhilber, D.; Rossow, T.; Welker, P.; Licha, K.; Haag, R., Biocompatible Functionalized Polyglycerol Microgels with Cell Penetrating Properties. *Angewandte Chemie International Edition* **2009,** *48* (41), 7540-7545.
159. Steinhilber, D.; Sisson, A. L.; Mangoldt, D.; Welker, P.; Licha, K.; Haag, R., Synthesis, Reductive Cleavage, and Cellular Interaction Studies of Biodegradable, Polyglycerol Nanogels. *Advanced Functional Materials* **2010,** *20* (23), 4133-4138.

160. Steinhilber, D.; Seiffert, S.; Heyman, J. A.; Paulus, F.; Weitz, D. A.; Haag, R., Hyperbranched polyglycerols on the nanometer and micrometer scale. *Biomaterials* **2011,** *32* (5), 1311–1316.
161. Rossow, T.; Heyman, J. A.; Ehrlicher, A. J.; Langhoff, A.; Weitz, D. A.; Haag, R.; Seiffert, S., Controlled Synthesis of Cell-Laden Microgels by Radical-Free Gelation in Droplet Microfluidics. *Journal of the American Chemical Society* **2012,** *134* (10), 4983-4989.
162. Asadian-Birjand, M.; Sousa-Herves, A.; Steinhilber, D.; Cuggino, J. C.; Calderon, M., Functional nanogels for biomedical applications. *Current medicinal chemistry* **2012,** *19* (29), 5029-43.
163. Anselmo, A. C.; Zhang, M.; Kumar, S.; Vogus, D. R.; Menegatti, S.; Helgeson, M. E.; Mitragotri, S., Elasticity of Nanoparticles Influences Their Blood Circulation, Phagocytosis, Endocytosis, and Targeting. *ACS Nano* **2015,** *9* (3), 3169-3177.
164. Myerson, J. W.; Braender, B.; Mcpherson, O.; Glassman, P. M.; Kiseleva, R. Y.; Shuvaev, V. V.; Marcos-Contreras, O.; Grady, M. E.; Lee, H.-S.; Greineder, C. F.; Stan, R. V.; Composto, R. J.; Eckmann, D. M.; Muzykantov, V. R., Flexible Nanoparticles Reach Sterically Obscured Endothelial Targets Inaccessible to Rigid Nanoparticles. *Advanced Materials* **2018,** *30* (32), 1802373.
165. Zhang, X.; Malhotra, S.; Molina, M.; Haag, R., Micro- and nanogels with labile crosslinks - from synthesis to biomedical applications. *Chemical Society Reviews* **2015,** *44* (7), 1948-1973.
166. Steinhilber, D.; Witting, M.; Zhang, X.; Staegemann, M.; Paulus, F.; Friess, W.; Küchler, S.; Haag, R., Surfactant free preparation of biodegradable dendritic polyglycerol nanogels by inverse nanoprecipitation for encapsulation and release of pharmaceutical biomacromolecules. *Journal of Controlled Release* **2013,** *169* (3), 289–295.
167. Zhang, X.; Achazi, K.; Steinhilber, D.; Kratz, F.; Dernedde, J.; Haag, R., A facile approach for dual-responsive prodrug nanogels based on dendritic polyglycerols with minimal leaching. *Journal of Controlled Release* **2014,** *174*, 209-216.
168. Wei, X.; Luo, Q.; Sun, L.; Li, X.; Zhu, H.; Guan, P.; Wu, M.; Luo, K.; Gong, Q., Enzyme- and pH-Sensitive Branched Polymer–Doxorubicin Conjugate-Based Nanoscale Drug Delivery System for Cancer Therapy. *ACS Applied Materials & Interfaces* **2016,** *8* (18), 11765–11778.
169. Thornton, P. D.; Mart, R. J.; Webb, S. J.; Ulijn, R. V., Enzyme-responsive hydrogel particles for the controlled release of proteins: designing peptide actuators to match payload. *Soft Matter* **2008,** *4* (4), 821–827.
170. Zhang, X.; Malhotra, S.; Molina, M.; Haag, R., Micro- and nanogels with labile crosslinks - from synthesis to biomedical applications. *Chemical Society Reviews* **2015**.
171. Tahara, Y.; Akiyoshi, K., Current advances in self-assembled nanogel delivery systems for immunotherapy. *Advanced Drug Delivery Reviews* **2015,** *95*, 65-76.
172. Kwon, G. S., Polymeric micelles for delivery of poorly water-soluble compounds. *Crit Rev Ther Drug Carrier Syst* **2003,** *20* (5), 357-403.
173. Nishiyama, N.; Matsumura, Y.; Kataoka, K., Development of polymeric micelles for targeting intractable cancers. *Cancer Science* **2016,** *107* (7), 867-874.
174. Cabral, H.; Kataoka, K., Progress of drug-loaded polymeric micelles into clinical studies. *Journal of Controlled Release* **2014,** *190*, 465-476.
175. O'Reilly, R. K.; Hawker, C. J.; Wooley, K. L., Cross-linked block copolymer micelles: functional nanostructures of great potential and versatility. *Chemical Society Reviews* **2006,** *35* (11), 1068-1083.
176. Panyam, J.; Labhasetwar, V., Biodegradable nanoparticles for drug and gene delivery to cells and tissue. *Adv Drug Deliv Rev* **2003,** *55* (3), 329-47.
177. Soppimath, K. S.; Aminabhavi, T. M.; Kulkarni, A. R.; Rudzinski, W. E., Biodegradable polymeric nanoparticles as drug delivery devices. *Journal of controlled release : official journal of the Controlled Release Society* **2001,** *70* (1-2), 1-20.
178. Nair, L. S.; Laurencin, C. T., Biodegradable polymers as biomaterials. *Progress in Polymer Science* **2007,** *32* (8), 762-798.
179. Jain, J. P.; Chitkara, D.; Kumar, N., Polyanhydrides as localized drug delivery carrier: an update. *Expert Opin Drug Deliv* **2008,** *5* (8), 889-907.
180. Teasdale, I.; Brüggemann, O., Polyphosphazenes: Multifunctional, Biodegradable Vehicles for Drug and Gene Delivery. *Polymers* **2013,** *5* (1), 161-187.

181. Zhao, Z.; Wang, J.; Mao, H.-Q.; Leong, K. W., Polyphosphoesters in drug and gene delivery. *Advanced Drug Delivery Reviews* **2003,** *55* (4), 483-499.
182. Vauthier, C.; Dubernet, C.; Chauvierre, C.; Brigger, I.; Couvreur, P., Drug delivery to resistant tumors: the potential of poly(alkyl cyanoacrylate) nanoparticles. *Journal of controlled release : official journal of the Controlled Release Society* **2003,** *93* (2), 151-60.
183. Nicolas, J.; Couvreur, P., Synthesis of poly(alkyl cyanoacrylate)-based colloidal nanomedicines. *Wiley interdisciplinary reviews. Nanomedicine and nanobiotechnology* **2009,** *1* (1), 111-127.
184. Heller, J.; Barr, J., Poly(ortho esters)From Concept to Reality. *Biomacromolecules* **2004,** *5* (5), 1625-1632.
185. Siegel, S. J.; Kahn, J. B.; Metzger, K.; Winey, K. I.; Werner, K.; Dan, N., Effect of drug type on the degradation rate of PLGA matrices. *European journal of pharmaceutics and biopharmaceutics : official journal of Arbeitsgemeinschaft fur Pharmazeutische Verfahrenstechnik e.V* **2006,** *64* (3), 287-93.
186. Hrkach, J.; Von Hoff, D.; Ali, M. M.; Andrianova, E.; Auer, J.; Campbell, T.; De Witt, D.; Figa, M.; Figueiredo, M.; Horhota, A.; Low, S.; McDonnell, K.; Peeke, E.; Retnarajan, B.; Sabnis, A.; Schnipper, E.; Song, J. J.; Song, Y. H.; Summa, J.; Tompsett, D.; Troiano, G.; Van Geen Hoven, T.; Wright, J.; LoRusso, P.; Kantoff, P. W.; Bander, N. H.; Sweeney, C.; Farokhzad, O. C.; Langer, R.; Zale, S., Preclinical Development and Clinical Translation of a PSMA-Targeted Docetaxel Nanoparticle with a Differentiated Pharmacological Profile. *Science Translational Medicine* **2012,** *4* (128), 128ra39-128ra39.
187. Puri, A.; Loomis, K.; Smith, B.; Lee, J. H.; Yavlovich, A.; Heldman, E.; Blumenthal, R., Lipid-based nanoparticles as pharmaceutical drug carriers: from concepts to clinic. *Crit Rev Ther Drug Carrier Syst* **2009,** *26* (6), 523-80.
188. Barenholz, Y., Doxil(R)--the first FDA-approved nano-drug: lessons learned. *Journal of controlled release : official journal of the Controlled Release Society* **2012,** *160* (2), 117-34.
189. Muehlmann, L. A.; Rodrigues, M. C.; Longo, J. P.; Garcia, M. P.; Py-Daniel, K. R.; Veloso, A. B.; de Souza, P. E.; da Silva, S. W.; Azevedo, R. B., Aluminium-phthalocyanine chloride nanoemulsions for anticancer photodynamic therapy: Development and in vitro activity against monolayers and spheroids of human mammary adenocarcinoma MCF-7 cells. *Journal of nanobiotechnology* **2015,** *13*, 36.
190. Devalapally, H.; Zhou, F.; McDade, J.; Goloverda, G.; Owen, A.; Hidalgo, I. J.; Silchenko, S., Optimization of PEGylated nanoemulsions for improved pharmacokinetics of BCS class II compounds. *Drug Delivery* **2015,** *22* (4), 467-474.
191. Neslihan Gursoy, R.; Benita, S., Self-emulsifying drug delivery systems (SEDDS) for improved oral delivery of lipophilic drugs. *Biomedicine & Pharmacotherapy* **2004,** *58* (3), 173-182.
192. Bouchemal, K.; Briançon, S.; Perrier, E.; Fessi, H., Nano-emulsion formulation using spontaneous emulsification: solvent, oil and surfactant optimisation. *International Journal of Pharmaceutics* **2004,** *280* (1), 241-251.
193. Fernandez, P.; André, V.; Rieger, J.; Kühnle, A., Nano-emulsion formation by emulsion phase inversion. *Colloids and Surfaces A: Physicochemical and Engineering Aspects* **2004,** *251* (1), 53-58.
194. Ostertag, F.; Weiss, J.; McClements, D. J., Low-energy formation of edible nanoemulsions: Factors influencing droplet size produced by emulsion phase inversion. *Journal of Colloid and Interface Science* **2012,** *388* (1), 95-102.
195. Mura, S.; Bui, D. T.; Couvreur, P.; Nicolas, J., Lipid prodrug nanocarriers in cancer therapy. *Journal of Controlled Release* **2015,** *208*, 25-41.
196. Danhier, F., To exploit the tumor microenvironment: Since the EPR effect fails in the clinic, what is the future of nanomedicine? *Journal of Controlled Release* **2016,** *244*, 108-121.
197. Lammers, T.; Kiessling, F.; Hennink, W. E.; Storm, G., Drug targeting to tumors: principles, pitfalls and (pre-) clinical progress. *Journal of controlled release : official journal of the Controlled Release Society* **2012,** *161* (2), 175-87.
198. Nagel, G.; Tschiche, H. R.; Wedepohl, S.; Calderón, M., Modular approach for theranostic polymer conjugates with activatable fluorescence: Impact of linker design on the stimuli-induced release of doxorubicin. *Journal of Controlled Release* **2018,** *285*, 200-211.

199. Câmara, A. L. d. S.; Nagel, G.; Tschiche, H. R.; Cardador, C. M.; Muehlmann, L. A.; Oliveira, D. M. d.; Alvim, P. Q.; Azevedo, R. B.; Calderón, M.; Longo, J. P. F., Acid-sensitive lipidated doxorubicin prodrug entrapped in nanoemulsion impairs lung tumor metastasis in a breast cancer model. *Nanomedicine* **2017,** *12* (15), 1751-1765.
200. Thiam, A. R.; Farese, R. V., Jr.; Walther, T. C., The biophysics and cell biology of lipid droplets. *Nature reviews. Molecular cell biology* **2013,** *14* (12), 775-786.
201. Weigelt, B.; Peterse, J. L.; van 't Veer, L. J., Breast cancer metastasis: markers and models. *Nat Rev Cancer* **2005,** *5* (8), 591-602.
202. Tang, Y.; Soroush, F.; Sheffield, J. B.; Wang, B.; Prabhakarpandian, B.; Kiani, M. F., A Biomimetic Microfluidic Tumor Microenvironment Platform Mimicking the EPR Effect for Rapid Screening of Drug Delivery Systems. *Scientific reports* **2017,** *7* (1), 9359.

6 APPENDIX

6.1 Supporting information

6.1.1 Modular approach for theranostic polymer conjugates with activatable fluorescence: impact of linker design on the stimuli-induced release of doxorubicin

Supporting Information

Modular approach for theranostic polymer conjugates with activatable fluorescence: impact of linker design on the stimuli-induced release of doxorubicin

Gregor Nagel[a], Harald R. Tschiche[b], Stefanie Wedepohl[a], Marcelo Calderón[a,*]

[a] *Freie Universität Berlin, Institute of Chemistry and Biochemistry, Takustr. 3, 14195 Berlin, Germany.*

[b] *German Federal Institute for Risk Assessment (BfR), Department of Product Research and Nanotechnology, Max-Dohrn-Str. 8-10, 10589 Berlin, Germany.*

*Corresponding author:

Prof. Dr. Marcelo Calderón

Freie Universität Berlin, Institute of Chemistry and Biochemistry

Takustrasse 3, 14195 Berlin (Germany)

Tel.: +49 30 838 459368

E-mail: marcelo.calderon@fu-berlin.de

Homepage: http://www.bcp.fu-berlin.de/chemie/calderon

Table of content:	Page
I. General information	**S3**
II. Equations	**S5**
III. Figures and Schemes	**S6**
IV. Experimental data	**S11**

I. General information

Plate reader

After cells and samples were added, the microplates (Sarstedt or Brand) were covered with optically clear adhesive seal sheets (Absolute QPCR Seal, Thermo Scientific) and placed into a Tecan Infinite M200 Pro microplate reader heated to 37 °C. Fluorescence of Dox was monitored every 5 min over 16 h using an excitation wavelength of 490 nm (9 nm bandwidth) and an emission wavelength of 590 nm (20 nm bandwidth).

GPC

Gel permeation chromatography (GPC) analysis were performed on a Shimadzu Prominenze-i LC-2030 liquid chromatography system equipped with a Shimadzu RID-20A refractive index detector. The GPC column used was a Shodex OHpak SB-806M HQ with OHpak SB-G 6B as guard column. Solvents with HPLC grade by Fisher Chemical were employed. The oven temperature was set to 30 °C. The method included a flow 0.5 mL/min with an isocratic mobile phase (PBS 10 mM phosphate, 50 mM NaCl, pH 7.4). The injection volume was 50 μL and the UV-detectors were to 490 and 650 nm). GPC data was analyzed by Shimadzu LabSolution Version 5.85 software.

Dynamic Light Scattering (DLS) Measurements

DLS measurements were performed on a Malvern Zeta-sizer Nano-ZS ZEN 3600 instrument equipped with a He-Ne laser (532 nm) and a fixed detector oriented at 173°. Conjugate solutions (0.5 mL, 1 mg/mL) were analyzed in quartz fluorescence cuvettes with a round aperture. The autocorrelation functions of backscattered light were analyzed using the Zeta-sizer DTS software from Malvern to determine the size distribution by intensity and the polydispersity index. The measurements were performed at 25 °C in water, equilibrating the system at this temperature for 120 s. Measurements were performed in triplicate of which the mean value is given.

II. Equations

Equation S1. Quenching efficiency

$$\mathrm{QE} = 100 \times \left(1 - \frac{FI_{to}}{FI_{max}}\right) \quad [2]$$

QE=Quenching efficiency, FI_{to}=fluorescence intensity at t=0, FI_{max}=fluorescence intensity after cleavage

Equation S2. relative FRET efficiency

$$E_{rel} = \frac{FI_A}{FI_D + FI_A} \quad [1]$$

E_{rel}=relative efficiency, I_A=acceptor fluorescence intensity, I_D=donor fluorescence intensity

III. Figures and Schemes

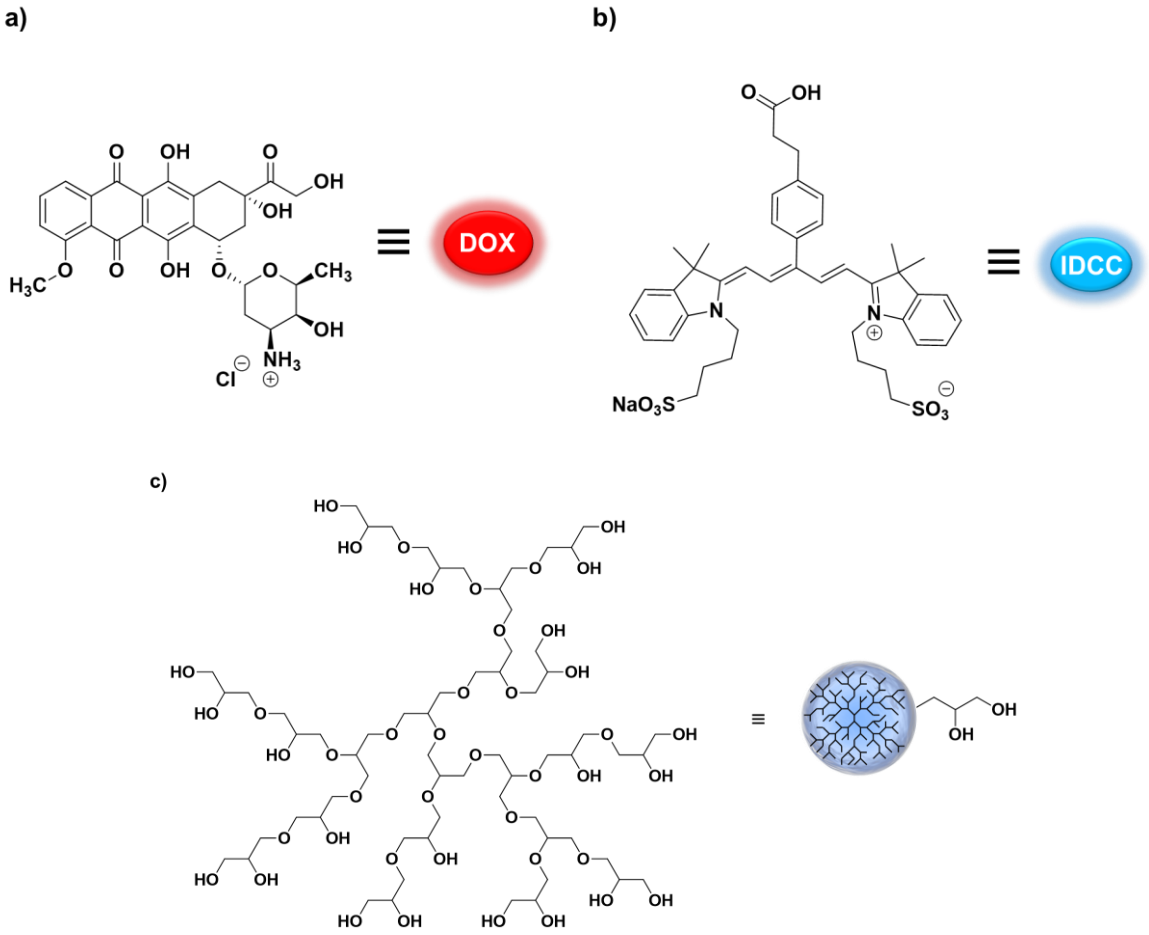

Fig. S1. Structures of building blocks of theranostic polymer conjugates: (a) Doxorubicin (Dox) HCl salt, (b) symmetric indodicarbocyanine (IDCC) dye with carboxyl group, (c) representative structure of dendritic polyglycerol (dPG).

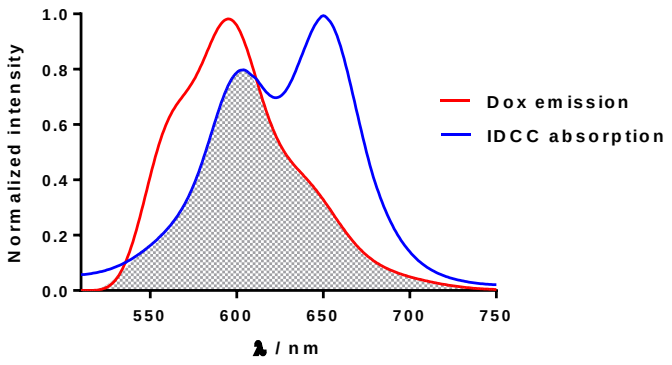

Fig. S2: Spectral overlap of Dox emission spectrum and absorption spectrum of IDCC.

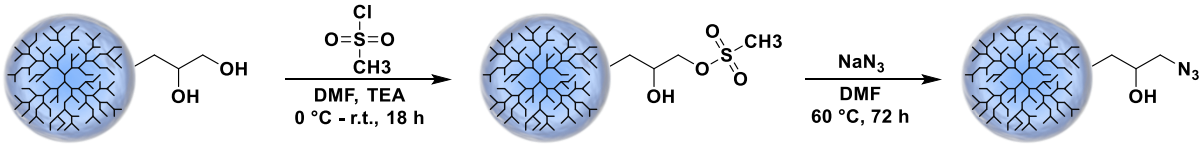

Scheme S1. Functionalization of dPG with azide groups in two steps.

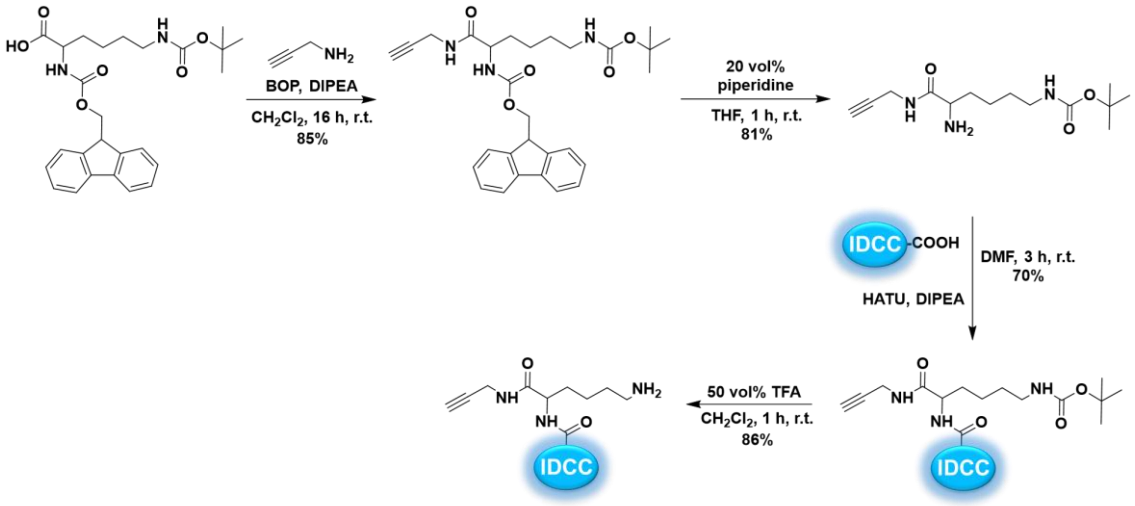

Scheme S2. Synthesis of N_{α}-IDCC-propargyl-*L*-lysine.

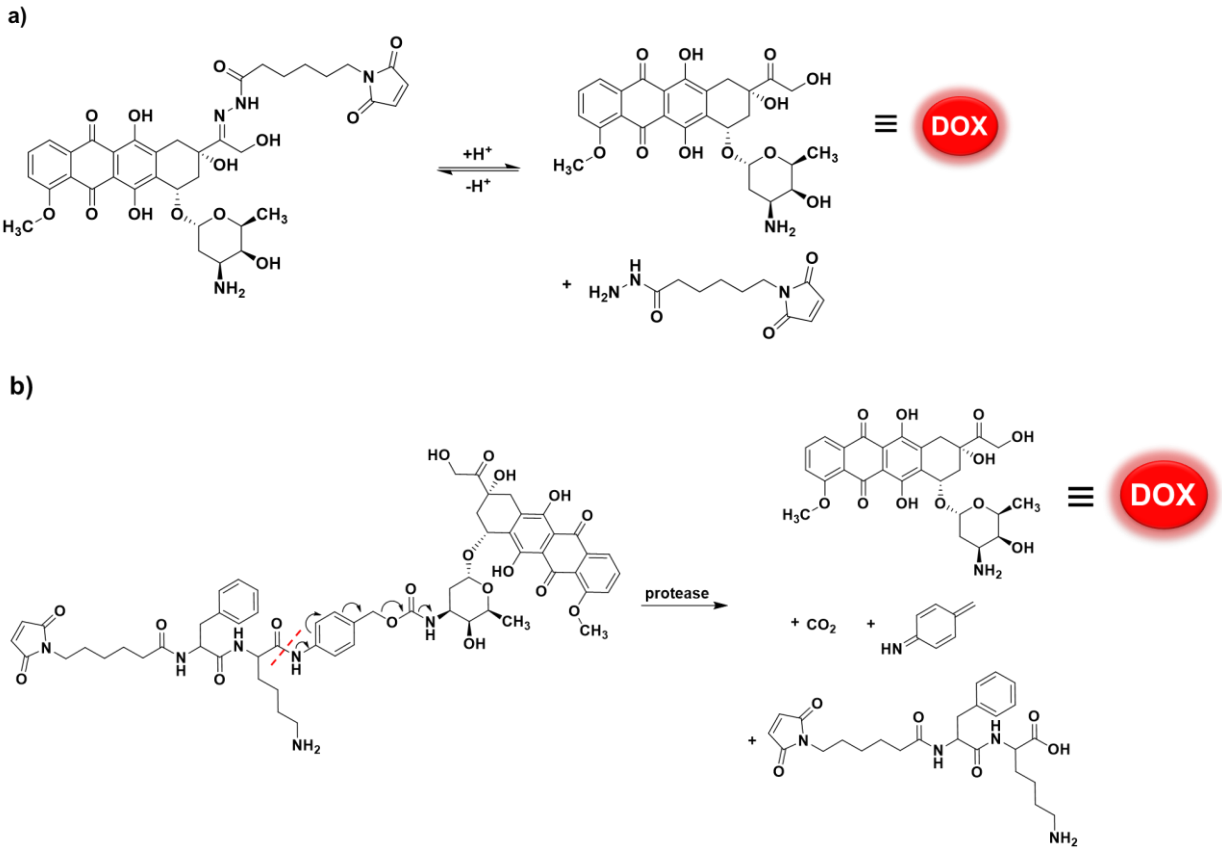

Scheme. S3. (a) Cleavage mechanism for pH-sensitive aldoxorubicin; (b) cleavage mechanism for protease-sensitive mal-Phe-Lys-PABC-Dox. Both mechanisms result in native Dox.

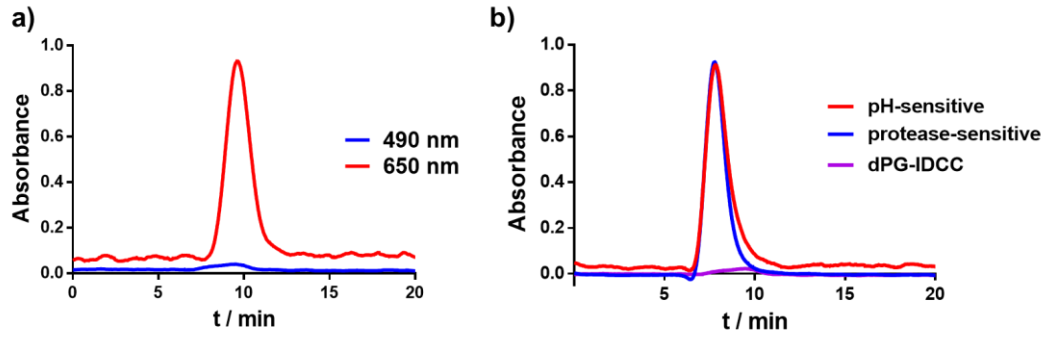

Fig. S3. GPC chromatograms of (a) dPG-IDCC with detection at 490 nm and 650 nm and (b) the TPC and dPG-IDCC with absorbance at 490 nm (Dox absorption maximum).

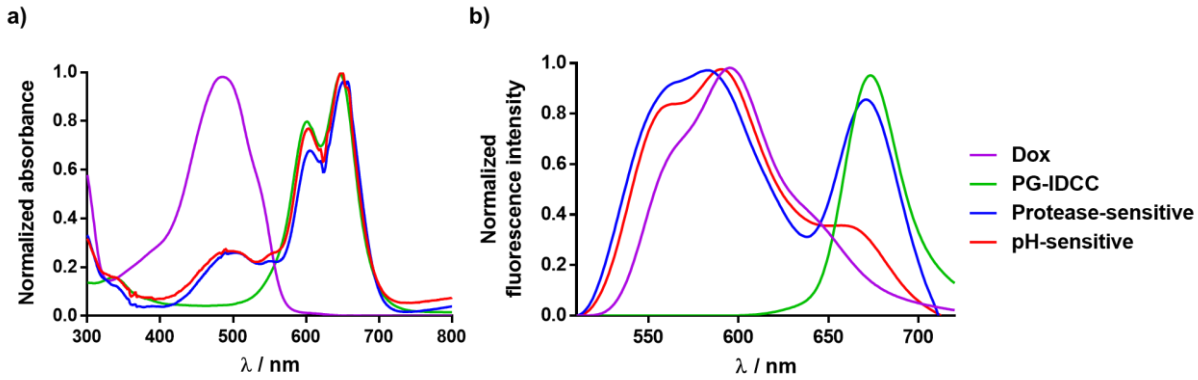

Fig. S4. Normalized (a) UV/Vis spectra and (b) fluorescence spectra of free Dox, dPG-IDCC (carrier) and the TPC (Excitation for Dox, protease- and pH-sensitive TPB: 490 nm; excitation for dPG-IDCC: 600 nm).

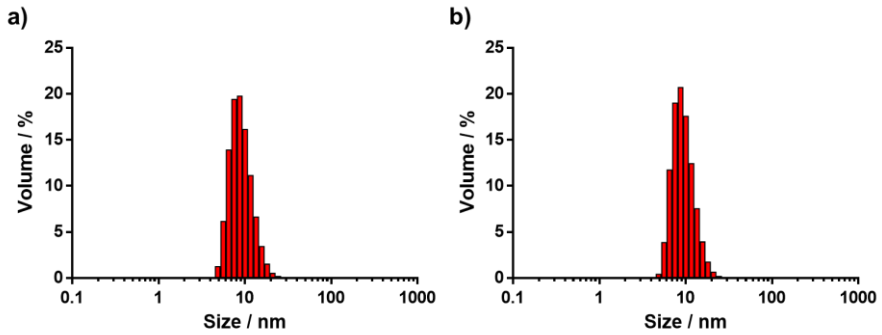

Fig. S5. Means of hydrodynamic diameter of (a) pH-sensitive and (b) protease-sensitive TPC by DLS.

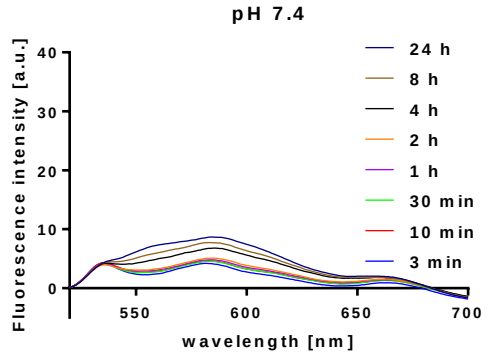

Fig. S6. Fluorescence spectra of protease-sensitive conjugates incubated at pH 7.4 over a period of 24 h.

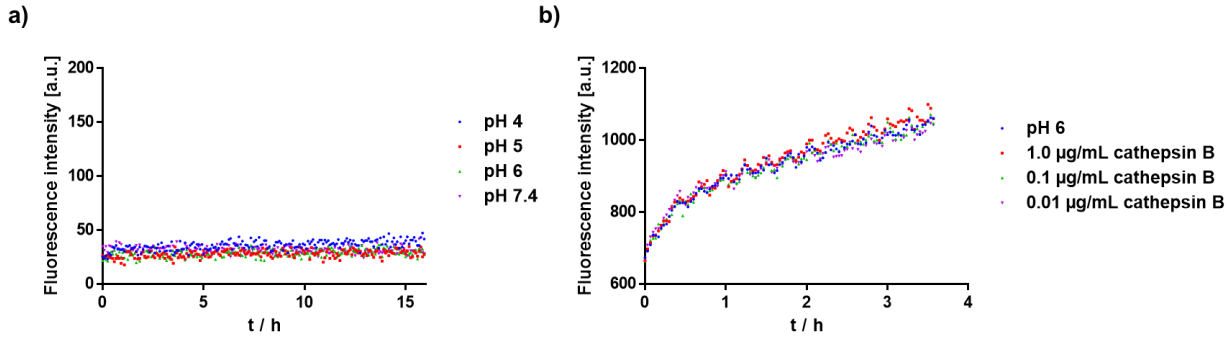

Fig. S7. (a) Fluorescence signal (Ex.: 490 nm, Em.: 590 nm) of protease-sensitive TPC incubated at different pH over time and (b) ph-sensitive TPC at different cathepsin B concentrations.

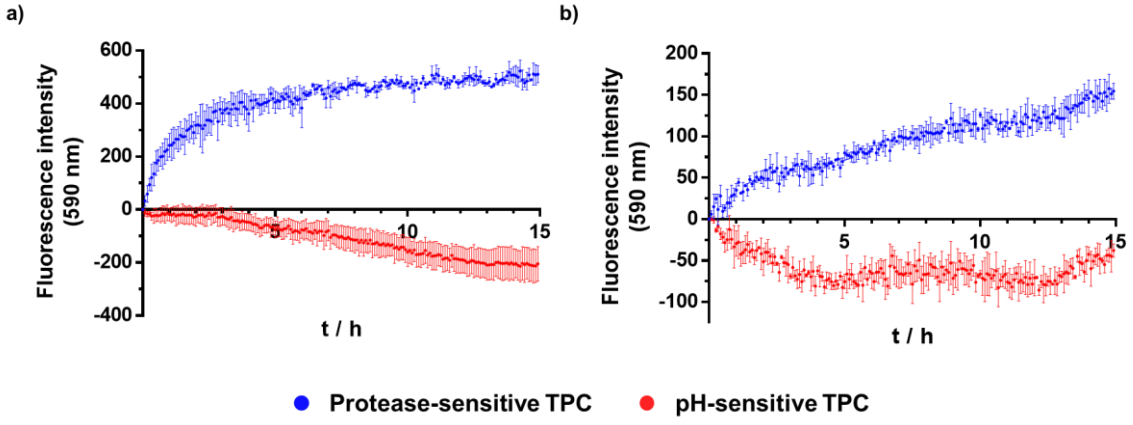

Fig. S8. pH-sensitive and protease-sensitive TPC incubated in cell-conditioned media incubated with (a) HeLa and (b) KB-V1. Error bars indicate SEM from two independent measurements.

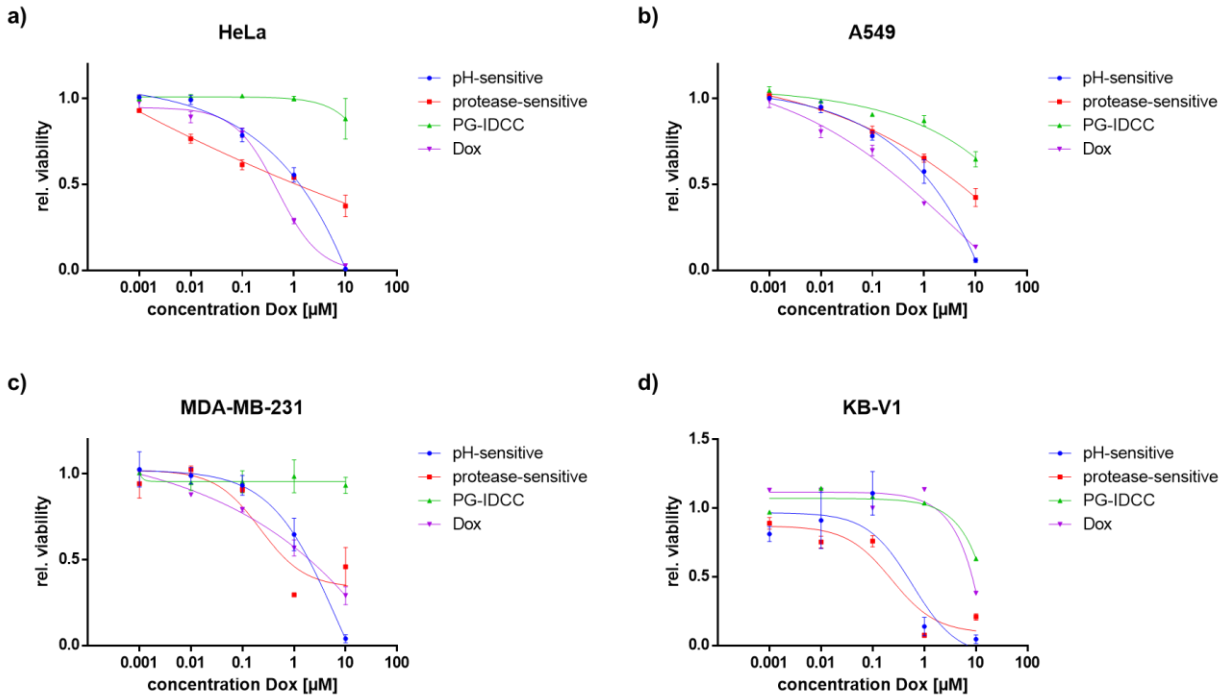

Fig. S9. Dose-response relationship for (a) HeLa, (b) A549, (c) KB-V1 and (d) MDA-MB-231 cells treated with pH-sensitive, enzyme-sensitive conjugates, PG-IDCC or Dox after 48 h.

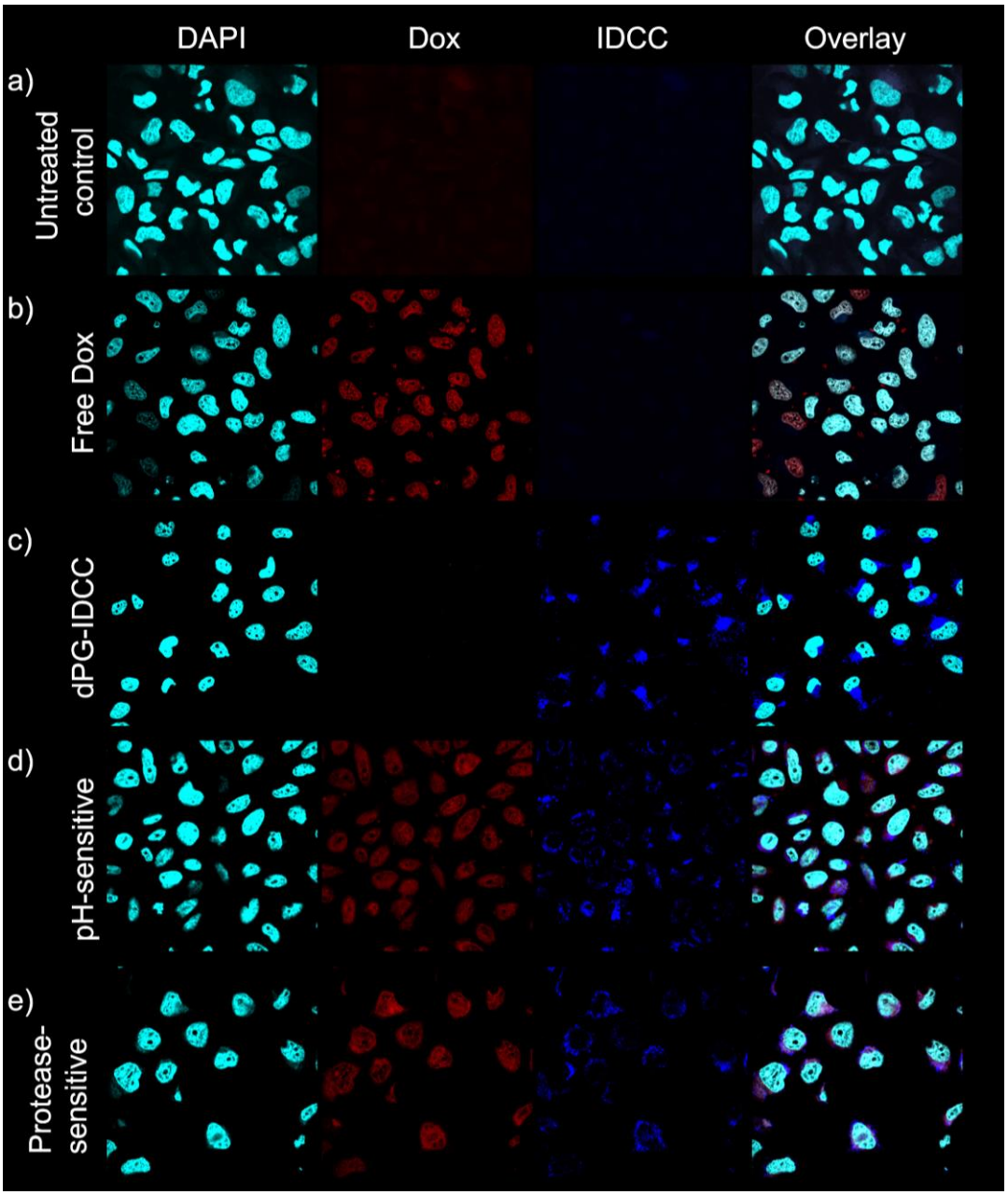

Fig. S10. Confocal laser scanning microscopy images of fixed, (a) untreated HeLa cells and HeLa cells incubated with (b) free Dox, (c) polymeric carrier dPG-IDCC, (d) pH-sensitive and (e) protease-sensitive TPC for 3 h.

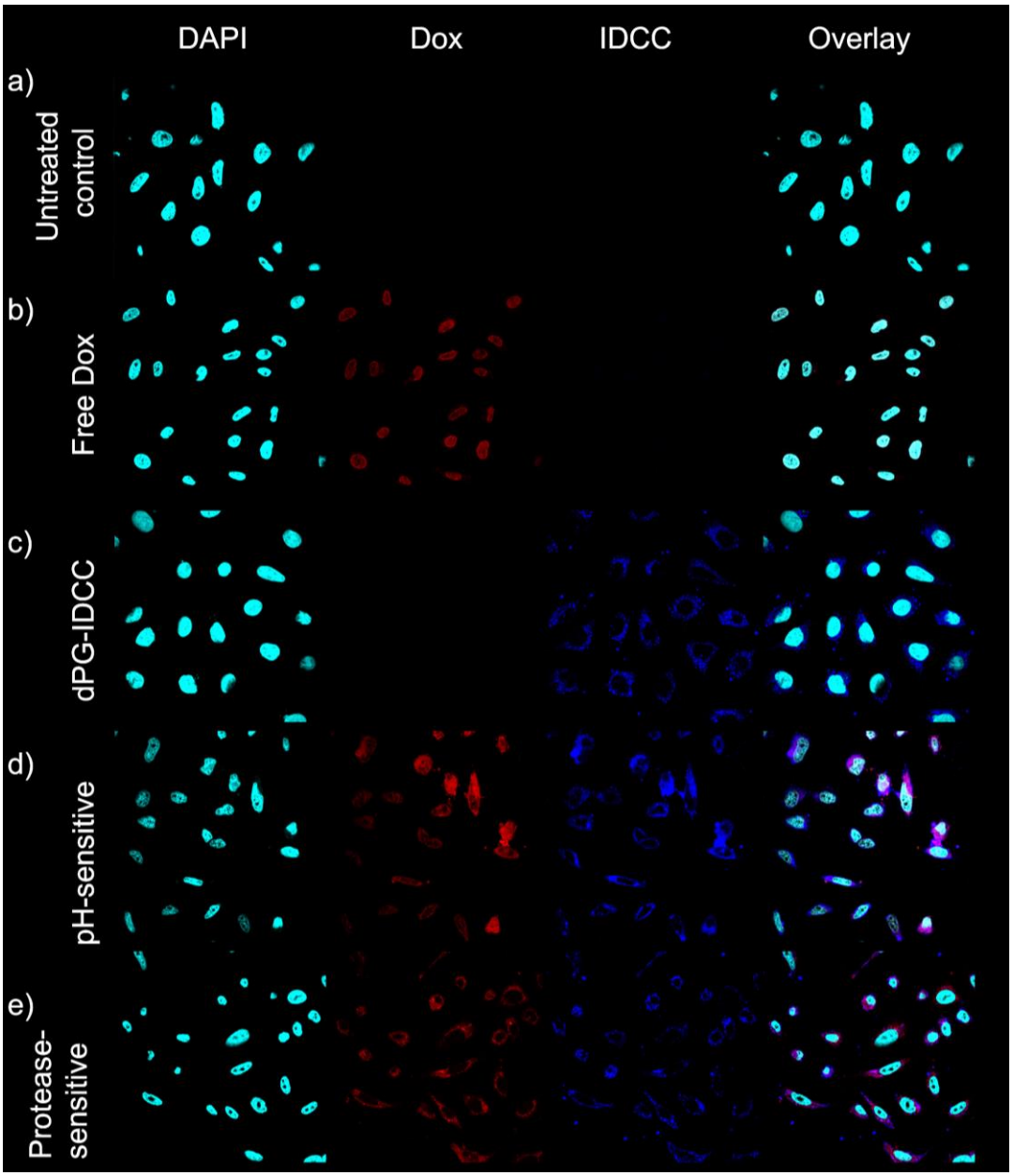

Fig. S11. Confocal laser scanning microscopy images of fixed, (a) untreated A549 cells and A549 cells incubated with (b) free Dox, (c) polymeric carrier dPG-IDCC, (d) pH-sensitive and (e) protease-sensitive TPC for 3 h.

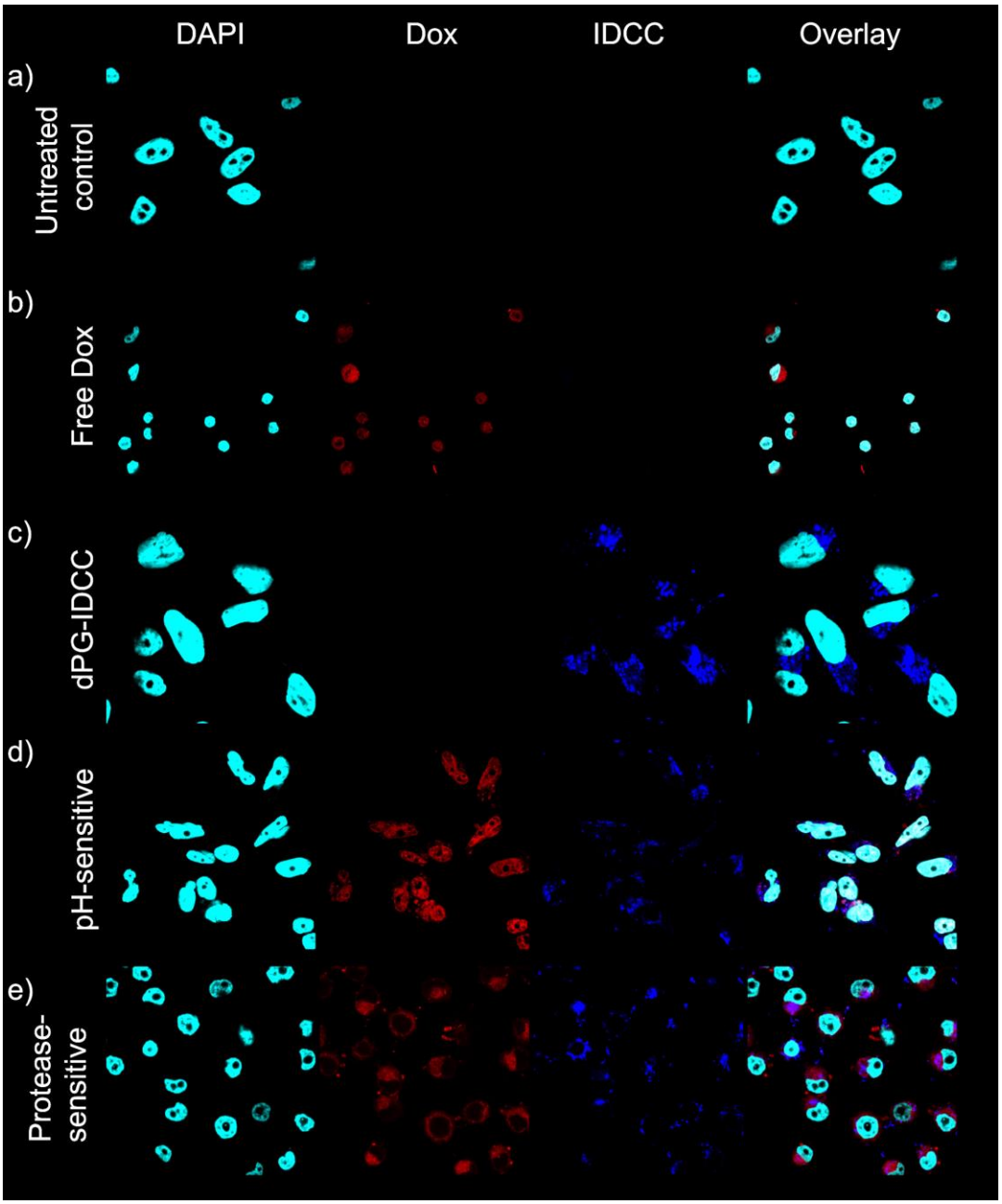

Fig. S12. Confocal laser scanning microscopy images of fixed, (a) untreated KB-V1 cells and KB-V1 cells incubated with (b) free Dox, (c) polymeric carrier dPG-IDCC, (d) pH-sensitive and (e) protease-sensitive TPC for 3 h.

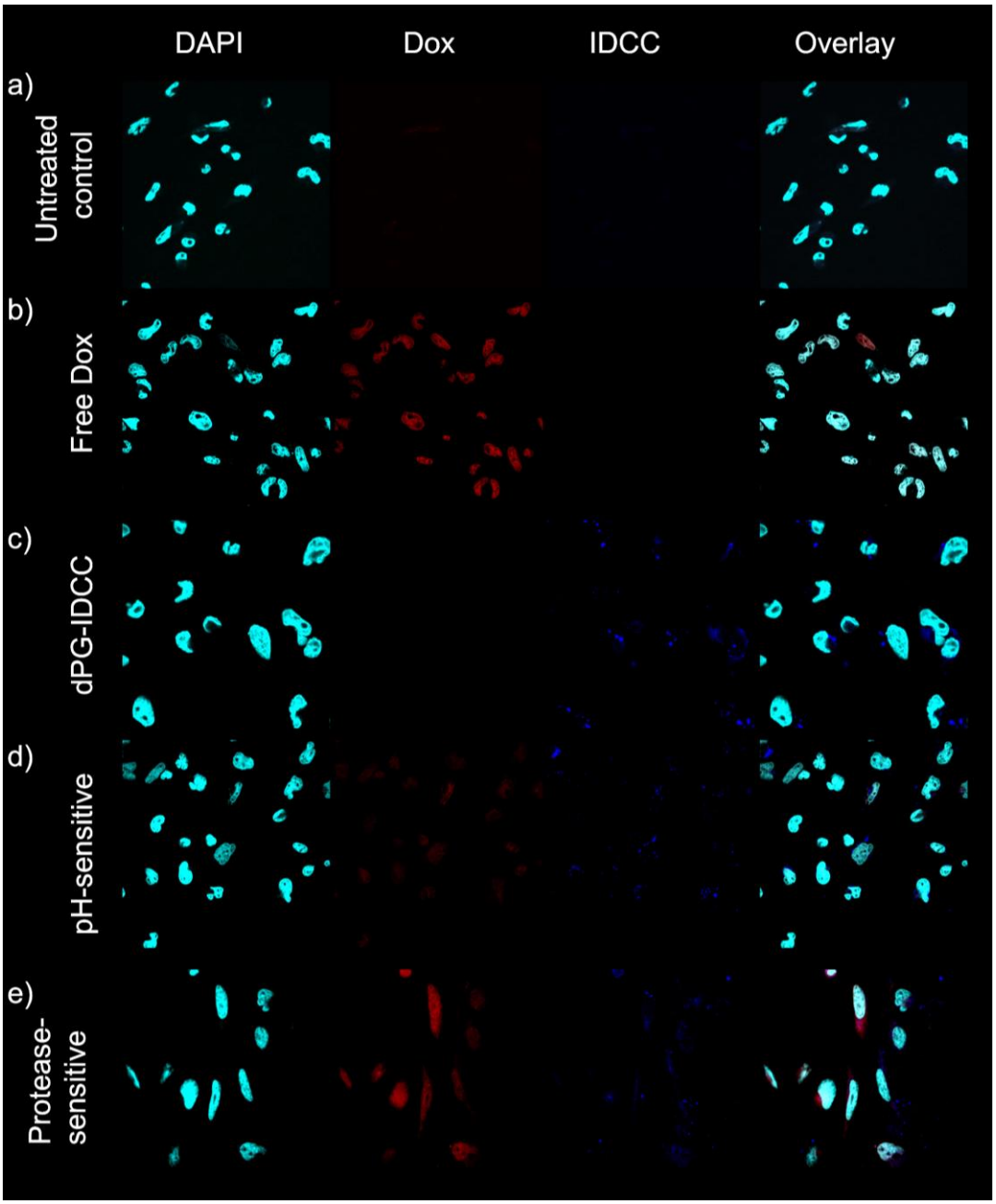

Fig. S13. Confocal laser scanning microscopy images of fixed, (a) untreated MDA-MB-231 cells and MDA-MB-231 cells incubated with (b) free Dox, (c) polymeric carrier dPG-IDCC, (d) pH-sensitive and (e) protease-sensitive TPC for 3 h.

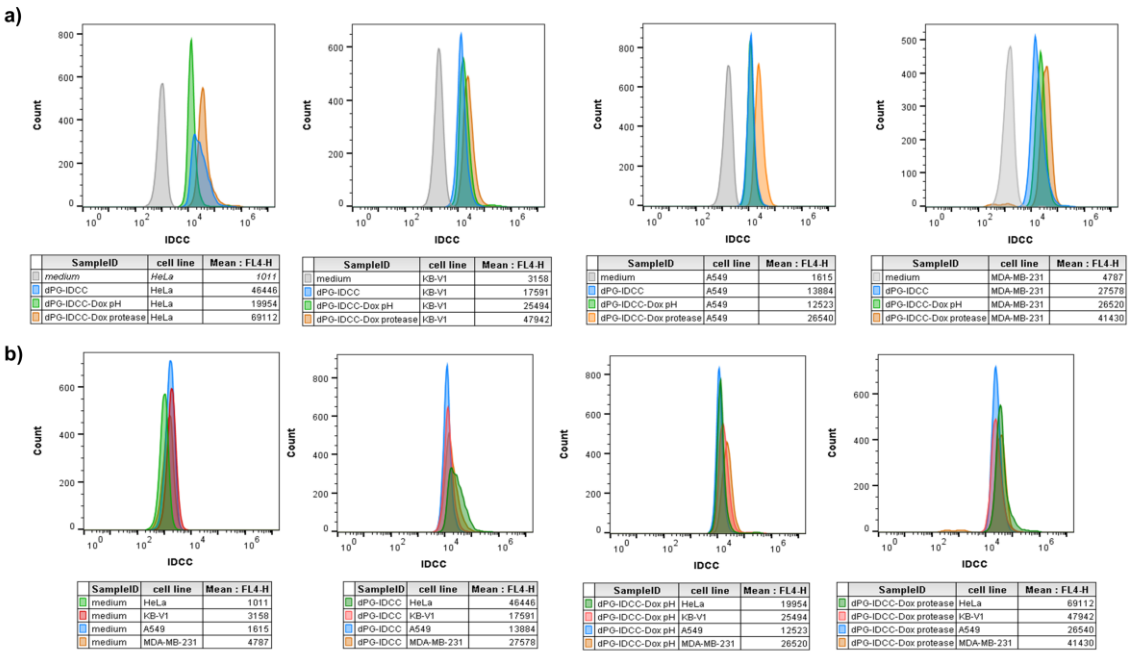

a)

SampleID	cell line	Mean : FL4-H
medium	*HeLa*	*1011*
dPG-IDCC	HeLa	46446
dPG-IDCC-Dox pH	HeLa	19954
dPG-IDCC-Dox protease	HeLa	69112

SampleID	cell line	Mean : FL4-H
medium	KB-V1	3158
dPG-IDCC	KB-V1	17591
dPG-IDCC-Dox pH	KB-V1	25494
dPG-IDCC-Dox protease	KB-V1	47942

SampleID	cell line	Mean : FL4-H
medium	A549	1615
dPG-IDCC	A549	13884
dPG-IDCC-Dox pH	A549	12523
dPG-IDCC-Dox protease	A549	26540

SampleID	cell line	Mean : FL4-H
medium	MDA-MB-231	4787
dPG-IDCC	MDA-MB-231	27578
dPG-IDCC-Dox pH	MDA-MB-231	26520
dPG-IDCC-Dox protease	MDA-MB-231	41430

b)

SampleID	cell line	Mean : FL4-H
medium	HeLa	1011
medium	KB-V1	3158
medium	A549	1615
medium	MDA-MB-231	4787

SampleID	cell line	Mean : FL4-H
dPG-IDCC	HeLa	46446
dPG-IDCC	KB-V1	17591
dPG-IDCC	A549	13884
dPG-IDCC	MDA-MB-231	27578

SampleID	cell line	Mean : FL4-H
dPG-IDCC-Dox pH	HeLa	19954
dPG-IDCC-Dox pH	KB-V1	25494
dPG-IDCC-Dox pH	A549	12523
dPG-IDCC-Dox pH	MDA-MB-231	26520

SampleID	cell line	Mean : FL4-H
dPG-IDCC-Dox protease	HeLa	69112
dPG-IDCC-Dox protease	KB-V1	47942
dPG-IDCC-Dox protease	A549	26540
dPG-IDCC-Dox protease	MDA-MB-231	41430

Fig. S14. Flow cytometry a) comparison of internalization of dPG-IDCC and the TPC into HeLa, KB-V1, A549 and MDA-MB-231 (left to right) and b) comparison of internalization between the cell lines of medium, dPG-IDCC, pH-sensitive TPC and protease-sensitive TPC (left to right).

IV. Experimental Data

Synthesis of N_α-Fmoc-N_ε-Boc-propargyl-*L*-lysine

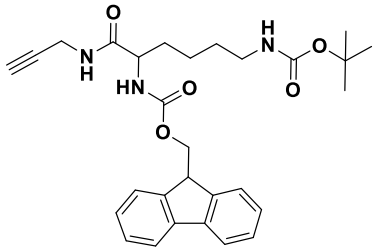

N_α-Fmoc-N_ε-Bocl-*L*-lysine (0.50 g, 1.07 mmol, 1.0 equiv.) was dissolved in 15 mL CH_2Cl_2 and (Benzotriazol-1-yloxy)tris(dimethylamino)phosphonium hexafluorophosphate (BOP, 0.568 g, 1.28 mmol, 1.2 equiv.), DIPEA (1.12 mL, 6.6 mmol, 3.0 equiv.) and propargyl amine (64.8 mg, 1.18 mmol, 1.1 equiv.) was added to the solution. After the reaction was stirred for 16 h at room temperature, solvent was evaporated and the residue was redissolved in 100 mL ethyl acetate. The organic layer was washed three times with 1 mol/L $KHSO_4$ solution, once with H_2O, three times with 5% $NaHCO_3$ solution and three times with saturated NaCl solution. The organic layer was dried over $NaSO_4$, filtered and concentrated in vacuum. Though the crude product N_α-Fmoc-$N\varepsilon$-Boc-propargyl-*L*-lysine contained propargyl amine it was used in the next step without further purification. Yield 85%.

^{1}H-NMR (400 MHz; MeOD-d4): δ (ppm) = 7.75 (d, 2H), 7.57 (d, 2H), 7.38 (t, 2H), 7.31 (t, 2H), 6.78 (bs, 1H), 5.70-5.63 (m, 1H), 4.68 (bs, 1H), 4.38 (d, 2H), 4,16-4.22 (m, 2H), 4.03-3.97 (m, 2H), 3.09 (s, 2H), 2.14 (t, 1H), 1.61-1.89 (m, 2H), 1.42 (s, 9H), 1.54-1.31 (m, 4H); **HRMS (ESI-TOF):** $C_{29}H_{35}N_3O_5Na^+$ $[M+Na]^+$ calculated**:** 528.2474; found**:**528.2493.

Synthesis of N_ε-Boc-propargyl-*L*-lysine-NH_2

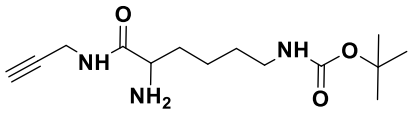

N_α-Fmoc-N_ε-Boc-propargyl-*L*-lysine (0.40 g, 0.79 mmol, 1.0 equiv.) was dissolved in 20% piperidine in THF (10 mL). After the mixture was stirred for 1 h, solvent was removed under vacuum, and the residue was co-evaporated three times with toluene and three times with chloroform. The residue was purified by column chromatography with CH_2Cl_2/MeOH (9:1 v/v) as eluent. N_ε-Boc-propargyl-*L*-lysine-NH_2 was obtained as yellow oil. Yield 81%.

^{1}H-NMR (400 MHz; MeOD-d4): δ (ppm) =3.96 ((t, *J* = 3.2 Hz,, 2H), 3.31 (t, *J* = 6.6 Hz, 1H), 3.01 (t, *J* = 6.9 Hz, 2H), 2.58 (t, *J* = 2.6 Hz, 1H), 1.41 (s, 9H), 1.71–1.26 (m, 6H); **HRMS (ESI-ToF)**: m/z = $C_{14}H_{26}N_3O_3^+$ $[M+H]^+$ calculated: 284.1969; measured: 284.1985.

Synthesis of N_α-IDCC-Nε-Boc-propargyl-*L*-lysine

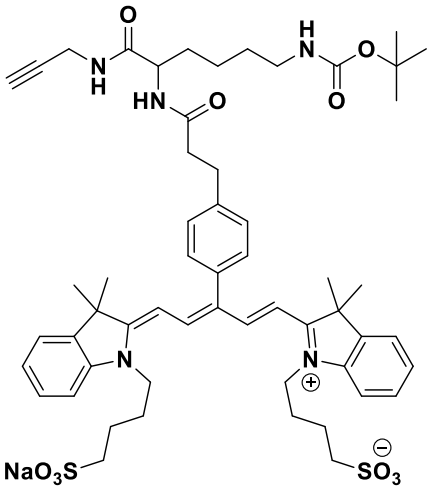

The reaction was performed under dry conditions. IDCC-COOH (0.230 g, 0.28 mmol, 1.0 equiv.), (1-[Bis(dimethylamino)methylene]-1H-1,2,3-triazolo[4,5-b]pyridinium 3-oxid hexafluorophosphate (HATU) (0.183 g, 0.48 mmol, 1.7 equiv.), *N*,*N*-diisopropylethylamine (DIPEA, 0.817 mL, 4.69 mmol, 5.5 equiv.) were dissolved in DMF (3 mL). The mixture was stirred for 30 min at room temperature, before N_ε-Boc-propargyl-*L*-lysine-NH_2 (0.122 g, 0.43 mmol, 1.5 equiv.) was added and the solution mixture was stirred for 3 h .The reaction was quenched by precipitation in diethyl ether. The suspension was filtered through a G4 glass frit. The blue solid was purified by column chromatography (reversed phase C18 43g, water/methanol; linear gradient 0-100%). Yield 70%.

^{1}H-NMR (700 MHz MeOD-d4):δ= 8.33 (d, *J* = 14.0 Hz, 2H), 7.53 (d, *J* = 7.5 Hz, 2H), 7.49 (d, J= 7.5 Hz, 2H), 7.43-7.18 (m, 8H), 5.82 (d, *J* = 14.0 Hz, 2H), 4.30 (dd, J = 9.1 Hz, 5.0 Hz, 1H), 3.97 (ddd, *J = 17.4 Hz*, *2.5 Hz*, 2H), 3.81 (m, 4H), 3.15- 2.97 (m, 4H), 2.83-2.68 (m, 6H), 2.54 (t, J = 2.5 Hz, 1H), 1.94-1.65 (m, 8H), 1.77 (s, 12H), 1.62-1.31 (m, 6H), 1.41 (s, 9H) ppm; **HRMS (ESI-TOF):** $C_{56}H_{72}N_5Na_2O_{10}S_2^+$ $[M+Na]^+$ calculated: 1084.4511; found: 1084.4623.

Synthesis of N_α-IDCC-propargyl-*L*-lysine-NH_2

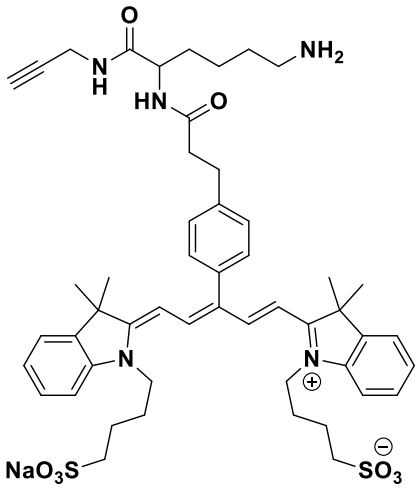

N_α-IDCC-N_ε-Boc-propargyl-*L*-lysine (50 mg, 0.047 mmol, 1.0 equiv.) was dissolved in 0.5 mL CH_2Cl_2 and 0.5 mL trifluoroacetic acid (TFA) were added. After 1 h at room temperature, the solvent and TFA were removed under vacuum. The blue solid was purified by column chromatography (reversed phase C18 43g, water/methanol; linear gradient 0-100%). Yield: 86%.

^{1}H-NMR (700 MHz, MeOD-d4): δ= 8.33 (d, *J* = 13.9 Hz, 2H), 7.54 (d, *J* = 7.5 Hz, 2H), 7.49 (d, *J* = 7.4 Hz, 2H), 7.40-7.24 (m, 8H), 5.82 (d, *J* = 13.9 Hz, 2H), 4.33 (dd, *J* = 9.1 Hz, 5.0 Hz, 1H), 3.97 (ddd, *J* = 25.5 Hz, 17.4 Hz, 2.5 Hz, 2H), 3.81 (m, 4H), 3.06 (tq, *J* = 19.1 Hz, 6.4 Hz, 5.6 Hz, 2H), 2.99 (t, *J* = 7.2 Hz, 2H), 2.84-2.67 (m, 6H), 2.54 (t, *J* = 2.6 Hz, 1H), 1.93-1.49 (m, 14H), 1.77 (s, 12H) ppm; **HRMS (ESI-TOF):** $C_{51}H_{65}N_5O_8S_2^+$ $[M+H]^+$ calculated: 940.4347; found: 940.4368; $C_{51}H_{65}N_5NaO_8S_2^+$ $[M+Na]^+$ calculated: 962.4167; found: 962.4197; $C_{51}H_{64}N_5Na_2O_8S_2^+$ $[M+2Na]^+$ calculated: 984.3986; found: 984.4013.

UV/Vis spectra of N_α-IDCC-propargyl-*L*-lysine in MeOH:

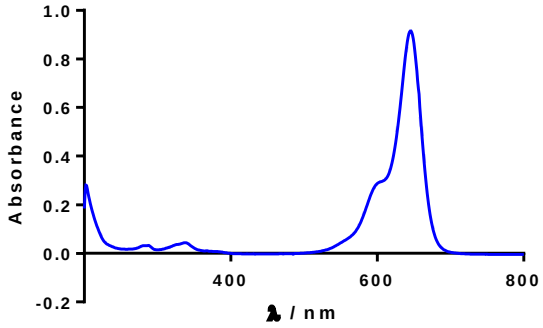

Mass spectrum (ESI-TOF) of N_α-IDCC-propargyl-*L*-lysine

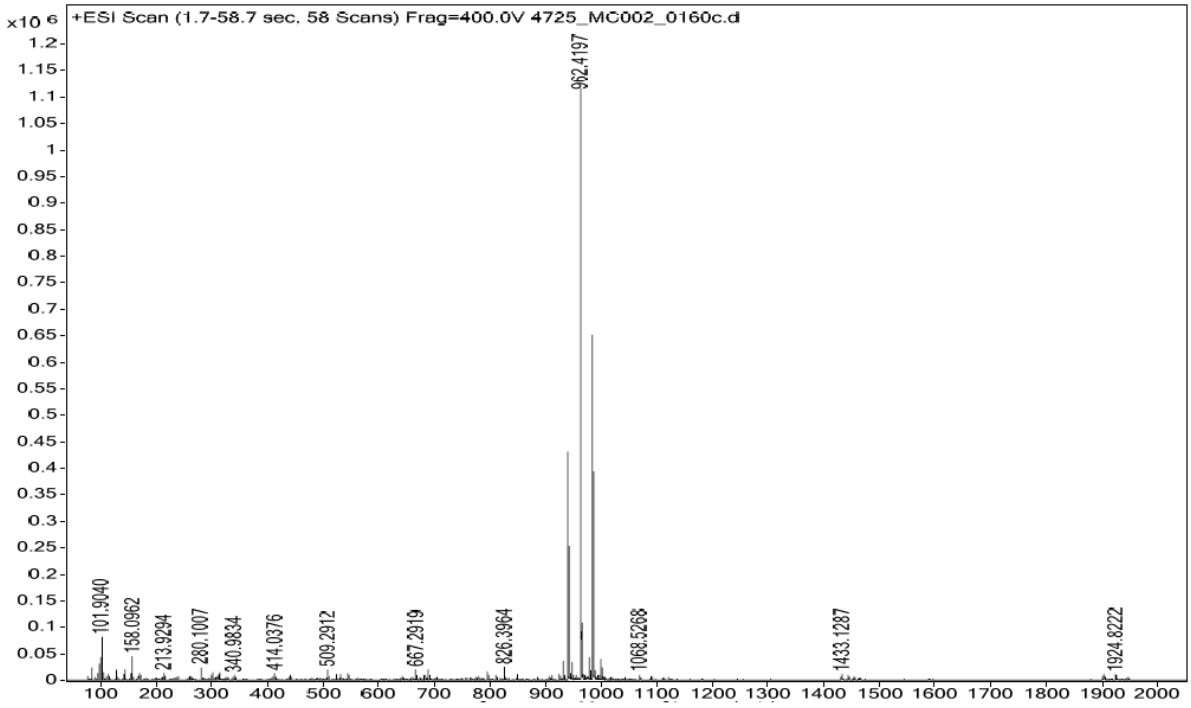

Zoom of mass spectrum (ESI-TOF) of N_α-IDCC-propargyl-*L*-lysine

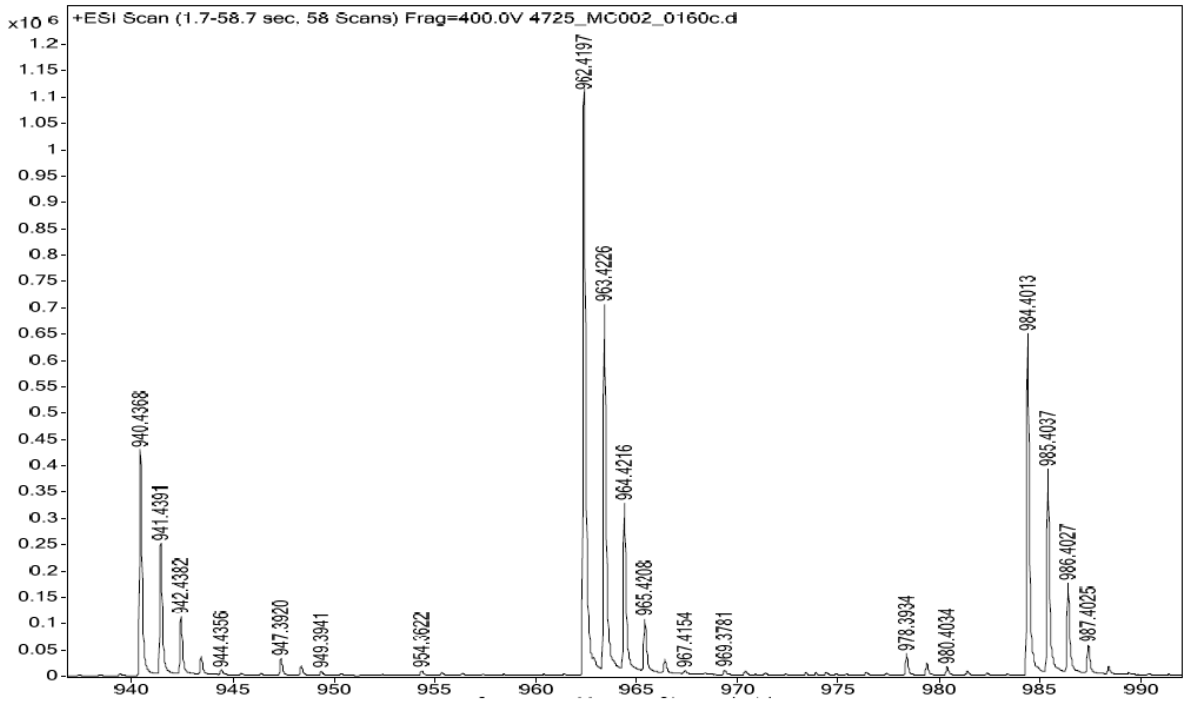

Synthesis of dPG-N_α-IDCC-propargyl-*L*-lysine

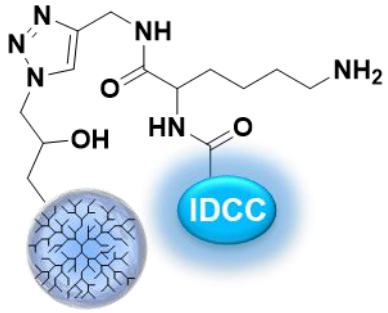

208 kDa dPG (0.070 g, 0.00034 mmol, 1.0 equiv.) with 1% of azide functionalization was dissolved in a mixture of 2 mL H_2O and 2 mL MeOH. To this solution N_α-IDCC-propargyl-*L*-lysine (0.49 mg, 0.00050 mmol, 1.5 equiv.), sodium ascorbate (0.020 mg, 0.00010 mmol, 0.3 equiv.) and copper sulphate pentahydrate (0.038 mg, 0.00015 mmol, 0.45 equiv.) were added. The pH of the solution was adjusted to pH 8 - 9 by DIPEA, purged with N_2 and then stirred for one overnight. The crude mixture was purified by ultrafiltration (MWCO 5000 g/mol) using H_2O/MeOH (1:1 v/v) as solvent with one running-circle EDTA solution to remove all copper content. The product was obtained as a blue honey-like solid. The product was characterized by UV-Vis spectroscopy, fluorescence spectroscopy, and GPC. The conjugate has a loading of 3.2 µg IDCC ($4.0 \cdot 10^{-3}$ µmol) per mg conjugate determined by UV/Vis spectroscopy, using the molar extinction coefficient ε_{650}=106000 M^{-1} $cm^{-1}$of IDCC. Conjugate formation was proven by faster polymer band on SEC compared to the free dye and by GPC. Yield 73%.

UV/Vis spectra of dPG- N_α-IDCC-propargyl-*L*-lysine in H_2O:

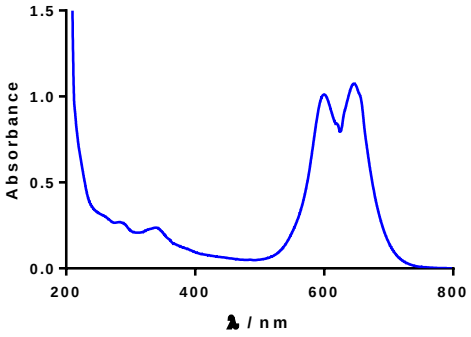

Synthesis of (6-maleimidocaproyl) hydrazone derivative of doxorubicin (aldoxorubicin)

The pH-sensitive (6-maleimidocaproyl) hydrazone derivative of doxorubicin (aldoxorubicin), was synthesized starting from 6-aminocaproic acid following a procedure from literature.[1]

^{1}H-NMR (500 MHz, MeOD-d_4): δ = 7.91 (s, 1H), 7.90 (d, *J* = 1.9 Hz, 1H), 7.65 (dd, *J* = 5.7, 4.1 Hz, 1H), 6.98 (s, 2H), 5.77 (t, *J* = 4.8 Hz, 1H), 5.51 (s, 1H), 5.46 (d, *J* = 6.2 Hz, 1H), 5.30

(d, *J* = 2.9 Hz, 1H), 4.95 (t, *J* = 6.7 Hz, 1H), 4.40 (dd, *J* = 7.6, 4.8 Hz, 2H), 4.03 (q, *J* = 6.5, 6.1 Hz, 1H), 3.98 (s, 3H), 3.57 (d, *J* = 4.3 Hz, 1H), 3.25 – 3.20 (m, 2H), 2.75 (d, *J* = 17.3 Hz, 1H), 2.21 (dd, *J* = 15.4, 7.7 Hz, 1H), 2.14 (dd, *J* = 13.4, 6.8 Hz, 1H), 2.07 (s, 2H), 1.89 (td, *J* = 12.6, 3.5 Hz, 1H), 1.73 (dd, *J* = 12.0, 4.1 Hz, 1H), 1.55 – 1.42 (m, 1H), 1.30 (q, *J* = 7.7 Hz, 3H), 1.16 (d, *J* = 6.5 Hz, 3H), 1.02 (p, *J* = 7.9 Hz, 2H) ppm; **HRMS (ESI-TOF)**: $C37H43N4O13^+$ $[M+H]^+$ calculated: 751.2821; found: 751.2861; $C37H42N4NaO13^+$ $[M+Na]^+$ calculated: 773.2641; found: 773.2664.

^{1}H-NMR of (6-maleimidocaproyl) hydrazone derivative of doxorubicin (aldoxorubicin)

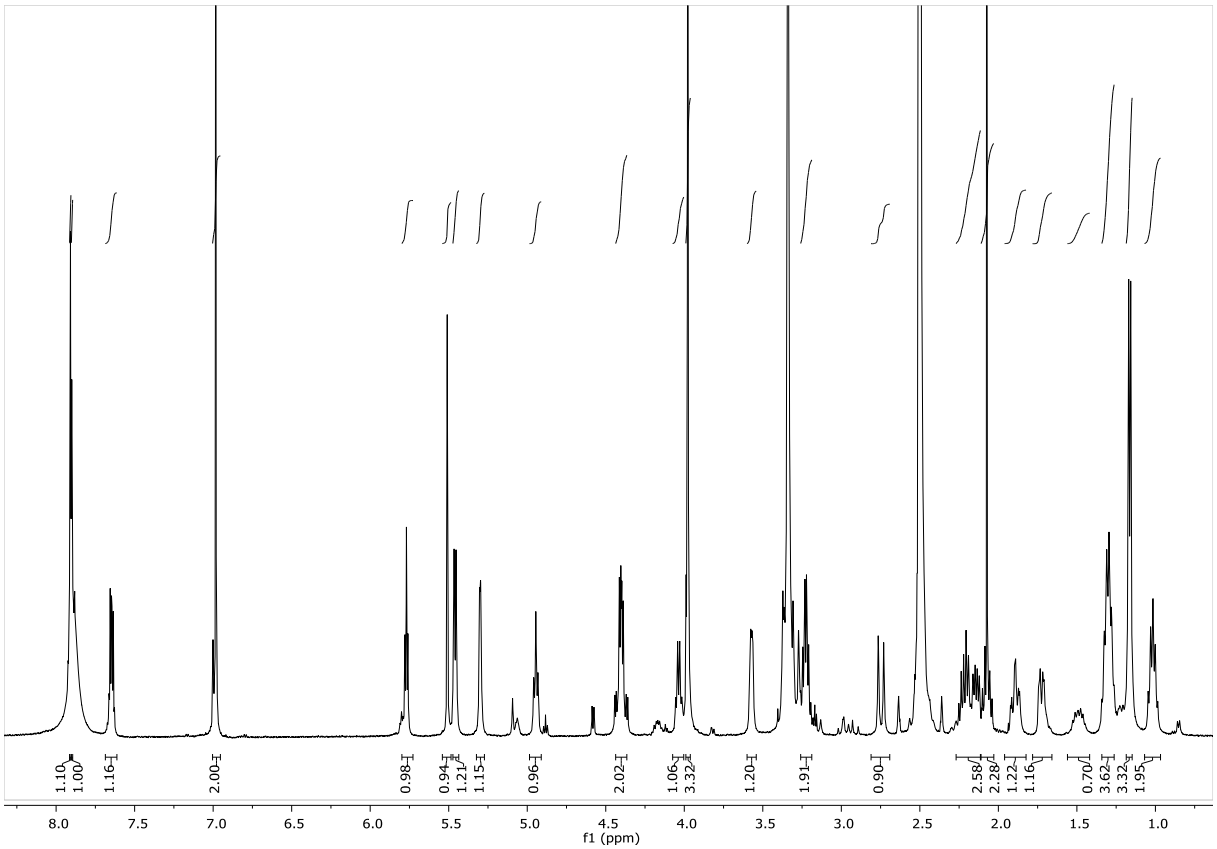

Mass spectrum (ESI-TOF) of (6-maleimidocaproyl) hydrazone derivative of doxorubicin (aldoxorubicin)

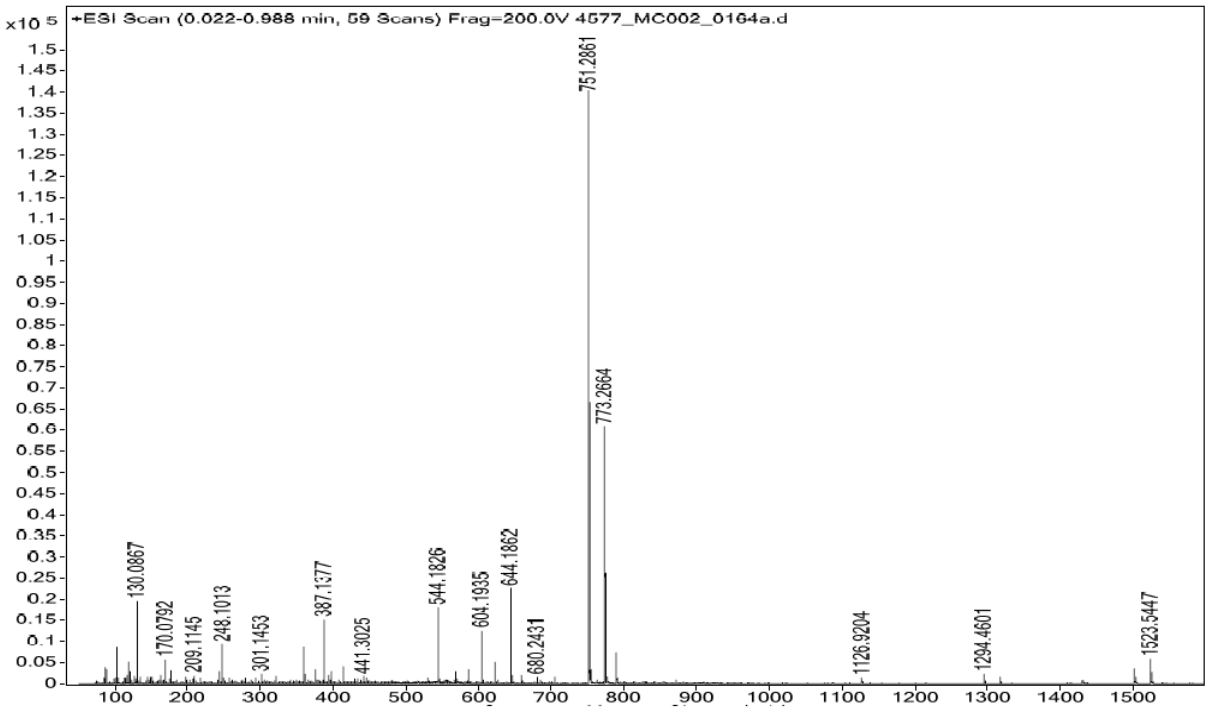
+ESI Scan (0.022-0.988 min, 59 Scans) Frag=200.0V 4577_MC002_0164a.d
x10 5
751.2861
773.2664
130.0867
544.1826
644.1862
604.1935
387.1377
248.1013
170.0792
209.1145
301.1453
441.3025
680.2431
1126.9204
1294.4601
1523.5447

Synthesis of mal-Phe-Lys-PABC-Dox

Mal-Phe-Lys-PABC-Dox was synthesized following slightly modified literature procedure.[2-3]

^{1}H NMR (700 MHz MeOD-d4): δ= 7.81 (s, 1H), 7.75 (s, 1H), 7.46 (dd, *J* = 8.3, 4.0 Hz, 2H), 7.28 (d, *J* = 8.3 Hz, 2H), 7.23 - 7.12 (m, 5H), 7.07 (s, 1H), 6.80 (s, 2H), 5.40 (d, *J* = 3.7 Hz, 1H), 5.11 – 5.00 (m, 2H), 4.76 (d, *J* = 4.5 Hz, 2H), 4.42 (dd, *J* = 9.1, 5.1 Hz, 1H), 4.27 (d, *J* = 6.7 Hz, 1H), 3.97 (s, 3H), 3.92 (d, *J* = 11.5 Hz, 1H), 3.65 (s, 1H), 3.42 (t, *J* = 7.2 Hz, 2H), 3.06 (d, *J* = 17.7 Hz, 1H), 2.97 – 2.85 (m, 4H), 2.37 (d, *J* = 14.3 Hz, 1H), 2.22 – 2.11 (m, 2H), 1.96 (td, *J* = 13.1, 4.0 Hz, 1H), 1.86 (dq, *J* = 13.6, 6.2 Hz, 1H), 1.80 (dd, *J* = 13.1, 4.6 Hz, 1H), 1.76 – 1.61 (m, 3H), 1.56 – 1.39 (m, 6H), 1.29 (d, *J* = 6.4 Hz, 3H), 1.18 (dt, *J* = 16.2, 7.6 Hz, 2H) ppm; **HRMS (ESI-TOF):** $C_{60}H_{69}N_6O_{18}^+$ $[M+H]^+$ calculated: 1161.4663; found: 1161.4675.

^{1}H-NMR of mal-Phe-Lys-PABC-Dox (protease-sensitive prodrug).

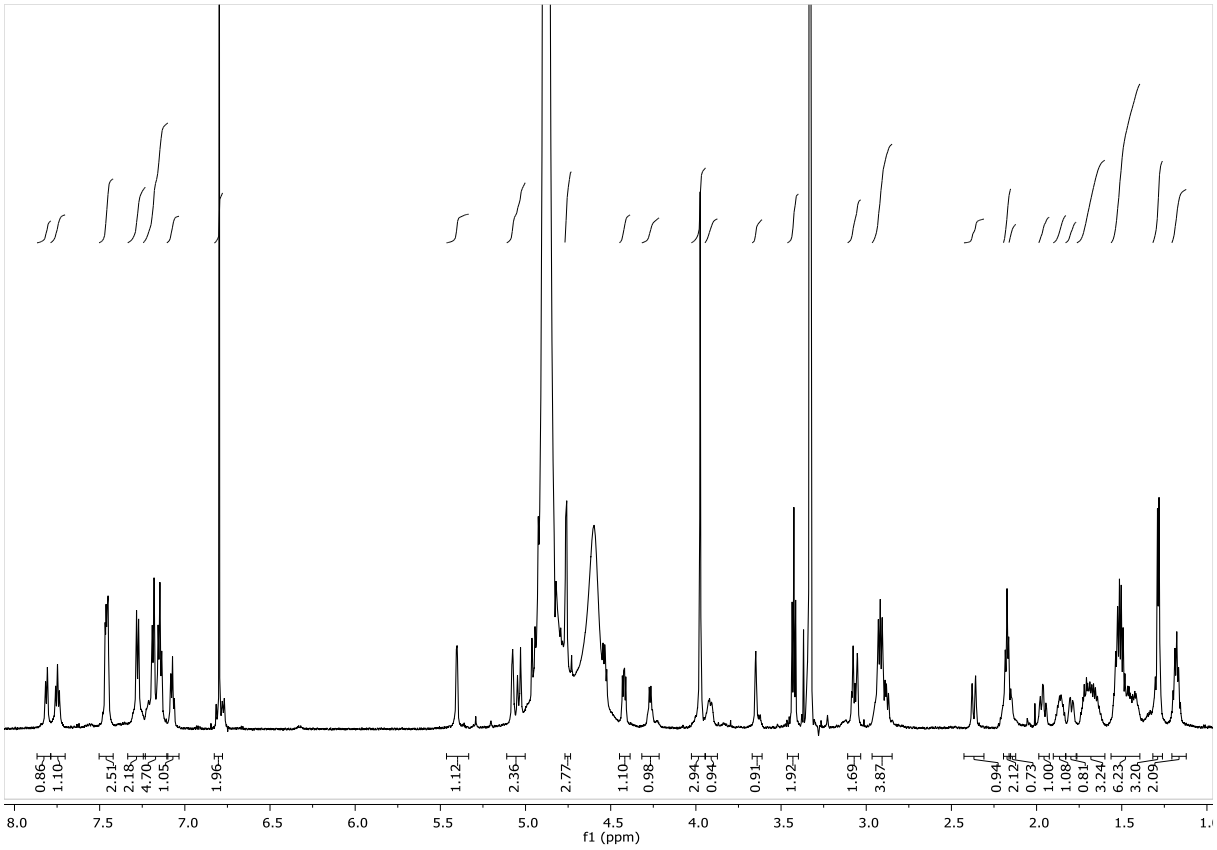

Mass spectrum (ESI-TOF) of mal-Phe-Lys-PABC-Dox (protease-sensitive prodrug)

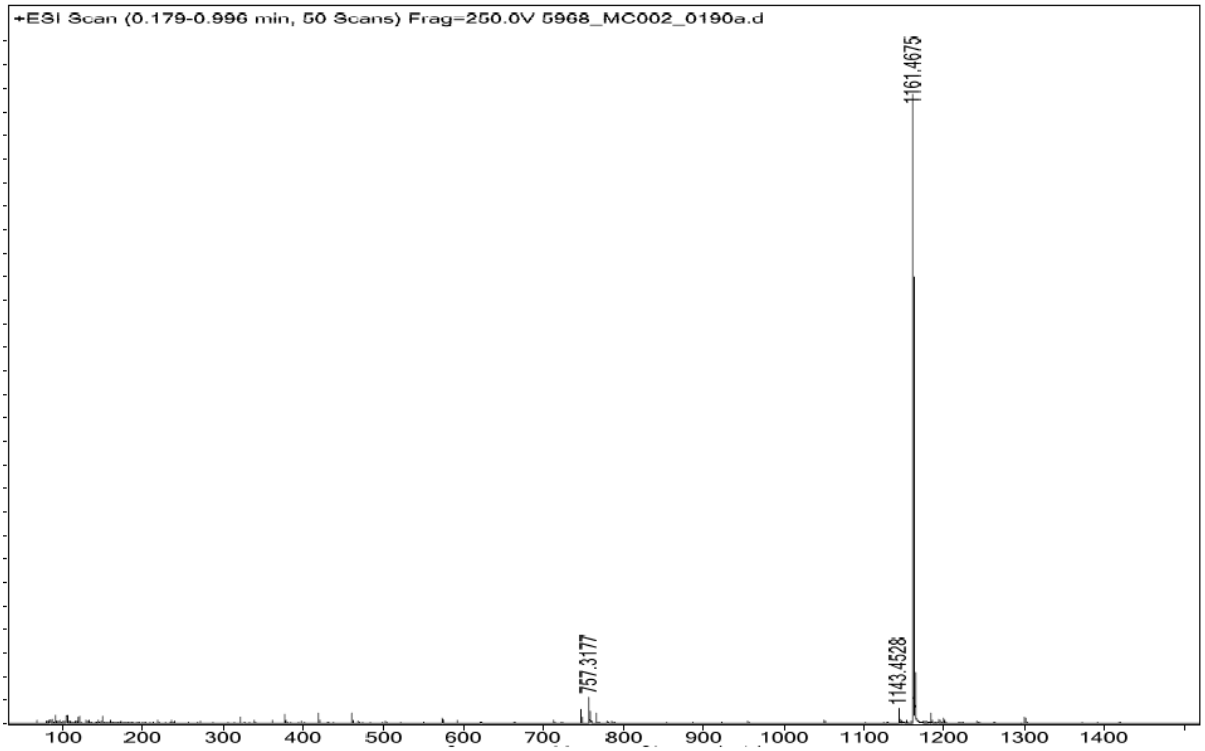

Synthesis of dPG-N_α-IDCC-propargyl-*L*-lysine-SH

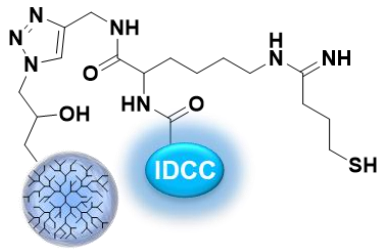

To a solution of dPG-N_α-IDCC-propargyl-*L*-lysine (20 mg, 0.0001 mmol, 1.0 equiv.) in 2 mL phosphate buffer (PB, 50 mM, pH 7.4), 2-iminothiolane (0.04 mg, 0.00029 mmol, 3.0 equiv.) was added and the reaction mixture was stirred for 20 min. The following reaction was performed in situ.

Theranostic polymer conjugate (TPC) – pH-sensitive

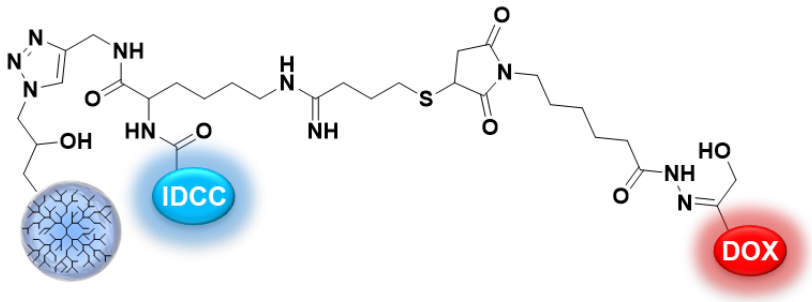

After thiolation with 2-iminothiolane, 1 mL of a PB (50 mM, pH 7.4) solution containing (6-maleimidocaproyl) hydrazone derivative of doxorubicin (aldoxorubicin, 0.36 mg, 0.0005 mmol, 5.0 equiv.) was added dropwise. The reaction mixture was stirred for 3 h. Afterwards the solution was purified by SEC using a Sephadex LH20 superfine gel followed by a Sephacryl G25 superfine HR column eluted with PB (50mM, pH 7.4). The conjugate loading was determined by UV/Vis spectroscop with $3.4 \cdot 10^{-3}$ µmol Dox (2.0 µg) and $4.0 \cdot 10^{-3}$ µmol IDCC (3.2 µg) per mg polymer, using the molar extinction coefficients ε_{495}=10590 M^{-1} $cm^{-1}$for Dox and ε_{650}=106000 M^{-1} cm^{-1} for IDCC. Conjugate formation was proven by faster polymer band on SEC compared to the free dye and by the detection of UV-absorption at 490 nm at the retention time of the polymer by GPC (Fig. S3). Yield 71%

UV/Vis spectra of pH-sensitive TPC:

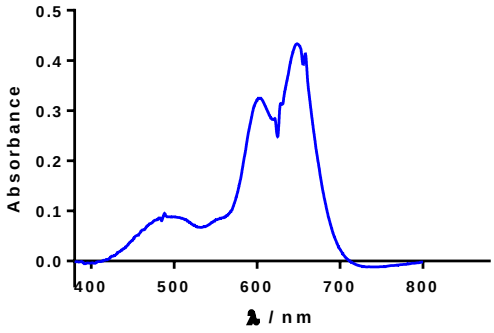

Theranostic polymer conjugate (TPC) – protease-sensitive

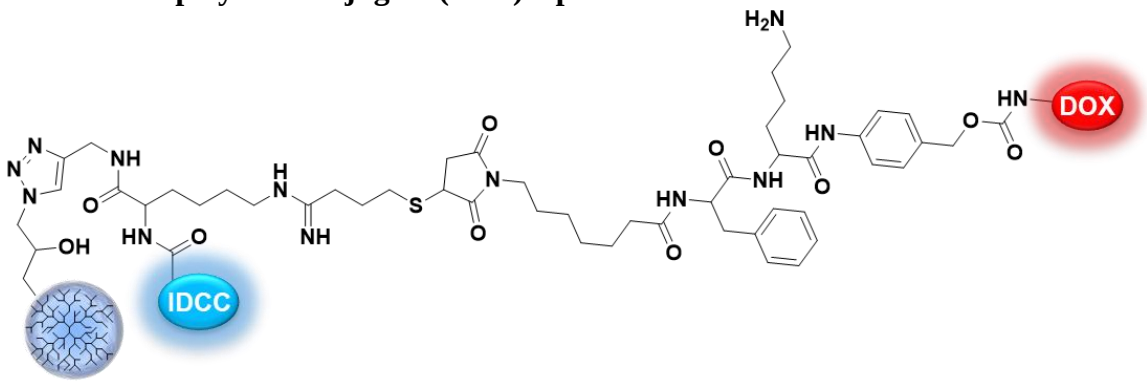

After thiolation with 2-iminothiolane, 1 mL of a PB (50 mM, pH 7.4) solution containing mal-Phe-Lys-PABC-Dox (protease-sensitive prodrug, 0.56 mg, 0.0005 mmol, 5.0 equiv.) was added dropwise. The reaction mixture was stirred for 3 h. Afterwards the solution was purified by SEC using a Sephadex LH20 superfine gel followed by a Sephacryl G25 superfine HR column eluted with PB (50mM, pH 7.4). The conjugate had a loading of $3.20 \cdot 10^{-3}$ µmol Dox (1.9 µg) and $4.0 \cdot 10^{-4}$ µmol IDCC (3.2 µg) per mg polymer determined by UV/Vis spectroscopy, using the molar extinction coefficients ε_{495}=10590 M^{-1} $cm^{-1}$for Dox[4] and ε_{650}=106000 M^{-1} cm^{-1} for IDCC. Conjugate formation was proven by faster polymer band on SEC compared to the free dye and by the detection of UV-absorption at 490 nm at the retention time of the polymer by GPC (Fig. S3). Yield 74%.

UV/Vis spectra of protease-sensitive TPC:

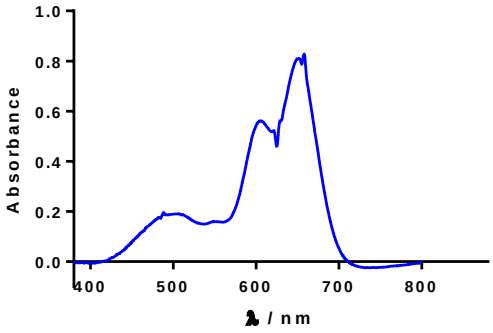

[1] D. Willner, P. A. Trail, S. J. Hofstead, H. D. King, S. J. Lasch, G. R. Braslawsky, R. S. Greenfield, T. Kaneko, R. A. Firestone, *Bioconjugate Chemistry* **1993**, *4*, 521-527.

[2] G. M. Dubowchik, R. A. Firestone, L. Padilla, D. Willner, S. J. Hofstead, K. Mosure, J. O. Knipe, S. J. Lasch, P. A. Trail, *Bioconjugate Chemistry* **2002**, *13*, 855-869.

[3] K. Abu Ajaj, R. Graeser, I. Fichtner, F. Kratz, *Cancer Chemother Pharmacol* **2009**, *64*, 413-418.

[4] F. Kratz, T. Roth, I. Fichiner, P. Schumacher, H. Fiebig, C. Unger, *Journal of Drug Targeting* **2000**, *8*, 305-318.

6.1.2 Acid-sensitive lipidated doxorubicin prodrug entrapped in nanoemulsion impairs lung tumor metastasis in a breast cancer model

Methods

C16-Dox pH-sensitive properties analysis

Water-insoluble C16-DOX was dispersed in phosphate buffer saline (PBS, Termo Fisher), pH 7.2, at 25 °C and, after 1 minute, the pH was adjusted with an excess of PBS (pH 3) to pH 3. During this process, the fluorescence (Excitation: 488 nm/Emission: 588 nm) of the system was recorded using Lumina Fluorescent and Luminescent chamber (IVIS Spectrum, Caliper, USA). Data was represented as the relative fluorescent unit (RFU).

*Quantification of doxorubicin in **NE**-C16-**DOX***

Dox was spectrometrically quantified by its absorption at 580 nm (Spectra Max). The standard curve was prepared with solutions of free Dox in ultrapure water at concentrations ranging from 0.0125 to 1.0 mg mL^{-1}.The data was collected in triplicate, and a linear regression was performed to determine the amount of Dox in the formulations. The theoretical amount of Dox in NE-C16-Dox was experimentally confirmed by UV/Vis measurements and a spectrophotometric correlation between C16-Dox (mg mL^{-1} in NE dispersion) and free Dox (mg mL^{-1} in PBS) (Figure S3A).

NE-C16-Dox pH-mediated Dox Release

Doxorubicin release from nanoemulsions was conducted by cellulose dialysis tubing using dialysis bag-diffusion (Spectrum Lab.com) method with a molecular cut-off of 10,000 Da. Dialysis tubes (AMICON, Milipore), containing 1 mL of NE C16-DOX solution, were placed in an *in vitro* release medium containing 7 mL 0.1 M potassium phosphate buffer pH 7.4 or 1 M acetate buffer pH 4. Both assemblies were kept at room temperature and mixed on a stir plate.

At different point times, 1 mL samples were withdrawn from the outer compartment and replaced with fresh release medium to maintain the same conditions. DOX concentrations in the samples were determined by spectrophotometry measurements at (580 nm). The drug concentration was calculated from the measured absorbance using a calibration curve.

In addition to the dialysis bag experiment, we evaluated Dox release by centrifugation (14,000 rpm; 20 minutes) of the NE-C16-Dox in Amicon tubes. As these tubes have filtering membranes with 10,000 Da pores, it is possible to separate the released free Dox. For that, the NE were kept under different pH conditions (7.2 and 2) for 6 hours. After centrifugation, the released Dox fluorescence (Excitation: 488 nm/Emission: 588 nm) was observed at the bottom of the tube using Lumina Fluorescent and Luminescent chamber (IVIS Spectrum, Caliper, USA).

Dox Internalization

Dox internalization was assessed in 4T1 cells incubated with NE-C16-DOX (equivalent to 100 µg Dox mL^{-1}) and free DOX (100 µg mL^{-1}) at 37 °C and 5% CO_2. After different time points (15, 30, 60 and 120 min) the supernatant was removed, cells trypsinized, inactivated, centrifuged, suspended in PBS and read by flow cytometry. Untreated cells were used as negative control. Dox fluorescence data were collected on a FACS (BD Biosciences) and all data analyzed using FlowJo Software (Tree Star Inc).

Hemolytic Analysis

The hemolytic capacity of NE C16-DOX was analyzed *in vitro* by a hemolytic activity assay using BALB/c mouse erythrocytes. The whole blood was centrifuged at 3000 RPM for 5 minutes at 10 °C and then suspended in 10 mL of saline (NaCl 150 mM). This procedure was repeated twice to remove all the plasma components. The samples were incubated for 120 minutes

with different concentrations of NE-C16-Dox and blank nanoemulsion at room temperature and then centrifuged again at 402.48 g for 5 minutes at 10 °C. The positive control was produced by suspending the red blood cells in distilled water, and the negative control in 150 mM NaCl. The supernatant was transferred to a 96-well plate, and the supernatants were measured using a spectrophotometer with a microplate reader at a wavelength of 540 nm (Bio-Rad, Hercules, CA). The data represent a triplicate analysis.

Maximum Tolerated Dose

Twenty-four healthy female BALB/c mice (8 weeks of age) were randomly distributed among the following 6 experimental groups (n=4 per group): NE-C16-DOX (40 mg kg^{-1}); NE-C16-DOX (20 mg kg^{-1}); free DOX (20 mg kg^{-1}); free DOX (10 mg kg^{-1}); free DOX (5 mg kg^{-1}) and NE-Blank. For all treatments the doses of DOX were equivalent. Four animals without treatment were used as a control. The experimental groups were treated intraperitoneally (each injection represents 20% of total dose) once a day for 5 consecutive days. Body weight and clinical observations were monitored after infection. On day 14, all 28 animals were euthanized; hearts were weighed, fixed overnight with 4% paraformaldehyde and proceeded to histological analyses according to Bicalho et all. (2013) [1].

Hemogram and Histology

For blood collection, mice were anesthetized with ketamine (100 mg kg^{-1}) and xylazine (20 mg kg^{-1}). Blood samples (1 mL) were collected by cardiac puncture using syringe containing EDTA (Ethylenediamine tetraacetic acid). Hematological analyses were conducted in an automated hematology system (Sysmex pocH-100iV Diff), which was calibrated for mice blood. After blood collection, mice were euthanized with an excess of anesthetic (xylazine and ketamine),

organs were dissected, weighed, and processed for histological analysis as described by Longo et al. 2016 [2].

Immunofluorescence and Immunohistochemical

The immunofluorescence and immunohistochemical analyses were conducted as described by Longo et al. 2016 [2]. For the immunofluorescence, the GR1 and CD11b markers (Termo Fisher) were detected in liver tissue sections. The antibodies against these two markers were coupled with red and green fluorochromes, respectively. The combination of these two markers identify the myeloid derived suppressor cells (MDSC) in liver tissue. For immunohistochemical analysis, CD34 was used to identify hematopoietic stem cell to confirm the extramedullary hematopoiesis. Figures S12 A and B represent the CD11b (green) and GR1 (red) expression in liver tissue. Figure S9C represent liver tissue stained with DAPI for nucleus identification and Figure S9D shows the area where both markers were identify together. The MDSC, doubled marked with CD11b and GR1, are highlighted with a circle.

Results

MRN and Mass Spectroscopy

^{1}H-NMR (400 MHz, DMSO): δ = 7.92 – 7.83 (m, 2H), 7.62 (dd, J = 6.3, 3.1 Hz, 1H), 5.82 (t, J = 4.8 Hz, 1H), 5.48 (s, 1H), 5.30 (s, 1H), 4.94 (q, *J* = 7.2, 6.6 Hz, 1H), 4.41 (t, *J* = 4.4 Hz, 2H), 4.05 (t, *J* = 6.7 Hz, 1H), 3.96 (s, 3H), 3.90 (ddd, *J* = 8.9, 3.8, 2.2 Hz, 1H), 3.28 – 3.19 (m, 3H), 3.22 – 3.10 (m, 1H), 2.79 (d, *J* = 17.1 Hz, 1H), 2.73 – 2.57 (m, 2H), 2.45 (t, *J* = 3.0 Hz, 1H), 2.33 – 2.21 (m, 1H), 2.21 – 2.06 (m, 2H), 1.89 (dd, *J* = 13.9, 10.1 Hz, 1H), 1.73 (d, *J* = 12.4 Hz, 1H), 1.55 – 1.41 (m, 3H), 1.39 – 1.26 (m, 4H), 1.23 – 1.12 (m, 27H), 1.08 (t, *J* = 7.0 Hz, 2H), 0.83 (t, *J* = 6.7 Hz, 3H).

HRMS (High resolution mass spectrometry) (ESI-TOF) (ESI-Time-of-Flight LC/MS mass spectrometer 6210 from Agilent Technologies): m/z calculated for ([M+H$^+$]):1009.5279; found: 1009.5220 (Figure S1A). The compound was further confirmed by ESI-TOF mass spectrometry where the found mass is in good accordance to the calculated mass (Figure S1B).

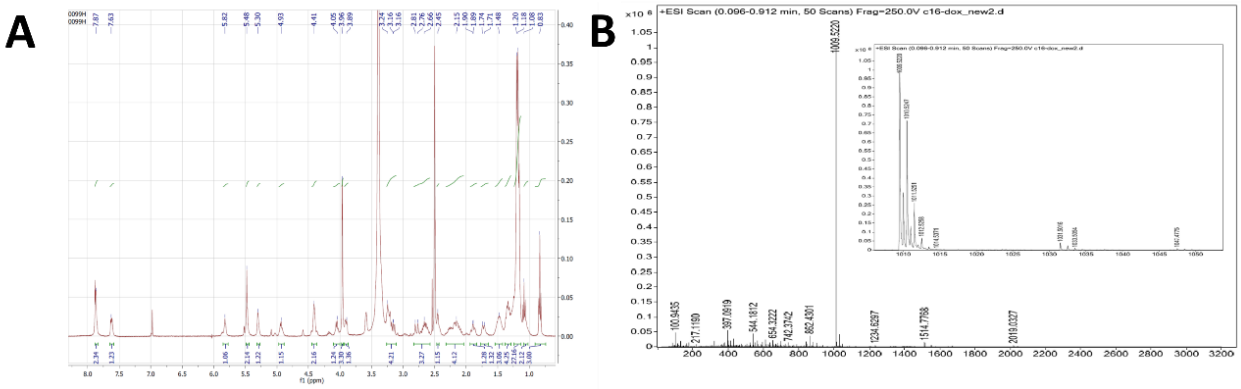

Figure S1. a) C16-Dox weight and structure analyzed by magnetic nuclear resonance spectroscopy (MNR). b) C16-Dox mass spectroscopy.

C16-Dox pH-sensitive properties analysis

The responsiveness of C16-Dox towards acidic pH-values was confirmed in an experimental set-up, following the solubilization of the prodrug at acidic pH. For that, C16-Dox was dispersed in PBS (pH 7.2), and the Dox fluorescence (Ex.: 488 nm/Em.: 590 nm) was recorded in a fluorescence chamber. After reducing the pH to 3, a significant increase in fluorescence intensity was observed over time, indicating that the displacement of the Dox molecule from the C16-Dox aggregates in acidic conditions due to a cleavage of the hydrazone bonds (Figure S2). In section S2A, the increase in fluorescence is seen to depend on pH and time. In section S2B, a quantitative representation of this experimental set-up is presented.

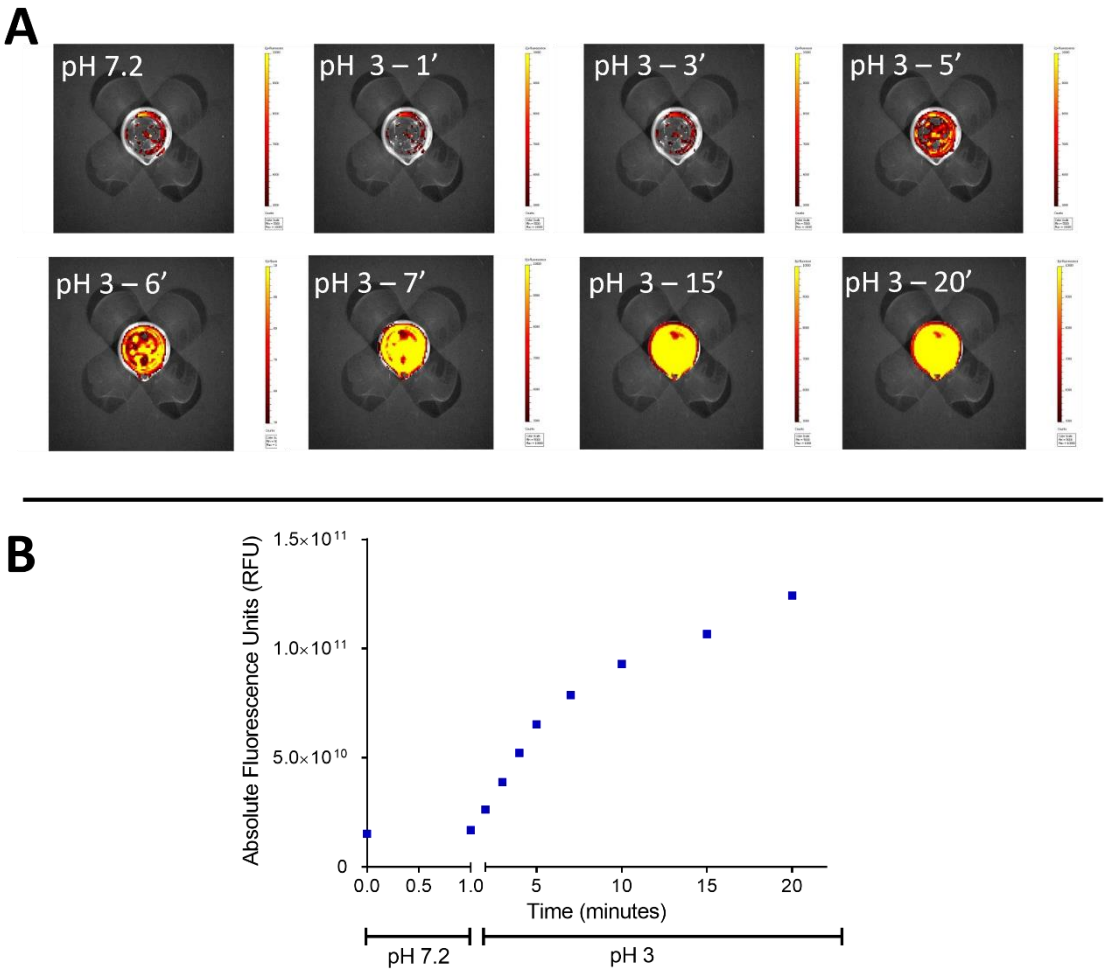

Figure S2. pH-responsiveness of C-16. Images shows Dox displacement from C16 after reducing pH: a) Qualitative representation of fluorescence intensity over time in pH 7.2 and 3; b) Quantitative image analysis in Absolute Fluorescence Intesity (RFU) over time.

NE-C16-Dox Characterization

In order to measure the amount of Dox concentration in the NE, a spectrophotometric correlation between C16-Dox (mg mL^{-1} in NE dispersion) and free Dox (mg mL^{-1} in PBS) was traced (Figure S3A). Both solutions presented a positive linear correlation, and the correlation tests confirmed (~55% w/w) the theoretical content of Dox in C16-Dox (54% w/w) experimentally. The tested NE-C16-Dox had the following final Dox concentrations: 0.22, 0.44, and 0.66 mg Dox mL^{-1} respectively.

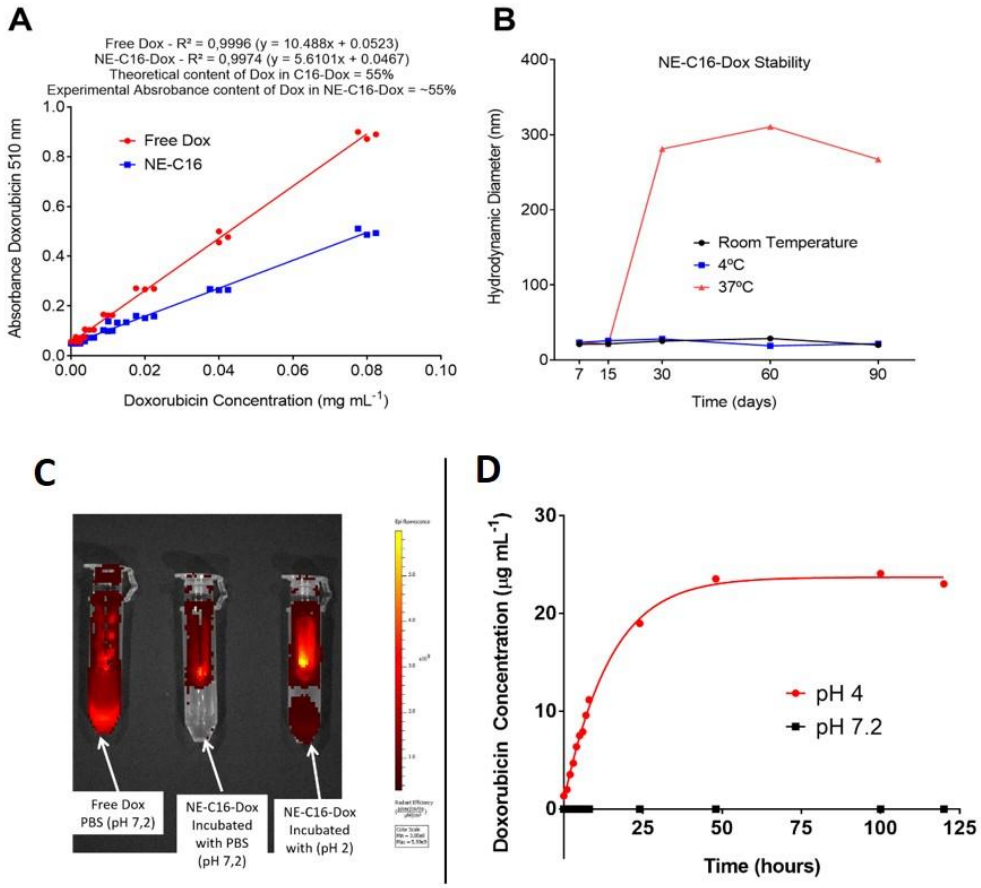

Figure S3. NE C16-DOX characterization: a) Theoretical DOX amount confirmation and calculation in NE C16-DOX by UV/Vis; b) NE C16-DOX Hydrodynamic Diameter stability in different environment over time. c) Qualitative evaluation of Dox release by fluorescence in amicon tubes; d) Quantitative evaluation of Dox release profile by dialysis experiments. Dox was quantified by spectrophotometry measurement at 580 nm.

The release of free Dox from the NE-C16-Dox nanocarrier, a key feature of this system, was evaluated qualitatively by centrifugation experiments and quantitatively by dialysis experiments. In both, a porous membrane allowed the permeation of free Dox, but not of NE-C16-Dox, from the NE dispersion to a collector compartment. Figure S3C shows Amicon tubes with Dox under different conditions. Free Dox solution can pass the membrane, and the molecule is detected at the bottom of the tube after centrifugation. In NE-C16-Dox, a pH-

dependent release is qualitatively observed (Figure S3C), where under acidic conditions (pH 2) the Dox molecule is released from the NE, while at physiological pH (7.2) Dox fluorescence is observed only in the upper part of the tube.

Long-term stability of NE-C16-Dox

The long-term NE-C16-Dox stability was evaluated measuring the hydrodynamic diameter, as well as the polidispersity index. As presented in Figure S3B, it is possible to note that the NE was stable in 4 ^{0}C and room temperature. At 37 ^{0}C, the formulation was stable for two weeks.

Dox Internalization

The absolute fluorescence intensity analysis, obtained in the cytometry experiments, shows that cells treated with NE-C16-Dox presented a more intense signal compared to the cells treated with free Dox. Furthermore, Dox fluorescence was detected in almost all cells (98%) in the first 15 minutes of exposure (Figure S4A) when associated to the NE, while for the free Dox treatment its fluorescence was detected in 65% of the cells in the same period, achieving more than 90% of positive cells only after 120 minutes of exposure to free Dox solution (Figure S4D).

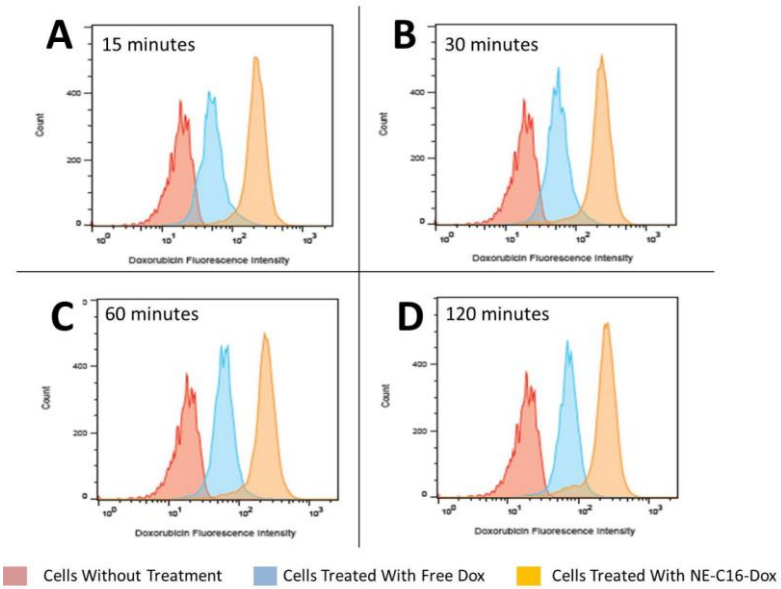

Figure S4. Dox internalization in 4T1 cells quantified by Flow Cytometry after Free Dox and NE C16-DOX exposure over time.

Maximum Tolerated Dose

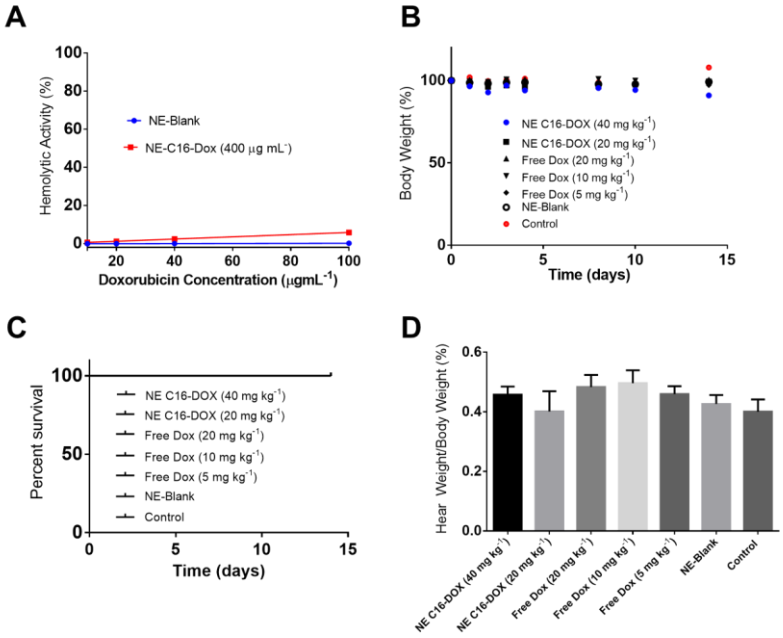

Figure S5: Maximum tolerated dose experiments in mice: A) Hemolytic activity assay analysis after treatment with NE Blank (blue) and NE-C16-Dox (red); B) Changes in mice body weight over 15 days after different treatments; C) Mice survival percentage over 15 days after different treatments; D) Changes in mice heart weight/mice body weight ratio over 15 days after different treatments. Error bars indicate the standard error of the mean (SEM) in 5 independent animal measurements.

Maximum Tolerated Dose

After *in vitro* evaluations, the potential *in vivo* effects of the NE-C16-Dox were evaluated in murine models. The first step was to establish the maximum tolerated dose (MTD) of the formulation in healthy mice. It is well known that the adverse effects of Dox, particularly its potentially severe cardiotoxicity, are dose-limiting, intensely lowering its therapeutic index. For the MTD study, healthy mice were evaluated for 15 days after different treatments. In a previous hemolytic assay, it was observed that neither blank NE and NE-C16-Dox induced significant hemolysis (Figure S5A), indicating that these formulations are safe for systemic parenteral administrations. These data are highlighted here due to some literature reports that link the toxicity of nanoemulsions to the surfactant used for oil droplet stabilization [3], an event that was not noticed with the experimental protocols used in this study.

In our MDT experiments, we neither observed weight loss (Figure S5B), mouse death (Figure S5C), nor a difference in heart weight (Figure 6D) in all the experimental treatments. In this experimental design, we compared the NE-C16-Dox MTD (20 and 40 mg Dox kg^{-1}) with the free Dox MTD (5, 10, and 20 mg kg^{-1}). It is important to highlight that free Dox at the higher concentration (40 mg kg^{-1}) was not used because previous experiments (unpublished data) showed that this dose is too toxic and causes mouse mortality at 10 days after drug administration.

The data show that NE-C16-Dox is more tolerated by healthy mice at concentrations of at least twice those of the free drug, probably due to its lower systemic toxicity in comparison to free Dox. Prevention of drug toxicity is one of the goals of drug delivery systems [4, 5] and has been the aim of various studies. The increased tolerability of Dox associated with NE-C16-Dox may

be due to the change in its pharmacokinetics, which is discussed below, or even to altered intracellular dynamics, as discussed before.

It is worth noting that the histopathological analysis of the heart in the MDT study (Figure S6) showed that the intensity of cardiac injury induced by NE-C16-Dox, even in the higher concentration treatments (NE-C16-Dox 40 mg Dox kg^{-1}), was less intense in comparison to that induced by free Dox.

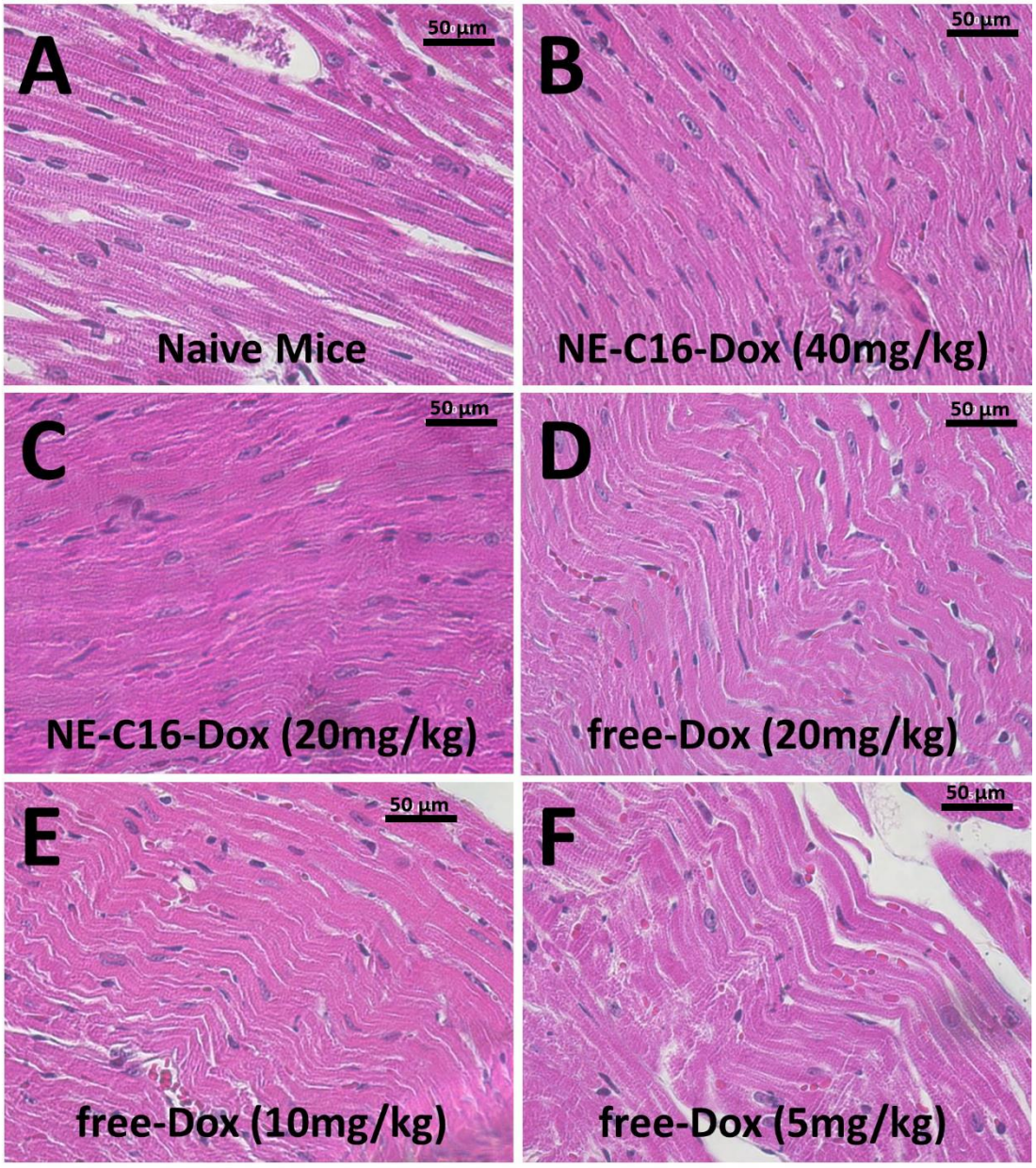

Figure S6. Heart histopatological analysis in mice after different treatments.

Dox Biodistribution

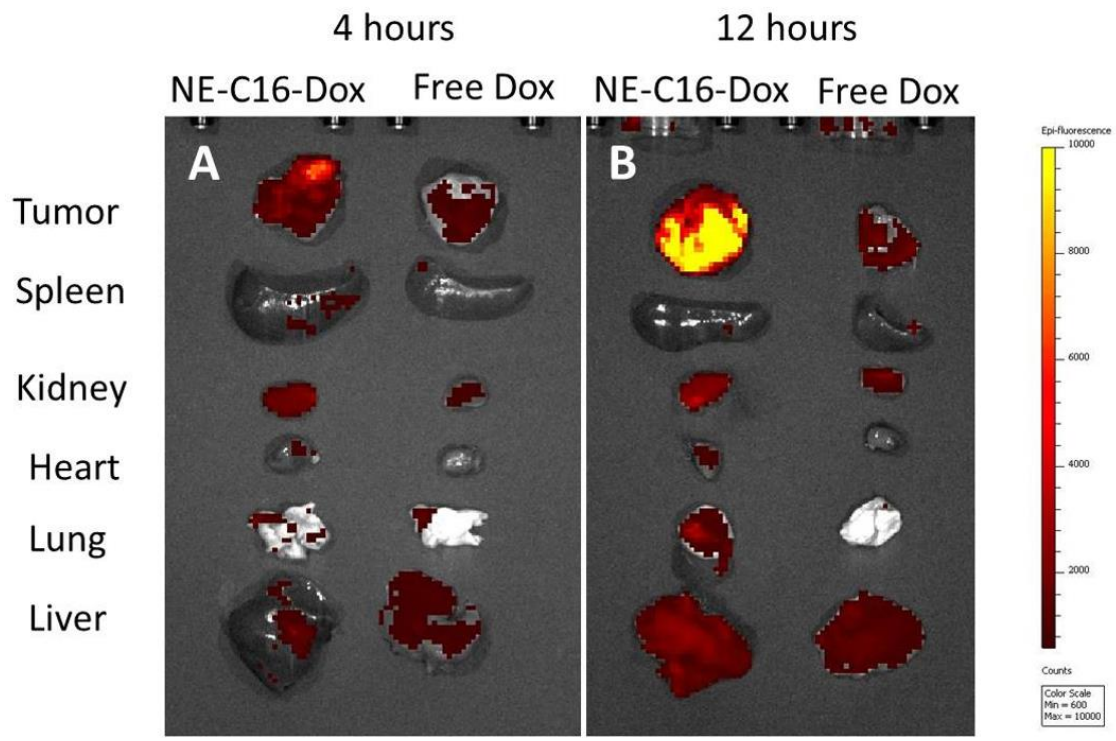

Figure S7: Qualitative Dox biodistribution in tumor-bearing mice 4 and 12 hours after treatment with NE C16-Dox (4 mg kg^{-1}) and Free Dox (4 mg kg^{-1}). A scale bar of emission quantification is placed in the right part of the figure. Yellow emission indicates higher Dox quantification, while red emission denotes lower quantification.

Lung Microtomography

Figure S8A and B represents the morphological aspects of bidimensional and tree dimensional lungs micro-CT images. Following the color scale, it is possible to note the significant density differences in the bidimensional images among the experimental groups. Noteworthy, the X-ray densities from lungs of animals treated with NE-C16-Dox are similar to those of the naïve control lungs.

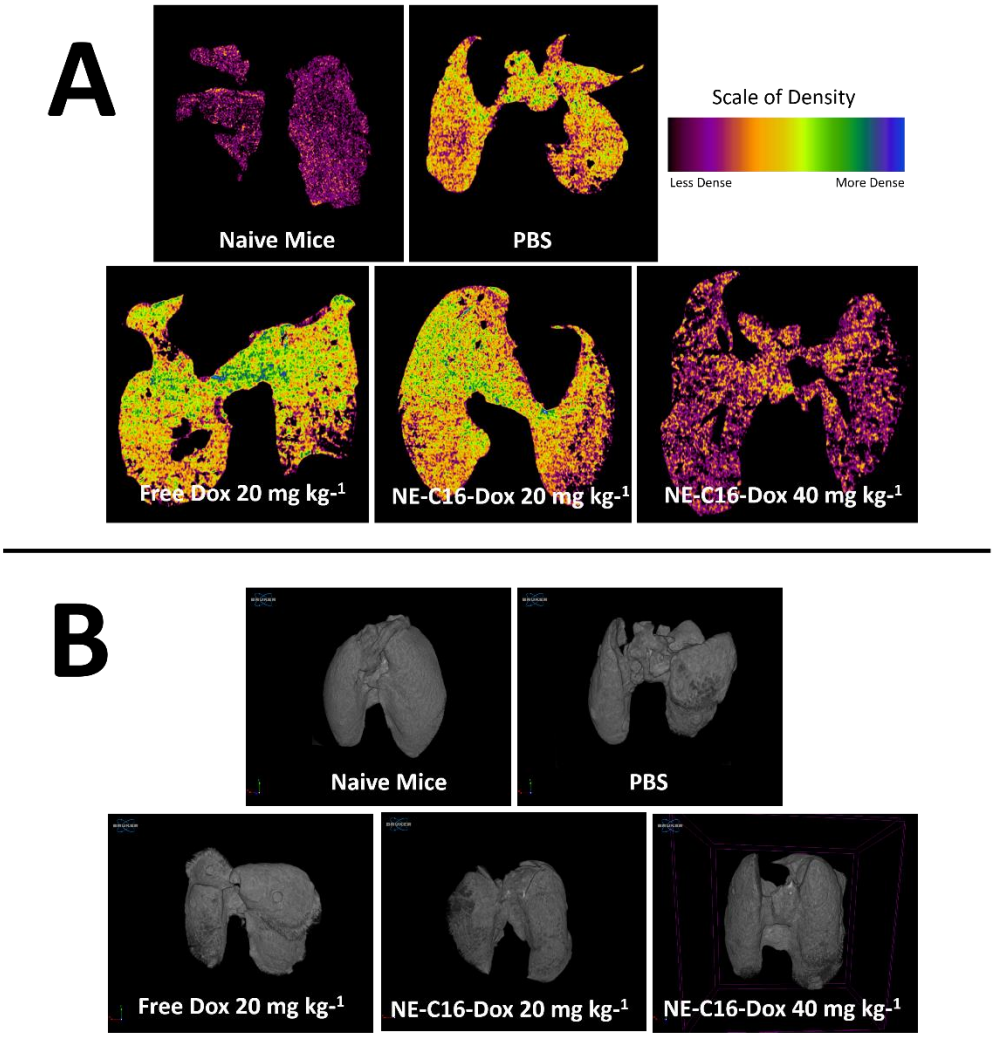

Figure S8. Mouse lung densities by X-ray in a micro computed tomography (micro-CT): a) Bidimensional cross section from mice lungs after treatments; b) a 3 dimensional aspect of mice lungs after different treatments are represented.

Lung Histopathology

Figure S9A represents the normal histological aspect of naïve control mice lungs, without metastatic proliferating cells. In Figure S9D, it is possible to note the presence of a dense tissue with metastatic tumor cells. In a higher magnification view (Figure S9F-arrow), it is possible to confirm the typical morphology of colonies of 4T1 cells in the lung tissue. Noteworthy, the

lungs from mice treated with NE-C16-Dox (40 mg kg^{-1}) presented a histological pattern similar (Figure S9B) to that of untreated control mice.

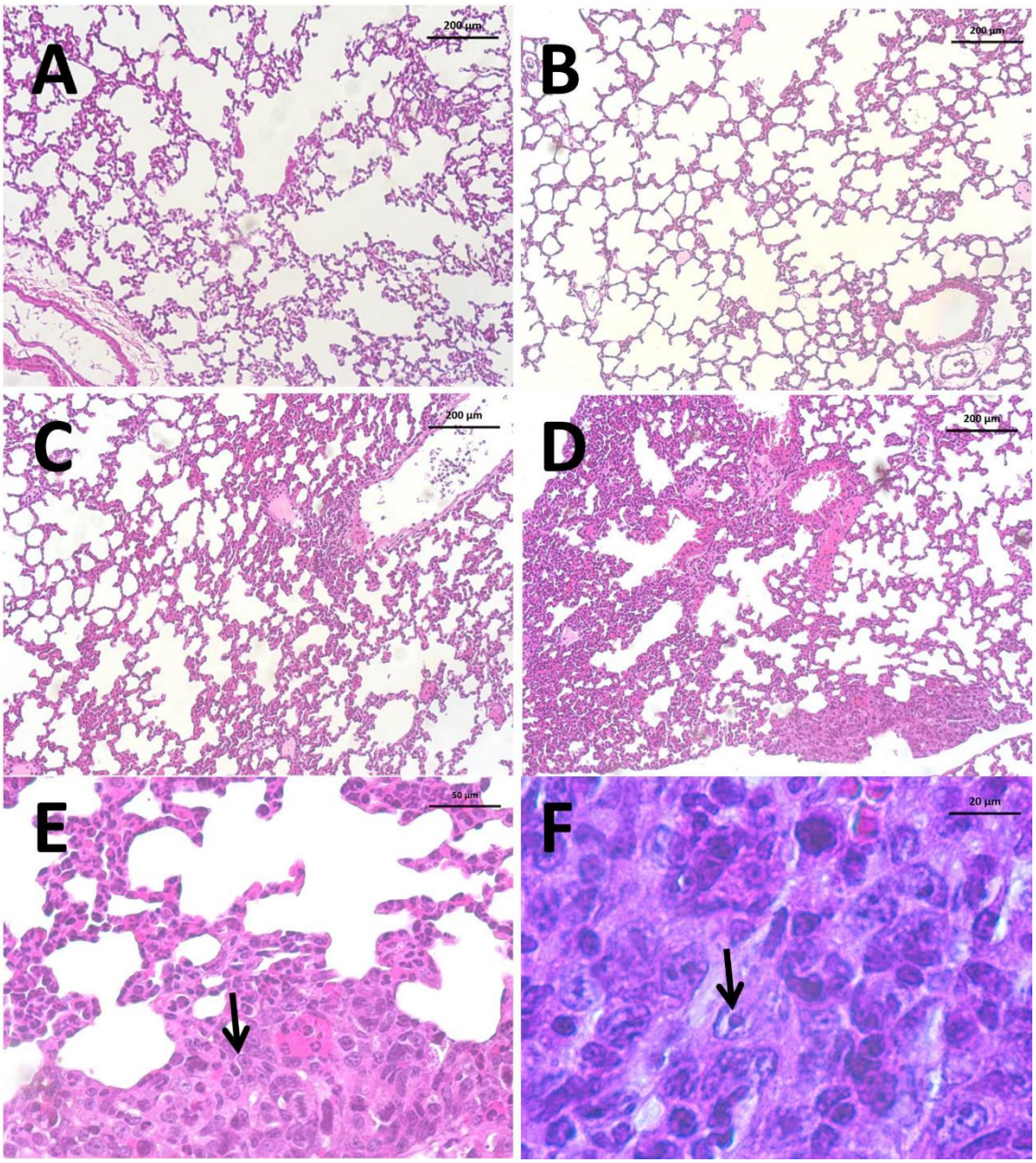

Figure S9. Lung histopatological photomicrographs. Photomicrographs represent normal naïve mice lungs histology (a); NE-C16-Dox (40 mg kg^{-1}) (b); NE-C16-Dox (20 mg kg^{-1}) (c); Free Dox (20 mg kg^{-1}) (d); and PBS treated (e) mice respectively. In section (f) a higher magnification highlight the 4T1 metastatic cells proliferating among lung tissue.

Hemogram

Figure S10 shows the blood cell counting for the different experimental groups. The absolute red blood cells (RBC) counting was statistically equal for the treated groups. On the other hand, the total white blood cell (WBC) counting presented significant increases in all experimental groups compared to the naive group (Figure S10A). The differential WBC counting showed an inversion of blood cell populations in all tumor-bearing mice, compared to naive mice (Figure S10B). The most frequently WBC in naive mice were the lymphocytes (SCC, >75%), which presented reduced percentages in all others experimental groups. The decrease in lymphocyte cell percentages is followed by a significant increase in monocyte (MCC) proportion. The percentage of neutrophils (LCC) did not vary among experimental groups.

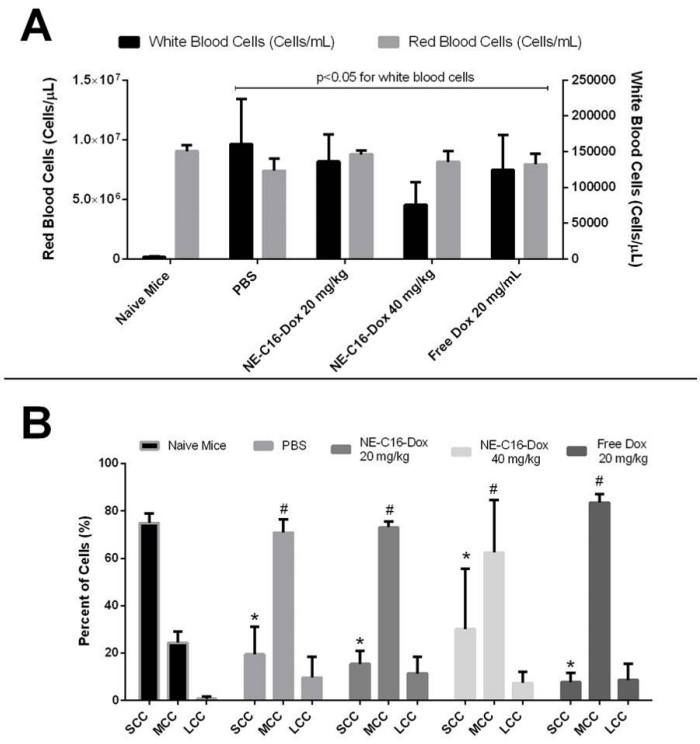

Figure S10. Hematological analysis: a) Counting of Red and White blood cells in different experimental groups; b) Counting of white blood cells types after different treatments. Error bars indicate the standard error of the mean (SEM) in 5 independent animal measurements.

Immunofluorescence and immunohistochemical analyses

Figure S11 shows the CD34 expression in liver histological sections. This procedure was used to confirm the presence of extramedullary hematopoiesis in the liver. The brown spots represent the immunohistochemical stain. CD34 is also expressed in endothelial cells that were used as internal control of the reaction (Figure S11A). In Figure S11B, the positive CD34 cells are clearly identified among the negative CD34 hepatocytes. These cells are atypical in adult mice, and confirm the presence of hematopoietic cells proliferating among normal liver tissue. Figure 12 represent the immunofluorescent confirmation of MDSC in liver tissue. Thus, specific myeloid cell line is characterized by the double expression of GR1 and CD11b.

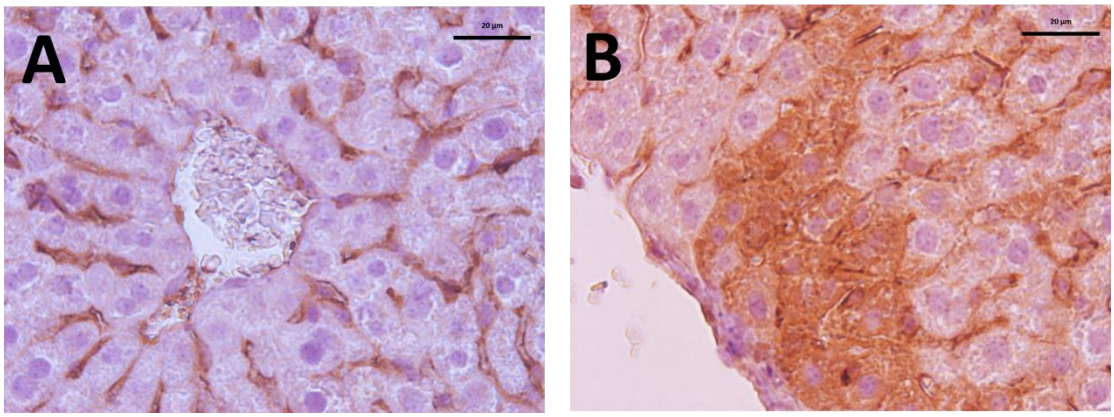

Figure S11. Liver immunohistochemical images staining in brown the CD34 expression. In section (a) the normal liver histology showing the normal CD34 expression in endothelial cells. In (b) CD34 is expressed specifically in hematopoietic cells.

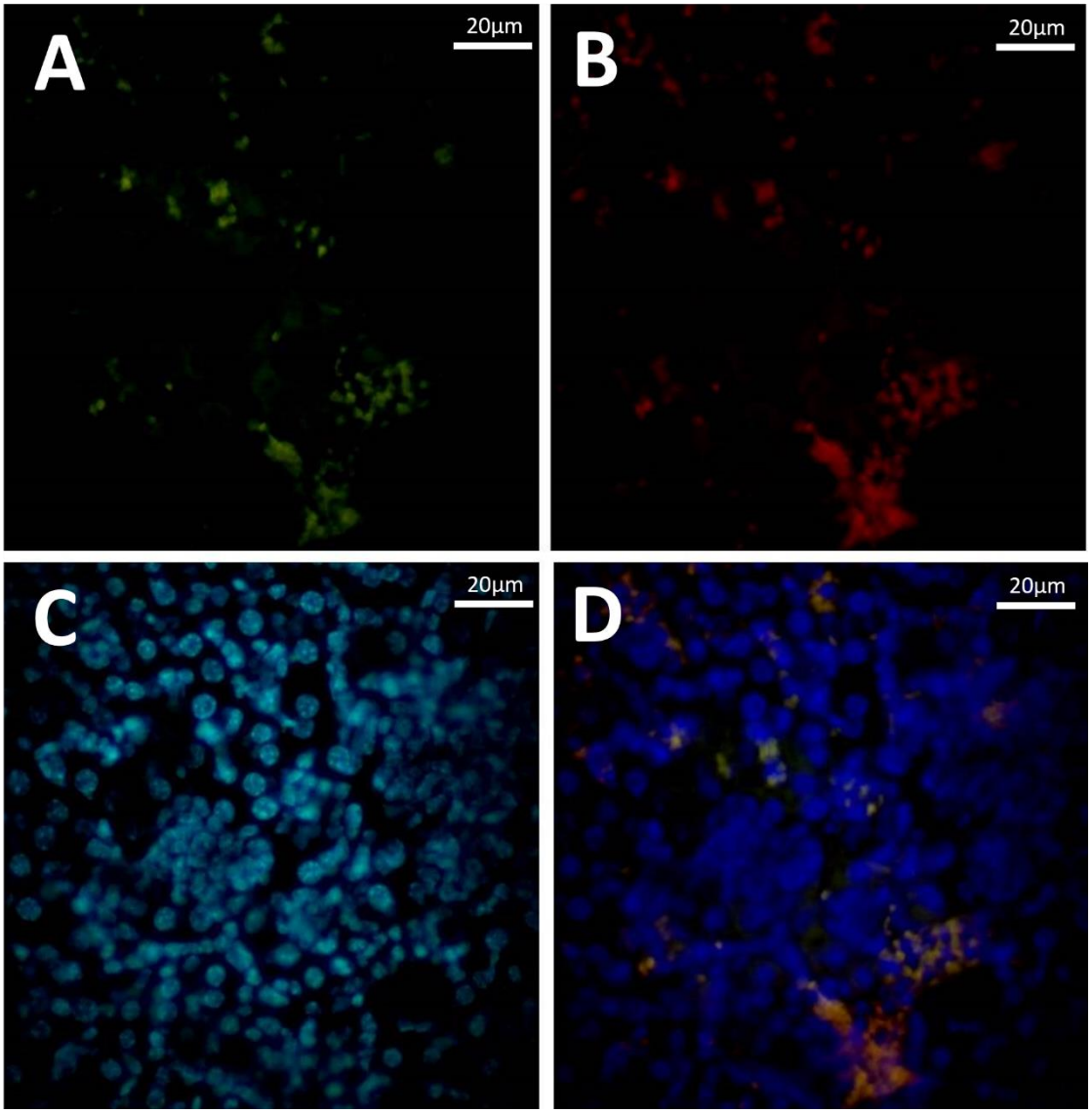

Figure S12. Represents immunofluorescent of MDSC (myeloid derived suppressor cells) in liver tissue. This specific myeloid cell line is characterized by the double expression of GR1 (red) in section (b) and CD11b (green) in section (a). Section (c) represents nuclei staining (DAPI) and section (d) represents the images superposition, confirming the double expression of MDSC.

References

1. Bicalho, L. S.; Longo, J. P. F.; Cavalcanti, C. E. O.; Simioni, A. R.; Bocca, A. L.; de Almeida, S.; de Fátima Menezes, M.; Tedesco, A. C.; Azevedo, R. B., Photodynamic therapy leads to complete remission of tongue tumors and inhibits metastases to regional lymph nodes. *Journal of biomedical nanotechnology* **2013,** *9* (5), 811-818.

2. Longo, J. P. F.; Muehlmann, L. A.; Miranda-Vilela, A. L.; Portilho, F. A.; de Souza, L. R.; Silva, J. R.; Lacava, Z. G. M.; Bocca, A. L.; Chaves, S. B.; Azevedo, R. B., Prevention of Distant Lung Metastasis

After Photodynamic Therapy Application in a Breast Cancer Tumor Model. *Journal of Biomedical Nanotechnology* **2016,** *12* (4), 689-699.
3. Nornoo, A. O.; Osborne, D. W.; Chow, D. S.-L., Cremophor-free intravenous microemulsions for paclitaxel: I: formulation, cytotoxicity and hemolysis. *International journal of pharmaceutics* **2008,** *349* (1), 108-116.
4. Gabizon, A.; Shmeeda, H.; Grenader, T., Pharmacological basis of pegylated liposomal doxorubicin: impact on cancer therapy. *European Journal of Pharmaceutical Sciences* **2012,** *45* (4), 388-398.
5. Al-Jamal, K. T.; Al-Jamal, W. T.; Wang, J. T.-W.; Rubio, N.; Buddle, J.; Gathercole, D.; Zloh, M.; Kostarelos, K., Cationic poly-L-lysine dendrimer complexes doxorubicin and delays tumor growth in vitro and in vivo. *ACS nano* **2013,** *7* (3), 1905-1917.

6.1.3 Matrix metalloproteinase-sensitive multistage nanogels enhance drug transport in 3D tumor model

Supporting information

Matrix metalloproteinase-sensitive multistage nanogels enhance drug transport in 3D tumor model

Gregor Nagel, Ana Sousa-Herves, Stefanie Wedepohl, Marcelo Calderon

[a] *Freie Universität Berlin, Institute of Chemistry and Biochemistry, Takustr. 3, 14195 Berlin, Germany.*

*Corresponding author:

Prof. Dr. Marcelo Calderón

Freie Universität Berlin, Institute of Chemistry and Biochemistry

Takustr. 3, 14195 Berlin (Germany)

Tel.: +49 30 838 459368

E-mail: marcelo.calderon@fu-berlin.de

Homepage: http://www.bcp.fu-berlin.de/chemie/calderon

Table of content:	Page
I. General information	**S3**
II. Figures and Schemes	**S4**
III. Experimental data	**S10**

I. General information

Plate reader

After samples and protease were added, the microplates (Sarstedt or Brand) were covered with optically clear adhesive seal sheets (Absolute QPCR Seal, Thermo Scientific) and placed into a Tecan Infinite M200 Pro microplate reader heated to 37 °C. Fluorescence of methoxy coumarine was monitored every 5 min over 16 h using an excitation wavelength of 320 nm (9 nm bandwidth) and an emission wavelength of 405 nm (20 nm bandwidth).

GPC

Gel permeation chromatography (GPC) analysis were performed on a Shimadzu Prominenze-i LC-2030 liquid chromatography system equipped with a Shimadzu RID-20A refractive index detector. The GPC column used was a Shodex OHpak SB-806M HQ with OHpak SB-G 6B as guard column. Solvents with HPLC grade by Fisher Chemical were employed. The oven temperature was set to 30 °C. The method included a flow 0.5 mL/min with an isocratic mobile phase (PBS 10 mM phosphate, 50 mM NaCl, pH 7.4). The injection volume was 50 µL and the UV-detectors were set to 490 and 650 nm. GPC data was analyzed by Shimadzu LabSolution Version 5.85 software.

Dynamic Light Scattering (DLS) Measurements

DLS measurements were performed on a Malvern Zeta-sizer Nano-ZS ZEN 3600 instrument equipped with a He-Ne laser (532 nm) and a fixed detector oriented at 173°. Conjugate solutions (0.5 mL, 1 mg/mL) were analyzed in quartz fluorescence cuvettes with a round aperture. The autocorrelation functions of backscattered light were analyzed using the Zeta-sizer DTS software from Malvern to determine the size distribution by intensity and the polydispersity index. The measurements were performed at 25 °C in water, equilibrating the system at this temperature for 120 s. Measurements were performed in triplicate of which the mean value is given.

II. Figures and Schemes

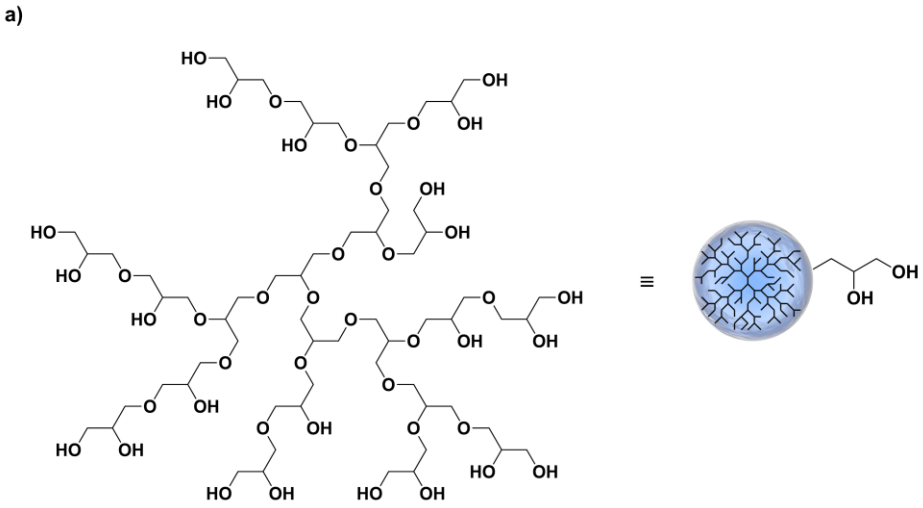

Figure S1. Representative structure of dendritic polyglycerol (dPG).

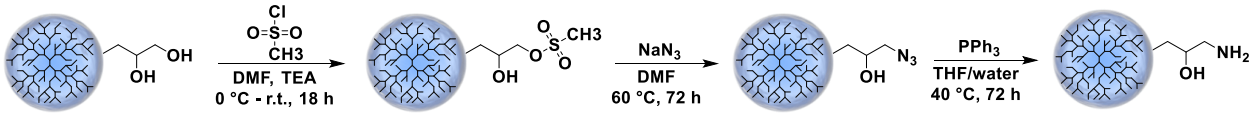

Scheme S1. Functionalization of dPG with amine groups in three steps.

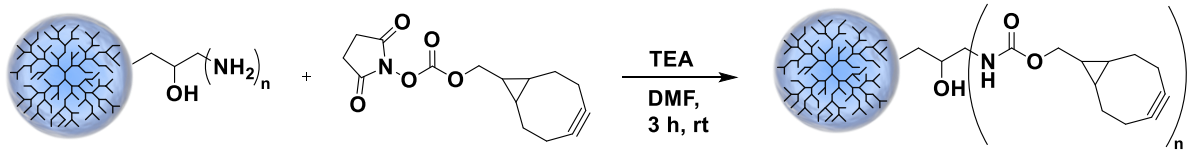

Scheme S2. Functionalization of dPG with bicyclo[6.1.0]non-4-yn (dPG-BCN).

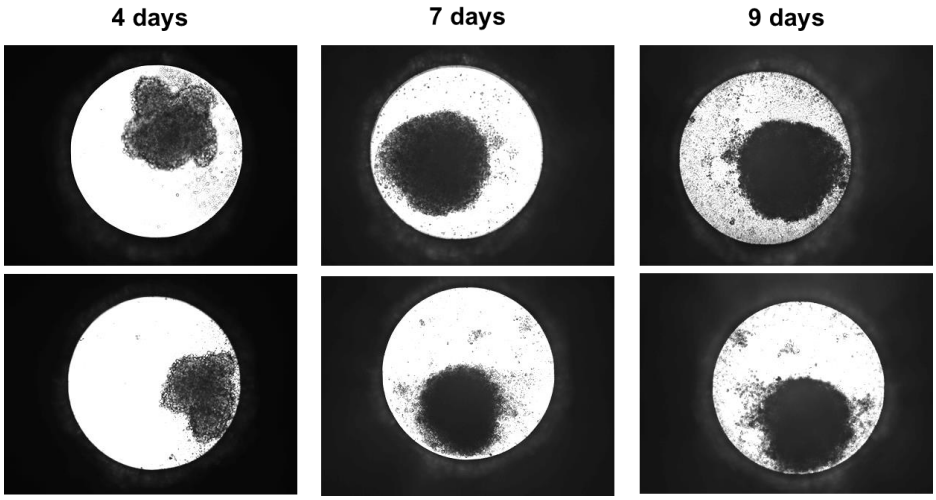

Figure S2. Morphology of multicellular tumor spheroids (MCTS) over time. After 7 days dense, circular spheroids with sizes around 500 µm were obtained.

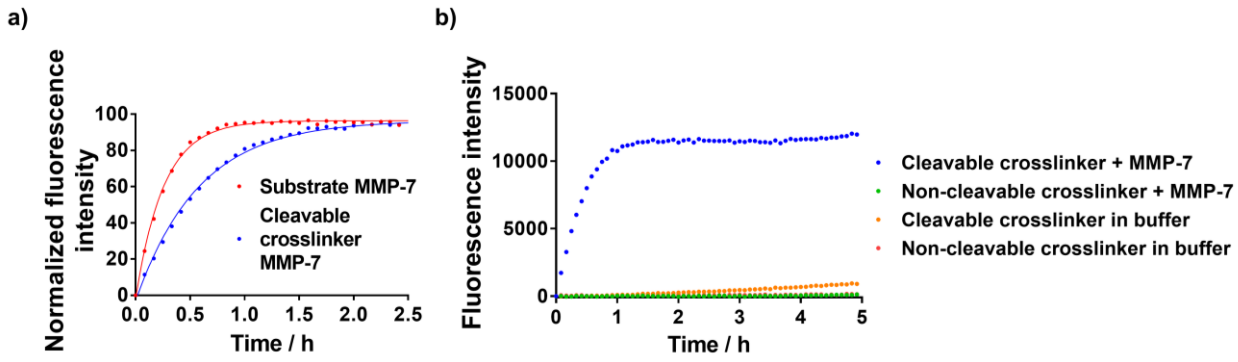

Figure S3. (a) Change of fluorescence intensity (Ex: 320 nm; Em: 405 nm) over time for a commercial substrate and cleavable fluorogenic peptide crosslinker incubated with matrix metalloprotease 7 (MMP-7) at 37 °C. Time constants: Substrate 0.26 h; crosslinker: 0.58 h with same concentration. (b) Change of Fluorescence intensity (Ex: 320 nm; Em: 405 nm) over time for cleavable and non-cleavable fluorogenic peptide crosslinker incubated in buffer or in the presence of MMP-7 at 37 °C.

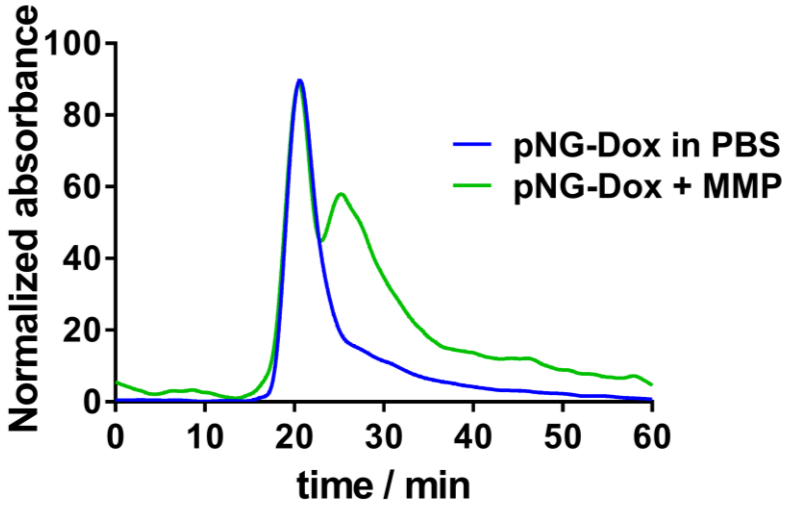

Figure S4. Normalized gel permeation chromatography traces of multistage pNG-Dox before and after incubation with MMP-7 for 16 h.

Table S1: Time constants of degradation rate determined from the exponential fit of the fluorescence intensities over time.

pNG	Time constant (1/K; h)
pNG3	1.3
pNG6	3.7
pNG8	6.6
pNG11	8.5

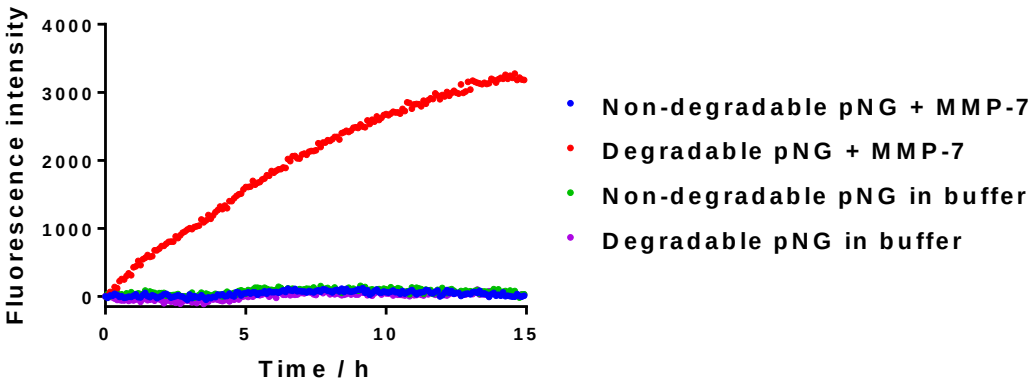

Figure S5. Change of fluorescence intensity (Ex: 320 nm; Em: 405 nm) over time for pNG incubated in buffer or in the presence of MMP-7 at 37 °C.

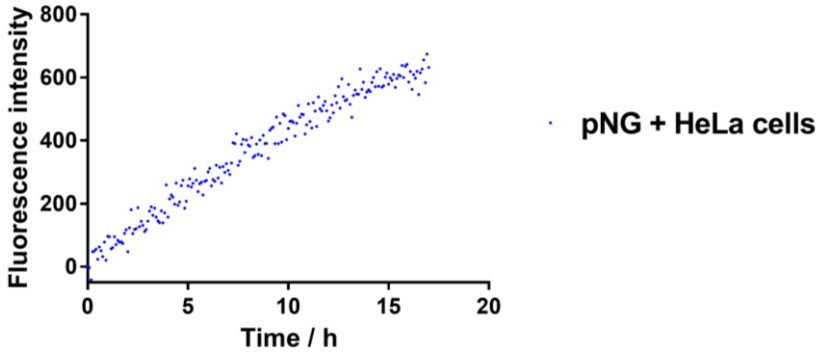

Figure S6. Change of fluorescence intensity (Excitation (Ex): 320 nm; Emission (Em): 405 nm) over time for peptide-crosslinked nanogel (pNG) incubated with Hela cells (10E5 cells/mL) at 37 °C.

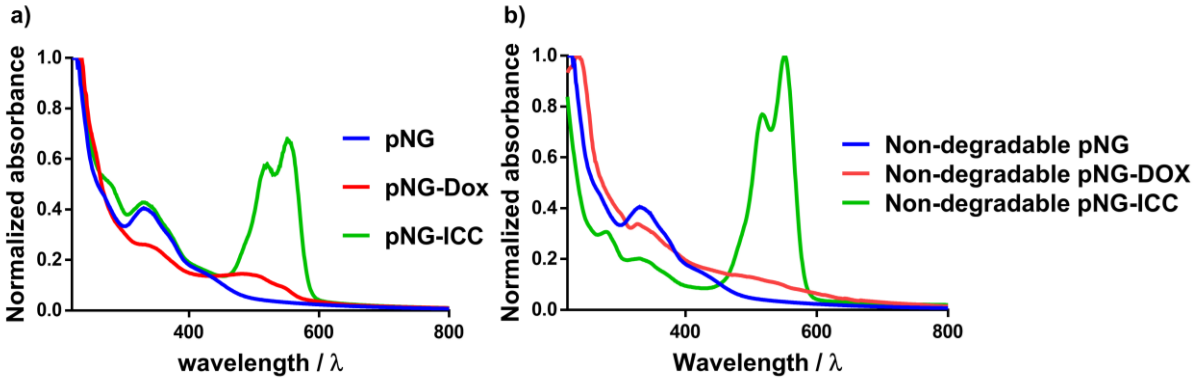

Figure S7. UV/Vis-spectra of (a) degradable and (b) non-degradable pNGs including unfunctionalized pNGs, multistage pNG-Dox, and labeled pNG-ICC.

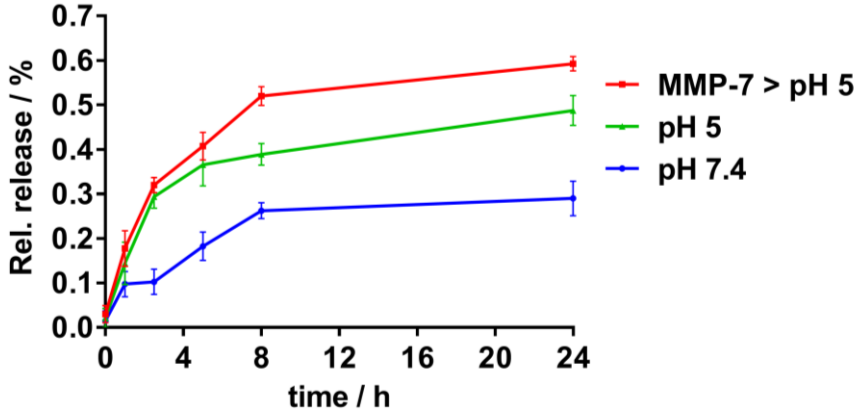

Figure S8. Release of DOX from multistage pNGs under different conditions. The red squares describe the release at pH 5 after the pNG-Dox was digested with MMP-7 over night.

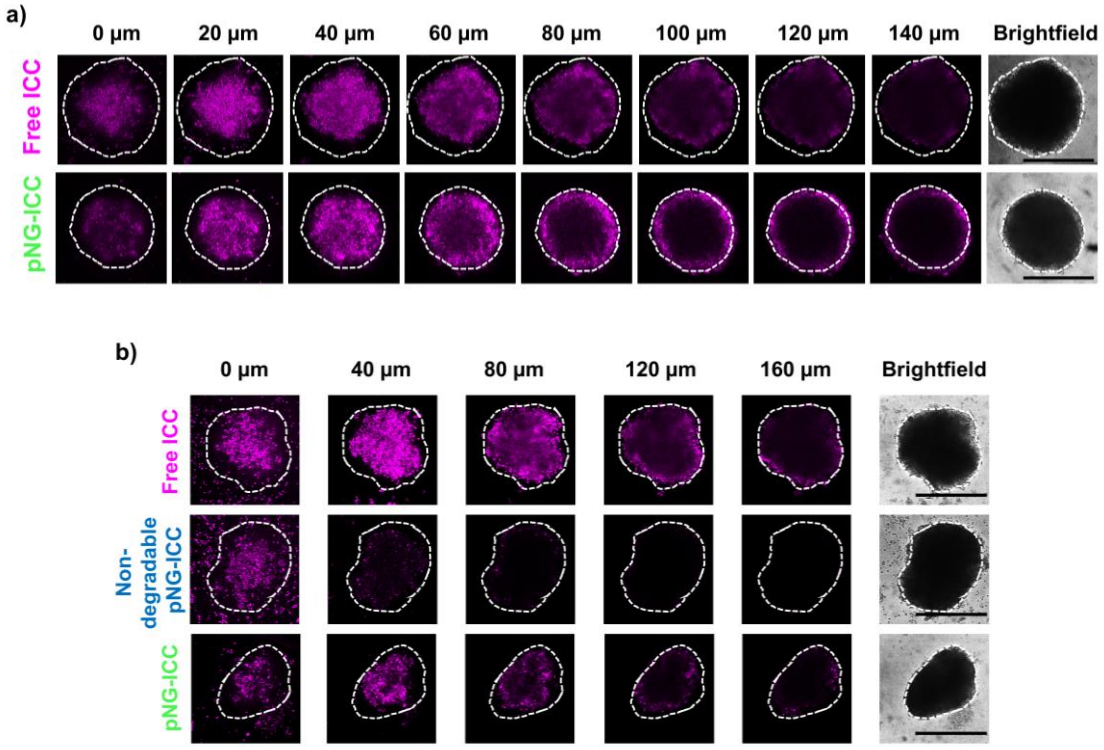

Figure S9. Two examples of Z-stack optical sections using CLSM of live spheroids incubated for 16 h with free ICC, degradable, or non-degradable pNG-ICC. The white dotted line displays the outside margin of the spheroids in the brightfield image. The black bars in the brightfield images represent 500 µm.

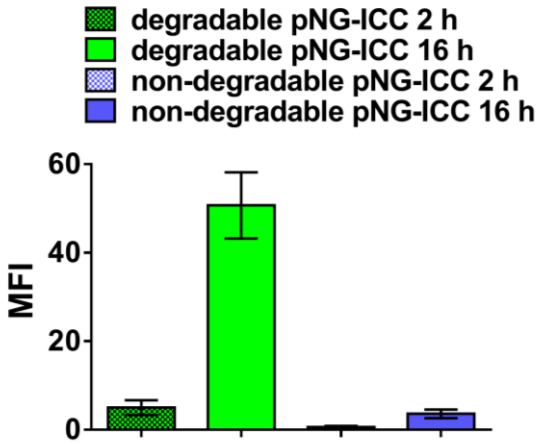

Figure S10. Mean fluorescence intensity over the area of spheroid sections after 2 h and 16 h incubation.

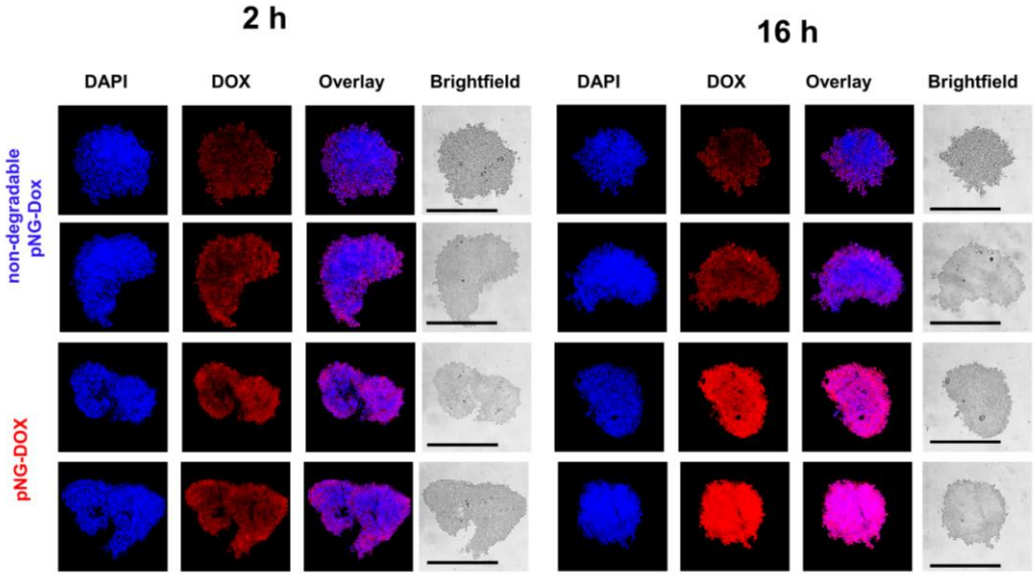

Figure S11. CLSM images of MCTS cryosections with 20-fold magnification. MCTS were incubated degradable and non-degradable pNG-DOX for (a) 2 h and (b)16 h, respectively. Images were obtained with flattened spheroids and optical sectioning

III. Experimental Data

Synthesis of (6-maleimidocaproyl) hydrazone derivative of doxorubicin (aldoxorubicin)

The pH-sensitive (6-maleimidocaproyl) hydrazone derivative of doxorubicin (aldoxorubicin), was synthesized starting from 6-aminocaproic acid following a procedure from literature.[1]

^{1}H-NMR (500 MHz, MeOD-*d*$_4$): δ = 7.91 (s, 1H), 7.90 (d, *J* = 1.9 Hz, 1H), 7.65 (dd, *J* = 5.7, 4.1 Hz, 1H), 6.98 (s, 2H), 5.77 (t, *J* = 4.8 Hz, 1H), 5.51 (s, 1H), 5.46 (d, *J* = 6.2 Hz, 1H), 5.30 (d, *J* = 2.9 Hz, 1H), 4.95 (t, *J* = 6.7 Hz, 1H), 4.40 (dd, *J* = 7.6, 4.8 Hz, 2H), 4.03 (q, *J* = 6.5, 6.1 Hz, 1H), 3.98 (s, 3H), 3.57 (d, *J* = 4.3 Hz, 1H), 3.25 – 3.20 (m, 2H), 2.75 (d, *J* = 17.3 Hz, 1H), 2.21 (dd, *J* = 15.4, 7.7 Hz, 1H), 2.14 (dd, *J* = 13.4, 6.8 Hz, 1H), 2.07 (s, 2H), 1.89 (td, *J* = 12.6, 3.5 Hz, 1H), 1.73 (dd, *J* = 12.0, 4.1 Hz, 1H), 1.55 – 1.42 (m, 1H), 1.30 (q, *J* = 7.7 Hz, 3H), 1.16 (d, *J* = 6.5 Hz, 3H), 1.02 (p, *J* = 7.9 Hz, 2H) ppm; **HRMS (ESI-TOF)**: $C37H43N4O13^+$ $[M+H]^+$ calculated: 751.2821; found: 751.2861; $C37H42N4NaO13^+$ $[M+Na]^+$ calculated: 773.2641; found: 773.2664.

^{1}H-NMR of (6-maleimidocaproyl) hydrazone derivative of doxorubicin (aldoxorubicin)

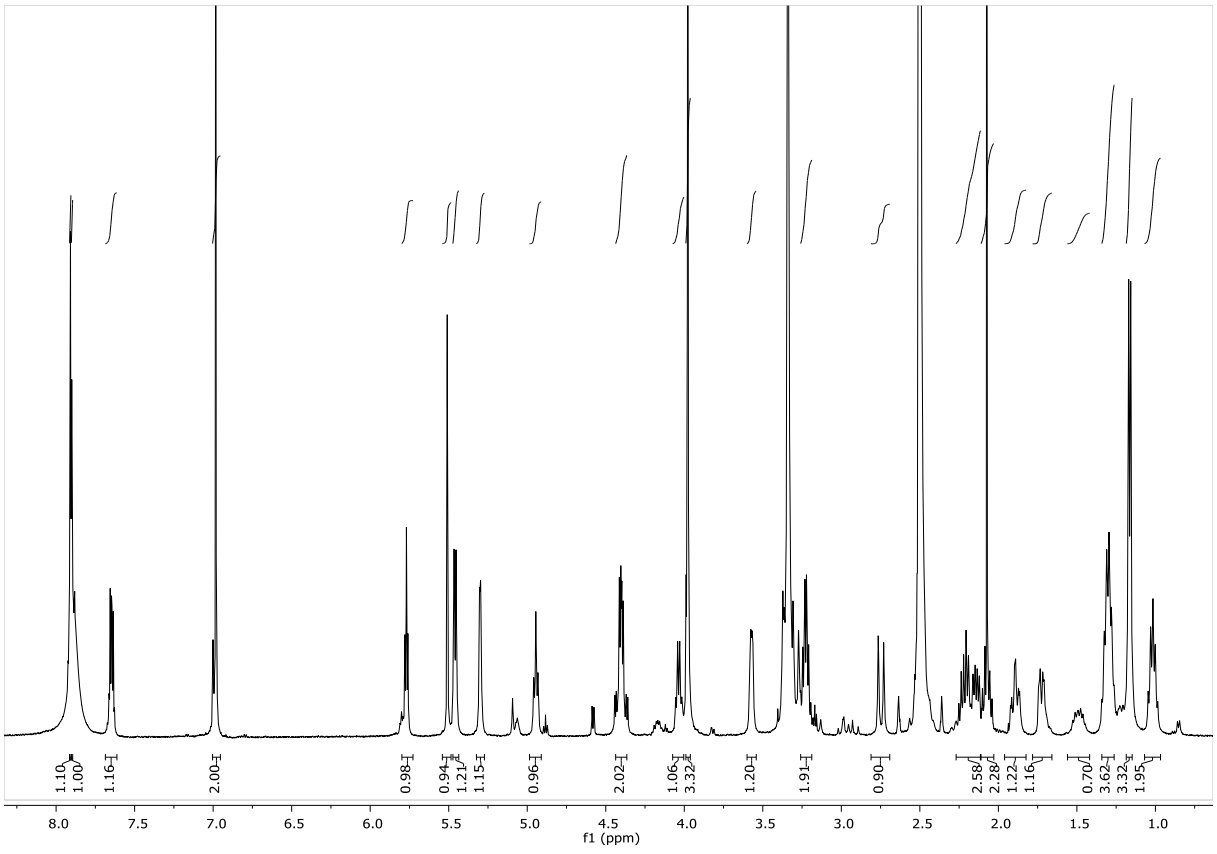

Mass spectrum (ESI-TOF) of (6-maleimidocaproyl) hydrazone derivative of doxorubicin (aldoxorubicin)

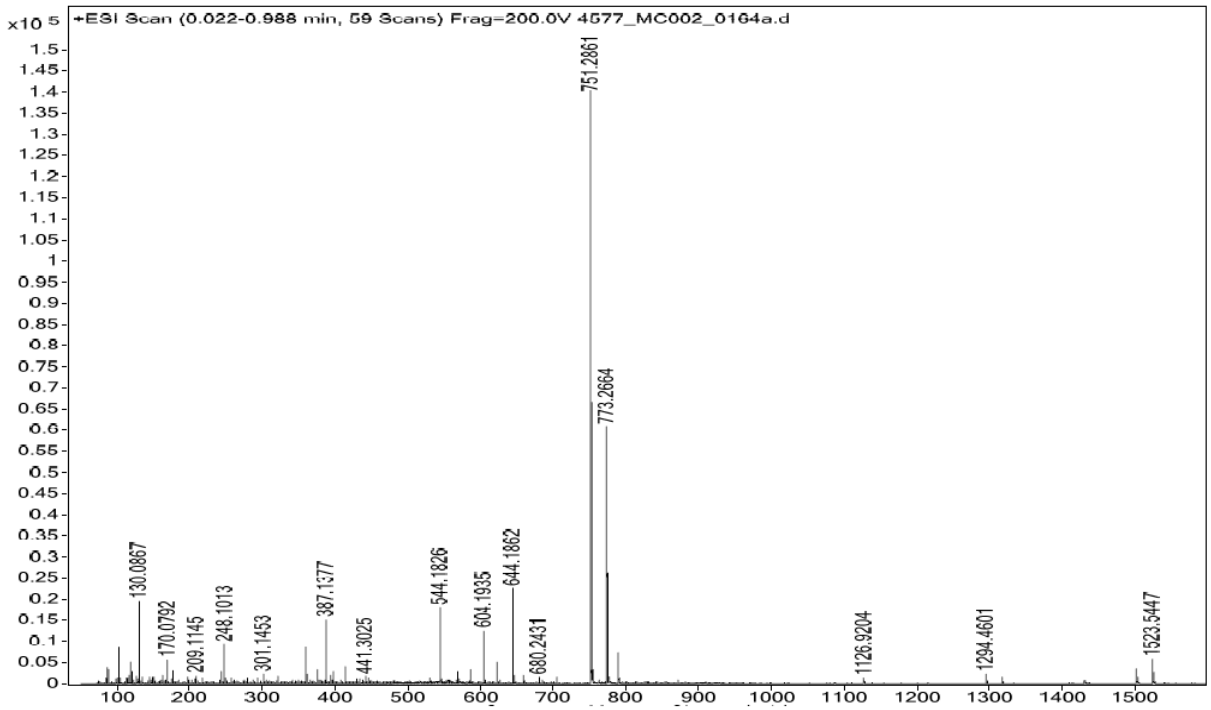

Snthesis of dPG-(1R,8S,9s)-Bicyclo[6.1.0]non-4-yn-9-ylmethyl (dPG-BCN)

^{1}H-NMR (500 MHz, D_2O): δ (ppm) = 4.24-3.42 (m, 5H, dPG backbone), 2.31-2.14 (m, 6H, cyclooctyne), 1.60-1.28 (m, 2H, cyclooctyne), 0.98-0.80 (m, 3H, cyclopropane).

4.2% functionalization

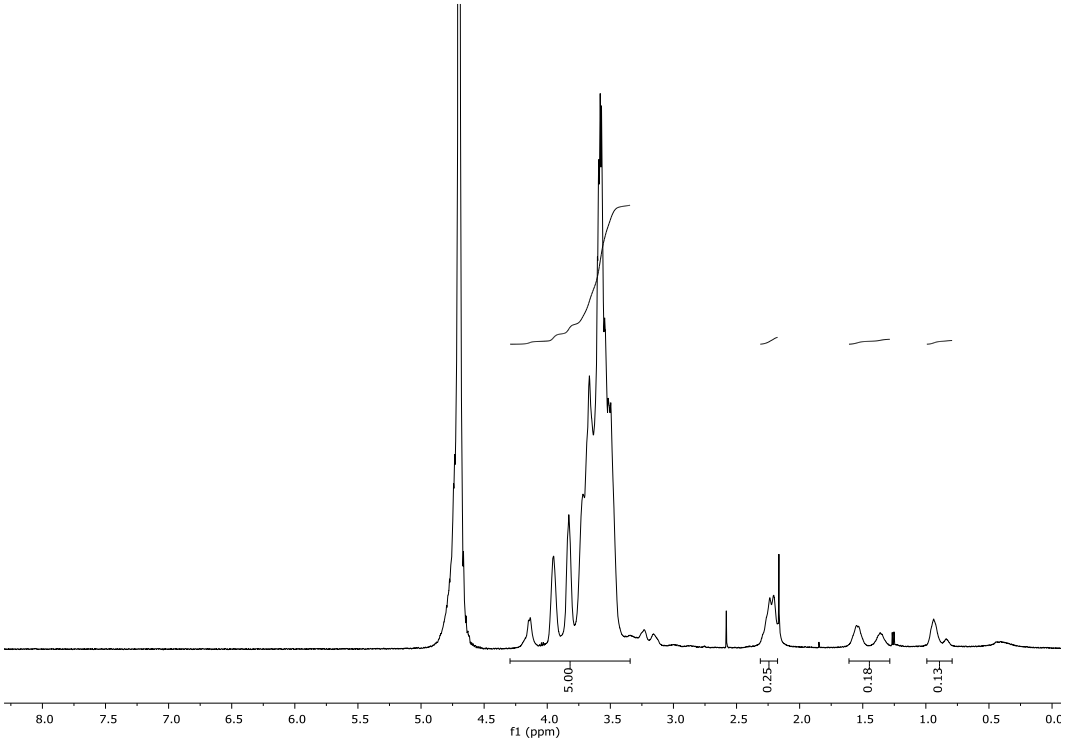

8. % functionalization

^{1}H-NMR (500 MHz, MeOD-d_4): δ (ppm) = 4.24-3.42 (m, 5H, dPG backbone), 2.42-2.50 (m, 6H,
cyclooctyne), 1.69-1.28 (m, 2H, cyclooctyne), 1.02-0.80 (m, 3H, cyclopropane).

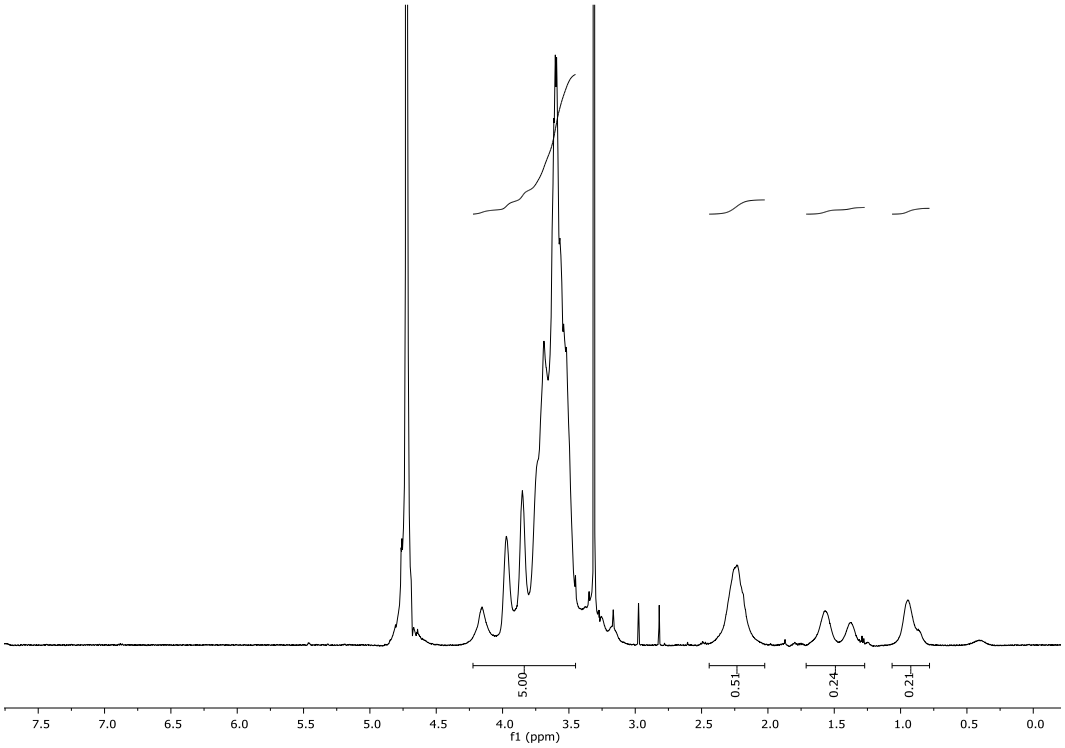

1. Willner, D.; Trail, P. A.; Hofstead, S. J.; King, H. D.; Lasch, S. J.; Braslawsky, G. R.; Greenfield, R. S.; Kaneko, T.; Firestone, R. A., (6-Maleimidocaproyl)hydrazone of doxorubicin. A new derivative for the preparation of immunoconjugates of doxorubicin. *Bioconjugate Chemistry* **1993,** *4* (6), 521-527.

6.2 Publications & conference contributions

Publications:

1. H. R. Krüger, **G. Nagel**, S. Wedepohl, M. Calderón, Dendritic polymer imaging systems for the evaluation of conjugate uptake and cleavage. *Nanoscale* **2015**, 9, 3838-3844.
2. A. L. dos Santos Câmara‡, **G. Nagel**‡, H. R. Tschiche, C. Magalhães Cardador, L. A. Muehlmann, D. Mara de Oliveira, P. Queiroz Alvim, R. Bentes Azevedo, M. Calderón, J. P. Figueiró Longo, Acid-sensitive lipidated doxorubicin prodrug entrapped in nanoemulsion impairs lung tumor metastasis in a breast cancer model. Nanomedicine (Lond.) **2017**, 12, 1751–1765.
3. M. Kar, L. Fechner, **G. Nagel**, E. Glitscher, G. Noe Rimondino, M. Calderón, Chapter 12 Responsive Nanogels for Anti-cancer Therapy, in: Nanogels for Biomedical Applications. The Royal Society of Chemistry, **2018**, 210-260.
4. S. Jung, **G. Nagel**, M. Giulbudagian, M. Calderón, A. Patzelt, F. Knorr, J. Lademann, Temperature-Enhanced Follicular Penetration of Thermoresponsive Nanogels. Zeitschrift für Physikalische Chemie **2018**, 232, 805-817.
5. M. L. Picchio, J. C. Cuggino, **G. Nagel**, S. Wedepohl, R. J. Minari, C. I. Alvarez Igarzabal, L. M. Gugliotta, M. Calderón, Crosslinked casein-based micelles as a dually responsive drug delivery system. Polymer Chemistry **2018**, 9, 3499-3510.
6. **G. Nagel**, H. R. Tschiche, S. Wedepohl, M. Calderón, Modular approach for theranostic polymer conjugates with activatable fluorescence: Impact of linker design on the stimuli-induced release of doxorubicin. Journal of Controlled Release **2018**, 285, 200–211.
7. **G. Nagel**, A. Sousa Hervés, S. Wedepohl, M. Calderón, Matrix metalloproteinase-sensitive multistage nanogels enhance drug transport in 3D tumor model. Manuscript submitted.

‡ Equal contributions

Conference Contributions

1. **G. Nagel**, H. R. Krüger, S. Wedepohl and M. Calderón, Dendritic Polymer Imaging Systems for the Evaluation of Conjugate Uptake and Cleavage. European Polymer Congress of the European Polymer Federation, Dresden, Germany **2015**.
2. **G. Nagel**, H. R. Krüger, S. Wedepohl, M. Calderón, Evaluation of Drug Release from Theranostic Macromolecular Prodrugs by Different Triggers. 11th International Symposium on Polymer Therapeutics: From Laboratory to Clinical Practice. Valencia, Spain **2016**.
3. **G. Nagel**, A. L. dos Santos Câmara, H. R. Krüger, C. Cardador, L. A. Muehlmann, R. Bentes Azevedo, M. Calderón, J. P. Figueiró Longo. Nanoemulsions from Lipophilic, pH-sensitive Doxorubicin Prodrug Impairs Tumor Growth and Prevents Distant Lung Metastasis in a Breast Cancer Mice Model. 11th International Symposium on Polymer Therapeutics: From Laboratory to Clinical Practice. Valencia, Spain **2016**.
4. **G. Nagel**, H. R. Krüger, S. Wedepohl, M. Calderón, Following Cellular Uptake and Internal Drug Release of Polymer-Drug Conjugates by Fluorescent Turn-on Probes. Polydays, Potsdam, Germany **2016**.
5. **G. Nagel**, H. Tschiche, S. Wedepohl and M. Calderón, Comparison of Endogenous Triggers for the Drug Release from Polymer-Drug Conjugates by Fluorescent Turn-on Probes. 19th Frühjahrssymposium des JungChemikerForums, Mainz, Germany **2017**.
6. **G. Nagel**, S. Wedepohl, M. Calderón, Protease-sensitive Nanogels with Fluorogenic Reporter for Dermal Drug Delivery. European Symposium on Controlled Drug Delivery, Egmond aan Zee, Netherlands **2018**.

6.3 Curriculum Vitae

Der Lebenslauf ist in der Online-Version aus Gründen des Datenschutzes nicht enthalten.